Kinematic Analysis, Optimization and Programming of Parallel Robotic Manipulators

by

Clément Gosselin

B.Eng. (Université de Sherbrooke), 1985

Department of Mechanical Engineering

McGill University

Montréal, Canada

A thesis submitted to the Faculty of Graduate Studies and Research

in partial fulfillment of the requirements for the degree of

Doctor of Philosophy

June 15, 1988

Abstract

This thesis presents an extensive study of the kinematics of parallel manipulators. The latter are considered here as a subset of a more general class of kinematic chains called *complex kinematic chains* which are defined as chains in which there exists at least one link having a degree of connectivity greater than or equal to three. The degree of connectivity of a link is defined here as the number of rigid bodies that are directly attached to this link by kinematic pairs.

The first portion of the thesis is devoted to the study of simple kinematic chains which are the basic elements from which complex kinematic chains, and hence parallel manipulators, are constructed. The analysis of complex kinematic chains is then pursued through their graph representation and through the derivation of the associated Jacobian matrix. The three types of singularities pertaining to this class of kinematic chains are identified using the latter concept. They are illustrated with some examples. This also leads to an unambiguous definition of parallel manipulators based on their graph representation.

Parallel manipulators are then analyzed in detail. The analysis includes the solution of the direct and inverse kinematic problems, the velocity and acceleration inversions and an investigation of the singularities. These problems are discussed in a general framework before special cases are introduced. The kinematic design optimization of parallel manipulators is then undertaken using some performance criteria such as symmetry, workspace, local dexterity and global dexterity. A new performance index called *global conditioning index (GCI)* is also defined.

Finally, the kinematic inversion of redundant parallel manipulators is approached as a local dexterity maximization problem. The concept of *trajectory map* is introduced and an algorithm for the generation of smooth trajectories is given.

Résumé

Cette thèse présente une étude détaillée de la cinématique des manipulateurs à architecture parallèle. Ces manipulateurs constituent en fait un sous-ensemble d'une classe plus générale de chaînes cinématiques que l'on appelle *chaînes cinématiques complexes*, ces dernières étant définies comme les chaînes cinématiques possédant au moins un membre dont le degré de connectivité est supérieur ou égal à trois. Le degré de connectivité d'un membre est défini ici comme le nombre de membres lui étant directement attachés par des liaisons cinématiques.

La première partie de la thèse traite des chaînes cinématiques simples, celles-ci étant les éléments de base à partir desquels les chaînes cinématiques complexes et, par conséquent, les manipulateurs parallèles sont construits. Cette section permet d'introduire des concepts importants tels que la mobilité des mécanismes, l'optimisation de la qualité de transmission et l'identification des différentes configurations ou ramifications.

L'analyse des chaînes cinématiques complexes est alors entreprise grâce au concept de graphe associé et de matrice Jacobienne associée. Cette dernière méthode permet d'identifier les trois types de singularités pouvant être rencontrées dans les chaînes cinématiques complexes. Des exemples sont fournis afin d'illustrer ces trois catégories. De plus, l'approche basée sur la théorie des graphes conduit à une définition non équivoque des manipulateurs parallèles en tant que sous-ensemble des chaînes cinématiques complexes.

Les manipulateurs parallèles sont ensuite analysés de façon approfondie. Cette analyse inclut la solution des problèmes cinématiques direct et inverse de même que la dérivation des relations inverses de vitesse et d'accélération. Une étude des singularités est également présentée. Ces problèmes sont d'abord discutés dans un contexte général, puis des cas particuliers sont introduits. Les manipulateurs considérés sont de type: plan à 3 degrés de liberté, sphérique à 3 degrés de liberté, spatial à 3 degrés de liberté et spatial à 6 degrés de liberté.

L'optimisation cinématique des manipulateurs parallèles est alors entreprise en utilisant des critères de performance tels que la symétrie, le volume de travail, la dextérité locale et la dextérité globale. Un nouvel indice de performance appelé *indice de condition global* est également défini. Des solutions optimales sont obtenues pour les cas particuliers de manipulateurs mentionnés au paragraphe précédent.

Finalement, l'inversion cinématique des manipulateurs parallèles redondants est considérée comme un problème de maximisation de la dextérité locale. Le concept de *carte de trajectoire* est introduit et un algorithme permettant de générer des trajectoires continues est donné.

Acknowledgements

I am indebted to professor Jorge Angeles, my research supervisor, for his stimulating suggestions and for his patience in the long hours of discussion. His deep insight into kinematics and mathematics and his positive criticism throughout the course of this work were of great help to me.

I also wish to express my gratitude to the members of McRCIM for their technical assistance. Special thanks are due to Dr. Carlos S. López-Cajún, visiting professor, to Messrs. Ma Ou, Guo Lin, Meyer Nahon, and Miss Karen Anderson, graduate students, for the many enriching discussions that I have had with them, and to Mrs. Helga Symington who took the photographs included in this thesis.

I am also very grateful to my parents whose confidence in me and encouragement have greatly contributed to the completion of this work.

Finally, I would like to acknowledge the financial support of the Natural Sciences and Engineering Research Council.

To my parents

Contents

List of Figures

List of Tables

Claim of Originality

The author claims the originality of the ideas expressed in this thesis. The following contributions are of particular interest:

(i) the graphical representation of the mobility regions of planar and spherical four-bar linkages

(ii) the optimization of planar and spherical four-bar linkages as minimum-defect linkages using the orthogonal-decomposition method

(iii) the solution of the branch identification problem for wrist-partitioned manipulators using the eigenvalues of the Jacobian matrix

(iv) a general method to determine the degree-of-freedom of complex kinematic chains based on their topology and geometry

(v) a classification of all possible singularities encountered in complex kinematic chains in three different groups

(vi) a complete kinematic analysis and singularity analysis of four types of parallel manipulators

(vii) the definition of a new performance index (Global conditioning index) for the optimization of the global dexterity of serial or parallel manipulators

(viii) a workspace and dexterity optimization of four types of parallel manipulators

(ix) an algorithm for the kinematic inversion of redundant parallel manipulators using local dexterity maximization and the concept of trajectory map.

Some of the results reported in this thesis have been partly presented in the following publications and communications: Angeles et al. (1987), Gosselin and Angeles (1987*a*), (1987*b*), (1987*c*), (1987*d*), (1988*a*), (1988*b*), (1988*c*) and (1988*d*).

Chapter 1 INTRODUCTION

The constant evolution of the variety of products and goods to be manufactured and the evergrowing need for better efficiency lead to the development of new methods of production. This also applies to the manufacturing processes that make use of robotic manipulators to perform certain tasks.

Indeed, there is a great deal of effort directed towards the development of robots exhibiting better characteristics, e.g., the speed of operation, load carrying capacity, dynamic properties, reliability and repeatability. Apart from the work being done in control systems, algorithms and sensors, which will not be discussed here, researchers have been involved at two different levels, to aim at the foregoing objectives.

The first trend consists of the improvement of the performance of the different elements of a manipulator such as its actuators. The introduction and the development of direct-drive robots is an example of the research conducted at this level. (Asada et al. 1982; Asada and Kanade 1982; Asada and Youcef-Toumi 1987)

On the other hand, some researchers have been considering the possibility of designing robots with new kinematic architectures. As a matter of fact, most of the manipulators that are currently in use are of the serial type, i.e., their kinematic structure is simple and open. In such an architecture, each of the links is binary, i.e., it is attached to two other links, except for the end-effector and the base that are attached to only one other

link. However, although it readily leads to anthropomorphic arms and to simpler kinematic equations, this structure has some drawbacks, namely:

(i) only one of the motors is fixed; the remaining ones, accounting for a substantial part of the inertial load, are moving

(ii) due to the cantilever type of the links, the elastic flexibility is generally high which introduces positioning inaccuracies and undesired dynamical side effects

Since some applications require very stiff arms with important load-carrying capacities, the possibility of including closed kinematic chains into a robotic manipulator (Asada and Youcef-Toumi 1984; Bajpai and Roth 1986, Stoughton and Kokkinis 1987; Mohamed 1987), or even to build manipulators with a fully parallel architecture (Hunt 1983; Yang and Lee 1984; Mohamed and Duffy 1985; Fichter 1986; Inoue et al. 1985; Sugimoto 1987; Shirkhodaie and Soni 1987; Lee and Shah 1987), has been considered. Parallel robotic manipulators are characterized by the fact that the gripper is attached to the ground via several kinematic chains leading to a structure with multiple closed-loops. Parallel manipulators are expected to yield the following results:

(i) by allowing all of their motors, or at least the heavier ones, to be fixed, larger amounts of power will be available, thus increasing the load-carrying capacity and the speeds of operation

(ii) by full elimination or, at least, reduction of gear drives, accuracy will be increased, while production costs will be lowered

(iii) by elimination of cable transmissions, accuracy and reliability will be increased.

Moreover, parallel manipulators find applications in other fields such as flight simulators, walking machines and robot hands. In fact, the two latter mechanical systems can be considered as parallel manipulators with time varying kinematic parameters.

In this thesis, the kinematics of parallel manipulators is studied in detail. The objective is to obtain the kinematic equations constraining the motion of these manipulators and to use them to optimize the kinematic properties of the said manipulators with regard to two issues, design and programming. The approach adopted here is to consider this class of manipulators as a special case of a more general class of linkages called complex kinematic chains. Therefore, the next two chapters will be devoted to a review of some properties of simple and complex kinematic chains.

Some aspects of simple kinematic chains, such as mobility, transmission quality and branch identification, are critically reviewed because of their relevance to the study of parallel manipulators. This issue is covered in Chapter 2.

In Chapter 3, complex kinematic chains are regarded as a very general class of linkages. The graph representation of their topology is introduced and completed with a geometric representation, based on the Jacobian matrix, which leads to a method of determining the degree of freedom of any general complex chain for any of its configurations. The method is also applied to the investigation of singularities, which are shown to be of three different possible types.

Having discussed complex kinematic chains in general, parallel manipulators are introduced as a particular subset of these, their study being of greater interest in the context of robotics. Chapters 4 and 5 address the problems of analysis and optimization of these manipulators. The major issues in analysis are the solution of the direct and inverse kinematic problems, velocity and acceleration inversions, and singularity identification. Planar, spherical and spatial three-degree-of-freedom manipulators are considered together with a spatial six-degree-of-freedom manipulator. These particular manipulators have been chosen for they have emerged as the most promising cases according to a survey of the different possible parallel architectures for robotic applications (Hunt 1983). The optimization, dicussed in Chapter 5, focuses on the optimum design of manipulators based on performance indices related to workspace and dexterity. The concept of dexterity is defined here as a function of the condition number of the Jacobian matrix. A clear distinc-

tion is made between local and global dexterity, the latter, also termed *Global Conditioning Index (GCI)*, being a contribution of this thesis. This approach follows previous work on the subject (Salisbury and Craig 1982; Yoshikawa 1985; Angeles and Rojas 1987; Klein and Blaho 1987). The main objective of Chapter 5 is to obtain design guidelines for the parallel manipulators mentioned above, based on the foregoing criteria.

Since the tasks to be performed by a certain manipulator are, in general, unknown *a priori*, the design has to be based on criteria such as the ones presented above. However, a different problem arises when a *given* robot is required to produce a certain trajectory in the task space. If the number of controlled axes of the robot is equal to the number of variables associated with the given task, then the inverse kinematic algorithm is directly used for the programming of the robot. On the other hand, if the number of controlled axes of the robot is greater than the number of variables associated with the task, then the manipulator is said to be *redundant* with respect to this particular task and its motion can therefore be optimized because of the extra axes. The programming of these robots deserves special attention. Examples of such parallel robots are given in Chapter 6 where this problem is addressed. The trajectory is optimized using the local dexterity as an optimization criterion and using the concept of trajectory map developed here.

Chapter 2 SIMPLE KINEMATIC CHAINS

At the preliminary stage of this work, it is of interest to revisit some of the properties of simple kinematic chains. Simple chains are defined here as kinematic chains containing links having a degree of connectivity smaller than or equal to 2. It is recalled that the degree of connectivity of a link is understood here as the number of rigid bodies that are directly attached to the said link by kinematic pairs. Therefore, simple kinematic chains encompass both serial manipulators and closed single-loop linkages. The former have binary links and two links of connectivity one (the base and the end-effector), whereas the latter have only binary links.

The properties of kinematic chains studied in this chapter have been chosen for their particular relevance in the analysis or optimization of parallel manipulators. They allow the introduction of some concepts that will be extended or used as such in the forthcoming chapters, namely:

(i) the mobility analysis of planar and spherical four-bar linkages presented here is based on the concept of *linkage discriminant* which will be used later for the workspace analysis of planar and spherical parallel manipulators,

(ii) there is a connection between the concept of *transmission quality* used here to optimize planar and spherical four-bar linkages and the local and global dexterity of parallel manipulators which will be defined in Chapter 4,

(iii) the branch identification problem is discussed here for serial manipulators to stress its importance in the kinematics of manipulators in general. As a matter of fact, parallel manipulators usually have many more branches than the corresponding serial manipulators.

2.1 Mobility Analysis of Planar and Spherical Four-Bar Linkages

The identification of the mobility regions of linkages constitutes an important aspect of linkage design. In the context of CAD, the graphical representation of these regions is therefore an item of the utmost importance. The mobility region of a linkage is defined as the region, in the space of its parameters (or in a space defined with functions of these parameters), in which the input link has full rotatability, i.e., it can undergo a full rotation of 2π. However, it is often desirable to find the region in which the output link is fully rotatable. When these two regions are known, we can infer the region in which both the input and the output are fully rotatable, i.e., the *crank-crank* region by finding the intersection of the aforementioned regions. In a similar fashion, we can subtract the intersection from each of the original regions of mobility to obtain the *crank-rocker* and *rocker-crank* regions.

The mobility of planar and spherical linkages has been studied extensively in the past. Grashof (1883) first proposed inequalities describing the mobility of planar linkages. Further work on the subject produced other geometric (Gupta and Radcliffe 1971; Midha et al. 1985) and algebraic-geometric (Gupta 1980) criteria. These were meant to incorporate mobility conditions in design procedures. Similar mobility criteria were developed for spherical linkages (Freudenstein, 1965; Savage and Hall, 1970; Soni and Harrisberger, 1967; Duditza and Dittrich, 1969; Gupta 1986b).

More recently, the need for graphical representations of the mobility regions arose, the objective being to include them in CAD packages for linkage design. Risbourg (1983) gave a full description of the different regions for planar linkages based on Grashof's

inequalities. Barker and Lo (1986) presented a similar description and representation for spherical mechanisms.

The mobility analysis used here is an extension of the one given in (Gosselin and Angeles, 1987a). This is based on the concept of *linkage discriminant* which was first used in (Angeles and Callejas, 1984) for planar linkages and extended in (Angeles and Bernier, 1987a). Other studies using the concept of *linkage discriminant* for linkage mobility are (Williams and Reinholtz, 1986 & 1987).

The inequalities obtained by the mobility analysis of planar and spherical linkages lead to polyhedra in the 3-D space of linkage parameters. Moreover, these polyhedra, as shown here, have surprisingly symmetrical shapes and are formally identical for planar and spherical linkages.

2.1.1 Planar Linkages

The linkage parameters $k_i, (i = 1,2,3)$ used here are essentially those proposed first by Freudenstein (1954,1955). Moreover, they are identical to the ones used in (Angeles and Callejas, 1984; Angeles and Bernier, 1987a; Gosselin and Angeles, 1987a). They are recalled here for quick reference. A planar mechanism is shown in Fig. 2.1, where the link lengths are given by $a_i, (i = 1,\ldots,4)$. The linkage parameters $k_i, (i = 1,2,3)$ are then defined as:

$$k_1 = \frac{a_1^2 + a_2^2 - a_3^2 + a_4^2}{2a_2a_4}, \qquad k_2 = \frac{a_1}{a_2}, \qquad k_3 = \frac{a_1}{a_4} \tag{2.1}$$

The inverse transformation is given as follows:

$$a_1 = 1, \qquad a_2 = \frac{1}{k_2}, \qquad a_3 = \frac{\sqrt{k_2^2 + k_3^2 + k_2^2k_3^2 - 2k_1k_2k_3}}{|k_2k_3|}, \qquad a_4 = \frac{1}{k_3} \tag{2.2}$$

The input-output equation of the planar mechanism can then be expressed as:

$$A(\psi)T^2 + 2B(\psi)T + C(\psi) = 0 \tag{2.3}$$

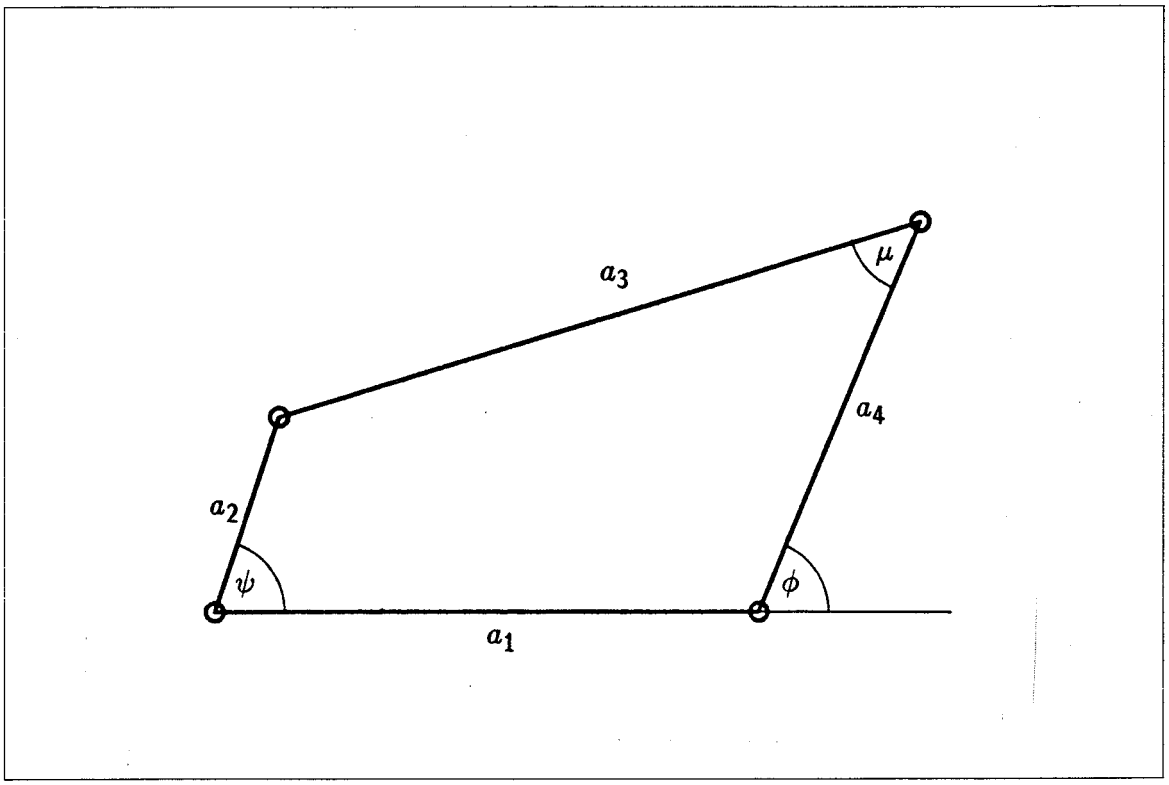

Figure 2.1 Planar four-bar linkage.

where

$$A(\psi) = k_1 - k_2 + (1 - k_3)\cos\psi \tag{2.4a}$$

$$B(\psi) = -\sin\psi \tag{2.4b}$$

$$C(\psi) = k_1 + k_2 - (1 + k_3)\cos\psi \tag{2.4c}$$

$$T = \tan(\phi/2) \tag{2.4d}$$

in which ψ and ϕ are the input and output angles respectively. The discriminant of the quadratic equation (2.3), known as the *linkage discriminant* (Angeles and Bernier 1987a), can be written as:

$$z(\psi) = B^2(\psi) - A(\psi)C(\psi) \tag{2.5a}$$

$$= \sin^2\psi - [k_1 - k_2 + (1 - k_3)\cos\psi][k_1 + k_2 - (1 + k_3)\cos\psi] \tag{2.5b}$$

which can be simplified to:

$$z(\psi) = (1 - k_1^2 + k_2^2) + 2(k_1 k_3 - k_2)\cos\psi - k_3^2\cos^2\psi \tag{2.5c}$$

The input link has full mobility if the discriminant is positive for every value of ψ, i.e., for $-1 \leq \cos\psi \leq 1$. Since eq.(2.5c) represents a parabola with negative curvature, this is the case if $z(0) \geq 0$ and $z(\pi) \geq 0$. If we denote by z_1 and z_2 the values of $z(\psi)$ for $\cos\psi = +1$ and $\cos\psi = -1$ respectively, we have:

$$\min_{-1 \leq \cos\psi \leq 1} z(\cos\psi) = \min(z_1, z_2) \tag{2.6}$$

and the full rotatability is attained if and only if $\min(z_1, z_2) \geq 0$ where:

$$z_1 \equiv z(\pi) = (1 + k_2)^2 - (k_1 + k_3)^2 \tag{2.7a}$$

$$z_2 \equiv z(0) = (1 - k_2)^2 - (k_1 - k_3)^2 \tag{2.7b}$$

It is then straightforward to show that these expressions lead to the following inequalities:

$$(k_1 + k_3)^2 \leq (1 + k_2)^2 \tag{2.8a}$$

and

$$(k_1 - k_3)^2 \leq (1 - k_2)^2 \tag{2.8b}$$

Each of these inequalities represents two regions of the (k_1, k_2, k_3) space which are bounded by two orthogonal planes. The line of intersection of these planes is parallel to plane $k_1 k_3$ and is located at $k_2 = -1$ for inequality (2.8a) and at $k_2 = +1$ for inequality (2.8b). Moreover, the projections of these two lines on plane $k_1 k_3$ give two lines orthogonal to each other and passing through the origin with an angle of +45 and -45 degrees, respectively, as shown in Fig. 2.2.

Hence, the intersection of the regions defined by inequalities (2.8a) and (2.8b) is given by a regular tetrahedron having its centroid at the origin and having edges of length $2\sqrt{2}$ and two open convexes (which are unbounded on one side) each sharing a common edge with the tetrahedron. This is represented in Fig. 2.3. The set of points of the (k_1, k_2, k_3) space located within these limits corresponds to the set of planar four-bar linkages having a fully rotatable input. It is pointed out that the origin of the (k_1, k_2, k_3) space, which is located inside this region, corresponds to the set of degenerate cases of

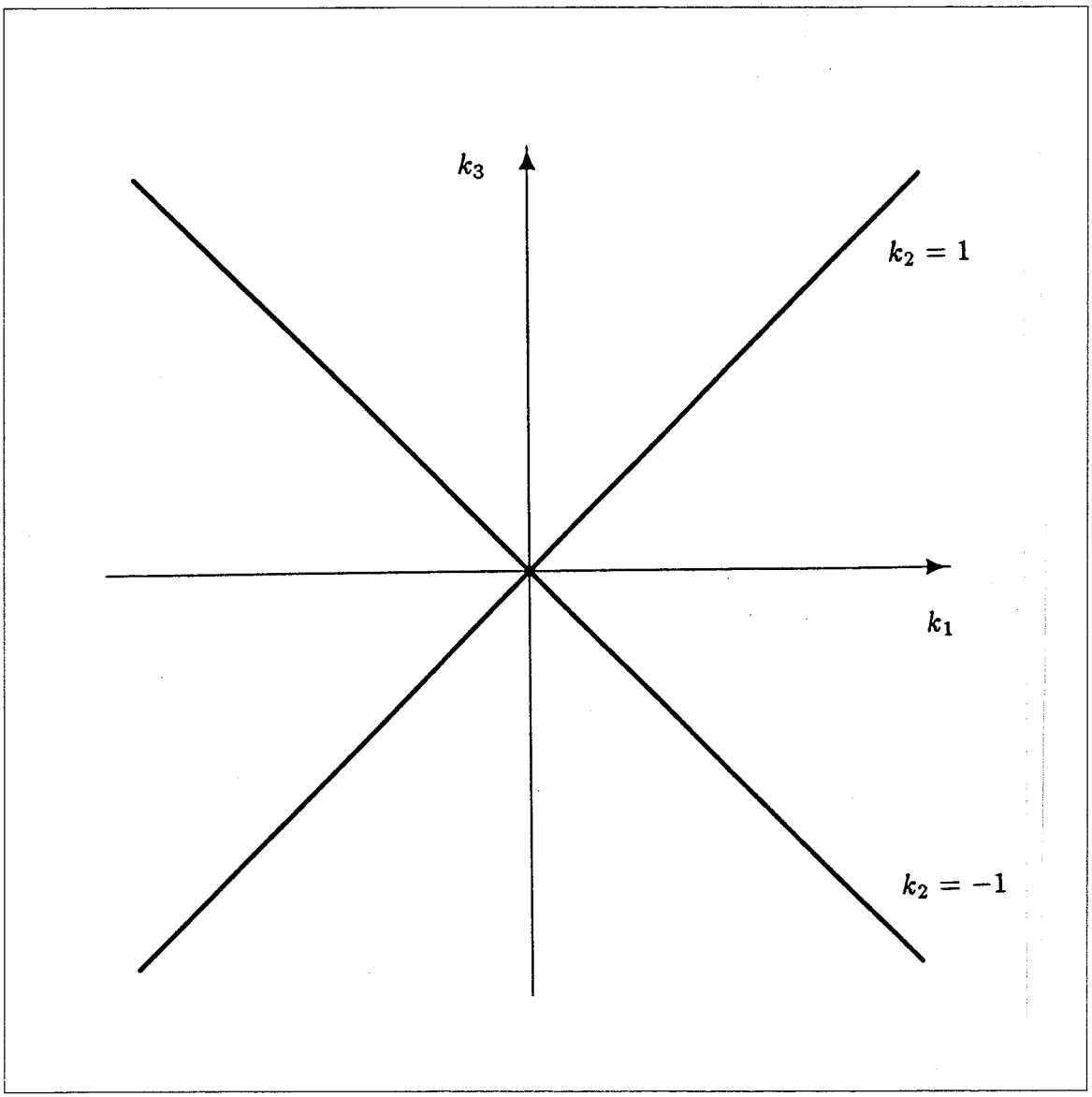

Figure 2.2 Projection, on the $k_1 k_3$ plane, of the lines constituting the intersection of the planes defined by eqs.(2.8a&b).

mechanisms for which $a_2 \to \infty$, $a_3 \to \infty$ and $a_4 \to \infty$, i.e., the planar PRRP mechanisms where the axes of the P pairs are parallel.

The mobility region is also represented in Fig. 2.4 where the tetrahedron is shown in yellow and the two open convexes in blue.

The foregoing analysis can now be applied to the output link by exchanging the

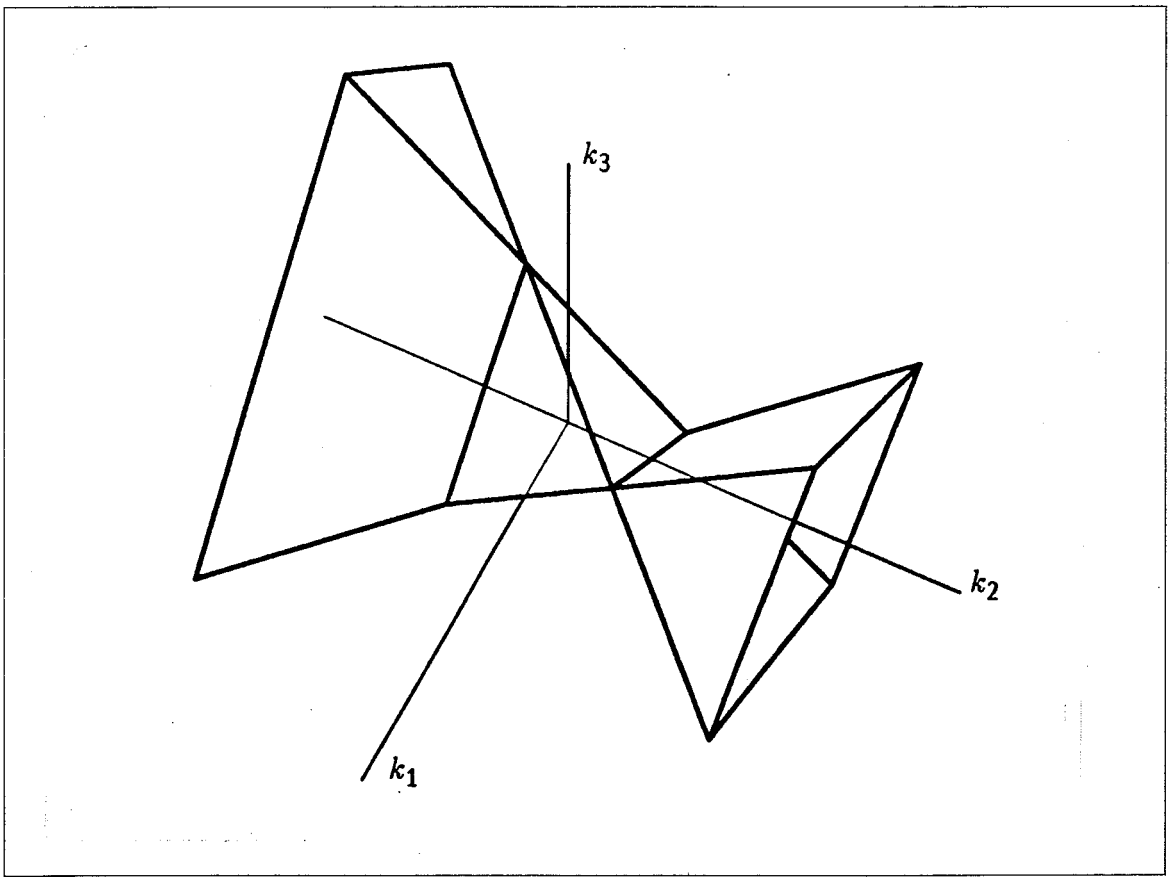

Figure 2.3 Mobility region for the input link of planar four-bar linkages.

role of the input and output links of the mechanism. To this end, eq.(2.3) is rewritten as:

$$A'(\phi)T^2 + 2B'(\phi)T + C'(\phi) = 0 \tag{2.9}$$

where

$$A'(\phi) = k_1 + k_3 + (k_2 + 1)\cos\phi \tag{2.10a}$$

$$B'(\phi) = -\sin\phi \tag{2.10b}$$

$$C'(\phi) = k_1 - k_3 + (k_2 - 1)\cos\phi \tag{2.10c}$$

$$T = \tan(\psi/2) \tag{2.10d}$$

The new discriminant obtained can then be expressed as:

$$\begin{aligned} \varsigma(\phi) &= [B'(\phi)]^2 - A'(\phi)C'(\phi) \\ &= (1 - k_1^2 + k_3^2) + 2(k_3 - 2k_1k_2)\cos\phi - k_2^2\cos^2\phi \end{aligned} \tag{2.11}$$

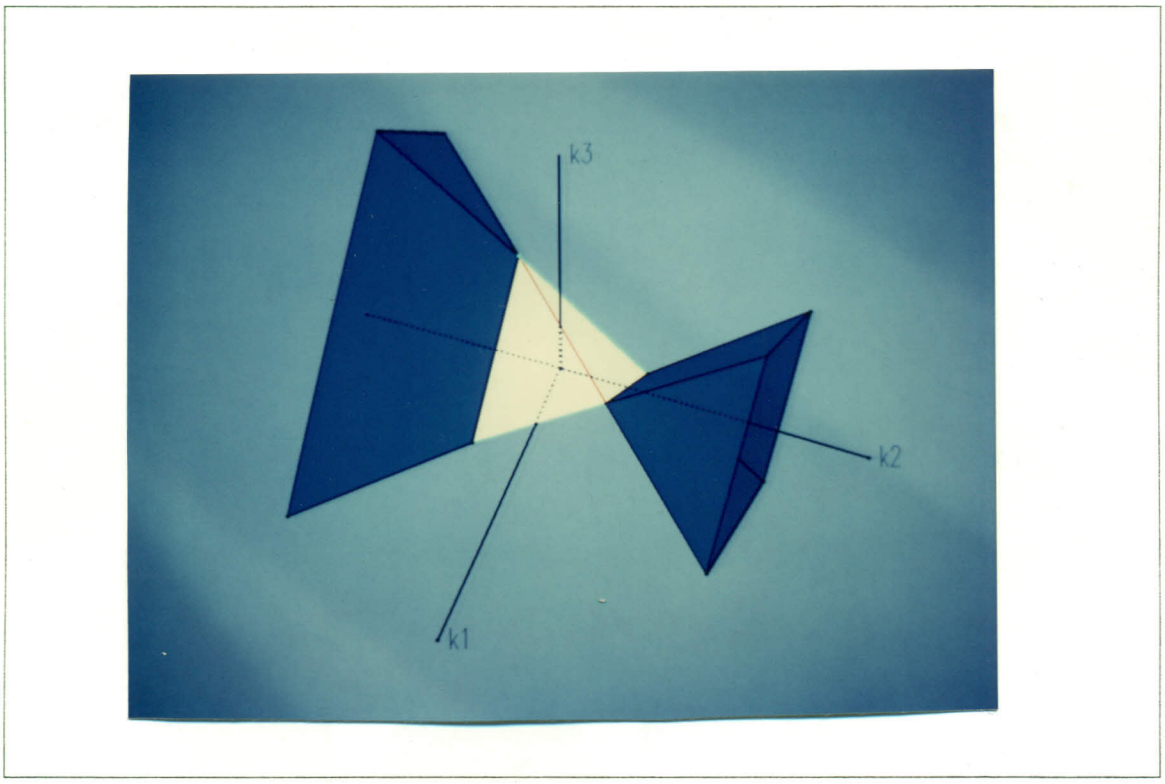

Figure 2.4 Mobility regions of planar four-bar linkages, crank-crank regions are shown in yellow and crank-rocker regions in blue.

The reasoning used above can be repeated here since we are again in the presence of a quadratic equation having a negative curvature. Therefore, the conditions for full mobility of the output link are $\varsigma(0) \geq 0$ and $\varsigma(\pi) \geq 0$. They lead to the following inequalities:

$$(k_1 + k_2)^2 \leq (1 + k_3)^2 \tag{2.12a}$$

and

$$(k_1 - k_2)^2 \leq (1 - k_3)^2 \tag{2.12b}$$

This result could have been expected since the exchange of the input and output links in eq.(2.1) is equivalent to exchanging the roles of k_2 and k_3.

The region described by inequalities (2.12a) and (2.12b) is shown in Fig. 2.5. Moreover, the central tetrahedron (in yellow) of this figure is regular and is related to that of Fig. 2.4 by a rotation about the origin that is a member of the *symmetry group* (Angeles 1982) of the tetrahedron of Fig. 2.4. Hence, the central tetrahedra of Figs. 2.4 and 2.5

are one and the same. Furthermore, the two open convexes (in red) are similar to the ones shown in blue in Fig. 2.4. Thus, the region defined by the tetrahedron is the one where both the input and output links have full mobility, i.e., where the linkages are of the *crank-crank* type. The open convexes then represent the regions where the linkages are of the *crank-rocker* type (in blue) and of the *rocker-crank* type (in red), respectively.

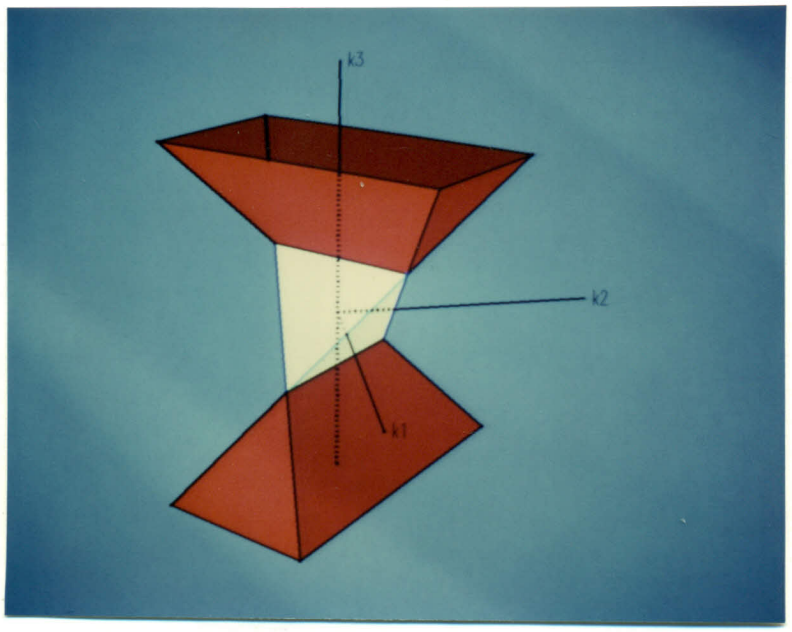

Figure 2.5 Mobility regions of planar four-bar linkages, crank-crank regions are shown in yellow and rocker-crank regions in red.

It can be observed that the open convexes are attached to the tetrahedron by its edges. To complete the symmetry of the whole spatial representation, we can define another set of open convexes (Fig. 2.6) attached to the tetrahedron by the two edges that are still free. Although this has not been shown, it is conjectured that this region (in green) contains unfeasible linkages. The rest of the space would then contain linkages of the *rocker-rocker* type. The proof of this hypothesis would require further work.

Notice that, in order to help the reader to grasp a global idea of the mobility

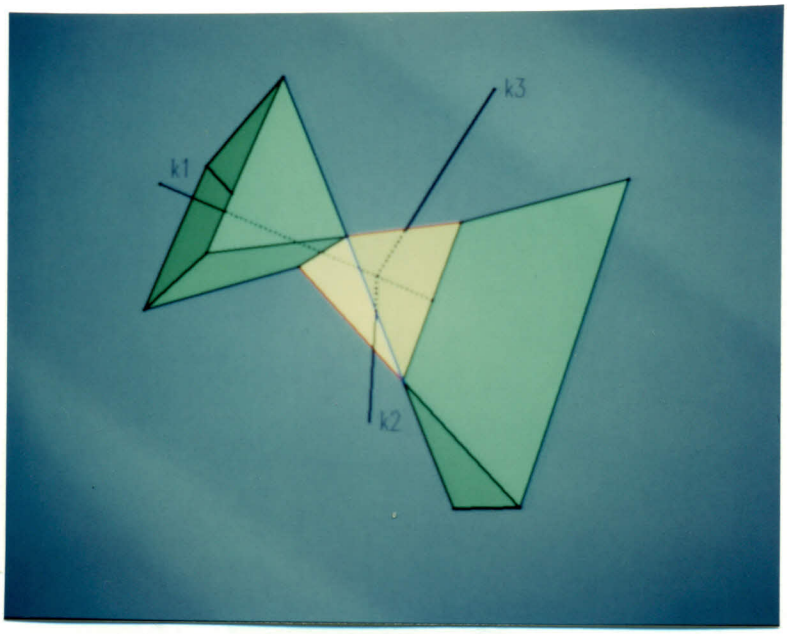

Figure 2.6 Mobility regions of planar four-bar linkages, crank-crank regions are shown in yellow and the regions containing unfeasible linkages in green.

regions in space, the edges of the tetrahedron in Figs. 2.4–2.6 have been drawn with the color of the open convex attached to it.

2.1.2 Spherical Linkages

Again, the linkage parameters $k_i, (i = 1, \ldots, 4)$ are identical to the ones used in (Angeles and Bernier, 1987a; Gosselin and Angeles, 1987a). The spherical mechanism is shown in Fig. 2.7, where the link angles are given by $\alpha_i, (i = 1, \ldots, 4)$. The linkage parameters are then defined as:

$$k_1 = \frac{\cos\alpha_1 \cos\alpha_2 \cos\alpha_4 - \cos\alpha_3}{\sin\alpha_1 \cos\alpha_2 \sin\alpha_4}, \qquad k_2 = \frac{\tan\alpha_2}{\tan\alpha_4}$$
$$k_3 = \frac{\tan\alpha_2}{\sin\alpha_1}, \qquad k_4 = \frac{\tan\alpha_2}{\tan\alpha_1} \tag{2.13}$$

A possible inversion of this transformation is given by:

$$\cos\alpha_1 = \frac{k_4}{k_3}, \qquad \sin\alpha_1 = \frac{\sqrt{k_3^2 - k_4^2}}{|k_3|}$$

$$\cos\alpha_2 = \frac{\mathrm{sgn}(k_3)}{\sqrt{1 + k_3^2 - k_4^2}}, \qquad \sin\alpha_2 = \sqrt{\frac{k_3^2 - k_4^2}{1 + k_3^2 - k_4^2}}$$

$$\cos\alpha_3 = \frac{k_2 k_4 - k_1(k_3^2 - k_4^2)}{|k_3|\sqrt{(1 + k_3^2 - k_4^2)(k_2^2 + k_3^2 - k_4^2)}} \tag{2.14a}$$

$$\sin\alpha_3 = \frac{1}{k_3}\sqrt{\frac{(k_3^2 - k_4^2)[k_2^2 + k_3^2(1 + k_2^2) + 2k_1 k_2 k_4 + (k_3^2 - k_1^2)(k_3^2 - k_4^2)]}{(1 + k_3^2 - k_4^2)(k_2^2 + k_3^2 - k_4^2)}}$$

$$\cos\alpha_4 = \frac{k_2}{\sqrt{k_2^2 + k_3^2 - k_4^2}}, \qquad \sin\alpha_4 = \sqrt{\frac{k_3^2 - k_4^2}{k_2^2 + k_3^2 - k_4^2}}\mathrm{sgn}(k_3)$$

In this inversion, it is assumed that:

$$k_4^2 \leq k_3^2 \tag{2.14b}$$

The input-output equation of the spherical mechanism can then also be written as the following quadratic equation:

$$A(\psi)T^2 + 2B(\psi)T + C(\psi) = 0 \tag{2.15}$$

where

$$A(\psi) = k_1 + 1 + (k_2 - k_4)\cos\psi \tag{2.16a}$$

$$B(\psi) = k_3 \sin\psi \tag{2.16b}$$

$$C(\psi) = k_1 - 1 + (k_2 + k_4)\cos\psi \tag{2.16c}$$

$$T = \tan(\phi/2) \tag{2.16d}$$

in which ψ and ϕ are the input and output angles, respectively. The discriminant of the quadratic equation (2.15) is then the ***linkage discriminant*** for the spherical mechanism. It is given by:

$$\begin{aligned} z(\psi) &= B^2(\psi) - A(\psi)C(\psi) \\ &= (k_4^2 - k_2^2 - k_3^2)\cos^2\psi + 2(-k_4 - k_1 k_2)\cos\psi + (1 - k_1^2 + k_3^2) \end{aligned} \tag{2.17}$$

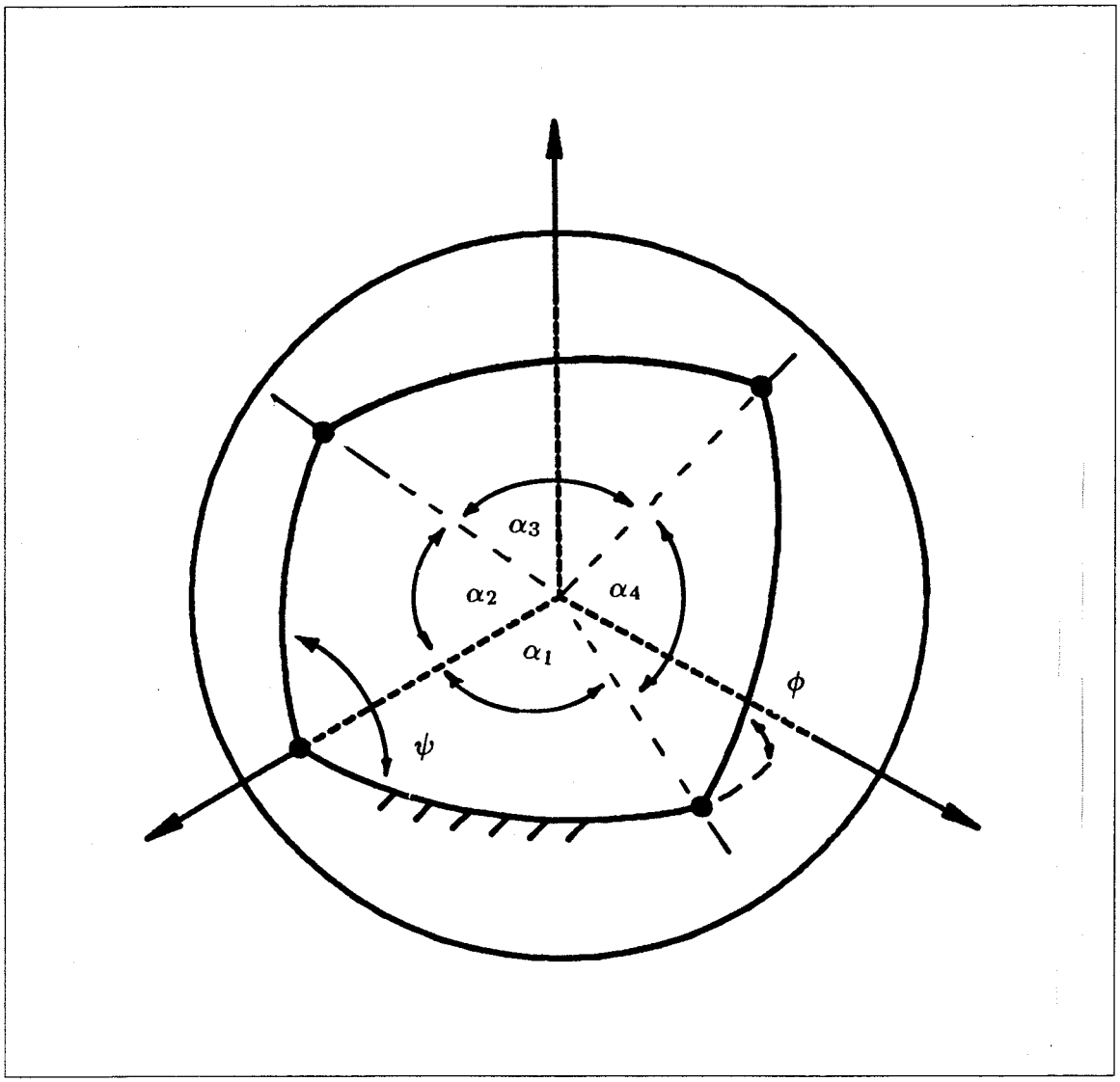

Figure 2.7 Spherical four-bar linkage.

where the coefficient of $\cos^2\psi$ can also be written as:

$$k_4^2 - k_2^2 - k_3^2 = -\frac{\tan^2\alpha_2}{\sin^2\alpha_4} \tag{2.18}$$

which clearly shows that it is negative definite, and hence the discriminant of equation (2.15) is a parabola in $\cos\psi$ with negative curvature, such as the discriminant appearing in eq.(2.5).

The arguments used in Section 2.1.1 for planar linkages can be repeated here. The full mobility of the input link is guaranteed by the positive definiteness of the discrimi-

nant over the whole range of values that ψ can attain, i.e., $0 \leq \psi \leq 2\pi$ or $-1 \leq \cos\psi \leq +1$. If we denote by z_1 and z_2 the values of $z(\psi)$ for $\cos\psi = -1$ and $\cos\psi = +1$—i.e. $z(0)$ and $z(\pi)$—respectively, the mobility conditions become:

$$\min_{-1 \leq \cos\psi \leq 1} z(\cos\psi) = \min(z_1, z_2) \geq 0 \tag{2.19}$$

where

$$z_1 \equiv z(-1) = (k_4 + 1)^2 - (k_2 - k_1)^2 \tag{2.20a}$$

$$z_2 \equiv z(+1) = (k_4 - 1)^2 - (k_2 + k_1)^2 \tag{2.20b}$$

which lead to:

$$(k_2 + k_1)^2 \leq (k_4 - 1)^2 \tag{2.21a}$$

and

$$(k_2 - k_1)^2 \leq (k_4 + 1)^2 \tag{2.21b}$$

Inequalities (2.21a&b) are very similar to inequalities (2.8a&b) and the associated region, which is shown in Fig. 2.8, is geometrically identical to the one obtained for planar linkages.

It is pointed out that, in this case, only three of the four parameters that we had defined (k_i, $i = 1, \ldots, 4$) play a role in the mobility, which allows us to obtain a tridimensional representation in the (k_1, k_2, k_4) space. The set of points located inside the limits of the tetrahedron and the open convexes correspond to the set of spherical four-bar linkages having a fully rotatable input link. The origin of the space used here represents the set of spherical mechanisms for which $\alpha_1 = \alpha_3 = \alpha_4 = 90°$, i.e., the spherical equivalent to planar PRRP linkages (Lichtencheldt and Luck 1979). The mobility region is also shown in Fig. 2.9.

The analysis is repeated by exchanging the role of the input and output links. Equation (2.15) is rewritten as:

$$A'(\phi)T^2 + 2B'(\phi)T + C'(\phi) = 0 \tag{2.22}$$

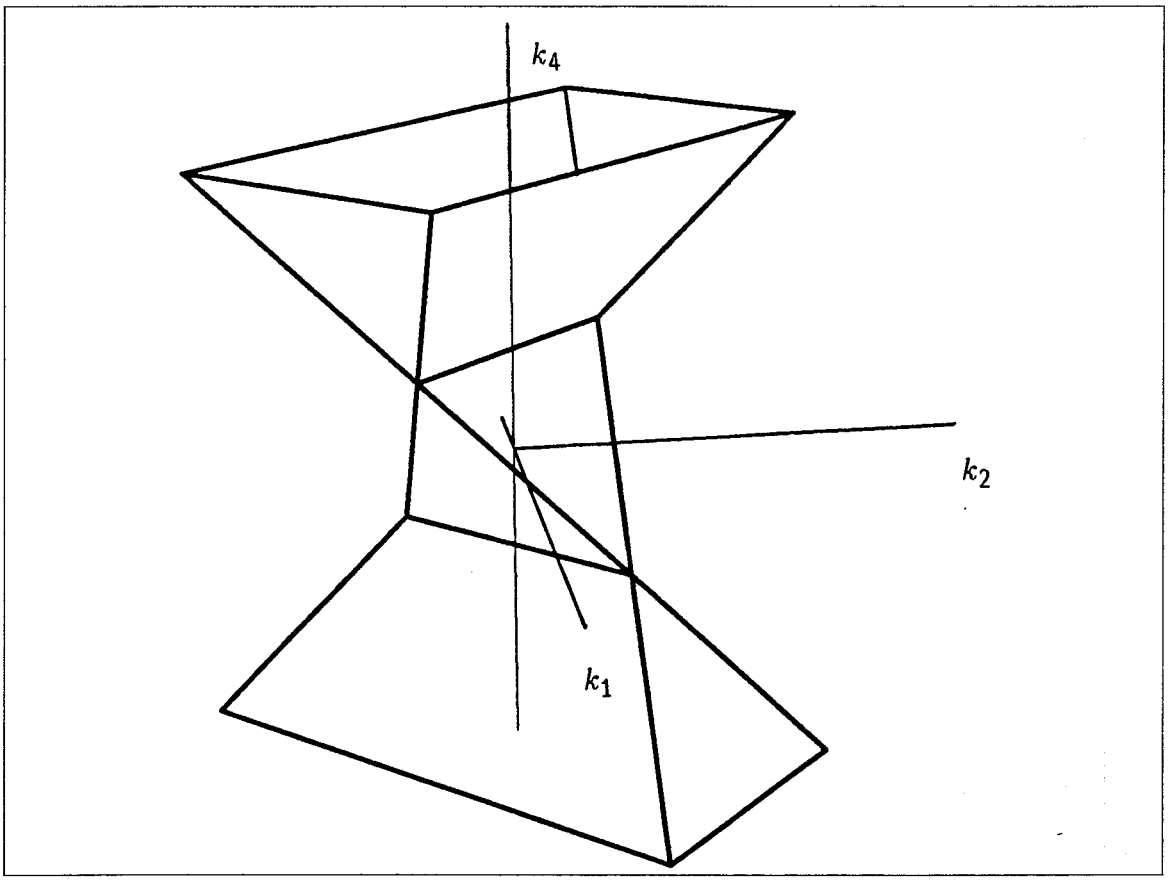

Figure 2.8 Mobility region for the input link of spherical four-bar linkages.

where

$$A'(\phi) = k_1 - k_2 - (1 + k_4)\cos\phi \tag{2.23a}$$

$$B'(\phi) = k_3 \sin\phi \tag{2.23b}$$

$$C'(\phi) = k_1 + k_2 - (1 - k_4)\cos\phi \tag{2.23c}$$

$$T = \tan(\psi/2) \tag{2.23d}$$

The new discriminant obtained can then be expressed as:

$$\begin{aligned}\varsigma(\phi) &= [B'(\phi)]^2 - A'(\phi)C'(\phi) \\ &= (k_4^2 - k_3^2 - 1)\cos^2\phi + 2(k_1 + k_2k_4)\cos\phi + (k_3^2 - k_1^2 + k_2^2)\end{aligned} \tag{2.24}$$

where the coefficient of $\cos^2\phi$ can be rewritten as:

$$(k_4^2 - k_3^2 - 1) = -\sec^2\alpha_1 \tag{2.25}$$

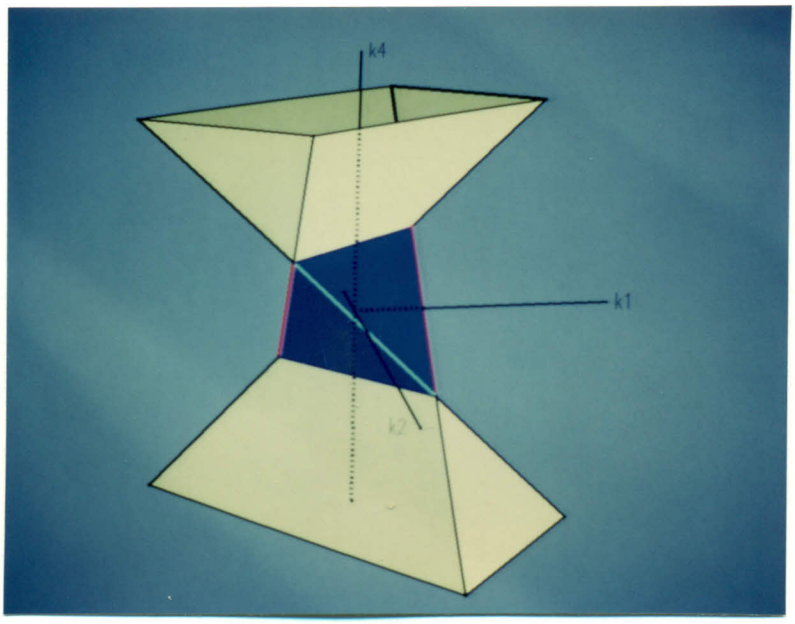

Figure 2.9 Mobility regions of spherical four-bar linkages, crank-crank regions are shown in yellow and crank-rocker regions in blue.

which clearly shows that it is negative definite, thus leading to the same conclusion as in dealing with the discriminant of eq.(2.17).

The conditions for full mobility of the output link are $\varsigma(0) \geq 0$ and $\varsigma(\pi) \geq 0$. They lead to the following inequalities:

$$(k_2 + k_4)^2 \geq (1 - k_1)^2 \tag{2.26a}$$

and

$$(k_2 - k_4)^2 \geq (1 + k_1)^2 \tag{2.26b}$$

The region described by inequalities (2.26a&b) constitutes a set of four open convexes which are shown in Fig. 2.9 (in yellow) and Fig. 2.10 (in red).

It is now apparent that the open convexes shown in Fig. 2.9 (in yellow) are the common intersection of the regions described by inequalities (2.21a&b) and (2.26a&b).

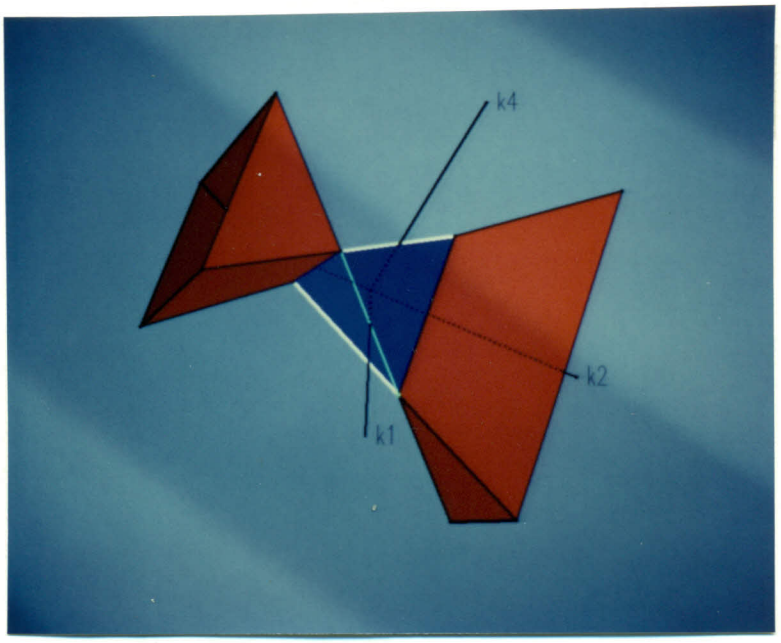

Figure 2.10 Mobility regions of spherical four-bar linkages, crank-rocker regions are shown in blue and rocker-crank regions in red.

Thus, this region is the one where both the input and output links have full mobility, i.e., where the linkages are of the *crank-crank* type. The tetrahedron then represents the region where the linkages are of the *crank-rocker* type (in blue) and the open convexes shown in Fig. 2.10 (in red) represent the region containing mechanisms of the *rocker-crank* type.

Again, to complete the symmetry of the whole spatial representation, we can define another set of open convexes (Fig. 2.11) attached to the tetrahedron by the two edges that are still free. In this case also, although it is not shown here, it is conjectured that this region (in green) contains unfeasible linkages. The rest of the space would then contain linkages of the *rocker-rocker* type. The proof of this hypothesis would also require a deeper investigation that may require tools other than the discriminant technique.

2.1.3 Example

An example problem making use of the mobility regions derived above is now

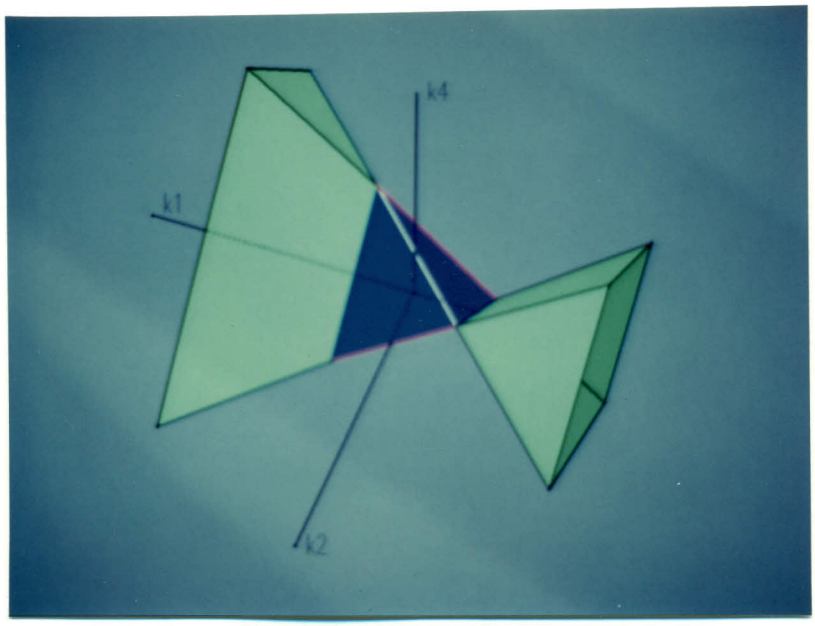

Figure 2.11 Mobility regions of spherical four-bar linkages, crank-rocker regions are shown in blue and the regions containing unfeasible linkages in green.

discussed. This example, which was presented in (Gupta 1986b), deals with a spherical robot wrist. The problem consists of determining the set of orientations of the end-effector that will allow it to undergo a full rotation about a given axis which is concurrent with the other three axes of the wrist. The angle defining the orientation of the end-effector, which becomes the unknown of the problem, is then associated with the value of α_1, i.e., the fixed link. It is assumed here that $0^\circ \leq \alpha_1 \leq 180^\circ$. The other angles of the wrist are given as $\alpha_2 = 30^\circ$,$\alpha_3 = 80^\circ$, and $\alpha_4 = 75^\circ$. Therefore, we have

$$k_1 = \frac{c_1 \cos\alpha_1 - c_2}{\sin\alpha_1} \qquad k_2 = c_3$$
$$k_3 = \frac{c_4}{\sin\alpha_1} \qquad k_4 = \frac{c_4}{\tan\alpha_1} \tag{2.27a}$$

where

$$c_1 = 0.26794 \qquad c_2 = 0.20759$$
$$c_3 = 0.15470 \qquad c_4 = 0.57735 \tag{2.27b}$$

which represents a curve in the (k_1, k_2, k_4) space. The values of angle α_1 corresponding to the portions of this curve that are inside the mobility region of the input link (Fig. 2.8)

are the values of α_1 for which the end-effector can undergo a full rotation. Notice that the end-effector is considered here as the input link of the spherical mechanism having a dimension of α_2. Inequalities (2.21a&b) lead to:

$$\left(\frac{(c_4^2-c_1^2)}{\tan^2\alpha_1}-\frac{c_2^2}{\sin^2\alpha_1}+\frac{2c_1c_2}{\sin\alpha_1\tan\alpha_1}+\frac{2(c_4+c_1c_3)}{\tan\alpha_1}-\frac{2c_2c_3}{\sin\alpha_1}+1-c_3^2\right)\geq 0 \quad (2.28a)$$

and

$$\left(\frac{(c_4^2-c_1^2)}{\tan^2\alpha_1}-\frac{c_2^2}{\sin^2\alpha_1}+\frac{2c_1c_2}{\sin\alpha_1\tan\alpha_1}-\frac{2(c_4+c_1c_3)}{\tan\alpha_1}+\frac{2c_2c_3}{\sin\alpha_1}+1-c_3^2\right)\geq 0 \quad (2.28b)$$

The following substitution is then introduced:

$$\cos\alpha_1=\frac{1-T^2}{1+T^2} \qquad \sin\alpha_1=\frac{2T}{1+T^2} \quad (2.29a)$$

where

$$T=\tan(\alpha_1/2) \quad (2.29b)$$

and inequalities (2.28a&b) can therefore be rearranged, which leads to:

$$AT^4-BT^3+CT^2+DT+E\geq 0 \quad (2.30a)$$

$$AT^4+BT^3+CT^2-DT+E\geq 0 \quad (2.30b)$$

where:

$$A=c_4^2-(c_1+c_2)^2 \quad (2.31a)$$

$$B=4(c_4+c_1c_3+c_2c_3) \quad (2.31b)$$

$$C=2(c_1^2-c_2^2-2c_3^2-c_4^2+2) \quad (2.31c)$$

$$D=4(c_4+c_1c_3-c_2c_3) \quad (2.31d)$$

$$E=c_4^2-(c_1-c_2)^2 \quad (2.31e)$$

Since we have $0^\circ\leq\alpha_1\leq 180^\circ$, then the range of interest of the variable T in inequalities (2.30a&b) is restricted to $T\geq 0$. The corresponding functions are plotted in Figs. 2.12–2.14, which clearly shows the different regions in which the inequalities are verified.

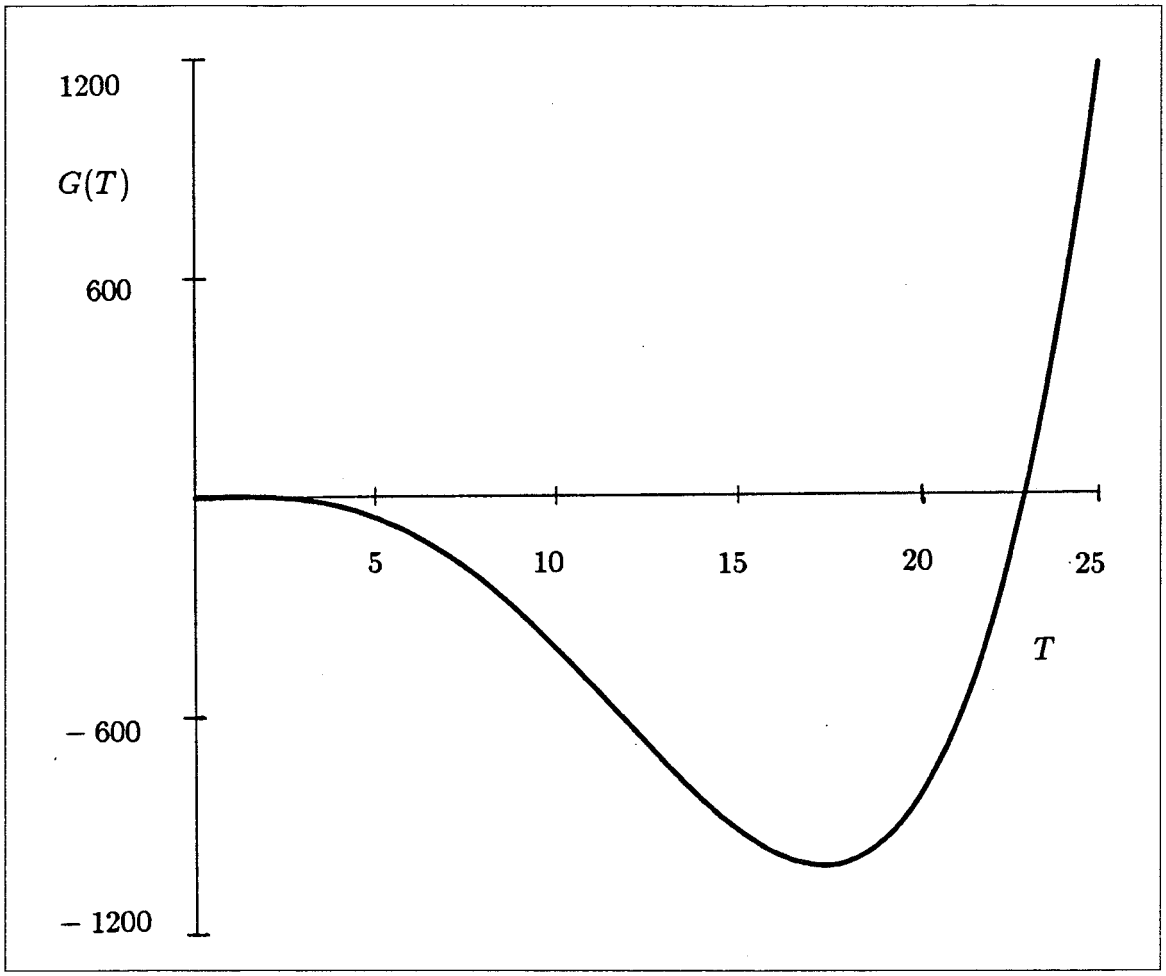

Figure 2.12 Function defined by the left-hand side of eq.(2.30a).

Notice that Fig. 2.13 is a zoom of Fig. 2.12 in the neighbourhood of the origin. The ranges of values of T for which the inequalities are not verified are:

$$0.222 \leq T \leq 0.315 \quad \text{and} \quad 1.92 \leq T \leq 22.9 \tag{2.32}$$

i.e.

$$25^\circ \leq \alpha_1 \leq 35^\circ \quad \text{and} \quad 125^\circ \leq \alpha_1 \leq 175^\circ \tag{2.33}$$

which is in full agreement with the results reported in (Gupta 1986b).

Finally, since the value of k_2 is constant, the curve described by equations (2.27a) can be represented in the plane given by $k_2 = 0.15470$, i.e., using a cross-sectional view of the solid of Fig. 2.8. This view is shown in Figs. 2.15 and 2.16. Portions AB and CD of the curve are clearly outside of the mobility region.

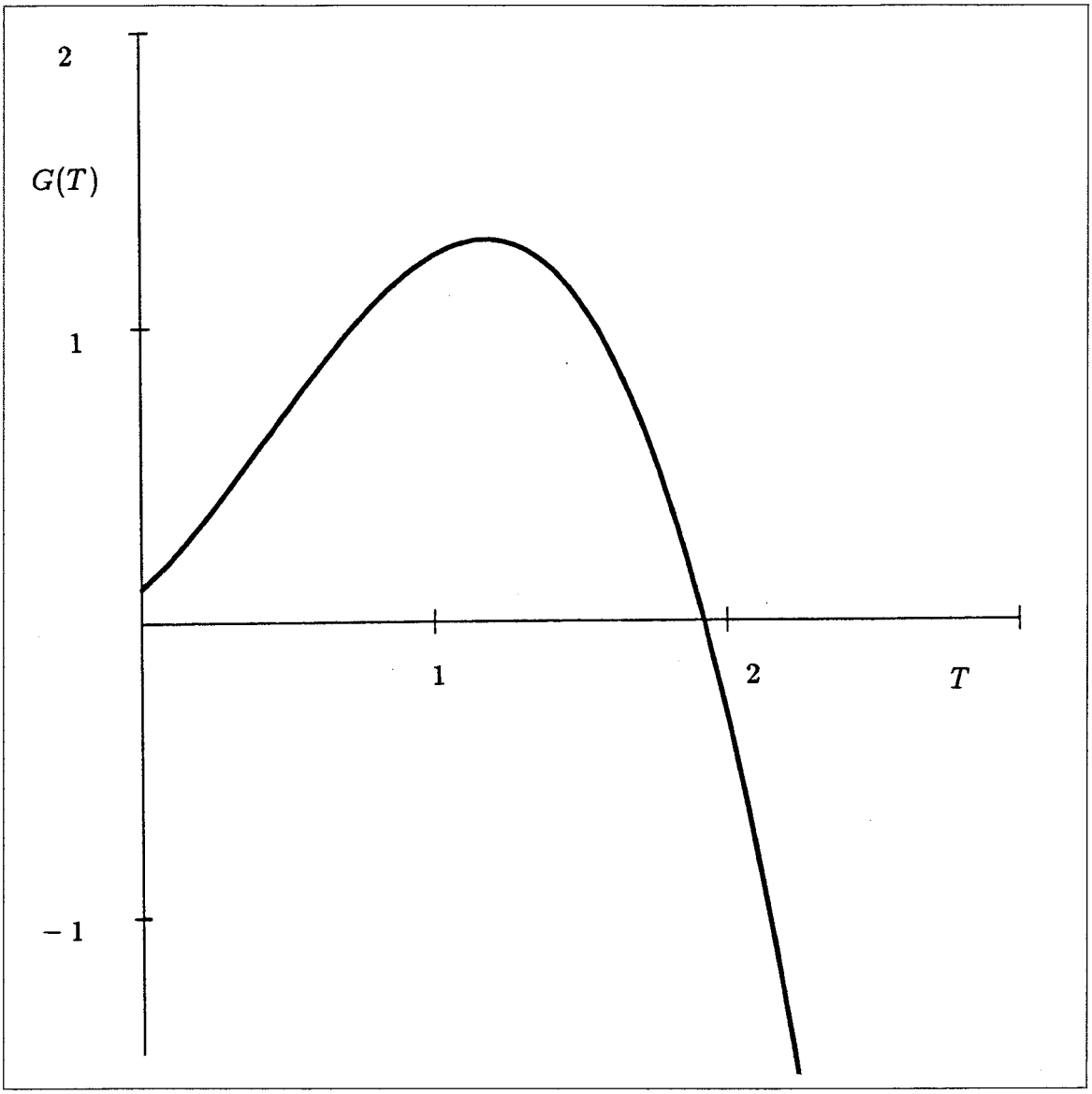

Figure 2.13 Zoom of Fig. 2.12 in the neighbourhood of the origin.

2.2 Optimization of Transmission-Quality

The linkage optimization problem aimed at maximizing the quality of transmission has been given due attention by many a researcher. Some of the authors that reported on the subject have used design charts (Hain 1967; Hall 1966; Soni 1974) while others used algebraic methods (Freudenstein and Primerose 1973; Gupta 1977) or numerical methods (Cleghorn and Fenton 1984) to tackle this problem. A crucial development in this context is

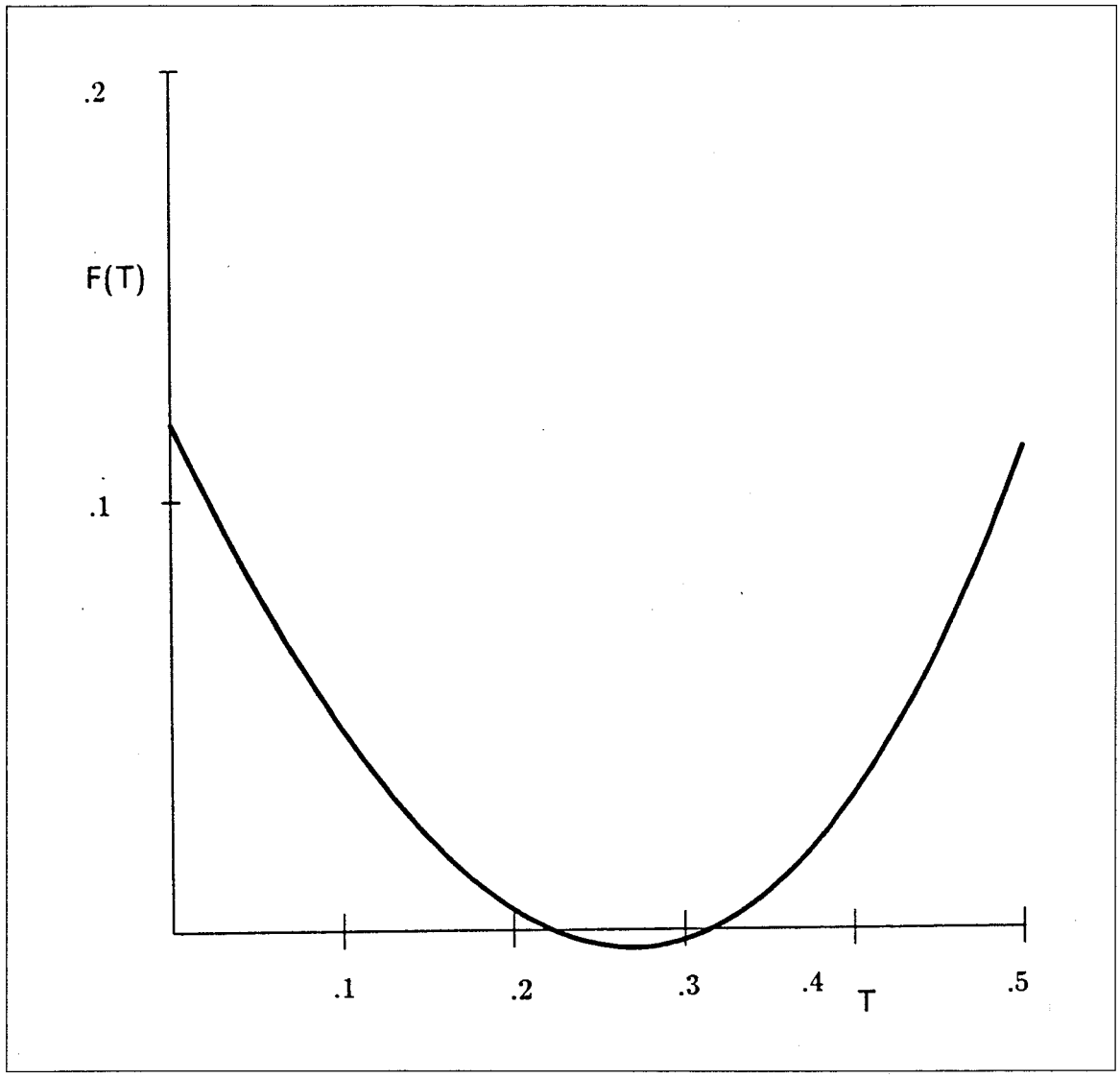

Figure 2.14 Function defined by the left-hand side of eq.(2.30*b*).

the concept of *transmission index*, introduced first by Sutherland and Roth (1973), which allows us to extend the concept of *transmission angle* to any spatial linkage. Moreover, it is shown in the foregoing reference that the maximization of the transmission quality is equivalent to a minimization of the positioning error, a result which is not to be neglected, especially when considering the extension of the concepts studied here to multiple degree-of-freedom systems. On the other hand, Gupta (1980) introduced a method of planar-linkage synthesis with an input crank, whose transmission angle is constrained to lie between 45° and 135°. This method was then extended to the *exact* synthesis of *RSSR*

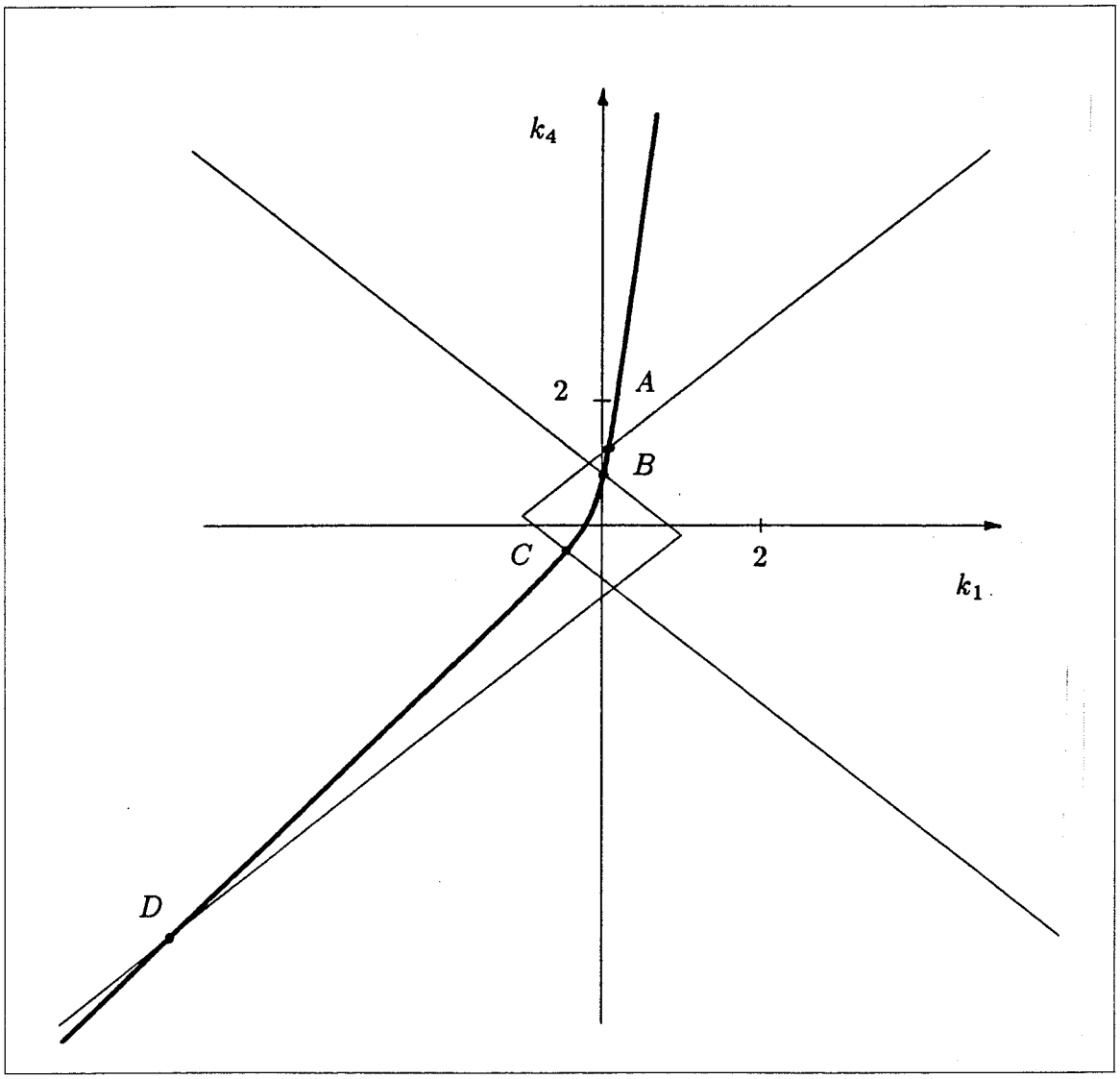

Figure 2.15 Curve defined by eq.(2.27a) in the plane $k_2 = c_3$, and the mobility regions in that plane.

linkages (Gupta and Kazerounian 1983). Furthermore, Tinubu and Gupta (1984) showed that a linkage optimization based on minimizing the structural error, rather than the *design error*, leads to branching-defect elimination. Moreover, the optimization of planar, spherical, and spatial linkages *having a quadratic input-output equation*, with a minimum design error and a maximum transmission quality, was presented in (Angeles 1986a). In this reference, the method used by the author is based on the Newton-Gauss algorithm for nonlinear least squares—see, for instance, (Wilde 1982 & 1983). On the other hand, the concept of *linkage discriminant*, which was used for the determination of the linkage

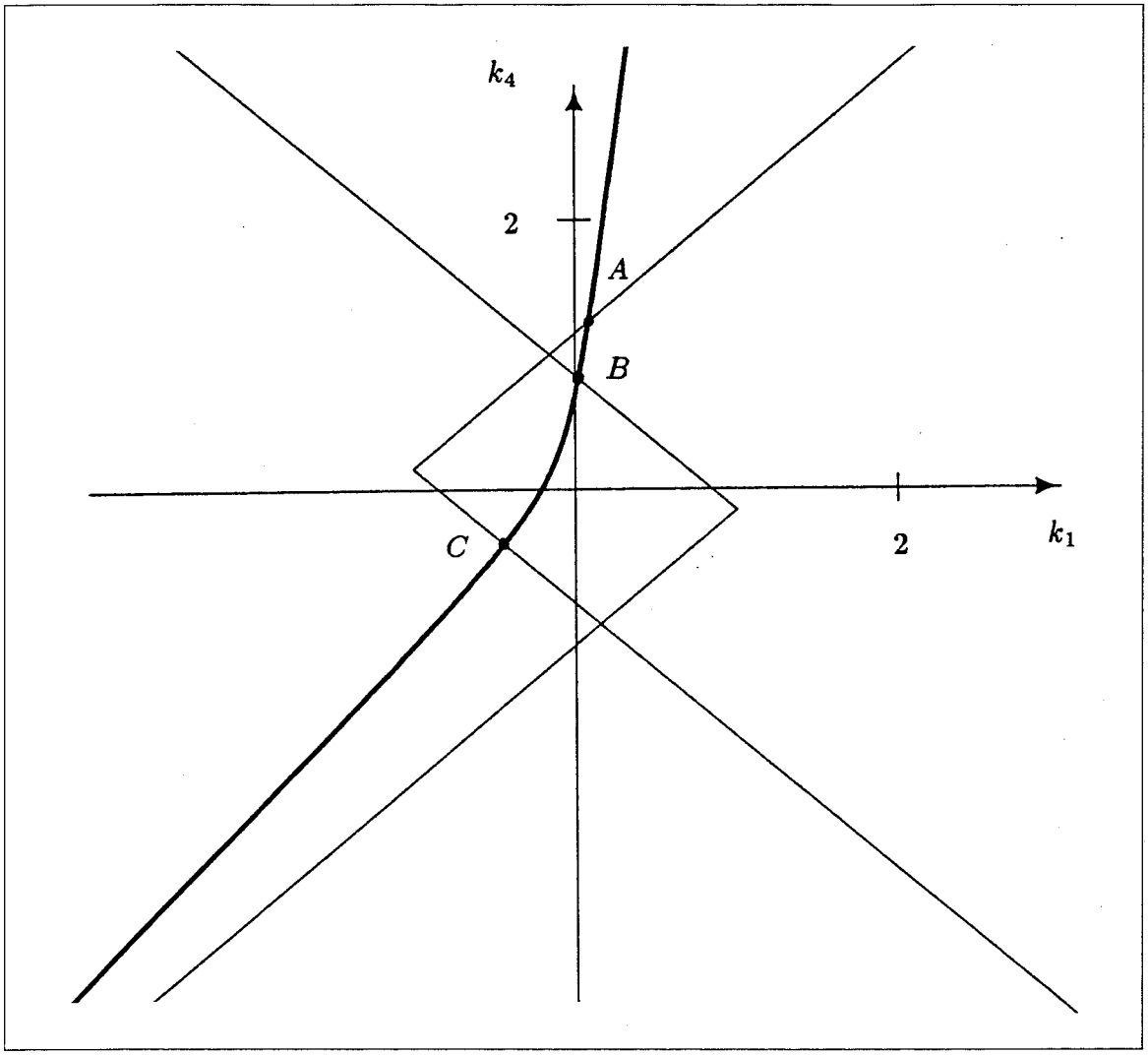

Figure 2.16 Zoom of Fig. 2.15 in the neighbourhood of the origin.

mobility region in Section 2.1, was applied to the optimization of linkages with maximum transmission quality and prescribed mobility characteristics (Angeles and Bernier 1987b).

In this section, results concerning the transmission quality of planar and spherical linkages are derived. A particular class of linkages, called here *zero-mean linkages*, is defined and analyzed in detail. Their mobility regions are introduced as a particular case of the ones presented in Section 2.1 for general planar and spherical 4-bar linkages. Some important theorems governing their mobility characteristics are also stated and guidelines for their design are given.

A more general class of linkages, called minimum-defect linkages, is also defined and this concept is applied to the design of quick-return mechanisms using the orthogonal-decomposition method, presented in (Angeles et al. 1987).

2.2.1 Definition of the Transmission Quality

The transmission quality of a four-bar linkage, which is to be maximized, was defined in (Angeles and Bernier 1987b) as the square root of the following positive definite quantity:

$$z = \frac{1}{2\pi}\int_0^{2\pi} \sin^2\mu d\psi \tag{2.34a}$$

where μ represents the *transmission angle* of the function-generating linkage under study. For brevity, the transmission quality is defined in what follows as z itself, rather than its square root. The *complement* of the transmission quality, which is to be minimized, is thus defined as:

$$z' = \frac{1}{2\pi}\int_0^{2\pi} \cos^2\mu d\psi \tag{2.34b}$$

and is termed the *transmission defect*. Hence,

$$z + z' = 1 \tag{2.34c}$$

and

$$0 < z' < 1 \tag{2.34d}$$

Of course, in these definitions, the input link is assumed to be of the crank type, for the associated integrals are not defined for input links of the rocker type. In the particular cases of planar and spherical linkages, the cosine of the transmission angle can be written as follows:

$$\cos\mu = c_1 + c_2\cos\psi \tag{2.35}$$

where c_1 and c_2 are constants depending only upon the linkage parameters, expressions for which will be given presently. Thus, for planar and spherical linkages, z' becomes

$$z' = c_1^2 + \frac{1}{2}c_2^2 \tag{2.36}$$

where c_1^2 and c_2^2 are *positive semidefinite* and *positive definite* quantities, respectively, as shown next, i.e.,

$$c_1^2 \geq 0, \quad c_2^2 > 0 \tag{2.37}$$

From the foregoing discussion, it is apparent that the transmission quality is maximized if the transmission defect is minimized. The practical application of this fact is that linkages with maximum transmission quality can be found using least-square based optimization algorithms, which aim intrinsically at minimizing a positive semidefinite performance index, rather than at its maximization.

For a general planar linkage as the one shown in Fig. 2.1, the cosine of the transmission angle is given as (Gupta 1977):

$$\cos\mu = \frac{a_3^2 + a_4^2 - a_1^2 - a_2^2 + 2a_1a_2\cos\psi}{2a_3a_4} \tag{2.38a}$$

or, in terms of the parameters $(k_i,\ i = 1,2,3)$ defined in the previous section, as

$$\cos\mu = \frac{\mathrm{sgn}(k_2k_3)(k_2 - k_1k_3 + k_3^2\cos\psi)}{\sqrt{k_2^2 + k_3^2 + k_2^2k_3^2 - 2k_1k_2k_3}} \tag{2.38b}$$

Constants c_1 and c_2 appearing in eqs.(2.35) and (2.36) are, then,

$$c_1 = \frac{\pm(k_2 - k_1k_3)}{\sqrt{k_2^2 + k_3^2 + k_2^2k_3^2 - 2k_1k_2k_3}}, \qquad c_2 = \frac{\pm k_3^2}{\sqrt{k_2^2 + k_3^2 + k_2^2k_3^2 - 2k_1k_2k_3}} \tag{2.39}$$

from which it is apparent that c_1^2 is positive semidefinite, whereas c_2^2 is positive definite.

For a general spherical linkage as the one shown in Fig. 2.7, where α_i, for $i = 1,\ldots,4$, denote the linkage dimensions, the cosine of the transmission angle, given in (Gupta 1987), is multiplied by factor $\sqrt{(1-\cos\alpha_3)/2}$, in order to render it compatible with the general definition of transmission index given in (Söylemez and Freudenstein 1982). This produces the following:

$$\cos\mu = \sqrt{\frac{1-\cos\alpha_3}{2}}\,\frac{\cos\alpha_1\cos\alpha_2 - \cos\alpha_3\cos\alpha_4 + \sin\alpha_1\sin\alpha_2\cos\psi}{\sin\alpha_3\sin\alpha_4} \tag{2.40}$$

Constants c_1 and c_2 of eqs.(2.35) and (2.36) are now defined by:

$$c_1 = \sqrt{\frac{1-\cos\alpha_3}{2}}\,\frac{\cos\alpha_1\cos\alpha_2 - \cos\alpha_3\cos\alpha_4}{\sin\alpha_3\sin\alpha_4} \tag{2.41a}$$

$$c_2 = \sqrt{\frac{1-\cos\alpha_3}{2}}\,\frac{\sin\alpha_1\sin\alpha_2}{\sin\alpha_3\sin\alpha_4} \tag{2.41b}$$

or, in terms of the parameters $(k_i,\ i = 1,\ldots,4)$:

$$c_1 = F\gamma_1 \quad , \quad c_2 = F\gamma_2 \tag{2.41c}$$

where

$$F = \sqrt{\frac{|k_3|\sqrt{(1+k_3^2-k_4^2)(k_2^2+k_3^2-k_4^2)} - k_2k_4 + k_1(k_3^2-k_4^2)}{2|k_3|\sqrt{(1+k_3^2-k_4^2)(k_2^2+k_3^2-k_4^2)}}} \tag{2.41d}$$

and

$$\gamma_1 = \frac{k_1k_2 + k_4}{\sqrt{k_2^2 + k_3^2(1+k_2^2) + 2k_1k_2k_4 + (k_3^2-k_1^2)(k_3^2-k_4^2)}} \tag{2.41e}$$

$$\gamma_2 = \frac{k_2^2 + k_3^2 - k_4^2}{\sqrt{k_2^2 + k_3^2(1+k_2^2) + 2k_1k_2k_4 + (k_3^2-k_1^2)(k_3^2-k_4^2)}} \tag{2.41f}$$

If none of the angles α_i, for $i = 1,\ldots,4$, is allowed to vanish, an issue that is given due attention in Section 2.2.3, it is clear that c_1^2 is positive semidefinite, and c_2^2 is positive definite—the positive definiteness of c_2^2 can also be readily realized from condition (2.14b). From expression (2.41d), neither c_1 nor c_2, and not even their squares, are smooth functions of the linkage-parameters $(k_i,\ i = 1,\ldots,4)$. This would prevent us from minimizing z^l using nonlinear least-square techniques, which rely on such smoothness. This is readily overcome by formulating the problem in the space of linkage dimensions, $\alpha_1, \alpha_2, \alpha_3, \alpha_4$, in which, from eqs. (2.41a&b), c_1 and c_2 are smooth functions.

2.2.2 Zero-Mean Linkages and their Properties

Minimum-defect linkages are defined as linkages having an input crank, for which the transmission defect, as given by equation (2.36), is a minimum. It has been shown

in Section 2.2.1 that the second term of the right-hand side of eq.(2.36) cannot vanish, whereas the first one can. This leads to the definition of a specific class of linkages, called *zero-mean linkages*, for which the value of c_1 is equal to zero. From eq.(2.35) it is apparent that c_1 and $\frac{1}{2}c_2^2$ are, in fact, the expected value and the variance of the cosine of the transmission angle, i.e.,

$$c_1 = E(\cos\mu) \tag{2.42a}$$

$$\frac{1}{2}c_2^2 = E[(\cos\mu - c_1)^2] \equiv \mathrm{Var}(\cos\mu) \tag{2.42b}$$

and hence the zero-mean adjective for linkages having a vanishing c_1.

2.2.2.1 Planar Zero-Mean Linkages

For planar linkages, the zero-mean condition leads to:

$$k_2 = k_1 k_3 \tag{2.43}$$

Thus, the transmission defect can be expressed as:

$$z' = \frac{1}{2}c_2^2 = \frac{k_3^2}{2(1 - k_1^2 + k_1^2 k_3^2)} \tag{2.44}$$

and the mobility conditions for an input crank derived in Section 2.1, i.e., inequalities $(2.8a\&b)$, reduce to the following:

$$(k_1 + k_3)^2 \leq (1 + k_1 k_3)^2 \tag{2.45a}$$

$$(k_1 - k_3)^2 \leq (1 - k_1 k_3)^2 \tag{2.45b}$$

The two foregoing inequalities can be readily reduced to a single one, namely,

$$(k_1^2 - 1)(1 - k_3^2) \leq 0 \tag{2.45c}$$

which represents the dashed region of the k_1-k_3 plane shown in Fig. 2.17. This region represents the domain of definition of zero-mean linkages, i.e., linkages having an input crank and for which $c_1 = 0$.

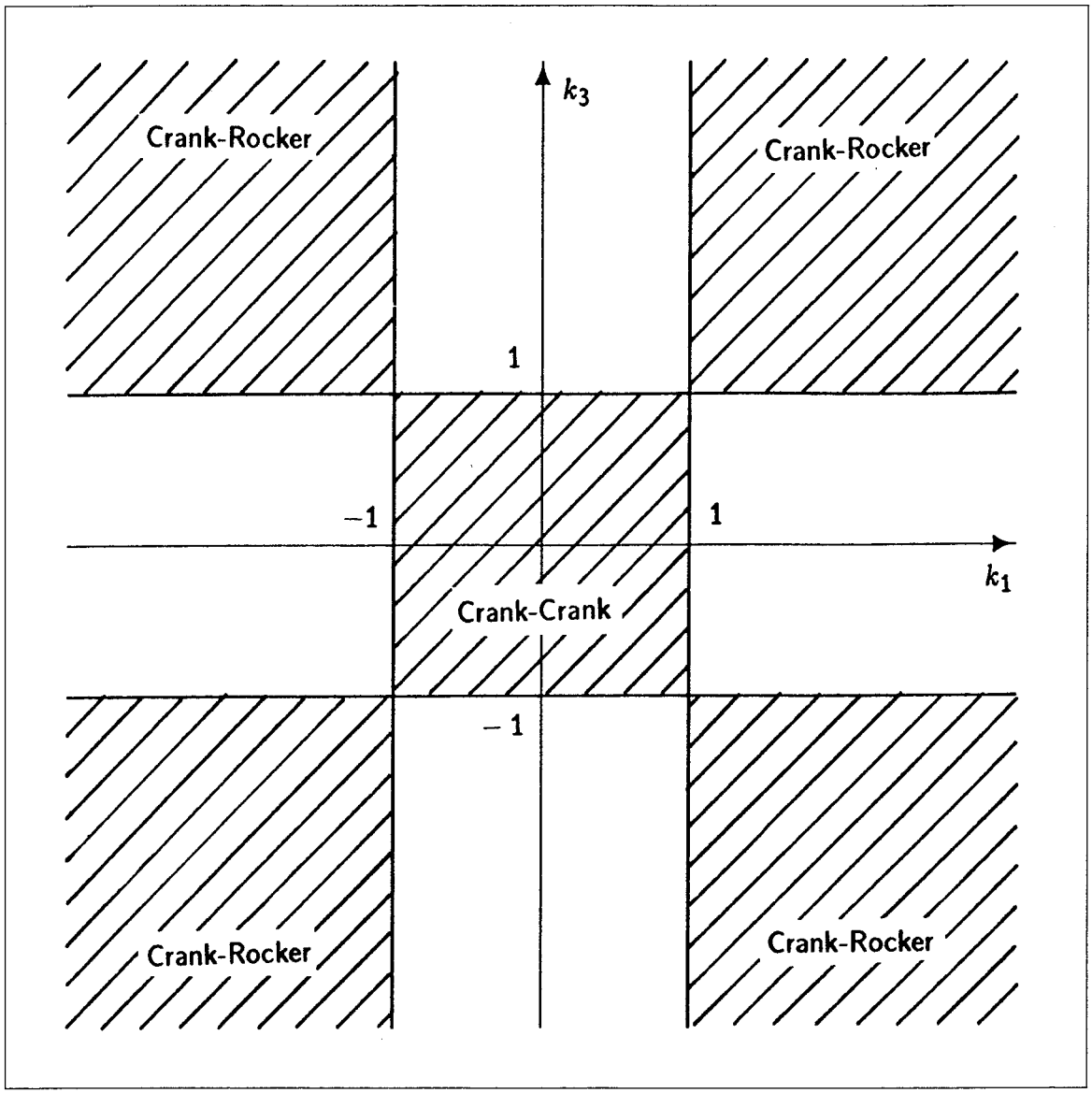

Figure 2.17 Domain of definition of planar zero-mean linkages.

Moreover, one can readily prove the following:

Theorem 2.1: *Zero-mean planar linkages are of the drag-link type when they correspond to points located in the inner square of the region of definition and of the crank-rocker type when they correspond to points located elsewhere within the said region.*

Proof: The conditions under which a planar four-bar linkage has a fully-rotatable output link are given in inequalities (2.12a&b). Substitution of the zero-mean condition in these

expresssions leads to:

$$(k_1^2 - 1)(1 + k_3)^2 \leq 0 \tag{2.46a}$$

and

$$(k_1^2 - 1)(1 - k_3)^2 \leq 0 \tag{2.46b}$$

which can be reduced to:

$$k_1^2 \leq 1 \tag{2.47}$$

Therefore, only the zero-mean linkages corresponding to points located in the inner square have a fully-rotatable output link, i.e., they are of the drag-link type. The other subregions represent zero-mean linkages of the crank-rocker type since their input link is a crank but their output link is not. This completes the proof.

A function-generation problem that arises rather frequently in applications calls for *quick-return mechanisms*. In this case, one is rather interested in linkages of the crank-rocker type. The motion of such linkages is defined by the time ratio of its two phases. If the first phase takes place as the input link sweeps an angle $\pi + \Delta\psi$, whereas the second phase—the return—as the input link sweeps an angle $\pi - \Delta\psi$, the time ratio T_R is defined as:

$$T_R = \frac{\pi + \Delta\psi}{\pi - \Delta\psi} \tag{2.48}$$

It was mentioned in theorem 2.1 that planar zero-mean linkages can be of the crank-rocker type. The following theorem is now proven:

Theorem 2.2: *Planar zero-mean linkages which are of the crank-rocker type have a time ratio of one.*

Proof: Consider the two geometric constructions of Fig. 2.18 where a planar crank-rocker linkage is shown in its two extreme positions. Moreover, the angle $\Delta\psi$ as defined in eq.(2.48) is given by:

$$\Delta\psi = \psi_2 - \psi_1 \tag{2.49a}$$

where ψ_1 and ψ_2 are assumed to be bounded as follows:

$$0 \leq \psi_1, \psi_2 \leq \pi \tag{2.49b}$$

Using the law of cosines, we can write:

$$\cos \psi_1 = \frac{a_1^2 - a_4^2 + (a_3 + a_2)^2}{2a_1(a_3 + a_2)} \tag{2.50a}$$

and

$$\cos \psi_2 = \frac{a_1^2 - a_4^2 + (a_3 - a_2)^2}{2a_1(a_3 - a_2)} \tag{2.50b}$$

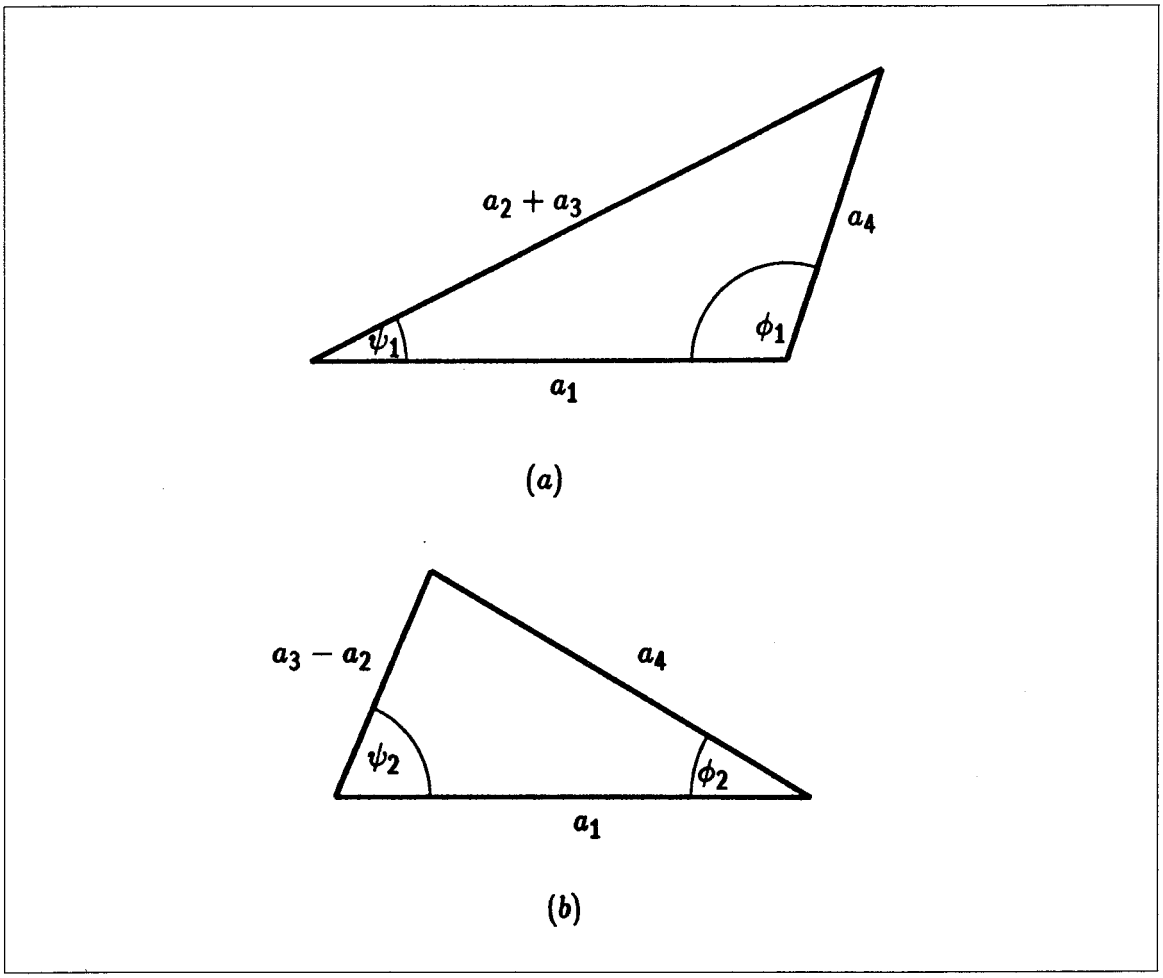

Figure 2.18 Limit positions of a planar four-bar linkage of the crank-rocker type.

If we now impose the zero-mean condition, i.e., if we substitute $a_1^2 + a_2^2$ by

$a_3^2 + a_4^2$, we obtain:

$$\cos\psi_1 = \cos\psi_2 = \frac{a_3}{a_1} \tag{2.51}$$

which, by virtue of relations (2.49a&b), leads to $\Delta\psi = 0$ and, from eq.(2.48), we have $T_R = 1$, which completes the proof.

Therefore, planar zero-mean linkages of the crank-rocker type cannot be candidates for quick-return mechanisms.

Planar zero-mean linkages which are of the drag-link type can be optimized by finding the minimum transmission defect for a given minimum value of the mechanism's *dimensional balance*. This is defined as the following real number:

$$b = (\frac{a_4}{a_2})^2 + (\frac{a_3}{a_2})^2 - 1 \tag{2.52a}$$

which turns out to be positive definite, for

$$b = k_1^2 k_3^2 \tag{2.52b}$$

It can be readily shown that $0 < b < 1$ for zero-mean linkages of the drag-link type since for these we have $|k_1| \leq 1$ and $|k_3| \leq 1$. Lines of constant balance and of constant transmission defect are plotted in Fig. 2.19. The optimum drag-link mechanism, for a given minimum balance b_m, is found at the point of tangency of the contour $b = b_m$ with a contour of constant transmission defect. This point can be readily determined in closed form. Indeed, linkages with a dimensional balance b_m verify the following equation:

$$b_m - k_1^2 k_3^2 = 0 \tag{2.53a}$$

whereas zero-mean linkages with a constant transmission defect z_0' verify

$$(\frac{1}{2} - k_1^2 z_0')k_3^2 - z_0'(1 - k_1^2) = 0 \tag{2.53b}$$

The solution of the nonlinear system of equations obtained when minimizing z_0' in eq.(2.53b) subjected to the constraint (2.53a) is the following:

$$k_3^2 = \frac{2b_m}{1 + b_m} \tag{2.54a}$$

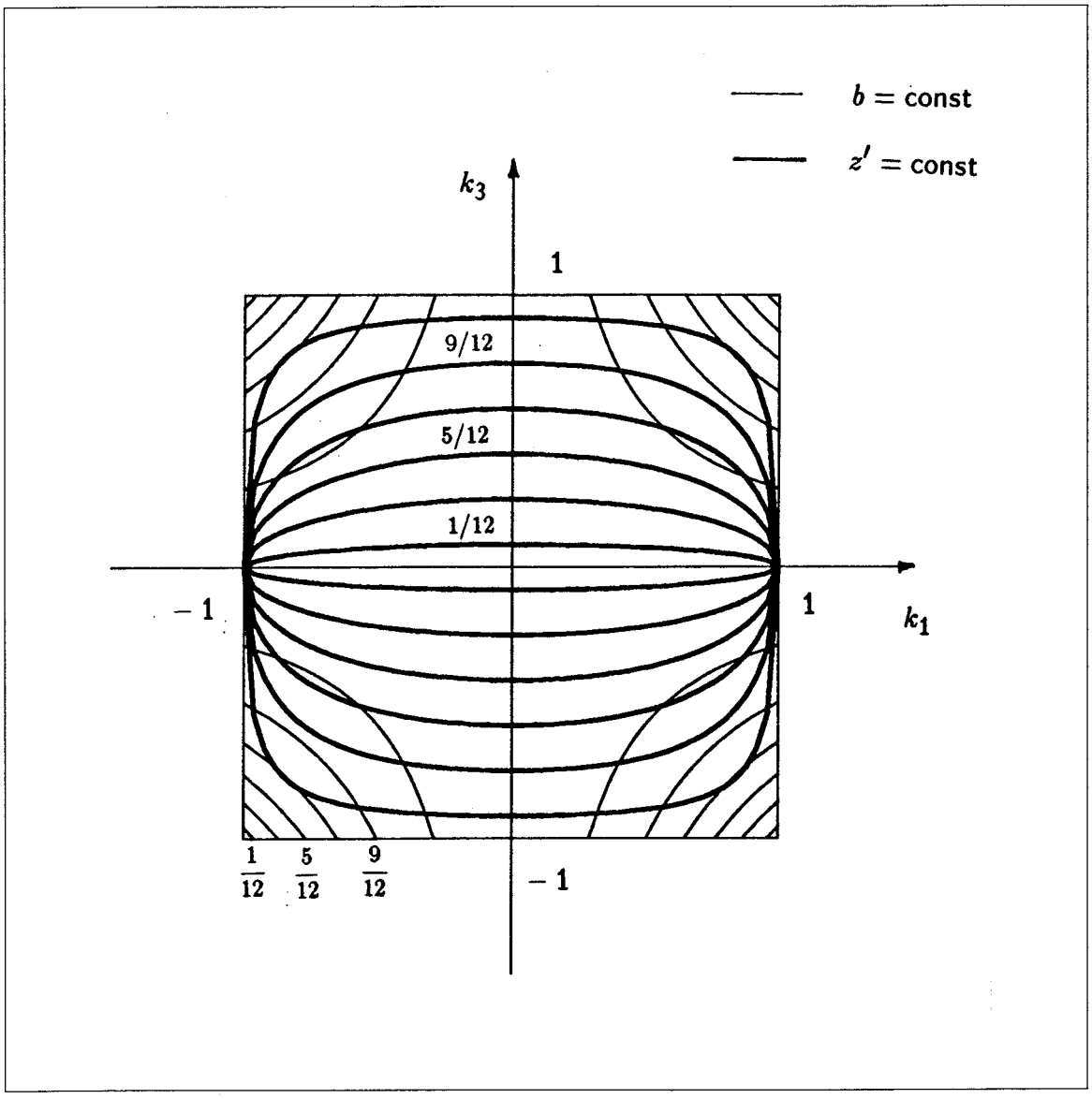

Figure 2.19 Lines of constant dimensional balance and of constant transmission defect for planar drag-link zero-mean linkages.

and

$$k_1^2 = \frac{b_m}{k_3^2} \tag{2.54b}$$

2.2.2.2 Spherical Zero-Mean Linkages

For spherical linkages, the zero-mean condition leads to:

$$k_4 = -k_1 k_2 \tag{2.55}$$

and the transmission defect can be written as:

$$z' = \frac{1}{2}c_2^2 = \frac{1}{4}AB \tag{2.56a}$$

where

$$A = \frac{|k_3|\sqrt{(1+k_3^2-k_1^2k_2^2)(k_2^2+k_3^2-k_1^2k_2^2)} + k_1k_2^2 + k_1(k_3^2-k_1^2k_2^2)}{|k_3|\sqrt{1+k_3^2-k_1^2k_2^2}} \tag{2.56b}$$

and

$$B = \frac{(k_2^2+k_3^2-k_1^2k_2^2)^{3/2}}{k_2^2+k_3^2(1+k_2^2)-2k_1^2k_2^2+(k_3^2-k_1^2)(k_3^2-k_1^2k_2^2)} \tag{2.56c}$$

The mobility conditions leading to an input crank, i.e., inequalities (2.21a&b), take on the form that follows, under condition (2.55):

$$(k_2-k_1)^2 \leq (1-k_1k_2)^2 \tag{2.57a}$$

and

$$(k_2+k_1)^2 \leq (1+k_1k_2)^2 \tag{2.57b}$$

which are equivalent to the following single inequality:

$$(k_1^2-1)(1-k_2^2) \leq 0 \tag{2.57c}$$

The region of the k_1k_2 plane defined by the foregoing inequality is represented in Fig. 2.20. This is the domain of definition of spherical zero-mean linkages. One now can prove the following:

Theorem 2.3: *Zero-mean spherical linkages are of the crank-rocker type when they correspond to points inside the inner square of the region of definition and of the drag-link type when they correspond to points located elsewhere within the said region.*

Proof: The conditions under which the spherical linkage has a fully rotatable output link were derived in Section 2.1 and are given in inequalities (2.26a&b). Upon substitution of the zero-mean condition, we obtain:

$$(k_2^2 - 1)(1 - k_1)^2 \geq 0 \tag{2.58a}$$

and

$$(k_2^2 - 1)(1 + k_1)^2 \geq 0 \tag{2.58b}$$

which can be reduced to

$$k_2^2 \geq 1 \tag{2.59}$$

Therefore, the linkages associated with points located in the peripheral sections of the mobility region are of the drag-link type and the ones corresponding to points inside the inner square are of the crank-rocker type. The proof is then completed.

Moreover, one has the following:

Theorem 2.4: *Zero-mean spherical linkages that are of the crank-rocker type have a time ratio of one.*

Proof: Consider now the two extreme configurations of the spherical linkage shown in Fig. 2.21. In this case, the angle $\Delta\psi$, defined in eq.(2.48), can be expressed as:

$$\Delta\psi = \psi_1 - \psi_2 \tag{2.60a}$$

where ψ_1 and ψ_2 are constrained as follows:

$$0 \leq \psi_1, \psi_2 \leq \pi \tag{2.60b}$$

Using the law of cosines for spherical triangles, one can also write:

$$\cos\psi_1 = \frac{\cos\alpha_4 - \cos\alpha_1\cos(\alpha_3 + \alpha_2)}{\sin\alpha_1\sin(\alpha_3 + \alpha_2)} \tag{2.61a}$$

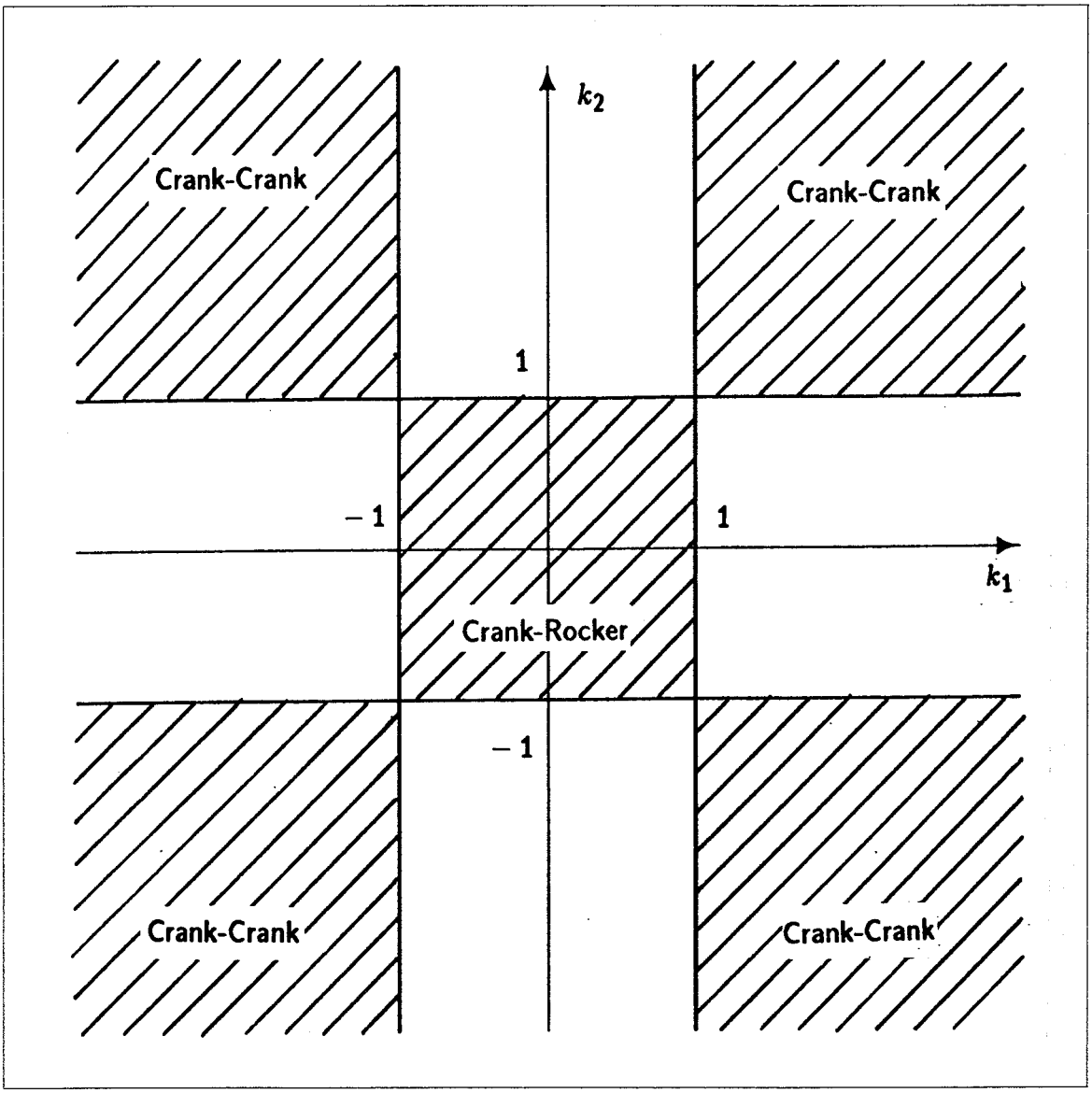

Figure 2.20 Domain of definition of spherical zero-mean linkages.

and

$$\cos\psi_2 = \frac{\cos\alpha_4 - \cos\alpha_1\cos(\alpha_3 - \alpha_2)}{\sin\alpha_1\sin(\alpha_3 - \alpha_2)} \tag{2.61b}$$

If we now introduce the zero-mean condition, i.e., if we substitute $\cos\alpha_4$ by r, where r is defined as

$$r = \frac{\cos\alpha_1\cos\alpha_2}{\cos\alpha_3} \tag{2.62a}$$

the following is derived:

$$\cos\psi_1 = \cos\psi_2 = \cot\alpha_1\tan\alpha_3 \tag{2.62b}$$

which, similarly to the planar case, leads to $\Delta\psi = 0$ and therefore $T_R = 1$, thereby completing the proof.

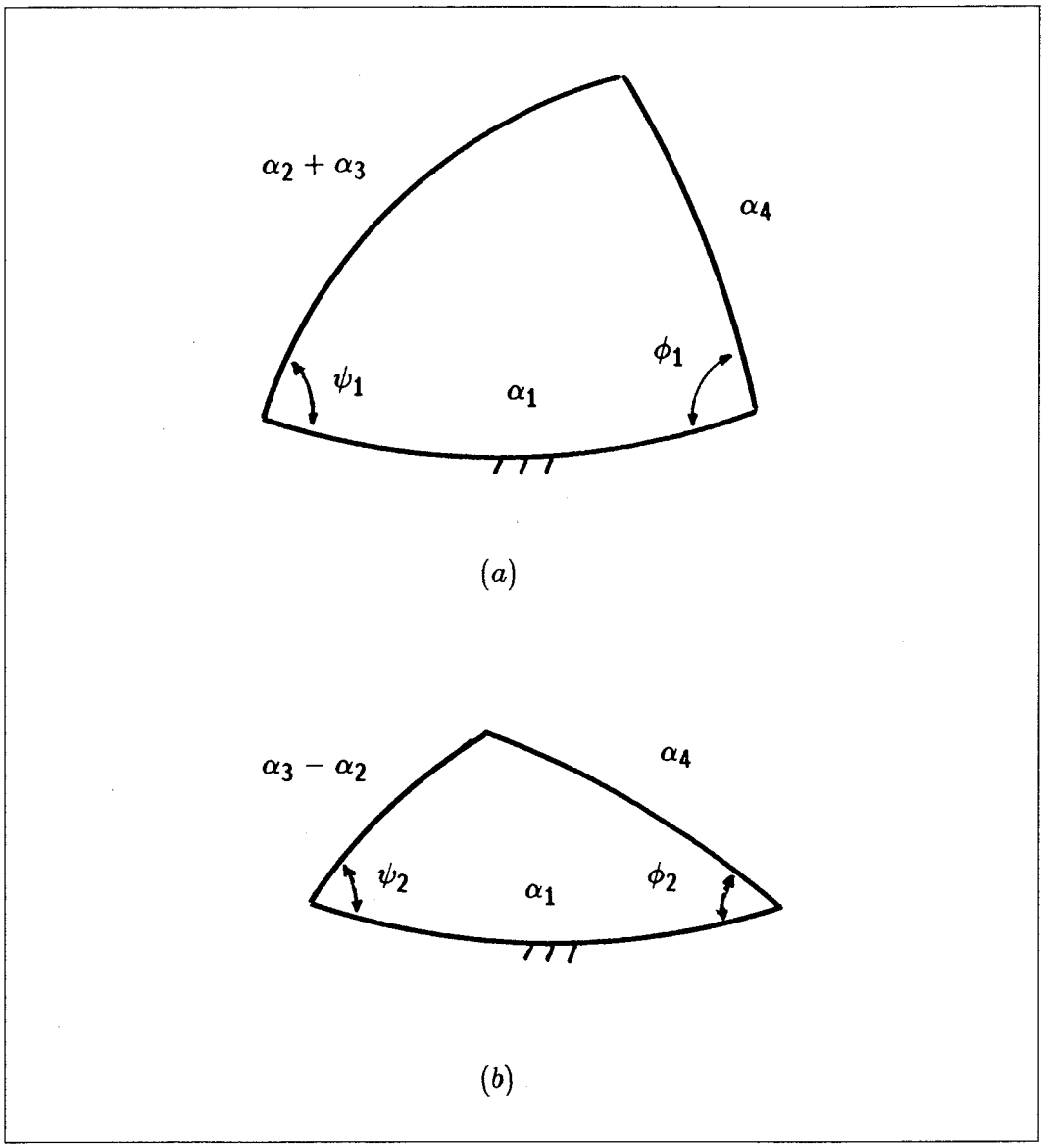

Figure 2.21 Limit positions of a spherical four-bar linkage of the crank-rocker type.

The fact that zero-mean crank-rocker linkages have a time ratio of unity disables them from being candidates for quick-return mechanisms. Hence, the optimization of quick-return mechanisms should be tackled with an alternate approach, which is done in the following Section.

2.2.3 Optimization of Quick-Return Mechanisms as Minimum-Defect Linkages

Quick-return mechanisms, as defined in Section 2.2.2, will now be designed using the concept of minimum-defect linkages. The problem then consists of minimizing the quadratic form of eq.(2.36) subjected to constraints on the time ratio and output swing angle of the linkage.

2.2.3.1 Planar Linkages

This is based on the approach introduced by Cleghorn and Fenton (1984). In order to set up the constraint equations of the problem at hand, the following transformations of the link lengths are introduced:

$$r_2 = \frac{a_2}{a_1}, \quad r_3 = \frac{a_3}{a_1}, \quad r_4 = \frac{a_4}{a_1} \tag{2.63}$$

and

$$q_1 = r_3 - r_2 \tag{2.64a}$$

$$q_2 = r_3 + r_2 \tag{2.64b}$$

The two extreme positions of the output link give rise to the geometric constructions of Fig. 2.18. Application of the *cosines law* to these triangles gives the following constraints (Cleghorn and Fenton 1984):

$$g_1 = r_4^2 - 1 - q_2^2 + 2q_2 \cos\psi_1 = 0 \tag{2.65a}$$

$$g_2 = r_4^2 - 1 - q_1^2 + 2q_1 \cos\psi_2 = 0 \tag{2.65b}$$

$$g_3 = q_2^2 - 1 - r_4^2 + 2r_4 \cos\phi_1 = 0 \tag{2.65c}$$

$$g_4 = q_1^2 - 1 - r_4^2 + 2r_4 \cos\phi_2 = 0 \tag{2.65d}$$

$$g_5 = \psi_2 - \psi_1 - \Delta\psi = 0 \tag{2.65e}$$

$$g_6 = \phi_1 - \phi_2 - \Delta\phi = 0 \tag{2.65f}$$

or, in vector form,

$$\mathbf{g} = \mathbf{0} \tag{2.65g}$$

where g_i denotes the i-th component of the 6-dimensional vector **g**, the time ratio being defined as in equation (2.48).

In the foregoing discussion, $\Delta\phi$ is the prescribed output swing angle, and $\Delta\psi$ is as defined in eq.(2.49a). Moreover, ψ_1, ψ_2, ϕ_1 and ϕ_2 are defined in Fig. 2.18.

The vector of design variables **x** will therefore be defined as:

$$\mathbf{x} = [\, r_4,\, q_1,\, q_2,\, \psi_1,\, \psi_2,\, \phi_1,\, \phi_2 \,]^T \tag{2.66}$$

The objective function to be minimized is defined as the linkage defect, i.e., as z', which can be readily expressed as the following quadratic form:

$$z' = \frac{1}{2}\mathbf{f}^T \mathbf{W}\, \mathbf{f} \tag{2.67a}$$

where $\mathbf{f} = [c_1 \quad c_2]^T$, with c_1 and c_2 defined as follows:

$$c_1 = \frac{q_1 q_2 + r_4^2 - 1}{r_4(q_1 + q_2)} \tag{2.67b}$$

$$c_2 = \frac{q_2 - q_1}{r_4(q_1 + q_2)} \tag{2.67c}$$

and

$$\mathbf{W} = \begin{bmatrix} 2 & 0 \\ 0 & 1 \end{bmatrix} \tag{2.67d}$$

The Jacobians of **f** and **g** with respect to **x**, **F** and **G**, respectively, are then readily derived as the following 2×7 and 6×7 matrices:

$$\mathbf{F} = \begin{bmatrix} f_{11} & f_{12} & f_{13} & 0 & 0 & 0 & 0 \\ f_{21} & f_{22} & f_{23} & 0 & 0 & 0 & 0 \end{bmatrix} \tag{2.68a}$$

where:

$$f_{11} = [-N/r_4^2 + 2]/(q_1 + q_2) \tag{2.68b}$$

$$f_{12} = [-N/(q_1 + q_2) + q_2]/r_4(q_1 + q_2) \tag{2.68c}$$

$$f_{13} = [-N/(q_1 + q_2) + q_1]/r_4(q_1 + q_2) \tag{2.68d}$$

$$f_{21} = (q_1 - q_2)/r_4^2(q_1 + q_2) \tag{2.68e}$$

$$f_{22} = [(q_1 - q_2)/(q_1 + q_2) - 1]/r_4(q_1 + q_2) \tag{2.68f}$$

$$f_{23} = [(q_1 - q_2)/(q_1 + q_2) + 1]/r_4(q_1 + q_2) \tag{2.68g}$$

$$N = q_1 q_2 + r_4^2 - 1 \tag{2.68h}$$

and

$$\mathbf{G} = [\,\mathbf{G}_1 \quad \mathbf{G}_2\,] \tag{2.69a}$$

where

$$\mathbf{G}_1 = \begin{bmatrix} 2r_4 & 0 & -2q_2 + 2\cos\psi_1 \\ 2r_4 & -2q_1 + 2\cos\psi_2 & 0 \\ -2r_4 + 2\cos\phi_1 & 0 & 2q_2 \\ -2r_4 + 2\cos\phi_2 & 2q_1 & 0 \\ 0 & 0 & 0 \\ 0 & 0 & 0 \end{bmatrix} \tag{2.69b}$$

and

$$\mathbf{G}_2 = \begin{bmatrix} -2q_2\sin\psi_1 & 0 & 0 & 0 \\ 0 & -2q_1\sin\psi_2 & 0 & 0 \\ 0 & 0 & -2r_4\sin\phi_1 & 0 \\ 0 & 0 & 0 & -2r_4\sin\phi_2 \\ -1 & 1 & 0 & 0 \\ 0 & 0 & 1 & -1 \end{bmatrix} \tag{2.69c}$$

which completes the formulation of the problem. This problem was solved numerically using the orthogonal-decomposition method (Angeles et al. 1987). This method is meant to minimize an objective function which is an m-dimensional quadratic form of n variables subjected to p nonlinear equality constraints. In this case, we have $m = 2$ with $n = 7$ variables subjected to $p = 6$ constraints.

Two examples of application of this method are presented here. They are taken from (Gupta 1977) for purposes of comparison. The results obtained using the aforementioned procedure are given in Table 2.1 and they are in full agreement with the results reported in that reference.

Several tests performed with this formulation of the problem for the design of planar linkages show that the procedure usually converges within 15 iterations.

2.2.3.2 Spherical Linkages

The formulation of this problem is similar to the one used in the planar case. The constraints are established using the extreme positions, which are shown in Fig. 2.21.

Optimum parameters	Case1 $\Delta\phi = 40°$ $\Delta\psi = -20°$	Case2 $\Delta\phi = 64°$ $\Delta\psi = 28°$
a_1	1.342	1.041
a_2	0.323	0.494
a_3	0.729	0.936
a_4	1.000	1.000
c_1	−0.2564	0.2929
c_2	0.5946	0.5494
z'	0.2425	0.2367

Table 2.1 Optimum planar four-bar linkages.

The *cosines law* for spherical triangles is applied on these two configurations. Moreover, since the link dimensions are now angles, the design variables will be chosen as the sines and the cosines of these, rather than as the angles themselves. This will simplify the formulation and will enhance the numerical stability of the problem, but will require additional constraints. The global set of constraints will then be:

$$g_1 = u_4 - u_1(u_2u_3 - v_2v_3) - v_1(u_2v_3 + v_2u_3)\cos\psi_1 = 0 \qquad (2.70a)$$

$$g_2 = u_4 - u_1(u_2u_3 + v_2v_3) - v_1(u_2v_3 - v_2u_3)\cos\psi_2 = 0 \qquad (2.70b)$$

$$g_3 = u_2u_3 - v_2v_3 - u_1u_4 - v_1v_4\cos\phi_1 = 0 \qquad (2.70c)$$

$$g_4 = u_2u_3 + v_2v_3 - u_1u_4 - v_1v_4\cos\phi_2 = 0 \qquad (2.70d)$$

$$g_5 = \psi_1 - \psi_2 - \Delta\psi = 0 \qquad (2.70e)$$

$$g_6 = \phi_1 - \phi_2 - \Delta\phi = 0 \qquad (2.70f)$$

$$g_7 = u_1^2 + v_1^2 - 1 = 0 \qquad (2.70g)$$

$$g_8 = u_2^2 + v_2^2 - 1 = 0 \qquad (2.70h)$$

$$g_9 = u_3^2 + v_3^2 - 1 = 0 \qquad (2.70i)$$

$$g_{10} = u_4^2 + v_4^2 - 1 = 0 \qquad (2.70j)$$

where

$$u_i = \cos\alpha_i \quad , \quad v_i = \sin\alpha_i \quad , \quad i = 1,\ldots,4 \qquad (2.70k)$$

or, in vector form,

$$\mathbf{g} = \mathbf{0} \tag{2.70l}$$

where g_i is the ith component of the 10-dimensional vector $\mathbf{g}$. The output swing angle is given by $\Delta\phi$ and $\Delta\psi$ is related to the time ratio by eq.(2.48). Angles ψ_1, ψ_2, ϕ_1 and ϕ_2 are defined in Fig. 2.21.

The objective function to be minimized will be the transmission defect. However, tests run with the program implementing the orthogonal-decomposition algorithm showed that the procedure is very strongly attracted by the degenerate case for which $\alpha_1 = \alpha_2 = \alpha_3 = \alpha_4 = 0$. One can easily verify that, in this case, all the constraints are satisfied—providing $\psi_1 - \psi_2 = \Delta\psi$ and $\phi_1 - \phi_2 = \Delta\phi$—and that the objective function goes to zero. To overcome this problem, we augment the objective function with the squares of the cosines of the link angles. This will force the angles of the mechanism to be as close as possible to 90°, which will lead to dimensionally well-balanced mechanisms. The objective function then becomes:

$$z' = \frac{1}{2}\mathbf{f}^T\mathbf{W}\mathbf{f} \tag{2.71}$$

where

$$\mathbf{f} = [\,\sqrt{2}c_1,\, c_2,\, \cos\alpha_1,\, \cos\alpha_2,\, \cos\alpha_3,\, \cos\alpha_4\,]^T \tag{2.72a}$$

Matrix W allows one to introduce some weights in the quadratic form. For example, if one assigns less importance to the dimensional balance of the mechanism—and gets closer to the original problem—, then W can be defined as

$$\mathbf{W} = \mathrm{diag}[1, 1, w, w, w, w] \tag{2.72b}$$

where w is a positive quantity smaller than 1.

Notice that, in this case, the vector of design variables will be defined as:

$$\mathbf{x} = [\,u_1,\, v_1,\, u_2,\, v_2,\, u_3,\, v_3,\, u_4,\, v_4,\, \psi_1,\, \psi_2,\, \phi_1,\, \phi_2\,]^T \tag{2.73}$$

Therefore, the Jacobians of $\mathbf{f}$ and $\mathbf{g}$ with respect to $\mathbf{x}$, denoted by $\mathbf{F}$ and $\mathbf{G}$, respectively, are written as the following 6×12- and 10×12 matrices:

$$\mathbf{F} = [\mathbf{F}_1 \quad \mathbf{F}_2 \quad \mathbf{F}_3] \tag{2.74a}$$

where

$$\mathbf{F}_1 = \begin{bmatrix} \frac{\sqrt{2}Qu_2}{v_3v_4} & 0 & \frac{\sqrt{2}Qu_1}{v_3v_4} & 0 & \left[\frac{-\sqrt{2}Qu_4}{v_3v_4} + \frac{\sqrt{2}(u_3u_4-u_1u_2)}{4Qv_3v_4}\right] \\ 0 & \frac{Qv_2}{v_3v_4} & 0 & \frac{Qv_1}{v_3v_4} & \frac{-v_1v_2}{4Qv_3v_4} \\ 1 & 0 & 0 & 0 & 0 \\ 0 & 0 & 1 & 0 & 0 \\ 0 & 0 & 0 & 0 & 1 \\ 0 & 0 & 0 & 0 & 0 \end{bmatrix} \tag{2.74b}$$

$$\mathbf{F}_2 = \begin{bmatrix} \frac{\sqrt{2}Q(u_3u_4-u_1u_2)}{v_3^2v_4} & \frac{-\sqrt{2}u_3Q}{v_3v_4} & \frac{\sqrt{2}Q(u_3u_4-u_1u_2)}{v_3v_4^2} \\ \frac{-Qv_1v_2}{v_4v_3^2} & 0 & \frac{-Qv_1v_2}{v_3v_4^2} \\ 0 & 0 & 0 \\ 0 & 0 & 0 \\ 0 & 0 & 0 \\ 0 & 1 & 0 \end{bmatrix} \tag{2.74c}$$

$$\mathbf{F}_3 = \mathbf{0}_{6\times4} \tag{2.74d}$$

in which $\mathbf{0}_{6\times4}$ denotes the 6×4 zero matrix, and Q is defined as

$$Q = \sqrt{\frac{1-u_3}{2}} \tag{2.74e}$$

with

$$\mathbf{G} = [\mathbf{G}_1 \quad \mathbf{G}_2 \quad \mathbf{G}_3 \quad \mathbf{G}_4] \tag{2.75a}$$

where

$$\mathbf{G_1} = \begin{bmatrix} (v_2v_3 - u_2u_3) & -(u_2v_3 + v_2u_3)\cos\psi_1 & -(u_1u_3 + v_1v_3\cos\psi_1) \\ -(u_2u_3 + v_2v_3) & (v_2u_3 - u_2v_3)\cos\psi_2 & -(u_1u_3 + v_1v_3\cos\psi_2) \\ -u_4 & -v_4\cos\phi_1 & u_3 \\ -u_4 & -v_4\cos\phi_2 & u_3 \\ 0 & 0 & 0 \\ 0 & 0 & 0 \\ 2u_1 & 2v_1 & 0 \\ 0 & 0 & 2u_2 \\ 0 & 0 & 0 \\ 0 & 0 & 0 \end{bmatrix} \tag{2.75b}$$

$$\mathbf{G}_2 = \begin{bmatrix} (u_1v_3 - v_1u_3\cos\psi_1) & -(u_1u_2 + v_1v_2\cos\psi_1) & (u_1v_2 - v_1u_2\cos\psi_1) \\ (-u_1v_3 + v_1u_3\cos\psi_2) & (-u_1u_2 + v_1v_2\cos\psi_2) & -(u_1v_2 + v_1u_2\cos\psi_2) \\ -v_3 & u_2 & -v_2 \\ v_3 & u_2 & v_2 \\ 0 & 0 & 0 \\ 0 & 0 & 0 \\ 0 & 0 & 0 \\ 2v_2 & 0 & 0 \\ 0 & 2u_3 & 2v_3 \\ 0 & 0 & 0 \end{bmatrix} \tag{2.75c}$$

$$\mathbf{G}_3 = \begin{bmatrix} 1 & 0 & v_1(u_2v_3 + v_2u_3)\sin\psi_1 \\ 1 & 0 & 0 \\ -u_1 & -v_1\cos\phi_1 & 0 \\ -u_1 & -v_1\cos\phi_2 & 0 \\ 0 & 0 & 1 \\ 0 & 0 & 0 \\ 0 & 0 & 0 \\ 0 & 0 & 0 \\ 0 & 0 & 0 \\ 2u_4 & 2v_4 & 0 \end{bmatrix} \tag{2.75d}$$

$$\mathbf{G}_4 = \begin{bmatrix} 0 & 0 & 0 \\ v_1(u_2v_3 - v_2u_3)\sin\psi_2 & 0 & 0 \\ 0 & v_1v_4\sin\phi_1 & 0 \\ 0 & 0 & v_1v_4\sin\phi_2 \\ -1 & 0 & 0 \\ 0 & 1 & -1 \\ 0 & 0 & 0 \\ 0 & 0 & 0 \\ 0 & 0 & 0 \\ 0 & 0 & 0 \end{bmatrix} \tag{2.75e}$$

which completes the formulation of this problem. Notice that, in this case, we have $n = 12$ variables subjected to $p = 10$ constraints and that we are aiming at minimizing a performance index for which $m = 6$.

Three examples are presented for this case, the results appearing in Table 2.2. Notice that in the first two examples given for this problem, we specified the same time ratio and output swing angle. However, in the second one, we have used some weights to give less importance to the terms $\cos^2\alpha_i$ in the objective function. The optimum linkage

Optimum parameters	Case1	Case2	Case3
$\Delta\phi$	70°	70°	90°
$\Delta\psi$	20°	20°	30°
Weights	1.	0.1	0.1
α_1(deg)	104.1	97.6	80.2
α_2(deg)	33.7	34.3	152.4
α_3(deg)	83.4	56.0	46.9
α_4(deg)	88.7	89.8	88.7
c_1	−0.13749	−0.06312	−0.09061
c_2	0.36078	0.31653	0.24891
z'	0.08399	0.05408	0.03919

Table 2.2 Optimum spherical four-bar linkages.

obtained, then, has a better transmission quality, but is dimensionally less balanced.

In the case of spherical linkages, convergence usually occurs within about 25 iterations.

2.3 Branch Identification for Regional Structures of Open-Loop Manipulators

This section concerns open-loop simple kinematic chains, i.e., serial manipulators. The problem addressed here is known as *branch identification*. This arises from the solution of the inverse kinematic problem for serial manipulators which may lead to many branches. However, when the robot is required to produce a certain trajectory in the Cartesian space, it is necessary, when obtaining the corresponding joint coordinates, that each of the points of the trajectory—in the joint space—belong to the same branch. It will be realized, in Chapter 4, that the branch identification problem for parallel manipulators can be solved as a series of such problems for serial manipulators. This is the rationale behind the discussion presented in this paragraph.

It has been shown in (Primrose 1986; Lee and Liang 1988) that the solution of the inverse kinematic problem for an arbitrary 6-axis serial manipulator can produce up to 16 different solutions, i.e., 16 branches. Sandor et al.(1986a) have developed inequalities that allow to identify the different branches.

An alternate method is derived here, based uniquely on the Jacobian matrix. The idea is to obtain a method to identify the branches by performing certain tests or computations on the Jacobian matrix. There should exist frame invariant properties of this matrix that would differ from one branch to another and which we could exploit. Some properties of a matrix that naturally arise are its determinant and its eigenvalues. These quantities are obviously frame independent since the determinant represents the local ratio of volume of the mapping defined by the matrix and the eigenvalues remain unchanged under similarity transformations. The problem is now reduced to regional structures of manipulators , i.e., three-degree-of-freedom kinematic structures used to position a point in space. This type of structure has a particular relevance for it is possible to treat wrist-partitioned manipulators as a regional structure plus a wrist that is used to orient the end-effector. The branching problem associated with the wrist is straightforward since the sine of the second angle of the wrist bears a different sign in each branch. This angle is, in fact, the transmission angle of the equivalent spherical four-bar linkage.

The branching problem of the regional structure, which in general may have up to four branches, is now solved using the properties of the Jacobian matrix mentioned above. Four cases may arise:

(i) the eigenvalues are all real and the determinant is positive

(ii) the eigenvalues are all real and the determinant is negative

(iii) only one of the eigenvalues is real and the determinant is positive

(iv) only one of the eigenvalues is real and the determinant is negative

An example of application of this method to a 3R regional structure taken from (Rastegar and Deravi 1987) is shown in Table 2.3. Unfortunately, the extension of this concept to a general 6-axis manipulator is not trivial.

Solution #	1	2	3	4
Eigenvalues	$0.20 + 2.93j$	$0.03 + 0.74j$	-2.31	-0.68
	$0.20 - 2.93j$	$0.03 - 0.74j$	3.72	0.81
	0.87	-0.87	0.87	-0.87
Determinant	7.45	-0.48	-7.45	0.48

Table 2.3 Branch identification for a 3R regional structure with $a_1 = 3$, $a_2 = 2$, $a_3 = 1$, $b_1 = b_2 = b_3 = 0$, $\alpha_1 = 0$ and $\alpha_2 = \pi/2$ for the configurations obtained when $x = 4$, $y = 1$ and $z = 1/2$.

Chapter 3 ANALYSIS OF COMPLEX KINEMATIC CHAINS

The subject of this thesis being the study of parallel manipulators, it is necessary to derive some results concerning the general class of linkages to which these manipulators belong, i.e., complex kinematic chains. It is recalled that these chains are defined as those containing at least one link having a degree of connectivity greater than or equal to three. However, if the only link of the chain having a degree of connectivity greater than or equal to three is the fixed link, then the chain can be treated as a set of uncoupled simple kinematic chains, i.e., it can be broken down into a number of cases similar to the ones that were studied in Chapter 2.

The possibility of applications of complex kinematic chains are numerous. Examples can be found even in the early work on machinery. Watt's and Stephenson's linkages, for instance, clearly constitute planar 6-link complex kinematic chains (Hunt 1978). More recently, with the advances in computer-aided synthesis of linkages, researchers have started to consider the use of complex kinematic chains as hard automation modules which are designed to perform a precise repetitive task. The inherent rigidity of complex kinematic chains is one of the important motivations behind these, because it leads to higher accuracy and load-carrying capacity. Some of the designs even include a certain flexibility, i.e., provision to perform alternate tasks by a simple change—which can be done within minutes or even seconds—in their linkage parameters; for instance, changing the distance or angle between two joints of the fixed link. Examples of the results obtained with this approach are found in (Sandor et al. 1984, 1985, 1986a, 1986b, Wang et al. 1987)

In this chapter, three aspects of the analysis of complex kinematic chains will be treated: the graph representation of their topology, the determination of their degree of freedom based on topology and geometry and their singularity analysis. A distinction has to be made here between the topology and the geometry of a kinematic chain, the former being the description of the chain through the type of kinematic pairs and the rigid bodies constituting the chain together with their relative connectivities, whereas the latter defines more precisely the linkage by giving its physical relative dimensions, in the form of its Hartenberg-Denavit parameters (Hartenberg and Denavit 1964) for instance. The final section of the chapter will be devoted to the introduction of parallel manipulators as a special case of complex kinematic chains.

3.1 Graph Representation of Complex Kinematic Chains

A kinematic chain can be described as a set of rigid bodies attached to each other by kinematic pairs, resulting in a mechanical network containing joints and links. Moreover, when at least one of the links but the fixed one has a degree of connectivity greater than or equal to three, the chain is said to be complex. The network defined by the chain is topologically analog to electrical networks made up of nodes and impedances (Davies 1981). Hence, *graph theory* offers a systematic way of representing the topology of complex kinematic chains. This is now shown and the results obtained here concerning the topology will be used in the next section for the derivation of a method allowing one to find the degree of freedom of any complex kinematic chain.

For the sake of consistency, and to render the presentation more systematic, we will define a joint as a kinematic pair coupling two rigid bodies and allowing no more than three degrees of freedom. Cylindrical (C), planar (E), screw (H), spherical (S), revolute (R) and prismatic (P) pairs are examples of joints. Once this is clear, we can write the graph associated with the kinematic chain, in which a point of the graph corresponds to a rigid body and an edge to a joint. A few definitions pertaining to graph theory (Harary 1969) are now recalled.

Definition 3.1 A *graph* G consists of a finite nonempty set $V = V(G)$ of p *points* together with a prescribed set X of q unordered pairs of distinct points of V. Each pair $x = \{u, v\}$ of points in X is a *line* or *edge* of G, and X is said to *join* u and v. We say that u and v are *adjacent points* of the graph.

Definition 3.2 A *subgraph* of G is a graph having all its points and lines in G.

Definition 3.3 A *spanning* subgraph of G is a subgraph containing all the points of G.

Definition 3.4 A *walk* on a graph is an alternating sequence of points and edges beginning and ending with points, in which each edge is incident with the two points immediately preceding and following it.

Definition 3.5 A *path* is a walk with all its points (and thus necessarily all its lines) distinct.

Definition 3.6 A graph is said to be *connected* if every pair of points are joined by a path.

Definition 3.7 A *cycle* or *loop* is defined as a *path* beginning and ending at the same point and including at least three points.

Definition 3.8 A *tree* is a connected graph which has no cycles.

As shown in (Davies 1981), only connected graphs in which every edge belongs to at least one cycle are needed, since the other cases represent trivial additions to the problem addressed here. They correspond to complex kinematic chains to which an uncoupled independent simple kinematic chain is added. An important issue to be covered now is the determination of the number of independent loops in a kinematic chain. This quantity is of great importance since it allows us to find a *basis* having a minimum *cardinality* for

the kinematic constraints of the chain, the cardinality of a set being defined as the number of elements that it contains. We can determine the number of independent loops in the kinematic chain by counting the number of independent cycles in the associated graph. The number of independent cycles in a connected graph is given by Euler's formula for graphs (Harary 1969), namely:

$$k = e - v + 1 \tag{3.1}$$

where e is the number of edges and v is the number of points (vertices). Notice that this equation has already been used in the context of kinematic chains, namely in (Davies 1981; Sheth and Uicker 1972; Kleinfinger and Khalil 1986).

The next step is now to identify a set of independent loops, i.e., a cycle basis of the graph. This can be done systematically by finding a *spanning tree* of the graph and then using the *chords* to complete the fundamental independent cycles. The following definition is needed:

Definition 3.9 A *spanning tree* of a connected graph is a connected subgraph in which all the points are present but in which there are no cycles. The omitted edges are called *chords* and each of the chords added to the tree completes a fundamental independent cycle of the original graph.

The topological analysis of complex kinematic chains is therefore completed since we have obtained, from its associated graph, the number of independent loops and a basis for these loops. It is to be noted that this basis need not be unique and that the use of any of the bases in setting up the kinematic constraint equations will lead to equivalent systems of equations.

As an example, Watt's linkage is shown in Fig. 3.1 together with its associated graph. A spanning tree and the corresponding chords, which allow us to identify a set of independent loops, are also included. It is recalled that the graph associated with a

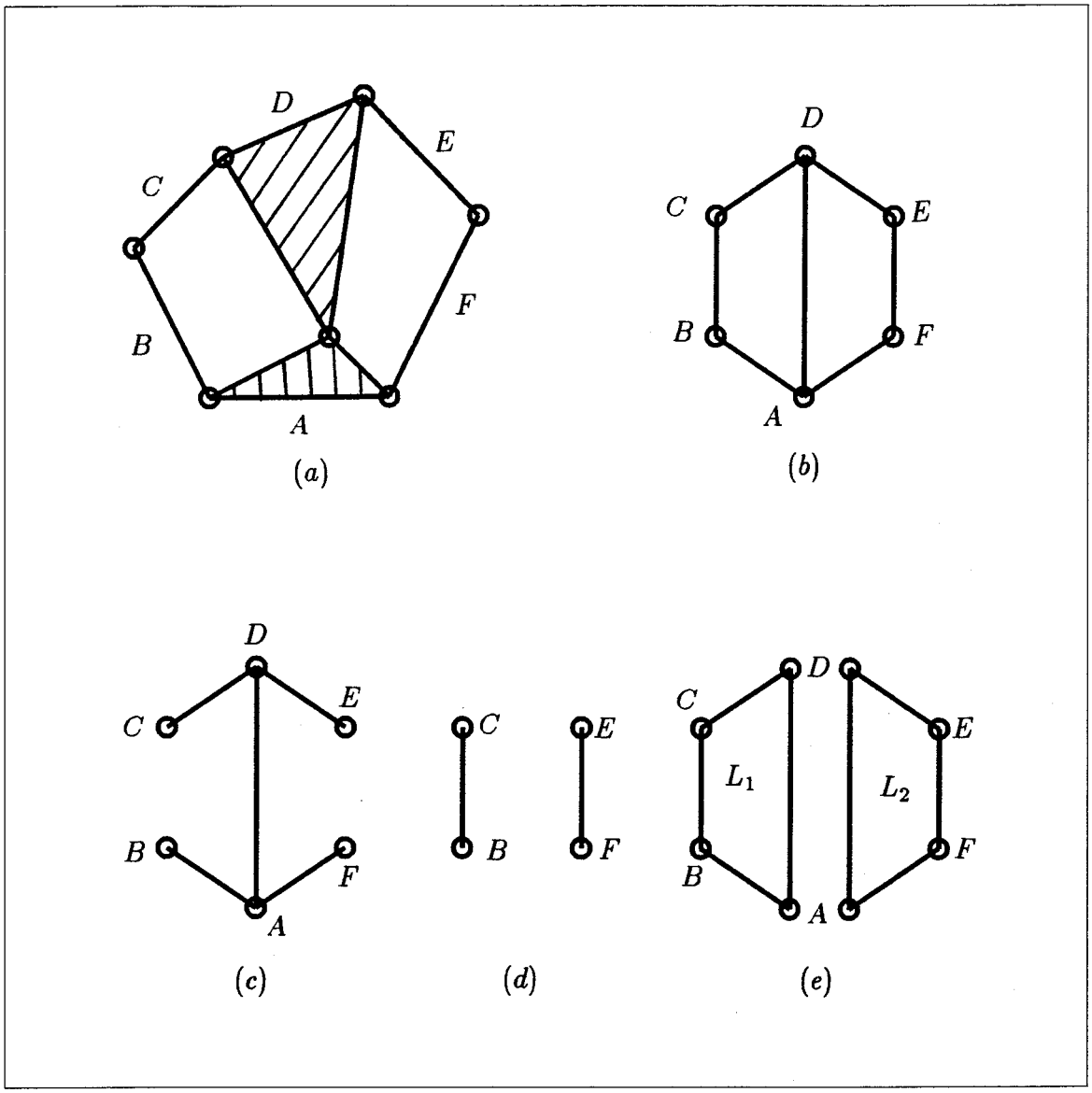

Figure 3.1 (*a*)Watt's linkage (*b*)associated graph (*c*)a spanning tree (*d*)the corresponding chords and (*e*)the associated set of independent loops.

kinematic chain, although very useful in the topological analysis, does not contain any information on its geometry.

One more important concept, in the context of graph representation of kinematic chains, is now defined.

Definition 3.10 The *non-powered subchain* of a kinematic chain is the subchain obtained when all the actuated joints are locked, i.e., when all the adjacent bodies connected

by actuated joints are rigidly coupled. When the linkage is in a non-singular configuration, the non-powered subchain has a degree of freedom of zero.

This concept can be illustrated by the following example: A two-degree-of-freedom planar complex kinematic chain is shown in Fig. 3.2a. The non-powered subchain shown in Fig. 3.2b is the one obtained when the actuated joints are the ones whose rotation angles are given by θ and ψ. The corresponding graph is shown in Fig. 3.2c. It is pointed out that, in this case, no closed-form solution for the output angle ϕ can be written in terms of the input angles. However, when the actuators are located on the joints whose rotation angle is denoted by θ and ϕ, the non-powered subchain becomes the one shown in Fig. 3.2d, with the associated graph of Fig. 3.2e. In this case, we can obtain a closed-form solution for the output angle ψ in terms of the input angles θ and ϕ. This is due to the fact that the fixed link of the non-powered subchain and the ternary floating rigid body are directly connected to each other by a kinematic pair, which generates the *short path* between the end nodes of the associated graph. Indeed, it can be readily seen, from Fig. 3.2a, that, given angles θ and ϕ, the position of point F can be computed using the input-output equation of the planar four-bar linkage. The position of points F and H being known, it is then straightforward to compute the position of point G and to determine angle ψ by making use of the four-bar linkage equation again.

3.2 Degree of Freedom of Complex Kinematic Chains

The determination of the degree of freedom (dof) of kinematic chains has attracted the attention of researchers for many years. The well known generalized Chebychev-Grübler-Kutzbach formulae, which rely only on the topology of the chains, can be used to find the dof of many simple and complex kinematic chains. An expression for this criterion, referred to as the *general mobility criterion* (Hunt 1978), can be written as:

$$l = 6(n - g - 1) + \sum_{i=1}^{g} f_i \tag{3.2}$$

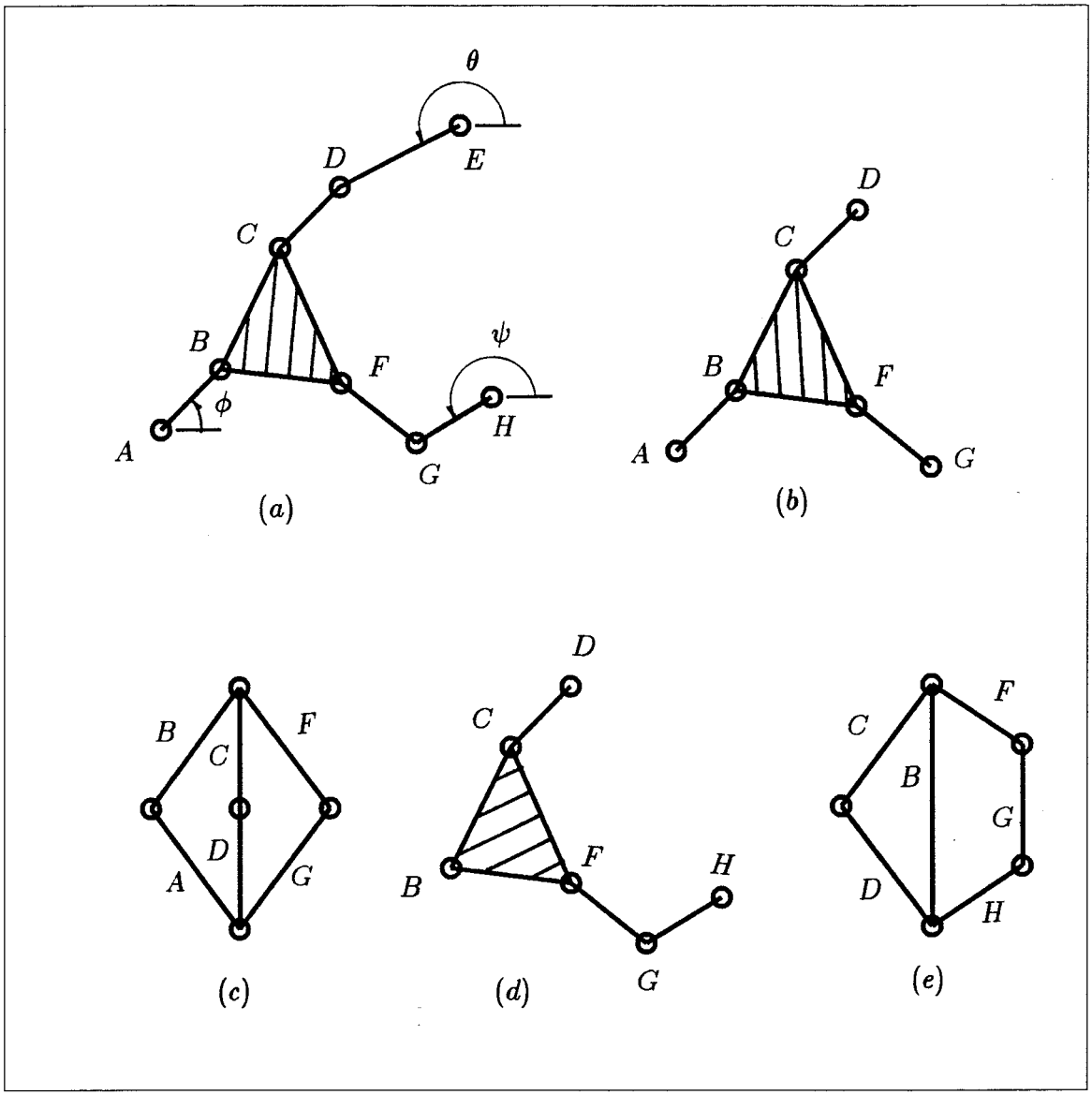

Figure 3.2 (*a*)Example of a 2 dof planar complex kinematic chain (*b*)non-powered subchain obtained when the actuated joint angles are θ and ψ (*c*)corresponding graph (*d*)non-powered subchain obtained when the actuated joint angles are θ and ϕ and (*e*)corresponding graph.

where l is the total number of degrees of freedom of the kinematic chain, n is the number of rigid bodies in the chain, g is the number of joints, and f_i is the number of degrees of freedom allowed by the ith joint.

However, this type of formulae are known to fail in cases such as the paradoxical kinematic chains (Hervé 1978). These exceptions arise when some special geometries are

present, as in the case of Bennett's (Bennett 1903) and Goldberg's mechanisms (Goldberg 1943), which are probably the best known examples. This suggests that general methods for the determination of the dof of kinematic chains should take into account their geometry as well as their topology (Eddie Baker 1980b, 1981; Davies 1981; Angeles 1987). The problem of finding the dof of complex kinematic chains, i.e., chains with multiple closed-loops, has also been addressed in this context (Eddie Baker 1980b, 1981; Davies 1981).

Using the results obtained on the topological description of complex kinematic chains, we will now derive a general method allowing us to determine the degree of freedom of any complex kinematic chain. It is assumed here that the graph associated with the complex kinematic chain has been obtained and that the independent loops have been identified, according to the procedure presented in Section 3.1.

The method developed here is an extension to complex kinematic chains, of the method described in (Angeles 1987), for simple closed kinematic chains. This method is based on the Jacobian matrix of the kinematic chain, a concept that is well known in the context of robot manipulators (Renaud 1980), and that was applied to closed kinematic chains in (Angeles 1987). It is interesting to notice that the idea of using the Jacobian matrix to find the degree-of-freedom of kinematic chains was first suggested in (Freudenstein 1962). The method developed in (Angeles 1987) will be recalled briefly here, for quick reference. It will then be formally extended to multiple closed-loop kinematic chains. An example of a linkage and two examples of parallel manipulators will be studied. These examples will bring about another interesting feature of the method, i.e., its ability to describe the singularities of multiple closed-loop manipulators.

3.2.1 Degree of Freedom of Simple Kinematic Chains

The method presented in (Angeles 1987) for the determination of the degree of freedom of simple kinematic chains can be summarized as follows:

Let a simple open kinematic chain be built with rotational (R) or prismatic (P)

pairs. As a matter of fact, screw (H), cylindrical (C), planar (E), and spherical (S) pairs can be synthesized as combinations of R and P pairs. Moreover, let this chain be constituted of (n+1) rigid bodies. The axis of the ith joint is defined by a point O_i on this axis and a unit vector $\mathbf{e}_i$ along this axis (Hartenberg and Denavit 1964). The motion of the $(i+1)$st rigid body with respect to the ith one is then defined by the rotation angle θ_i about this axis if the ith joint is rotational, or by the displacement s_i along this axis if the ith joint is prismatic.

In particular, the motion of the $(n+1)$st rigid body, called the end-effector, is described by the position vector $\mathbf{r}$ of one of its points P and by the orthogonal tensor $\mathbf{Q}$ giving its orientation. Velocities are then given by $\dot{\mathbf{r}}$ and ω, the angular velocity of the end-effector. If we denote by $\dot{\theta}$ the n-dimensional vector of joint rates and $\mathbf{t} = [\omega^T, \dot{\mathbf{r}}^T]^T$ as the 6-dimensional *twist* vector, then we can write:

$$\mathbf{J}\dot{\theta} = \mathbf{t} \tag{3.3}$$

where $\mathbf{J} = \mathbf{J}(\theta)$, the Jacobian matrix, is a function of the configuration of the chain. Matrix $\mathbf{J}$ is then defined as:

$$\mathbf{J} = \begin{bmatrix} \mathbf{e}_1 & \mathbf{e}_2 & \dots & \mathbf{e}_n \\ \mathbf{e}_1 \times \mathbf{r}_1 & \mathbf{e}_2 \times \mathbf{r}_2 & \dots & \mathbf{e}_n \times \mathbf{r}_n \end{bmatrix} \tag{3.4}$$

where $\mathbf{r}_i$ is the position vector of point P with respect to O_i. If the ith joint is prismatic, then the ith column of $\mathbf{J}$ is changed to: $\mathbf{c}_i = [\mathbf{0}^T, \mathbf{e}_i^T]^T$, where $\mathbf{0}$ is the 3-dimensional zero vector.

For simple closed kinematic chains, the end effector is coupled to the first link with a rotational or prismatic pair or a combination of these. The twist of the last link can then be written as:

$$\mathbf{t} = -\dot{\theta}_{n+1}\mathbf{c}_{n+1} \tag{3.5}$$

where $\mathbf{c}_{n+1}$ is defined similarly to $\mathbf{c}_i$. The vector of joint rates $\dot{\theta}$ can then be redefined as an $(n+1)$-dimensional vector having $\dot{\theta}_{n+1}$ as its last component. The Jacobian matrix is correspondingly redefined as an augmented $6 \times (n+1)$ matrix whose last column is $\mathbf{c}_{n+1}$. Equation (3.3) becomes:

$$\mathbf{J}\dot{\theta} = \mathbf{0} \tag{3.6}$$

The degree of freedom (l) of the chain is then equal to the dimension of the nullspace of **J**, i.e.:

$$l = \dim[\mathcal{N}(\mathbf{J})] \tag{3.7}$$

where $\mathcal{N}$ is the nullspace of **J**. The problem of finding the degree of freedom of a simple closed kinematic chain is then reduced to the determination of the dimension of the nullspace of a $6 \times (n+1)$ matrix, which is a common problem of numerical analysis. There are many ways of solving this problem. For instance, one can apply a Householder reflection technique to reduce the Jacobian matrix to a simpler form (Golub and Van Loan 1983), i.e.,

$$\mathbf{H}_r \ldots \mathbf{H}_1 \mathbf{J}^T = \begin{bmatrix} \mathbf{T} \\ \mathbf{0} \end{bmatrix} \tag{3.8}$$

where **T** is an $r \times 6$ matrix and **0** an $(n-r+1) \times 6$ zero matrix. Moreover, **T** is of the form $\mathbf{T} = [\mathbf{S}, \mathbf{U}]$ where **S** is an upper-triangular $r \times r$ matrix and **U** is an arbitrary $r \times (6-r)$ matrix, r being the rank of **J**.

The method described above has been successfully used in (Angeles 1987) for the determination of the degree of freedom of the Bennett mechanism which is a paradigm of mechanisms elusive to Chebychev-Grübler-Kutzbach formulae.

3.2.2 Extension to Complex Kinematic Chains

The extension of the method to complex kinematic chains is based essentially on the topological analysis of Section 3.1. Indeed, when all the independent loops of a complex kinematic chain have been found, the procedure described above is applied to each of these loops, which leads to:

$$\mathbf{J}_i \dot{\theta} = \mathbf{0}, \quad i = 1, \ldots, k \tag{3.9}$$

where k is recalled to be the number of independent loops and vector $\dot{\theta}$ includes all the joint rates of the whole chain. Joints which are not included in the ith loop will lead to a corresponding **0** column in the subjacobian matrix $\mathbf{J}_i$. It is also important, for consistency, to make sure that the positive direction of rotation around the axis (Hartenberg and Denavit

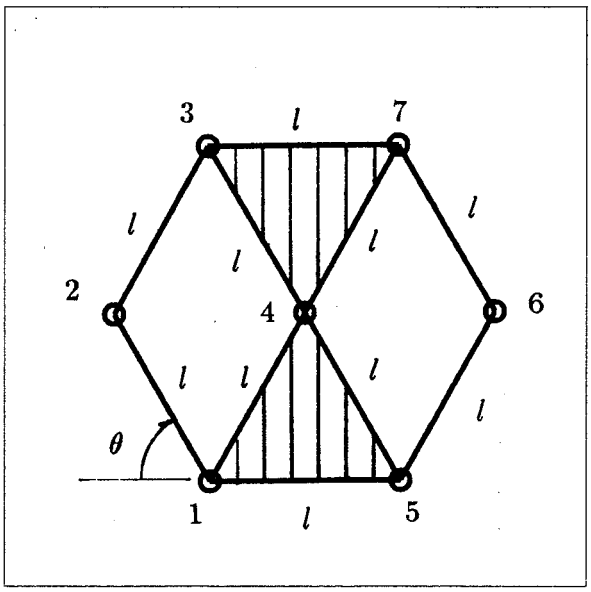

Figure 3.3 Special case of Watt's linkage, all link lengths are equal.

1964) of the ith joint be the same for each of the loops, i.e., that the definition of the joint rates is the same on each of the loops. The Jacobian matrix of the whole chain $\mathbf{J}$ can now be assembled as:

$$\mathbf{J} = \begin{bmatrix} \mathbf{J}_1 \\ \vdots \\ \mathbf{J}_k \end{bmatrix} \tag{3.10}$$

and hence, the kinematic joint-rate constraints of the overall chain can be written as

$$\mathbf{J}\dot{\theta} = \mathbf{0} \tag{3.11}$$

and hence

$$l = \dim(\mathcal{N}(\mathbf{J})) \tag{3.12}$$

i.e., the dof l of the complex kinematic chain is equal to the nullity of $\mathbf{J}$. This method will now be applied to the analysis of three different complex kinematic chains.

3.2.3 Examples

3.2.3.1 Application to Watt's Linkage

This linkage was described in Section 3.1 and a set of independent loops was identified in Fig. 3.1. The dimensions of the linkage considered here are shown in Fig. 3.3.

Since the topological analysis is already completed, we can directly apply the Jacobian method. The subjacobians will be 3×7 matrices for we have seven joints and the kinematic chain is planar. This is so because the angular velocity constraint leads to only one equation in a planar system, and the linear velocities are two-dimensional vectors. As a matter of fact, if we use complex numbers to denote the vectors in the plane, we have:

$$\mathbf{e} \times \mathbf{r}_i = e^{j\pi/2}\mathbf{r}_i \tag{3.13}$$

where $\mathbf{e} = [0, 0, 1]^T$ is a unit vector orthogonal to the plane and e is the basis of the natural logarithms. Therefore, if we denote the joints as in Fig. 3.3, we derive:

$$\mathbf{J}_1 = \begin{bmatrix} 1 & 1 & 1 & 1 & 0 & 0 & 0 \\ \mathbf{0}_2 & e^{j\pi/2}\mathbf{r}_2 & e^{j\pi/2}\mathbf{r}_3 & e^{j\pi/2}\mathbf{r}_4 & \mathbf{0}_2 & \mathbf{0}_2 & \mathbf{0}_2 \end{bmatrix} \tag{3.14a}$$

for the first loop and

$$\mathbf{J}_2 = \begin{bmatrix} 0 & 0 & 0 & 1 & 1 & 1 & 1 \\ \mathbf{0}_2 & \mathbf{0}_2 & \mathbf{0}_2 & e^{j\pi/2}\mathbf{r}'_4 & \mathbf{0}_2 & e^{j\pi/2}\mathbf{r}'_6 & e^{j\pi/2}\mathbf{r}'_7 \end{bmatrix} \tag{3.14b}$$

for the second loop, where $\mathbf{0}_2$ denotes the two-dimensional zero vector. The first row of the foregoing matrices arises from the angular velocity constraint—this is how the unity entries are obtained—and $\mathbf{r}_i$ and $\mathbf{r}'_i$ are the vectors connecting the ith joint to the 1st and 5th one respectively. These expressions can be rewritten in terms of angle θ (Fig. 3.3) as:

$$\mathbf{J}_1 = \begin{bmatrix} 1 & 1 & 1 & 1 & 0 & 0 & 0 \\ 0 & \sin\theta & (\sin\theta + \sqrt{3}/2) & \sqrt{3}/2 & 0 & 0 & 0 \\ 0 & \cos\theta & (\cos\theta - 1/2) & -1/2 & 0 & 0 & 0 \end{bmatrix} \tag{3.15a}$$

and

$$\mathbf{J}_2 = \begin{bmatrix} 0 & 0 & 0 & 1 & 1 & 1 & 1 \\ 0 & 0 & 0 & \sqrt{3}/2 & 0 & \sin(2\pi/3 - \theta) & [\sin(2\pi/3 - \theta) + \sqrt{3}/2] \\ 0 & 0 & 0 & 1/2 & 0 & -\cos(2\pi/3 - \theta) & [1/2 - \cos(2\pi/3 - \theta)] \end{bmatrix} \tag{3.15b}$$

The matrices can now be assembled as:

$$\mathbf{J} = \begin{bmatrix} \mathbf{J}_1 \\ \mathbf{J}_2 \end{bmatrix} \tag{3.16}$$

where the global Jacobian matrix $\mathbf{J}$ is of 6×7. Therefore, if $\mathbf{J}$ is of full rank, its nullity is of dimension 1 and the mechanism has a degree of freedom of 1, which is true in general. We

will now consider the link connecting joints 1 and 2 as the input link—the fixed link being the one connecting joints 1,4 and 5—and try to find configurations in which the mechanism would acquire an extra freedom. To this end, we will equate the joint rate corresponding to the input, i.e., $\dot{\theta}_1$, to zero. This can be accomplished by dropping the first column of **J**, which leads to:

$$\mathbf{J}' = \begin{bmatrix} 1 & 1 & 1 & 0 & 0 & 0 \\ \sin\theta & (\sin\theta + \sqrt{3}/2) & \sqrt{3}/2 & 0 & 0 & 0 \\ \cos\theta & (\cos\theta - 1/2) & -1/2 & 0 & 0 & 0 \\ 0 & 0 & 1 & 1 & 1 & 1 \\ 0 & 0 & \sqrt{3}/2 & 0 & \sin(2\pi/3 - \theta) & [\sin(2\pi/3 - \theta) + \sqrt{3}/2] \\ 0 & 0 & 1/2 & 0 & -\cos(2\pi/3 - \theta) & [1/2 - \cos(2\pi/3 - \theta)] \end{bmatrix} \tag{3.17}$$

The expansion of the determinant Δ of $\mathbf{J}'$ can then be reduced to:

$$\Delta = -\sin\theta\left(\frac{1}{2}\sin\theta + \frac{\sqrt{3}}{2}\cos\theta\right) \tag{3.18}$$

and the zeroing of this quantity leads to four solutions for θ, namely:

$$\theta = -\pi/3\,,\ 0\,,\ 2\pi/3\,,\ \pi \tag{3.19}$$

Each of these values of the input angle correspond to a configuration in which the linkage instantaneously acquires an extra degree of freedom, i.e., in which we can have a nonzero vector of joint rates even if the joint rate of the input is zero.

3.2.3.2 Planar Three-DOF Parallel Manipulator

A three-degree-of-freedom planar parallel manipulator is shown in Fig. 3.4. The three motors M_1, M_2 and M_3 are fixed and placed on the vertices of an equilateral triangle. Moreover, the corresponding link lengths on each of the legs are the same, i.e., the manipulator is symmetric. This manipulator will be studied in detail in Chapters 4 and 5, and the reader is referred to these chapters for a more detailed description of its characteristics.

In order to apply the method derived here to this manipulator, the associated graph has been drawn. This is shown in Fig. 3.5*a*. A spanning tree is shown in Fig. 3.5*b* and the associated independent loops are identified on Fig. 3.5*c*.

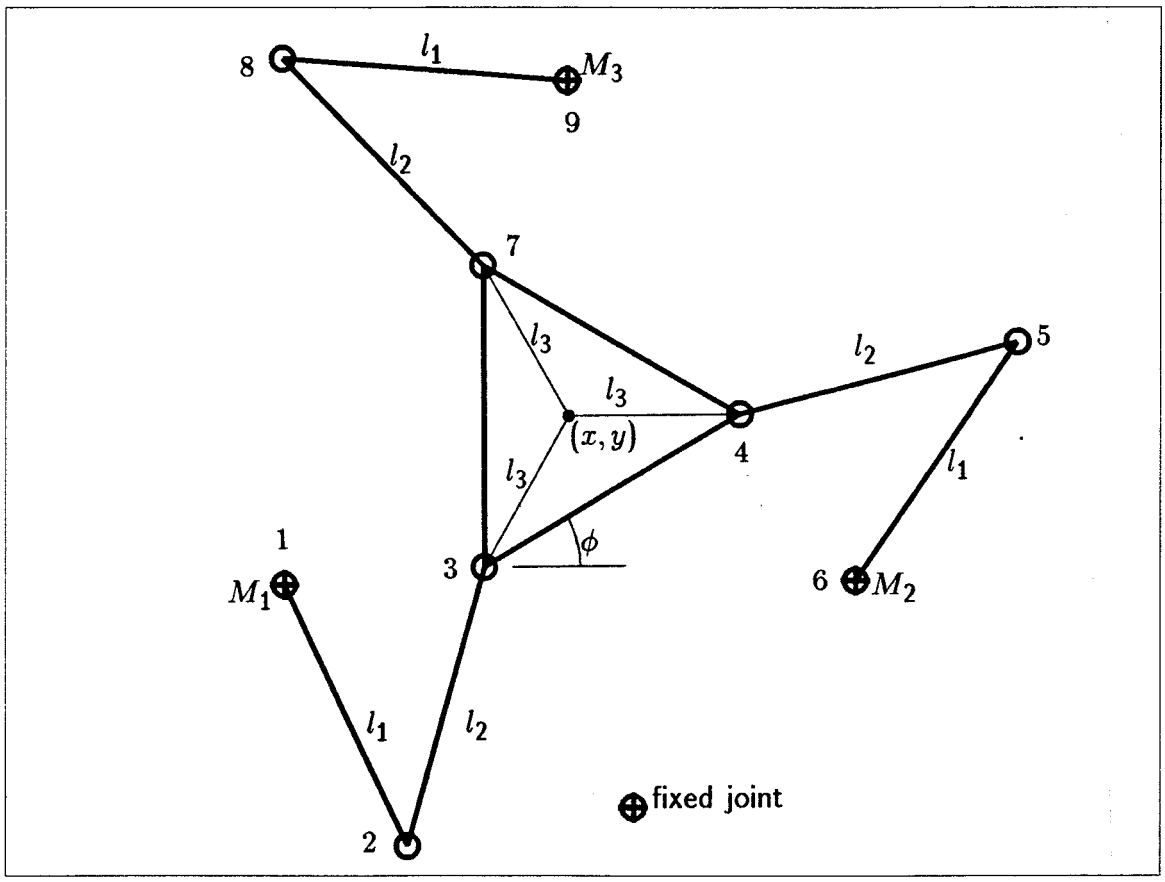

Figure 3.4 Planar three-degree-of-freedom parallel manipulator.

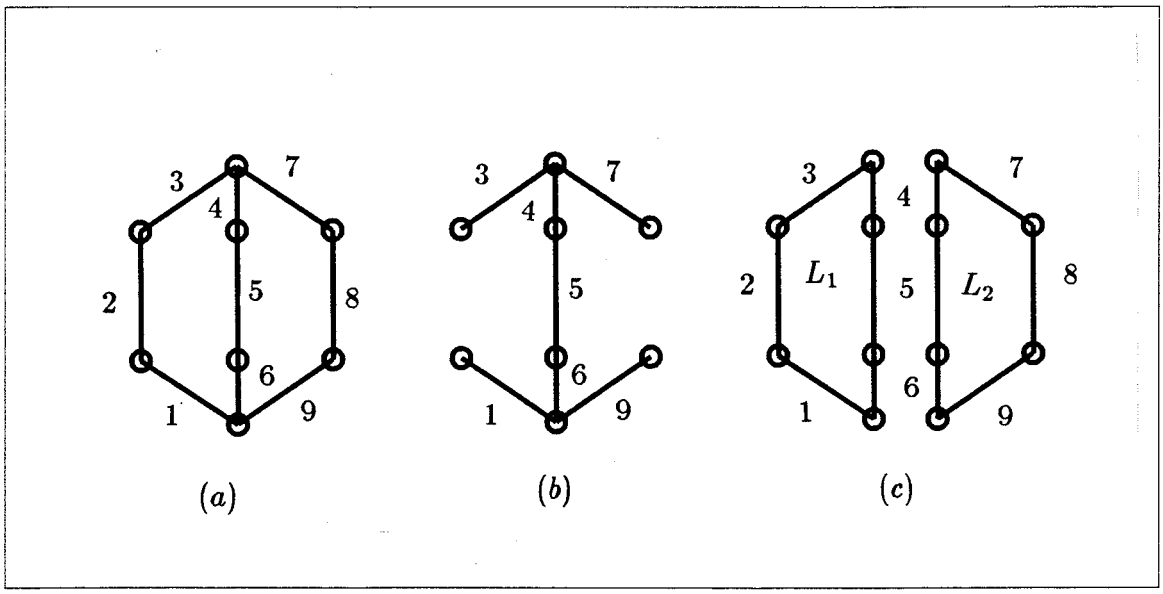

Figure 3.5 (*a*)Graph associated with the manipulator shown in Fig. 3.4 (*b*)a spanning tree and (*c*)the corresponding independent loops.

Since we have nine joints and the kinematic chain is, again, a planar chain, the subjacobians will be 3×9 matrices. If we use a notation identical to the one presented above, and if we denote the joints as indicated in Fig. 3.4, we derive:

$$\mathbf{J}_1 = \begin{bmatrix} 1 & 1 & 1 & 1 & 1 & 1 & 0 & 0 & 0 \\ e^{j\pi/2}\mathbf{r}_1 & e^{j\pi/2}\mathbf{r}_2 & e^{j\pi/2}\mathbf{r}_3 & e^{j\pi/2}\mathbf{r}_4 & e^{j\pi/2}\mathbf{r}_5 & \mathbf{0}_2 & \mathbf{0}_2 & \mathbf{0}_2 & \mathbf{0}_2 \end{bmatrix} \tag{3.20a}$$

and

$$\mathbf{J}_2 = \begin{bmatrix} 0 & 0 & 0 & 1 & 1 & 1 & 1 & 1 & 1 \\ \mathbf{0}_2 & \mathbf{0}_2 & \mathbf{0}_2 & e^{j\pi/2}\mathbf{r}'_4 & e^{j\pi/2}\mathbf{r}'_5 & e^{j\pi/2}\mathbf{r}'_6 & e^{j\pi/2}\mathbf{r}'_7 & e^{j\pi/2}\mathbf{r}'_8 & \mathbf{0}_2 \end{bmatrix} \tag{3.20b}$$

where, again, the first row of the subjacobian matrices arises from the angular velocity constraint and where $\mathbf{r}_i$ and $\mathbf{r}'_i$ are the two-dimensional vectors connecting the ith joint to the 6th and 9th one, respectively.

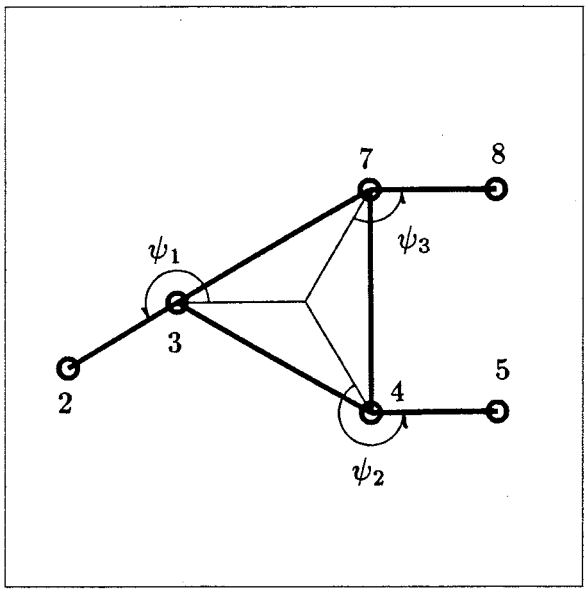

Figure 3.6 Definition of angles ψ_1, ψ_2 and ψ_3.

Moreover, angles ψ_1, ψ_2 and ψ_3 are defined as shown in Fig. 3.6, which leads to:

$$\mathbf{r}_1 = \begin{bmatrix} 1 \\ 0 \end{bmatrix} \tag{3.21a}$$

$$\mathbf{r}_2 = -\begin{bmatrix} x-1 \\ y \end{bmatrix} + l_3 \begin{bmatrix} \cos\phi_1 \\ \sin\phi_1 \end{bmatrix} - l_2 \begin{bmatrix} \cos(\phi_1+\psi_1) \\ \sin(\phi_1+\psi_1) \end{bmatrix} \tag{3.21b}$$

$$\mathbf{r}_3 = -\begin{bmatrix} x-1 \\ y \end{bmatrix} + l_3 \begin{bmatrix} \cos\phi_1 \\ \sin\phi_1 \end{bmatrix} \tag{3.21c}$$

$$\mathbf{r}_4 = -\begin{bmatrix} x-1 \\ y \end{bmatrix} + l_3 \begin{bmatrix} \cos\phi_2 \\ \sin\phi_2 \end{bmatrix} \tag{3.21d}$$

$$\mathbf{r}_5 = -\begin{bmatrix} x-1 \\ y \end{bmatrix} + l_3 \begin{bmatrix} \cos\phi_2 \\ \sin\phi_2 \end{bmatrix} - l_2 \begin{bmatrix} \cos(\phi_2+\psi_2) \\ \sin(\phi_2+\psi_2) \end{bmatrix} \tag{3.21e}$$

and

$$\mathbf{r}'_4 = -\begin{bmatrix} x-1/2 \\ y-\sqrt{3}/2 \end{bmatrix} + l_3 \begin{bmatrix} \cos\phi_2 \\ \sin\phi_2 \end{bmatrix} \tag{3.22a}$$

$$\mathbf{r}'_5 = -\begin{bmatrix} x-1/2 \\ y-\sqrt{3}/2 \end{bmatrix} + l_3 \begin{bmatrix} \cos\phi_2 \\ \sin\phi_2 \end{bmatrix} - l_2 \begin{bmatrix} \cos(\phi_2+\psi_2) \\ \sin(\phi_2+\psi_2) \end{bmatrix} \tag{3.22b}$$

$$\mathbf{r}'_6 = \begin{bmatrix} -1/2 \\ \sqrt{3}/2 \end{bmatrix} \tag{3.22c}$$

$$\mathbf{r}'_7 = -\begin{bmatrix} x-1/2 \\ y-\sqrt{3}/2 \end{bmatrix} + l_3 \begin{bmatrix} \cos\phi_3 \\ \sin\phi_3 \end{bmatrix} \tag{3.22d}$$

$$\mathbf{r}'_8 = -\begin{bmatrix} x-1/2 \\ y-\sqrt{3}/2 \end{bmatrix} + l_3 \begin{bmatrix} \cos\phi_3 \\ \sin\phi_3 \end{bmatrix} - l_2 \begin{bmatrix} \cos(\phi_3+\psi_3) \\ \sin(\phi_3+\psi_3) \end{bmatrix} \tag{3.22e}$$

where

$$\begin{aligned} \phi_1 &= \phi + \pi/6 \\ \phi_2 &= \phi + 5\pi/6 \\ \phi_3 &= \phi - \pi/2 \end{aligned} \tag{3.23}$$

angle ϕ being the angle defining the orientation of the gripper and x and y being the coordinates of the centroid of the gripper. Equations (3.20a) and (3.20b) lead to:

$$\mathbf{J} = \begin{bmatrix} 1 & 1 & 1 & 1 & 1 & 1 & 0 & 0 & 0 \\ 0 & -y_2 & -y_3 & -y_4 & -y_5 & 0 & 0 & 0 & 0 \\ 1 & x_2 & x_3 & x_4 & x_5 & 0 & 0 & 0 & 0 \\ 0 & 0 & 0 & 1 & 1 & 1 & 1 & 1 & 1 \\ 0 & 0 & 0 & -y'_4 & -y'_5 & -\sqrt{3}/2 & -y'_7 & -y'_8 & 0 \\ 0 & 0 & 0 & x'_4 & x'_5 & -1/2 & x'_7 & x'_8 & 0 \end{bmatrix} \tag{3.24}$$

where x_i, y_i and x'_i, y'_i are the x and y components of vectors $\mathbf{r}_i$ and $\mathbf{r}'_i$ respectively.

Since $\mathbf{J}$ is a 6×9 matrix, its nullity will be 3 if $\mathbf{J}$ is of full rank, i.e., the manipulator has, in general, three degrees of freedom. To analyze the singularities, we will set the rates of the powered joints to zero and see under which conditions the nullity of the reduced matrix can be greater than zero. It will become clear, in Section 3.3, that this type

of singularity corresponds to a singularity of the *second type* discussed in that section, i.e., a singularity for which the Cartesian rates of the gripper can be nonzero while the motor rates are zero. The zeroing of the motor rates can be accomplished here, by dropping the 1st, 6th and 9th columns of $\mathbf{J}$, which leads to:

$$\mathbf{J}' = \begin{bmatrix} 1 & 1 & 1 & 1 & 0 & 0 \\ -y_2 & -y_3 & -y_4 & -y_5 & 0 & 0 \\ x_2 & x_3 & x_4 & x_5 & 0 & 0 \\ 0 & 0 & 1 & 1 & 1 & 1 \\ 0 & 0 & -y'_4 & -y'_5 & -y'_7 & -y'_8 \\ 0 & 0 & x'_4 & x'_5 & x'_7 & x'_8 \end{bmatrix} \tag{3.25}$$

The foregoing Jacobian can be properly reduced by performing elementary operations on $\mathbf{J}'$—without affecting its rank—, which leads to:

$$\mathbf{J}' \sim \begin{bmatrix} 1 & 1 & 1 & 1 & 0 & 0 \\ 0 & (y_2 - y_3) & (y_2 - y_4) & (y_2 - y_5) & 0 & 0 \\ 0 & (x_2 - x_3) & (x_2 - x_4) & (x_2 - x_5) & 0 & 0 \\ 0 & 0 & 1 & 1 & 1 & 1 \\ 0 & 0 & 0 & (y'_4 - y'_5) & (y'_4 - y'_7) & (y'_4 - y'_8) \\ 0 & 0 & 0 & (x'_4 - x'_5) & (x'_4 - x'_7) & (x'_4 - x'_8) \end{bmatrix} \tag{3.26}$$

Substituting eqs.(3.21) and (3.22) in eq.(3.26) and expanding the determinant Δ will lead, after many simplifications, to the following:

$$\begin{aligned} \Delta \equiv \sin(2\pi/3 + \psi_3 - \psi 2)\,[\sin\psi_1 - \sin(\psi_1 - 2\pi/3)] \\ + \sin(\psi_1 - \psi_2 - 2\pi/3)\,[\sin(\psi_3 + 2\pi/3) - \sin\psi_3] \end{aligned} \tag{3.27}$$

which is next further reduced and set equal to zero as follows:

$$\Delta \equiv \sin(\psi_1 + \psi_2 + \psi_3) + 4\sin\psi_1 \sin\psi_2 \sin\psi_3 = 0 \tag{3.28}$$

There are two conditions under which this equation can be satisfied:

1. If $\psi_1 = \psi_2 = \psi_3 = n\pi$, $n = 0,1,2,\ldots$, then eq.(3.28) is obviously satisfied. This solution corresponds to configurations in which the secondary links of the three legs are concurrent. These links are defined as the ones joining the driving links to the gripper.

2. If $\psi_1 - \psi_2 = -\pi/3$ and $\psi_2 - \psi_3 = 2\pi/3$ then, substitution of these two equalities in eq.(3.28), leads to:

$$\sin(3\psi_1) + 4\sin^3\psi_1 - 3\sin\psi_1 = 0 \tag{3.29}$$

which is a trigonometric identity. This solution corresponds to the configurations for which the secondary links of the three legs are parallel.

These two conditions are exactly the same as the ones derived in (Hunt 1983) using screw theory; that is, the planar three-dof parallel manipulator is singular whenever its three secondary links are either concurrent or parallel. These results will also be confirmed in Chapter 4, where the singularities of the planar manipulator are analyzed following a different approach.

3.2.3.3 Spherical Three-DOF Parallel Manipulator

A spherical three-dof parallel manipulator is shown in Fig. 3.7. This manipulator will be studied in detail in Chapters 4 and 5. The three motors M_1, M_2 and M_3 are fixed and placed on the vertices of an equilateral triangle. Moreover, the manipulator is symmetric and all joint axes are concurrent. Furthermore, we denote by $\mathbf{u}_i$, $\mathbf{v}_i$ and $\mathbf{w}_i$ the unit vectors along the axis of the ith motor, the ith joint attached to the gripper and the ith intermediate joint, respectively.

The graph associated with this manipulator is identical to the one shown in Fig. 3.5a, and therefore, there are two independent loops. However, the linear velocity equations are irrelevant here since all the joint axes intersect and only the angular velocity constraints need to be considered. This leads to:

$$\mathbf{J}_1 = [\,\mathbf{u}_1 \quad \mathbf{w}_1 \quad \mathbf{v}_1 \quad \mathbf{u}_2 \quad \mathbf{w}_2 \quad \mathbf{v}_2 \quad \mathbf{0} \quad \mathbf{0} \quad \mathbf{0}\,] \tag{3.30a}$$

and

$$\mathbf{J}_2 = [\,\mathbf{0} \quad \mathbf{0} \quad \mathbf{0} \quad \mathbf{u}_2 \quad \mathbf{w}_2 \quad \mathbf{v}_2 \quad \mathbf{u}_3 \quad \mathbf{w}_3 \quad \mathbf{v}_3\,] \tag{3.30b}$$

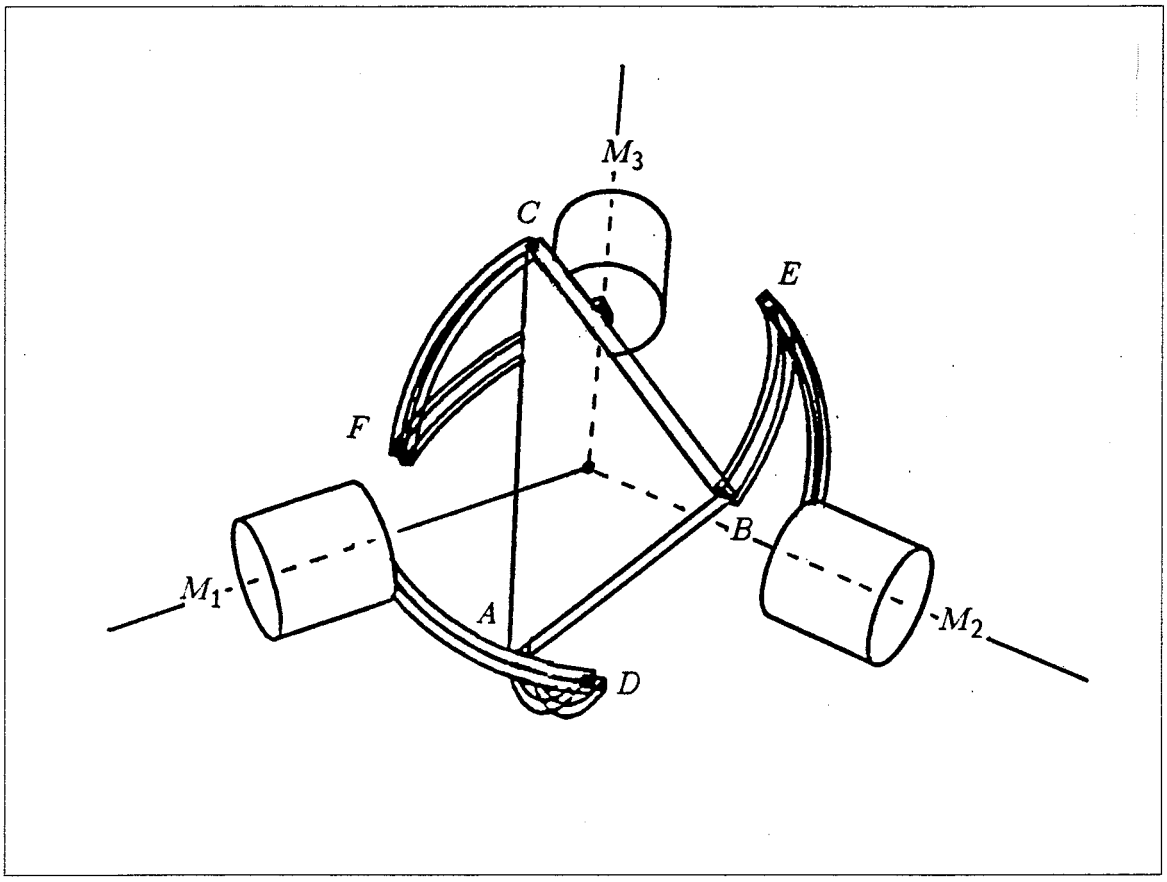

Figure 3.7 Spherical three-degree-of-freedom parallel manipulator.

These are next assembled as:

$$\mathbf{J} = \begin{bmatrix} \mathbf{J}_1 \\ \mathbf{J}_2 \end{bmatrix} \tag{3.31}$$

Again, matrix $\mathbf{J}$ is of 6×9, which means that, when it is of full rank, its nullity is 3 and the kinematic chain has three dof, as it should. To analyze the singularities, we set the motor rates to zero, as in the previous example, which leads to:

$$\mathbf{J}' = \begin{bmatrix} \mathbf{w}_1 & \mathbf{v}_1 & \mathbf{w}_2 & \mathbf{v}_2 & \mathbf{0} & \mathbf{0} \\ \mathbf{0} & \mathbf{0} & \mathbf{w}_2 & \mathbf{v}_2 & \mathbf{w}_3 & \mathbf{v}_3 \end{bmatrix} \tag{3.32}$$

and the condition under which $\det(\mathbf{J}')$ is equal to zero can be shown to be:

$$[(\mathbf{w}_1 \times \mathbf{v}_1) \times (\mathbf{w}_2 \times \mathbf{v}_2)] \cdot (\mathbf{w}_3 \times \mathbf{v}_3) = 0 \tag{3.33}$$

This result will be reproduced and interpreted in Chapter 4, where the singularities of the spherical parallel manipulator will be analyzed in detail following a different approach.

3.3 Singularities of Closed-Loop Kinematic Chains

The study of the kinematics of mechanical systems leads inevitably to the problem of singular configurations. These special configurations are defined as the ones in which the Jacobian matrix, i.e., the matrix relating the input rates to the output rates, becomes rank deficient. They correspond to configurations of the system that are usually undesirable since the degree of freedom is instantaneously changed. As a matter of fact, this is how the method presented in Section 3.2 allowed us to identify singular configurations. For serial manipulators, the singularity problem has been addressed by several authors, for instance: Sugimoto and Duffy (1982); Lai and Yang (1986); Litvin and Parenti Castelli (1985); Waldron et al. (1985); Litvin et al. (1985 & 1986); Hunt (1986 & 1987); Wang and Waldron (1987). Some researchers have also worked on the singularities of simple closed-loop kinematic chains (Eddie Baker 1980a; Sugimoto et al. 1982; Litvin at al. 1986 & 1987; Litvin and Tan 1987; Litvin and Fanghella 1987; Litvin and Wu 1987).

A singularity analysis for closed-loop kinematic chains is presented in this section. As demonstrated by the examples included here, this analysis is applicable to simple and complex closed-loop kinematic chains in general. The technique will be used in Chapter 4 for the singularity analysis of parallel manipulators.

3.3.1 Singularity Analysis

A complex kinematic chain consists of a set of rigid bodies connected to each other with joints and where the conditions specified in the first paragraph of this chapter are satisfied. The chain is also characterized by a set of inputs, denoted here by an n-dimensional vector θ, which correspond to the powered joints and by a set of output coordinates, denoted here by an m-dimensional vector $\mathbf{x}$. These input and output vectors depend on the nature and purpose of the kinematic chain. For instance, in a parallel manipulator, the input vector θ represents the set of actuated joints and the output vector $\mathbf{x}$ represents the Cartesian coordinates of the gripper. However, in general, the output does

not need to be a set of Cartesian coordinates and can also correspond to joint angles or displacements. Furthermore, although the number of inputs and outputs does not have to be equal, the number of independent inputs and outputs will always be the same and, therefore, vectors θ and $\mathbf{x}$ can be reduced or augmented to vectors of the same dimension which will be equal to the degree of freedom of the linkage. The input and output rates are then related through the Jacobian matrix of the chain as:

$$\dot{\theta} = \mathbf{J}\dot{\mathbf{x}} \tag{3.34}$$

As opposed to the convention used for serial manipulators, the Jacobian matrix is defined here as the one mapping the output rates into the input rates. The reason for that will become clear in Chapter 4. Moreover, eq.(3.34) can also be written as:

$$\dot{\mathbf{x}} = \mathbf{K}\dot{\theta} \tag{3.35}$$

where $\mathbf{K} = \mathbf{J}^{-1}$, $\mathbf{J}$ and $\mathbf{K}$ being configuration dependent.

As stated above, singularities occur in configurations where $\mathbf{J}$ is rank deficient. However, for general complex kinematic chains, a distinction can be made between three types of singularities which have different physical interpretations.

(i) The first type of singularity occurs when the following conditions are verified:

$$\det(\mathbf{K}) = 0 \tag{3.36a}$$

i.e

$$\det(\mathbf{J}) \rightarrow \infty \tag{3.36b}$$

The corresponding configuration is one in which the chain reaches either a boundary of its workspace, or an internal boundary limiting different subregions of the workspace where the number of solutions is not the same. In other words, this type of singularities consists of *the set of points where different branches of the inverse kinematic problem meet*, the inverse kinematic problem being understood here as the computation of the values of the input variables

from given values of the output variables. Since the nullity of $\mathbf{K}$ is nonzero, we can find a set of vectors $\dot{\theta}$ for which $\dot{\mathbf{x}}$ would be equal to zero and therefore some of the velocity vectors $\dot{\mathbf{x}}$ cannot be produced at the output. Typically, these would be velocities orthogonal to the boundary and directed towards the outside of the workspace.

(ii) The second type of singularity occurs when we have the following:

$$\det(\mathbf{J}) = 0 \tag{3.37a}$$

i.e.

$$\det(\mathbf{K}) \rightarrow \infty \tag{3.37b}$$

This corresponds to configurations in which the chain remains uncontrollable even when all the actuated joints are locked. As opposed to the first one, this type of singularity lies within the workspace of the chain and corresponds to *a point or set of points where different branches of the direct kinematic problem meet.* The direct kinematic problem is the one in which it is desired to obtain the values of the output variables from given values of the input variables. Since the nullspace of $\mathbf{J}$ is not empty, there exists a set of output rate vectors $\dot{\mathbf{x}}$ which will be mapped into the origin by $\mathbf{J}$, i.e., which will correspond to a velocity of zero of the input joints. The input rates are therefore not independent.

Both the first and second types of singularities correspond to *configurations* that can happen in a general complex kinematic chain.

(iii) The third type of singularity is of a slightly different nature than the first two, since it requires conditions on the linkage parameters. Indeed, if some specific conditions on the linkage parameters are satisfied, the chain can reach configurations where the first two types of singularities meet and the Jacobian matrix then becomes indeterminate. This corresponds to configurations in which the chain can undergo finite motions when its actuators are locked or in which a

finite motion of the inputs produces no motion of the outputs such as, for instance, a linkage having a constant branch (Russell 1988). For linkages having a quadratic input-output equation, the third type of singularity also corresponds to a case for which all three coefficients of the quadratic are equal to zero.

The three types of singularities will now be illustrated with some examples of closed-loop simple and complex kinematic chains.

3.3.2 Example 1: Planar *RRRP* Mechanism

A planar *RRRP* mechanism is shown in Fig. 3.8. This one-degree-of-freedom mechanism is often referred to as a crank-slider four-bar linkage. The crank angle θ is the input variable and the displacement of the slider, denoted as x, is the output.

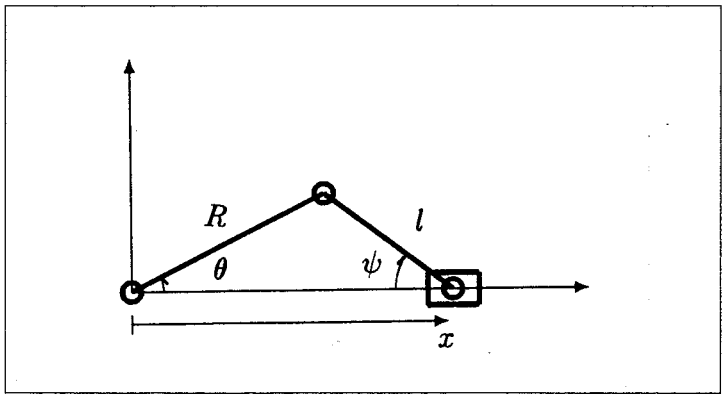

Figure 3.8 Planar *RRRP* mechanism.

Therefore, in this case, the Jacobian is a 1×1 matrix, i.e., a scalar, and will be denoted as J or K. From the geometry of the linkage, we can write:

$$x = R\cos\theta + l\cos\psi \tag{3.38a}$$

and

$$R\sin\theta = l\sin\psi \tag{3.38b}$$

substitution of eq.(3.38b) into eq.(3.38a) leads to:

$$x = R\cos\theta \pm l\sqrt{1 - r^2\sin^2\theta} \tag{3.39a}$$

where

$$r \equiv \frac{R}{l} \tag{3.39b}$$

and where the double sign arises from the fact that the direct kinematic problem has two branches. Upon differentiation with respect to time of eq.(3.39a), one obtains:

$$\dot{x} = K\dot{\theta} \tag{3.40a}$$

where

$$K = -R\left[\sin\theta \pm \frac{r\sin\theta\cos\theta}{\sqrt{1 - r^2\sin^2\theta}}\right] \tag{3.40b}$$

Therefore, the first type of singularity arises when $K = 0$, i.e., when $\theta = 0$ or π. In this configuration, eq.(3.39a) becomes:

$$x = \pm R \pm l \tag{3.41a}$$

and the links of length R and l are aligned, which corresponds to the limit of the workspace. Since K is equal to zero, the value of $\dot{x}$ will be equal to zero, whatever the value of $\dot{\theta}$ is.

The second type of singularity occurs when $J = 0$, i.e., when the denominator of K goes to zero. This condition leads to:

$$\sin\theta = \frac{l}{R} \tag{3.41b}$$

The corresponding configuration is shown in Fig. 3.9. This configuration is clearly within the range of motion of the output, i.e., within the workspace. Moreover, since the second term of eq.(3.39a) vanishes, the two branches of the direct kinematic problem meet. The output can undergo infinitesimal motion even if the input is locked.

As stated above, the third type of singularity requires that certain conditions on the linkage parameters be satisfied. For the example treated here, the condition is that the input and coupler links have the same length, i.e.,

$$R = l \tag{3.42}$$

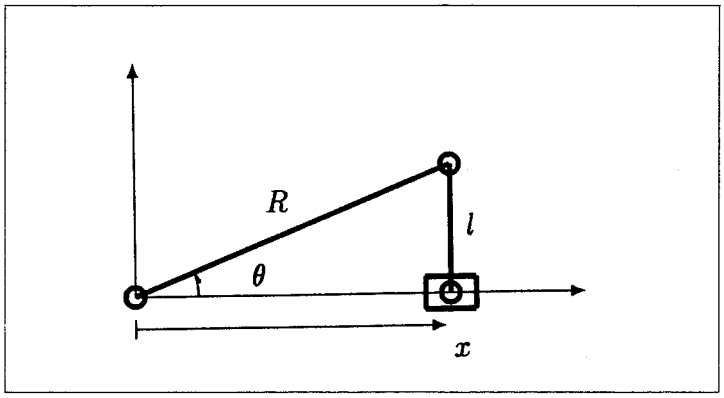

Figure 3.9 Second type of singularity for the planar *RRRP* mechanism.

Under this assumption, eq.(3.39a) can be rewritten as:

$$x = R\cos\theta \pm R\cos\theta \tag{3.43a}$$

or

$$x = \begin{cases} 0 \\ 2R\cos\theta \end{cases} \tag{3.43b}$$

which clearly shows that the mechanism has a constant branch. Therefore, when x is equal to zero, the input can undergo arbitrary rotations while the output remains at rest.

3.3.3 Example 2: Watt's Linkage

A linkage of this type is shown in Fig. 3.10. The link lengths used here are slightly more general than the ones used in Section 3.2. The mechanism has one degree of freedom, and the input and output variables are angles θ and ϕ, respectively. Again, the Jacobian is a scalar quantity.

From the geometry of the linkage, we can write:

$$x_1 = -\cos(\psi + \pi/3) \tag{3.44}$$

and

$$y_1 = \frac{\sqrt{3}}{2} + \sin(\psi + \pi/3) \tag{3.45}$$

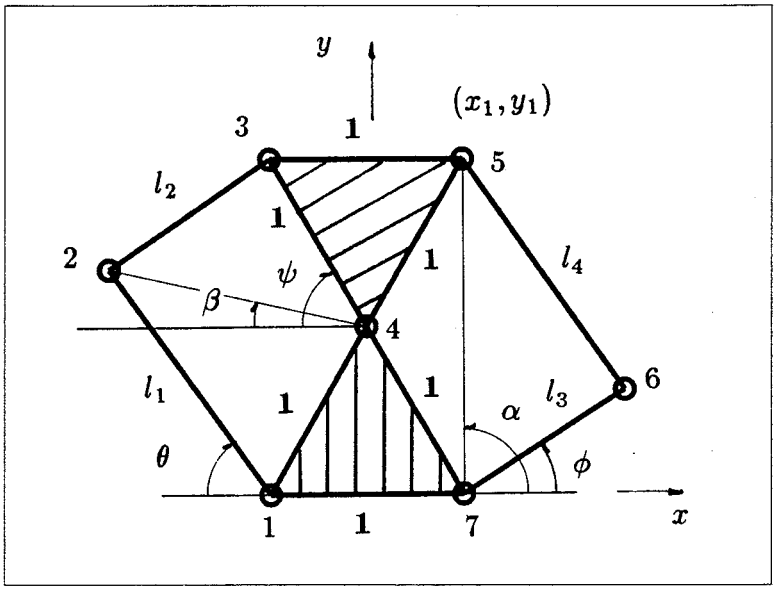

Figure 3.10 Watt's linkage.

and also:

$$\alpha = \tan^{-1}\left(\frac{y_1}{x_1'}\right) \tag{3.46a}$$

where

$$x_1' = x_1 - 1/2 \tag{3.46b}$$

and

$$\beta = \tan^{-1}\left(\frac{l_1 \sin\theta - \sqrt{3}/2}{l_1 \cos\theta + 1/2}\right) \tag{3.47}$$

Moreover, using the *law* of cosines, we obtain:

$$l_4^2 = l_3^2 + {x_1'}^2 + y_1^2 - 2l_3\sqrt{{x_1'}^2 + y_1^2}\cos(\alpha - \phi) \tag{3.48}$$

and

$$\begin{aligned} l_2^2 =& 1 + (l_1\cos\theta + 1/2)^2 + (l_1\sin\theta - \sqrt{3}/2)^2 \\ & - 2\sqrt{(l_1\cos\theta + 1/2)^2 + (l_1\sin\theta - \sqrt{3}/2)^2}\cos(\psi - \beta) \end{aligned} \tag{3.49}$$

Given a certain value of the input angle θ, angle ψ can be computed from eqs.(3.47) and (3.49) and then angle ϕ is obtained from eqs.(3.46) and (3.48). Upon differentiation of these equations with respect to time, the following is obtained:

$$\dot{\psi} = \dot{\beta} + \left[\frac{(\sqrt{3}l_1\sin\theta - l_1\cos\theta - l_1^2)(-1/2l_1\sin\theta - \sqrt{3}/2l_1\cos\theta)}{2\sin(\psi - \beta)[(1/2 + l_1\cos\theta)^2 + (l_1\sin\theta - \sqrt{3}/2)^2]^{3/2}}\right]\dot{\theta} \tag{3.50a}$$

where

$$\dot{\beta} = \left[\frac{l_1^2 + 1/2 l_1 \cos\theta - \sqrt{3}/2 l_1 \sin\theta}{(l_1 \cos\theta + 1/2)^2 + (l_1 \sin\theta - \sqrt{3}/2)^2} \right] \dot{\theta} \tag{3.50b}$$

and

$$\dot{\phi} = \dot{\alpha} + \frac{({x'_1}^2 + y_1^2 + l_4^2 - l_3^2)(x'_1 \dot{x}_1 + y_1 \dot{y}_1)}{2 l_3 \sin(\alpha - \phi)({x'_1}^2 + y_1^2)^{3/2}} \tag{3.51a}$$

where

$$\dot{\alpha} = \frac{x'_1 \dot{y}_1 - y_1 \dot{x}_1}{{x'_1}^2 + y_1^2} \tag{3.51b}$$

Therefore, the relation between the input and output velocities can be written as:

$$\dot{\phi} = K \dot{\theta} \tag{3.52}$$

where

$$K = \frac{N_1 N_2}{D_1 D_2} \tag{3.53a}$$

and

$$\begin{aligned} N_1 =& (l_1 \cos\theta - \sqrt{3} l_1 \sin\theta + l_1^2 + l_2^2)(1/2 l_1 \sin\theta + \sqrt{3}/2 l_1 \cos\theta) \\ &+ 2 \sin(\psi - \beta)(l_1^2 + 1/2 l_1 \cos\theta - \sqrt{2}/2 l_1 \sin\theta) \\ &\times \sqrt{1 - \sqrt{3} l_1 \sin\theta + l_1 \cos\theta + l_1^2} \end{aligned} \tag{3.53b}$$

$$N_2 = -\sin\psi({x'_1}^2 + y_1^2 + l_4^2 - l_3^2) - 2 l_3 \sin(\alpha - \phi)(1 + \cos\psi)\sqrt{{x'_1}^2 + y_1^2} \tag{3.53c}$$

$$D_1 = 2 \sin(\psi - \beta)(1 - \sqrt{3} l_1 \sin\theta + l_1 \cos\theta + l_1^2)^{3/2} \tag{3.53d}$$

$$D_2 = 2 l_3 \sin(\alpha - \phi)({x'_1}^2 + y_1^2)^{3/2} \tag{3.53e}$$

The first type of singularity occurs when $K = 0$, i.e., when

$$N_1 = 0 \qquad \text{or} \qquad N_2 = 0 \tag{3.54}$$

The first condition corresponds to the set of configurations in which links l_1 and l_2 are aligned, which clearly defines a boundary of the workspace. The second condition corresponds to configurations where link l_4 is aligned with the line connecting joints 4 and 5, which again defines a limit position of the output link. In these configurations, the velocity of the output is always zero, whatever the input velocity is.

The second type of singularity, i.e., the one in which the velocity of the output link can be nonzero even if the input velocity vanishes, occurs here when the denominator of K is equal to zero, i.e.:

$$D_1 = 0 \qquad \text{or} \qquad D_2 = 0 \tag{3.55}$$

The first condition can be rewritten as:

$$\sin(\psi - \beta) = 0 \tag{3.56}$$

which corresponds to configurations in which link l_2 is aligned with the line connecting joints 3 and 4. This type of configuration is shown in Fig. 3.11, where it is clear that the output link can undergo an infinitesimal motion even if the input is locked. The second condition can, in turn, be rewritten as:

$$\sin(\alpha - \phi) = 0 \tag{3.57}$$

which corresponds to configurations in which links l_3 and l_4 are aligned.

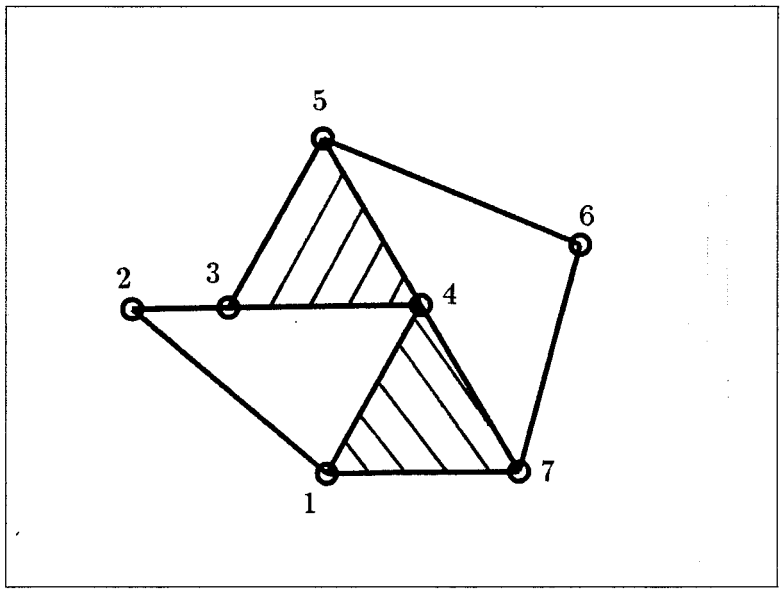

Figure 3.11 Second type of singularity for Watt's linkage.

The conditions on the link lengths required for the third type of singularity are given by the following:

$$l_1 = l_2 = 1 \qquad \text{or} \qquad l_3 = l_4 = 1 \tag{3.58}$$

When the first equality above is verified, the mechanism can reach configurations where joints 2 and 4 are superimposed, and the output can then undergo finite motions while the input is at rest. As a matter of fact, since links l_1 and l_2 are aligned with the lines connecting joints 1 and 4 and joints 3 and 4 respectively, they become kinematically irrelevant and the whole linkage is reduced to a four-bar planar linkage.

On the other hand, if the second equality of eq.(3.58) is verified, the mechanism can reach configurations where joints 4 and 6 are superimposed. In this case, links l_3 and l_4 become irrelevant and the linkage has a constant branch, i.e., a branch on which the output link remains at rest.

3.4 Characteristics of Parallel Manipulators

The purpose of this section is to introduce parallel manipulators as a subset of complex kinematic chains and to derive their characteristics.

First of all, the graph representation of parallel manipulators is always of the type shown in Fig. 3.5*a*. The graph is composed of a set of parallel paths connecting two *poles*, the poles being the base link and the gripper. Therefore, these two links are the only ones having a degree of connectivity greater than or equal to three. The number of joints in each of the parallel paths and the number of paths can vary.

Moreover, for the general case of a spatial manipulator, the number of loops can be related to the degree of freedom using the general mobility criterion (eq. 3.9) as:

$$l = 6(1 + pn) - 5p(n + 1) \tag{3.59}$$

where l is the number of degrees of freedom of the manipulator, n is the number of rigid bodies per leg of the manipulator disregarding the base and the end-effector and assuming that each joint has only one dof, and p is the number of legs, which corresponds to the number of paths connecting the two poles of the graph. Moreover, if we want to have a

fully parallel manipulator, i.e., one in which all the motors can be fixed to the ground, we need to have only one motor per leg, which leads to the following condition:

$$l = p \tag{3.60}$$

By substitution of eq.(3.60) in eq.(3.59), an equality describing all spatial fully parallel manipulators is obtained. This is expressed as:

$$p(n-6) = -6 \tag{3.61}$$

The solutions of this equation that are physically meaningful, i.e., the ones that correspond to feasible manipulators, are shown in Fig. 3.12. Point A is associated with the well known six-degree-of-freedom parallel device referred to as the Stewart platform (Stewart 1965). Point B, in turn, corresponds to a three-degree-of-freedom manipulator such as, for instance, the parallel part of the *ARTISAN* manipulator studied in Chapter 4. Point C is associated with a two-degree-of-freedom simple closed kinematic chain.

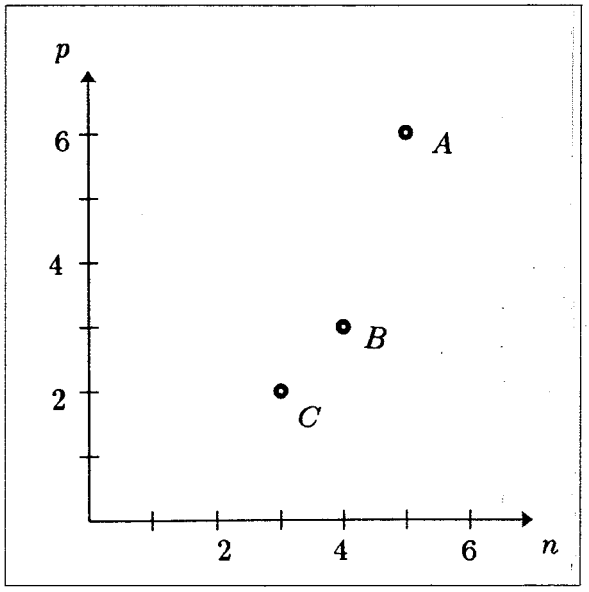

Figure 3.12 Spatial fully-parallel manipulators.

Although this thesis is devoted to the study of fully parallel manipulators, it is worth mentioning here that some researchers have proposed partially parallel structures for manipulators. Earl and Rooney (1983) have presented a topological investigation that

considers all these possibilities. In order to characterize the kinematic structure of such manipulators, the following index is now defined:

$$d = \frac{k}{l-1} \tag{3.62a}$$

with

$$0 \leq d \leq 1 \tag{3.62b}$$

where d is called the *degree of parallelism* of the manipulator, k is recalled to be the number of independent loops in the manipulator's graph, and l is the degree of freedom of the manipulator. The application of this criterion to a fully parallel manipulator gives a degree of parallelism of 1, whereas a degree of parallelism of zero is obtained for a serial manipulator. Intermediate architectures will give other results. For instance, the manipulator discussed in (Bajpai and Roth 1986) gives a degree of parallelism of 50% when the foregoing criterion is used. The index has a singularity when the degree of freedom of the chain is equal to one, in which case the value of d is one if there is at least one loop and zero otherwise.

Chapter 4 ANALYSIS OF PARALLEL MANIPULATORS

Some planar, spherical and spatial manipulators are introduced in this chapter. They all satisfy the definition given in Chapter 3, i.e., they all have a degree of parallelism of one. As pointed out in Chapter 1, the advantages of parallel manipulators make them suitable for many potential applications. However, since their structure is fundamentally different from the usual serial architecture, it is required that a detailed kinematic analysis be pursued. This analysis will allow us to obtain the equations constraining their motion, which include solutions to the *direct* and *inverse* kinematic problems as well as *velocity* and *acceleration inversions*. These results are of a primary importance for the control and trajectory planning of the manipulators. Moreover, the derivation of the Jacobian and the investigation of singularities presented here will be used in Chapter 5 for the optimization of the kinematic parameters of the manipulators.

As in the case of serial manipulators, the direct kinematic problem is defined here as the one in which the Cartesian coordinates of the gripper are obtained from the powered-joint angles. The inverse kinematic problem is therefore the one in which the powered-joint angles are computed from the Cartesian coordinates of the gripper. It is pointed out that the degree of difficulty involved in finding a solution to the direct kinematic problem of parallel manipulators differs from the one involved in the solution of the same problem for *corresponding serial manipulators*. The term *corresponding serial manipulator* used here refers to a serial manipulator having a kinematic structure identical to one of the legs of a given parallel manipulator. Therefore, the degree of difficulty involved in finding a solution

to the inverse kinematic problem of corresponding parallel and serial manipulators is the same, with the difference that, in the case of the parallel manipulator, only one joint angle per leg is needed and that the solution has to be repeated for each of the legs. However, the degree of difficulty involved in finding a solution to the direct kinematic problem of a parallel manipulator is much higher than for a corresponding serial manipulator. As a matter of fact, the solution of the direct kinematic problem for serial manipulators is straightforward since it amounts to a series of matrix multiplications and vector additions, whereas the solution of the same problem for the corresponding parallel manipulators usually requires the utilization of a numerical method, closed-form solutions being impossible to obtain. This is so because the graph representation of their non-powered subchain is usually symmetric and the gripper cannot be related directly to the fixed link of this subchain by any of the legs. Therefore, for parallel manipulators, the solution of the direct problem is, in general, not unique and both the inverse and the direct problems lead to multiple branches.

The velocity inversion gives the relationship between powered-joint rates and Cartesian rates of the manipulator's gripper and the acceleration inversion relates the corresponding accelerations. The Jacobian matrix derived for the velocity inversion is used in the singularity analysis and the results obtained are shown to be in agreement with those presented in Section 3.2.

4.1 Planar Three-Degree-of-Freedom Manipulator with Revolute Actuators

A planar parallel manipulator is represented in Fig. 4.1, all of whose joints are of the revolute type, and the three motors M_1, M_2, M_3 are fixed. The manipulator consists of a kinematic chain with three closed loops, namely M_1DABEM_2, M_2EBCFM_3, and M_3FCADM_1, the gripper being rigidly attached to triangle ABC. It is pointed out again here that only two of the aforementioned loops are kinematically independent according to the definition given in Chapter 3. This is clearly seen from the associated graph which was shown in Fig. 3.5a.

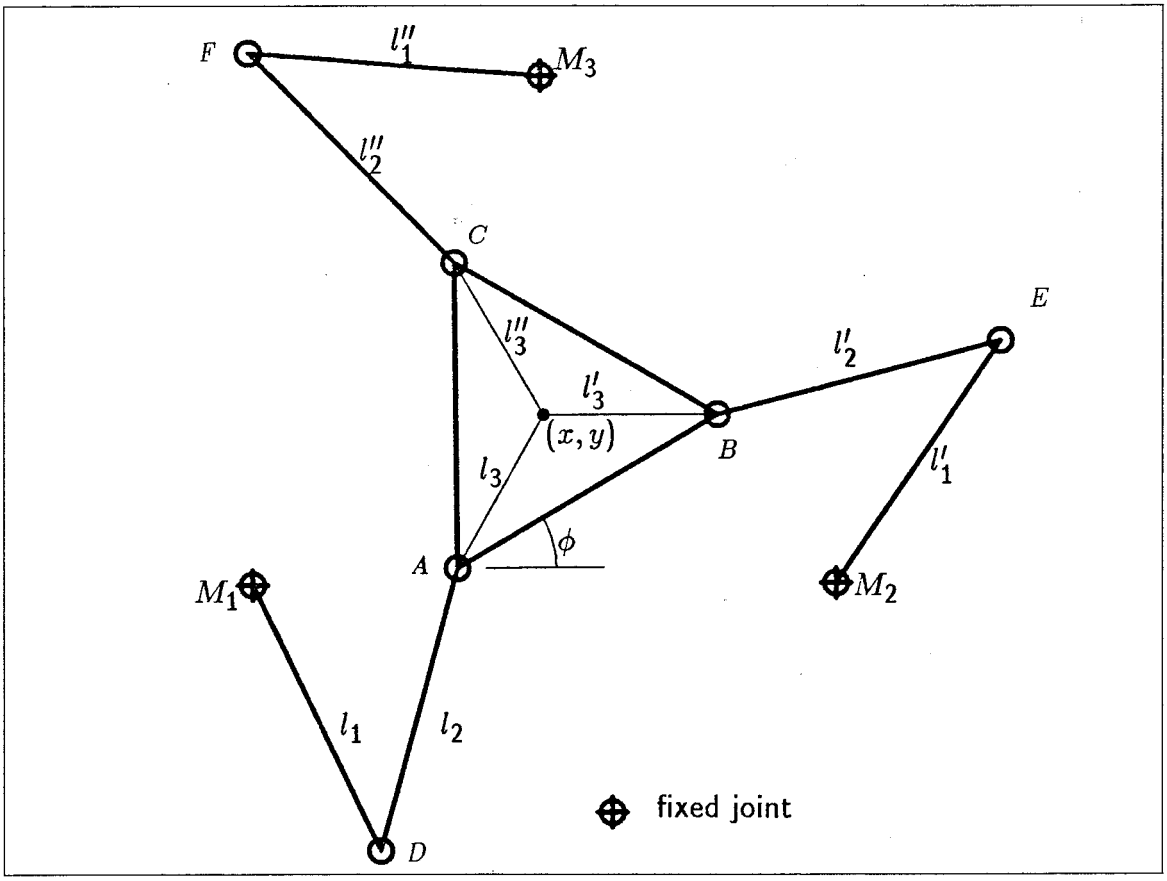

Figure 4.1 Planar three-degree-of-freedom parallel manipulator with revolute actuators.

Unlike the case of a mechanism, which, most of the time, is designed for a specific task, the tasks to be performed by a manipulator are unknown and unpredictable *a priori*. As a matter of fact, the manipulator studied here will be asked to arbitrarily position and orient the gripper in the plane of motion, following a certain trajectory that will be task dependent. Hence, there should not be any preferred general orientation for which the manipulator would have better properties. This suggests that the manipulator should be *symmetric*. Therefore, the motors will be located on the vertices of an equilateral triangle and the link lengths will be the same for each leg, i.e.,

$$l_i = l_i' = l_i'', \quad i = 1, 2, 3 \tag{4.1}$$

This assumption will be used throughout. Moreover, in what follows, the distance between any two of the motors will be set equal to unity, for normalization purposes.

Triangle ABC will be referred to as *the gripper*, for it is kinematically equivalent to this. It could be referred to as the end-effector, as well, but due to the kinematic structure involved, the gripper is not an end link.

The potential applications of this manipulator include pick-and-place operations over a plane surface, machining of plane surfaces, mobile base for a spatial manipulator and moving platform for a terrestrial vehicle simulator.

4.1.1 Inverse Kinematic Problem

As stated above, the manipulator aims at guiding the gripper through a certain trajectory in the Cartesian space, the Cartesian coordinates of the gripper being given by the position of its centroid $C(x,y)$ and the angle ϕ defining its orientation (Fig. 4.1). The inverse kinematic problem, therefore, consists of determining θ_1, θ_2 and θ_3 for given values of x, y and ϕ. It can be readily shown that the solution to this problem contains eight different branches. In fact, the solutions for the input angles θ_1, θ_2 and θ_3 are uncoupled and, moreover, the solution to each of these angles can be obtained from the input-output equation of a planar four-bar linkage for each leg, thus giving rise to a quadratic input-output equation, which thus contains two solutions, as shown, e.g., in (Angeles and Bernier 1987a). For instance, the solution for the first leg is shown in Fig. 4.2. In this figure, when the Cartesian coordinates (x,y,ϕ) are specified, we can consider the chain $CADM_1$ as a four-bar linkage for which the position of the input link, l_3, is given. Angle θ_1 can therefore be computed using the input-output equation mentioned above.

The same reasoning can be applied to each of the legs and a general solution is given here, for leg i, by:

$$\theta_i = \alpha_i \pm \psi_i, \quad i = 1,2,3 \tag{4.2}$$

where

$$\alpha_i = \text{atan2}(x_{2i}, y_{2i}) \tag{4.3}$$

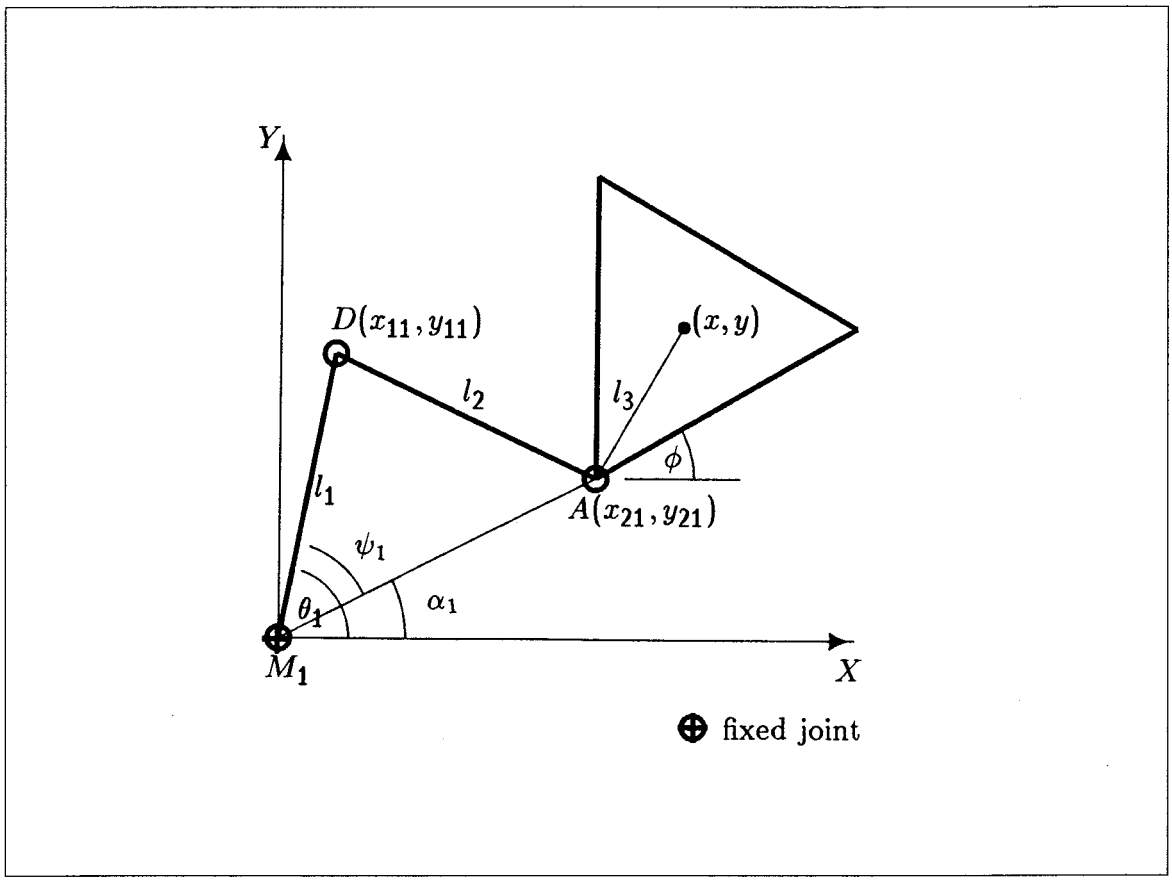

Figure 4.2 Analysis of the first leg.

and

$$\psi_i = \cos^{-1}\left[\frac{l_1^2 - l_2^2 + x_{2i}^2 + y_{2i}^2}{2l_1\sqrt{x_{2i}^2 + y_{2i}^2}}\right] \tag{4.4}$$

angle ψ_i being chosen on the main branch of the inverse cosine function, i.e., $0 \leq \psi_i \leq \pi$. Moreover, coordinates x_{2i} and y_{2i} are defined as:

$$x_{2i} = x - l_3 \cos\phi_i - x_{oi} \tag{4.5a}$$

$$y_{2i} = y - l_3 \sin\phi_i - y_{oi} \tag{4.5b}$$

whereas angles $\{\phi_i\}_1^3$ are given by

$$\phi_1 = \phi + \pi/6 \tag{4.6a}$$

$$\phi_2 = \phi + 5\pi/6 \tag{4.6b}$$

$$\phi_3 = \phi - \pi/2 \tag{4.6c}$$

and

$$\{x_{oi}\}_1^3 = \{0, 1, 1/2\} \tag{4.7a}$$

$$\{y_{oi}\}_1^3 = \{0, 0, \sqrt{3}/2\} \tag{4.7b}$$

are the positions of the centres of the motors. This completes the solution of the inverse kinematic problem.

4.1.2 Direct Kinematic Problem

As pointed out in the introduction of this chapter, the direct kinematic problem for parallel manipulators is more involved than the inverse problem. Indeed, even for the simple three-degree-of-freedom planar manipulator discussed here, no closed-form solution can be found. However, the following theorem was shown in (Hunt 1983):

Theorem 4.1: *The solution of the direct kinematic problem for the planar three-degree-of-freedom parallel manipulator leads to a maximum of 6 different branches.*

Proof: This result is obtained with the following reasoning: referring to Fig. 4.1, if the three input angles—i.e., the powered-joint angles—are specified, then the positions of points D, E and F are readily computed. Moreover, we can think of the chain $DABE$ as a four-bar linkage of which C is a point of the coupler link, generating a coupler curve. A solution for the closure of the whole kinematic chain (manipulator) is obtained whenever the coupler curve described by the motion of point C intersects the circle defined by the rotation of link FC around point F. Since the equation of the general coupler curve of a planar four-bar linkage—also called the tricircular sextic—is of the sixth degree (Hartenberg and Denavit 1964), the intersection of this curve with a circle has a maximum of six solutions, and hence, the direct kinematic problem of the planar three-degree-of-freedom manipulator has a maximum of six solutions, and the proof is completed.

The foregoing principle is now used to derive the equations that will lead to a simple formulation of the direct kinematic problem which is suitable for a numerical

solution. The notation used here is similar to the one used in (Ma and Angeles 1987). The four-bar linkage considered is shown in Fig. 4.3.

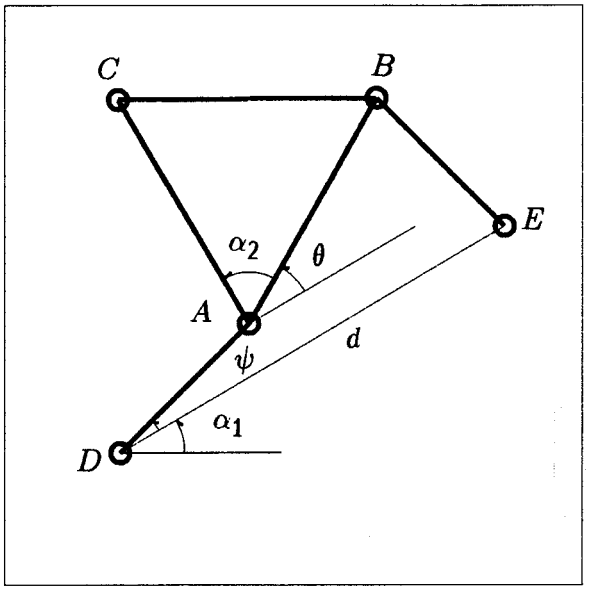

Figure 4.3 Planar four-bar linkage.

The position of point C of the coupler can be written as:

$$x_C = x_D + l_2 \cos(\alpha_1 + \psi) + \sqrt{3} l_3 \cos(\alpha_1 + \alpha_2 + \theta) \tag{4.8a}$$

$$y_C = y_D + l_2 \sin(\alpha_1 + \psi) + \sqrt{3} l_3 \sin(\alpha_1 + \alpha_2 + \theta) \tag{4.8b}$$

where

$$\alpha_2 = \pi/3 \tag{4.9}$$

$$\alpha_1 = \text{atan2}\left[\frac{y_E - y_D}{x_E - x_D}\right] \tag{4.10}$$

and

$$\theta_{1,2} = 2\tan^{-1}\left[\frac{B \pm \sqrt{B^2 - AC}}{A}\right] \tag{4.11}$$

with

$$A = m_1 - m_2 + (1 + m_3)\cos\psi \tag{4.12a}$$

$$B = \sin\psi \tag{4.12b}$$

$$C = m_1 + m_2 + (m_3 - 1)\cos\psi \tag{4.12c}$$

and

$$m_1 = \frac{-d^2 - 3l_3^2}{2\sqrt{3}l_2 l_3} \tag{4.13a}$$

$$m_2 = \frac{d}{l_2} \tag{4.13b}$$

$$m_3 = \frac{d}{\sqrt{3}l_3} \tag{4.13c}$$

$$d = \sqrt{(x_E - x_D)^2 + (y_E - y_D)^2} \tag{4.13d}$$

Therefore, the nonlinear equation to be solved is given by:

$$(x_C - x_F)^2 + (y_C - y_F)^2 = l_2^2 \tag{4.14}$$

Equation (4.14) can be solved for angle ψ using a numerical procedure. The secant method (Forsythe et al. 1977) has been implemented here. Moreover, the range of validity over which eq.(4.14) has real solutions is determined by the positive-semidefiniteness of the quantity under the square root in eq.(4.11), i.e.,

$$B^2 - AC \geq 0 \tag{4.15}$$

which, in the light of eqs.(4.12a,b,c), leads to:

$$(1 - m_1^2 + m_2^2) - 2(m_1 m_3 + m_2)X - m_3^2 X^2 \geq 0 \tag{4.16a}$$

where

$$X = \cos\psi \tag{4.16b}$$

Since the left-hand side of eq.(4.16a) represents a parabola with negative curvature, the roots of this parabola will give the limits of the range of validity of X from which the range of validity of ψ can be found. Due to the cosine function involved in eq.(4.16b), it may happen that we obtain two distinct ranges of validity for angle ψ, both of which should be considered. The roots of the parabola can be written as:

$$X_{1,2} = \frac{m_1 m_3 + m_2 \pm \sqrt{m_2^2 + m_3^2 + m_2^2 m_3^2 + 2m_1 m_2 m_3}}{-m_3^2} \tag{4.17}$$

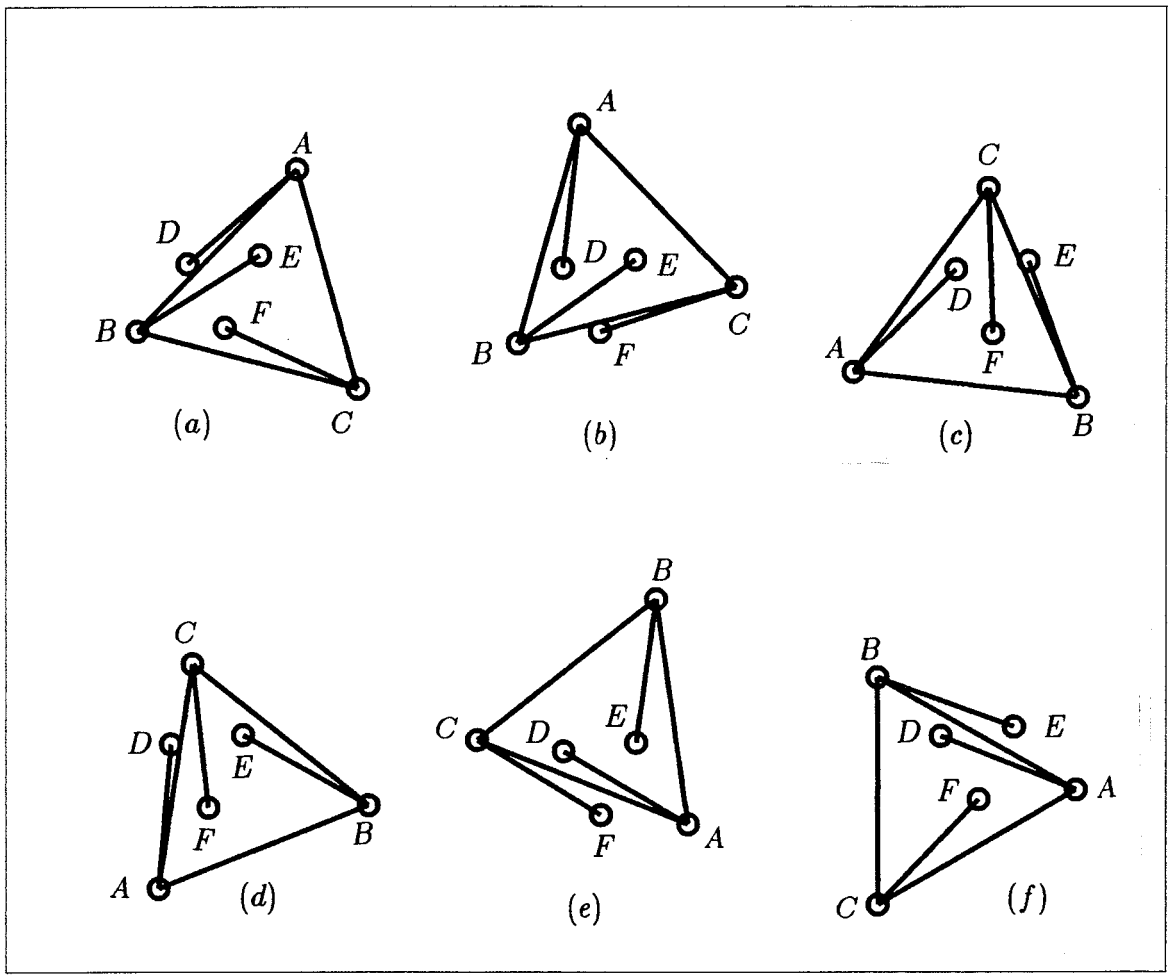

Figure 4.4 The six solutions of the direct kinematic problem for a given planar three-degree-of-freedom parallel manipulator in a given configuration.

Once the range of validity of ψ is known, we can use the secant method to obtain the solutions for angle ψ. By varying the value of the initial guess, we can obtain different solutions and, providing that a sufficient number of initial values is used, get all possible solutions. An example is shown in Fig. 4.4, where the configurations corresponding to each of the six solutions are displayed.

4.1.3 Velocity Inversion

The Jacobian matrix of a manipulator is generally defined as the matrix representing the transformation mapping the joint rates into the Cartesian velocities. However, since in the case of the closed-loop manipulator the inverse kinematic problem is easier

to solve than the direct one, the Jacobian matrix will be defined in terms of the inverse transformation, i.e.,

$$\mathbf{J}\dot{\mathbf{c}} = \dot{\theta} \tag{4.18}$$

where $\dot{\mathbf{c}}$ is the vector of Cartesian velocities, given here by $\dot{\mathbf{c}} = [\dot{x}, \dot{y}, \dot{\phi}]^T$ and $\dot{\theta}$ is the vector of joint rates, given here by $\dot{\theta} = [\dot{\theta}_1, \dot{\theta}_2, \dot{\theta}_3]^T$.

For the planar manipulator under study, the Jacobian matrix can be obtained by differentiation of eqs.(4.2–4.5) with respect to time. This leads to the following:

$$\mathbf{J} = \begin{bmatrix} a_1/d_1 & b_1/d_1 & c_1/d_1 \\ a_2/d_2 & b_2/d_2 & c_2/d_2 \\ a_3/d_3 & b_3/d_3 & c_3/d_3 \end{bmatrix} \tag{4.19}$$

where

$$a_i = 2l_1 y_{2i} \sqrt{x_{2i}^2 + y_{2i}^2} \sin\psi_i + \gamma_i E_i x_{2i} \tag{4.20a}$$

$$b_i = -2l_1 x_{2i} \sqrt{x_{2i}^2 + y_{2i}^2} \sin\psi_i + \gamma_i E_i y_{2i} \tag{4.20b}$$

$$c_i = 2l_1 l_3 \sqrt{x_{2i}^2 + y_{2i}^2} \sin\psi_i (x_{2i}\cos\phi_i + y_{2i}\sin\phi_i) + \gamma_i E_i l_3 (x_{2i}\sin\phi_i - y_{2i}\cos\phi_i) \tag{4.20c}$$

$$d_i = -2l_1 (x_{2i}^2 + y_{2i}^2)^{3/2} \sin\psi_i \tag{4.20d}$$

and

$$E_i = l_2^2 - l_1^2 + x_{2i}^2 + y_{2i}^2 \tag{4.21a}$$

Moreover,

$$\gamma_i = \pm 1 \tag{4.21b}$$

is a factor that depends on the branch we chose for the ith leg in the solution of the inverse kinematic problem.

However, the constraint on the kinematic closure of the ith leg can also be written as:

$$(x_{3i} - x_{4i})^2 + (y_{3i} - y_{4i})^2 = l_2^2 \tag{4.22a}$$

where

$$x_{3i} = x_{oi} + l_1 \cos\theta_i \tag{4.22b}$$

$$y_{3i} = y_{oi} + l_1 \sin\theta_i \tag{4.22c}$$

$$x_{4i} = x - l_3 \cos\phi_i \tag{4.22d}$$

$$y_{4i} = y - l_3 \sin\phi_i \tag{4.22e}$$

Differentiating both sides of eq.(4.22a) with respect to time, the Jacobian matrix can be rewritten as in eq.(4.19) with

$$a_i = x - x_{oi} - l_1 \cos\theta_i - l_3 \cos\phi_i \tag{4.23a}$$

$$b_i = y - y_{oi} - l_1 \sin\theta_i - l_3 \sin\phi_i \tag{4.23b}$$

$$c_i = -l_3[(y - y_{oi})\cos\phi_i - (x - x_{oi})\sin\phi_i] + l_1 l_3 \sin(\theta_i - \phi_i) \tag{4.23c}$$

$$d_i = l_1[(y - y_{oi})\cos\theta_i - (x - x_{oi})\sin\theta_i] + l_1 l_3 \sin(\theta_i - \phi_i) \tag{4.23d}$$

which is equivalent to eqs.(4.20a–d), except that now both the joint angles and the Cartesian coordinates are included in the expression. The computation of the Jacobian matrix using this method, therefore, requires that the inverse kinematic problem be solved first.

4.1.4 Acceleration Inversion

The relationship between the joint and Cartesian accelerations can be derived by differentiation of eq.(4.18). The following is obtained:

$$\mathbf{J}\ddot{\mathbf{c}} + \dot{\mathbf{J}}\dot{\mathbf{c}} = \ddot{\theta} \tag{4.24}$$

where $\ddot{\mathbf{c}} = [\ddot{x}, \ddot{y}, \ddot{\phi}]^T$ and $\ddot{\theta} = [\ddot{\theta}_1, \ddot{\theta}_2, \ddot{\theta}_3]^T$. The other quantities are assumed to be known from the velocity inversion. Therefore, the only matrix that has not been defined yet is the time derivative of the Jacobian matrix, denoted as $\dot{\mathbf{J}}$. The differentiation of eqs.(4.19) and (4.23a–d) leads to:

$$\dot{\mathbf{J}} = \begin{bmatrix} A_1 & B_1 & C_1 \\ A_2 & B_2 & C_2 \\ A_3 & B_3 & C_3 \end{bmatrix} \tag{4.25}$$

where

$$A_i = \frac{d_i\dot{a}_i - a_i\dot{d}_i}{d_i^2}, \qquad B_i = \frac{d_i\dot{b}_i - b_i\dot{d}_i}{d_i^2}, \qquad C_i = \frac{d_i\dot{c}_i - c_i\dot{d}_i}{d_i^2} \tag{4.26a}$$

with

$$\dot{a}_i = \dot{x} + l_1\dot{\theta}_i \sin\theta_i + l_2\dot{\phi}\sin\phi \tag{4.26b}$$

$$\dot{b}_i = \dot{y} - l_1\dot{\theta}_i \cos\theta_i - l_2\dot{\phi}\cos\phi \tag{4.26c}$$

$$\begin{aligned}\dot{c}_i =& l_3\dot{\phi}[(x - x_{oi})\cos\phi_i + (y - y_{oi})\sin\phi_i] + l_3[\dot{x}\sin\phi_i - \dot{y}\cos\phi_i] \\ &+ l_1 l_3(\dot{\theta}_i - \dot{\phi})\cos(\theta_i - \phi_i)\end{aligned} \tag{4.26d}$$

$$\begin{aligned}\dot{d}_i =& -l_1\dot{\theta}_i[(x - x_{oi})\cos\theta_i + (y - y_{oi})\sin\theta_i] - l_1[\dot{x}\sin\theta_i - \dot{y}\cos\theta_i] \\ &+ l_1 l_3(\dot{\theta}_i - \dot{\phi})\cos(\theta_i - \phi_i)\end{aligned} \tag{4.26e}$$

thereby completing the acceleration inversion.

4.1.5 Singularity Analysis

The three types of singularities discussed in Chapter 3 are now derived for the manipulator studied here. The physical significance of each of these types of singularities is also presented.

First type of singularities

It is recalled that the first type of singularities corresponds to the limit of the workspace and that it occurs when the determinant of the Jacobian matrix tends to infinity. This condition is encountered here when one of the denominators involved in the expression of the Jacobian tends to zero. From eq.(4.19) it is clear that this corresponds to:

$$d_i = 0, \qquad i = 1 \text{ or } 2 \text{ or } 3 \tag{4.27}$$

which, from eq.(4.20d), leads to:

$$\sin\psi_i = 0 \text{ or } \pi, \qquad i = 1 \text{ or } 2 \text{ or } 3 \tag{4.28}$$

This type of configuration is reached whenever the links of lengths l_1 and l_2 of one of the legs are aligned, as one can readily infer by inspection of Fig. 4.2. Moreover, since the solution of the inverse kinematic problem leads to two branches per leg, the corresponding quadratic equation leads to two solutions when the input Cartesian coordinates are located inside the workspace of the manipulator and to no real solution when the prescribed Cartesian coordinates are not within the workspace. Therefore, the limit of the workspace is defined by the set of points for which the quadratic equation will lead to only one solution, i.e., when we have the following condition in eq.(4.2):

$$\psi_i = \pm n\pi, \qquad n = 0,1,2,\ldots \qquad i = 1 \text{ or } 2 \text{ or } 3 \tag{4.29}$$

which is equivalent to eq.(4.28). Since in this type of configuration the ith leg is fully extended or folded, the set of Cartesian velocities of the gripper that correspond to a velocity of the point of attachment of the ith leg to the gripper along the folded or extended leg cannot be produced. This set of Cartesian velocities is given by the set of rotations of the gripper about an arbitrary point of a line passing through the ith point of attachment of the gripper and orthogonal to the ith leg.

Second type of singularities

The second type of singularities, which is located inside the workspace of the manipulator, occurs when the determinant of the Jacobian matrix tends to zero. For this type of configuration, the different motor rates are not independent any more and there exists a set of Cartesian velocities $\dot{\mathbf{c}}$ which are mapped into the zero vector by $\mathbf{J}$. These Cartesian velocities are then possible even when the rates of all motors are zero. These configurations can be inferred from eq.(4.19) by imposing the linear dependence of the columns of $\mathbf{J}$, i.e.,

$$k_1 a_i + k_2 b_i + k_3 c_i = 0, \qquad i = 1,2,3 \tag{4.30a}$$

for some real values of k_1, k_2, and k_3 for which

$$||\mathbf{k}|| \neq 0 \tag{4.30b}$$

where

$$\mathbf{k} = [k_1, k_2, k_3]^T \tag{4.30c}$$

By inspection of eqs.(4.30a) and (4.23a–d), two different cases for which the condition given by eqs.(4.30a&b) is satisfied can be identified. The first one is obtained when the lines along each of the three links of length l_2 intersect at the centroid of the gripper. In this case, we have

$$c_1 = c_2 = c_3 = 0 \tag{4.31}$$

and hence, eq.(4.30a) can be satisfied with $k_1 = k_2 = 0$ and arbitrary k_3. The last column of the Jacobian matrix is equal to zero and hence, the nullspace of **J** is given by $r[0, 0, 1]^T$ for any real r. The nullspace corresponds here to the set of pure rotations of the gripper about its centroid. This set of velocity vectors will produce motor rates of zero, due to the transitory additional degree of freedom. A configuration of this type is shown in Fig. 4.5.

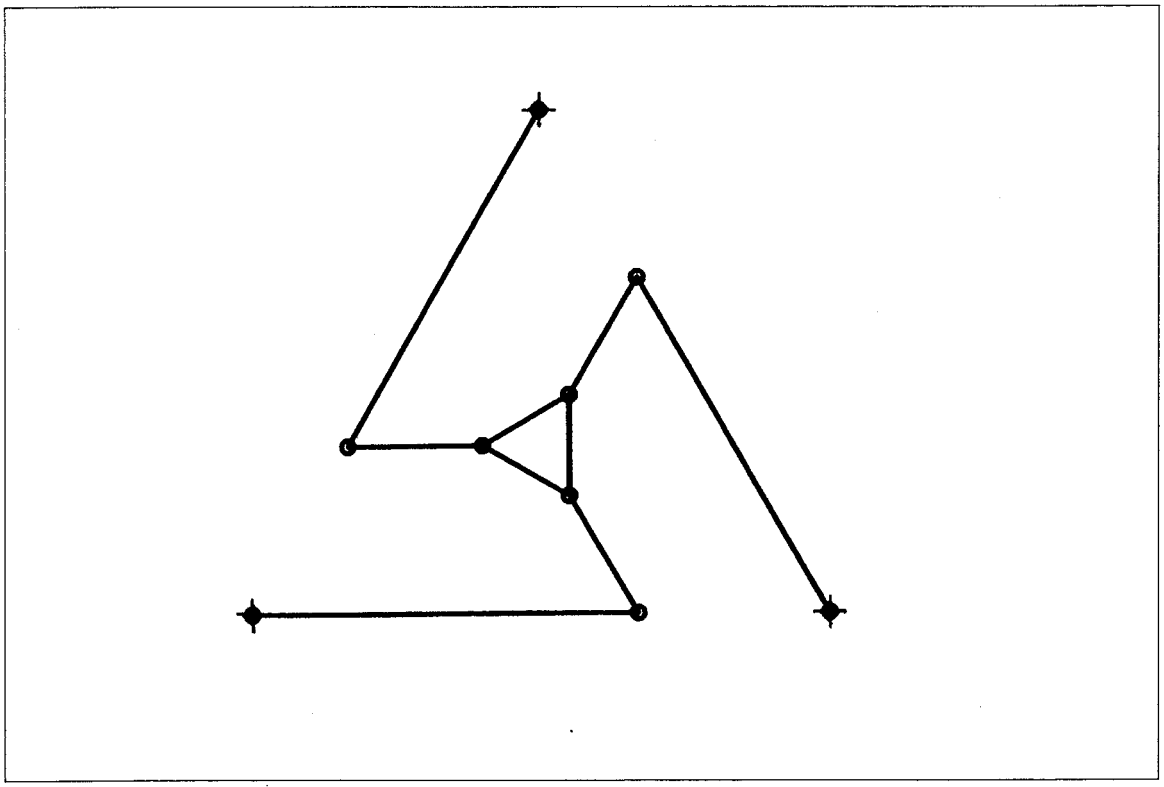

Figure 4.5 An example of the second type of singularity for the planar three-degree-of-freedom parallel manipulator.

The second case for which eq.(4.30a) can be verified is the set of configurations for which the three links of length l_2 are parallel. Indeed, by inspection of eq.(4.23a&b), we can define a set of vectors $\mathbf{v}_i$, $i = 1,2,3$ as two-dimensional vectors:

$$\mathbf{v}_i = [a_i,\ b_i]^T \tag{4.32}$$

where it is clear that $\mathbf{v}_i$ is the vector connecting the joint common to links l_1 and l_2 of the ith leg to the point of attachment of link l_2 of the same leg to the gripper, i.e., $\mathbf{v}_i$ is a vector along the two joint centres of the link of length l_2. Therefore, when the three links of length l_2 are parallel, we have

$$\mathbf{v}_1 = \pm\mathbf{v}_2 = \pm\mathbf{v}_3 \tag{4.33}$$

and the second column of $\mathbf{J}$ is a multiple of the first one. In this case, the nullspace of $\mathbf{J}$ represents the set of pure translations of the gripper along a direction orthogonal to $\mathbf{v}_i$, i.e., orthogonal to the three links of length l_2. A velocity of the gripper of that nature would produce motor rates of zero.

It is to be noticed that the results presented above for the second type of singularities of the revolute-based planar three-degree-of-freedom manipulator are in full agreement with the ones obtained in Chapter 3 with a different approach. This is so because the configurations derived here are the ones for which the manipulator instantaneously acquires an additional degree of freedom.

Third type of singularities

This type of singularities is characterized by the indeterminacy of the Jacobian matrix. In other words, some of the quantities involved in the expression of matrix $\mathbf{J}$ take on the form 0/0.

As mentioned in Chapter 3, this singularity is not only configuration- but also architecture-dependent. For the planar manipulator studied here, two situations may render the Jacobian matrix indeterminate. One of these two cases happens when we have:

$$l_1 = \frac{\sqrt{3}}{3} \quad \text{and} \quad l_2 = l_3 \tag{4.34}$$

With these constraints on the link lengths, we can reach a configuration where the tip of each of the three links of lengths l_1 meet at the centroid of the base triangle which coincides with the centroid of the gripper, since $l_2 = l_3$. The gripper can then undergo arbitrary rotations about its centroid while the motors remain at rest. This indeterminacy is due to the zeroing of both the c_i's and the d_i's when the gripper is oriented such that $\phi = 0$. At this particular point, both the first and second type of singularities meet.

The second case of degeneracy of the manipulator requires the following conditions:

$$l_1 = l_2 \quad \text{and} \quad l_3 = \frac{\sqrt{3}}{3} \tag{4.35}$$

In that case, the gripper is of the same size as the base triangle. Therefore, when the three vertices of the gripper are located at the centroid of the motors, and when angle ϕ is equal to zero, the motors can undergo arbitrary rotations while the gripper remains at rest. Again, the first two types of singularities meet here, i.e., when angles θ_1, θ_2, and θ_3 take on the values $-150°$, $-30°$, and $90°$ respectively, then both the c_i's and the d_i's are equal to zero.

4.2 Planar Three-Degree-of-Freedom Manipulator with Prismatic Actuators

The planar three-degree-of-freedom parallel manipulator studied in Section 4.1 can also be built using prismatic actuators. The *3R* architecture of the legs is changed to an *RPR* architecture where the prismatic joint is the one that is actuated. This is shown in Fig. 4.6, where, again, the distance between each of the M_i's—which do not refer to motors here but to free pin joints—is set equal to unity. The assumption of symmetry is also made here for the same reasons that were mentioned in Section 4.1. The potential advantages of this manipulator over the one based on revolute actuators are simpler kinematic equations and reduced mechanical interference. The applications for which this manipulator could be used are essentially the same as the ones mentioned for the revolute-based manipulator.

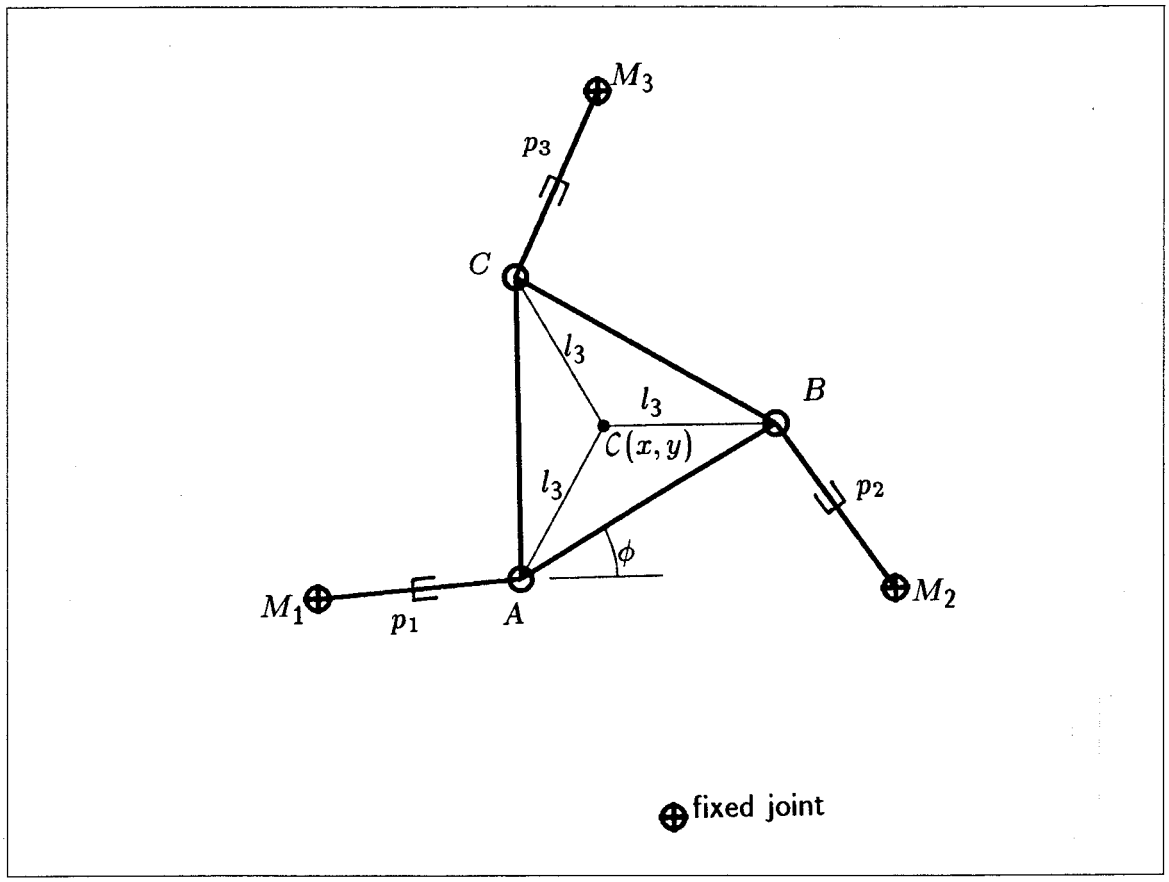

Figure 4.6 Planar three-degree-of-freedom parallel manipulator with prismatic actuators.

4.2.1 Inverse Kinematic Problem

Referring to Fig. 4.6, we denote by l_3 the dimension of the gripper, by p_i the length of the ith leg or actuator, and by (x_i, y_i) the coordinates of the point of attachment of the ith leg to the gripper. Moreover, the position of the point of attachment of the ith leg to the base is given by (x_{oi}, y_{oi}), quantities that are given in eqs.(4.7a&b). As in the case of the manipulator with revolute actuators, the Cartesian coordinates are given by the position of the centroid of the gripper $C(x, y)$ and by its orientation, defined here by angle ϕ. We can then write

$$x_i = x - l_3 \cos\phi_i - x_{oi}, \quad i = 1,2,3 \tag{4.36a}$$

$$y_i = y - l_3 \sin\phi_i - y_{oi}, \quad i = 1,2,3 \tag{4.36b}$$

where angles ϕ_i and the pairs (x_{oi}, y_{oi}) are given by eqs.(4.6a–c) and (4.7a&b) respectively.

The inverse kinematic problem, which has only one solution here, can then be solved using:

$$p_i = \sqrt{x_i^2 + y_i^2}, \qquad i = 1,2,3 \tag{4.37}$$

Therefore, given a certain position and orientation of the gripper, the required lengths of the actuators can be computed directly from eq.(4.37).

4.2.2 Direct Kinematic Problem

The solution of the direct kinematic problem for the manipulator with prismatic actuators is basically identical to the one encountered for the manipulator with revolute actuators. As a matter of fact, when the actuator lengths p_1, p_2, and p_3 are specified, point C can be considered as a point on the coupler of the four-bar linkage M_1ABM_2. The solutions of the direct kinematic problem are obtained when the curve described by this point of the coupler intersects a circle of radius p_3 centred at M_3. The problem leads to a maximum of 6 branches as shown in Section 4.1.2. The formulation given in that section can also be used here provided that some of the equations are rewritten. Indeed, for the four-bar linkage considered here, eqs.(4.8a&b) become:

$$x_C = x_{o1} + p_1 \cos\psi + \sqrt{3} l_3 \cos(\alpha_2 + \theta) \tag{4.38a}$$

$$y_C = y_{o1} + p_1 \sin\psi + \sqrt{3} l_3 \sin(\alpha_2 + \theta) \tag{4.38b}$$

where

$$\alpha_2 = \pi/3 \tag{4.38c}$$

and θ can be obtained from eqs.(4.11) and (4.12a–c), in which the m_i's are redefined as

$$m_1 = \frac{p_2^2 - 1 - p_1^2 - 3l_3^2}{2\sqrt{3} l_3 p_1} \tag{4.39a}$$

$$m_2 = \frac{1}{p_1} \tag{4.39b}$$

$$m_3 = \frac{1}{\sqrt{3} l_3} \tag{4.39c}$$

Therefore, the nonlinear equation to be solved becomes

$$(x_C - x_{o3})^2 + (y_C - y_{o3})^2 = p_3^2 \tag{4.40}$$

Equation (4.40) is similar to eq.(4.14) and can be solved for angle ψ using a numerical procedure. The ranges of validity of angle ψ, i.e., the ranges over which we can expect to find real solutions are found using eqs.(4.15) to (4.17).

4.2.3 Velocity Inversion

The Jacobian matrix of the planar manipulator with prismatic actuators is defined similarly to the one of the manipulator with revolute actuators given in eq.(4.19). We define:

$$\mathbf{J}\dot{\mathbf{c}} = \dot{\mathbf{p}} \tag{4.41}$$

where $\dot{\mathbf{c}} = [\dot{x}, \dot{y}, \dot{\phi}]^T$ is the vector of Cartesian velocities and $\dot{\mathbf{p}} = [\dot{p}_1, \dot{p}_2, \dot{p}_3]^T$ is the vector of linear actuator rates. The differentiation of eq.(4.37) leads to the following Jacobian matrix:

$$\mathbf{J} = \begin{bmatrix} a_1/p_1 & b_1/p_1 & c_1/p_1 \\ a_2/p_2 & b_2/p_2 & c_2/p_2 \\ a_3/p_3 & b_3/p_3 & c_3/p_3 \end{bmatrix} \tag{4.42}$$

where

$$a_i = x - x_{oi} - l_3 \cos\phi_i \tag{4.43a}$$

$$b_i = y - y_{oi} - l_3 \sin\phi_i \tag{4.43b}$$

$$c_i = (x - x_{oi}) l_3 \sin\phi_i - (y - y_{oi}) l_3 \cos\phi_i \tag{4.43c}$$

and the angles ϕ_i, for $i = 1,2,3$, are defined as in eq.(4.6a–c). The derivation of the relationship between Cartesian velocities and joint rates is thereby completed.

4.2.4 Acceleration Inversion

The differentiation of eq.(4.41) leads to the equation relating Cartesian accelerations with joint accelerations. Again, we obtain:

$$\mathbf{J}\ddot{\mathbf{c}} + \dot{\mathbf{J}}\dot{\mathbf{c}} = \ddot{\mathbf{p}} \tag{4.44}$$

where $\ddot{\mathbf{c}} = [\ddot{x}, \ddot{y}, \ddot{\phi}]^T$ is the vector of Cartesian accelerations and $\ddot{\mathbf{p}} = [\ddot{p}_1, \ddot{p}_2, \ddot{p}_3]^T$ is the vector of joint accelerations. The time derivative of the Jacobian matrix, $\dot{\mathbf{J}}$, is obtained by differentiation of eqs.(4.42) and (4.43a–c). Separating the different terms, we can write

$$\dot{\mathbf{J}} = \dot{\mathbf{J}}_1 - \dot{\mathbf{J}}_2 \tag{4.45a}$$

where

$$\dot{\mathbf{J}}_1 = \begin{bmatrix} A_1 & B_1 & C_1 \\ A_2 & B_2 & C_2 \\ A_3 & B_3 & C_3 \end{bmatrix} \tag{4.45b}$$

and

$$\dot{\mathbf{J}}_2 = \begin{bmatrix} D_1 & E_1 & F_1 \\ D_2 & E_2 & F_2 \\ D_3 & E_3 & F_3 \end{bmatrix} \tag{4.45c}$$

with

$$A_i = \frac{1}{p_i}(\dot{x} + l_3\dot{\phi}\sin\phi_i) \tag{4.46a}$$

$$B_i = \frac{1}{p_i}(\dot{y} - l_3\dot{\phi}\cos\phi_i) \tag{4.46b}$$

$$C_i = \frac{1}{p_i}(\dot{x}l_3\sin\phi_i + (x - x_{oi})l_3\dot{\phi}\cos\phi_i - \dot{y}l_3\cos\phi_i + (y - y_{oi})l_3\dot{\phi}\sin\phi_i) \tag{4.46c}$$

$$D_i = \frac{1}{p_i^2}(a_i\dot{p}_i) \tag{4.46d}$$

$$E_i = \frac{1}{p_i^2}(b_i\dot{p}_i) \tag{4.46e}$$

$$F_i = \frac{1}{p_i^2}(c_i\dot{p}_i) \tag{4.46f}$$

which completes the acceleration inversion.

4.2.5 Singularity Analysis

The singularities of the planar manipulator with prismatic actuators are now derived. Since the expression of the Jacobian matrix of this manipulator has similarities with the one of the manipulator with revolute actuators, it is expected that the singularities will occur in configurations of the same type.

First type of singularities

If we assume that the prismatic actuators of the manipulator have an infinite range of motion, the result is an infinitely large workspace and the first type of singularities occurs only when one of the actuators has a length of zero, i.e.:

$$p_i = 0, \quad i = 1 \text{ or } 2 \text{ or } 3 \tag{4.47}$$

From eq.(4.42), it is readily seen that this situation produces a Jacobian matrix whose determinant tends to infinity. This is so because the direction of the prismatic joint is undefined in these configurations.

However, in a real manipulator, the actuators have a finite range of motion, i.e,

$$p_{min} < p_i < p_{max} \tag{4.48}$$

and where p_{min} is, in general, different from zero. In this case, the first type of singularities happens when one of the actuators reaches one of its limits, i.e.,

$$p_i = p_{min} \quad \text{or} \quad p_i = p_{max}, \quad i = 1 \text{ or } 2 \text{ or } 3 \tag{4.49}$$

which corresponds to the limit of the workspace. Since one of the actuators cannot move further in one direction, a certain set of gripper velocities—pure rotations about an arbitrary point of a line orthogonal to the ith leg and passing through the point of attachment of that leg to the gripper—cannot be produced.

Second type of singularities

For purposes of analysis of the second type of singularities, we define a set of three two-dimensional unit vectors which are, respectively, orthogonal to the three lines connecting the centroid of the gripper to the points of attachment of the legs to the gripper. These vectors are given by

$$\mathbf{u}_i = \begin{bmatrix} \sin\phi_i \\ -\cos\phi_i \end{bmatrix}, \qquad i = 1, 2, 3 \tag{4.50}$$

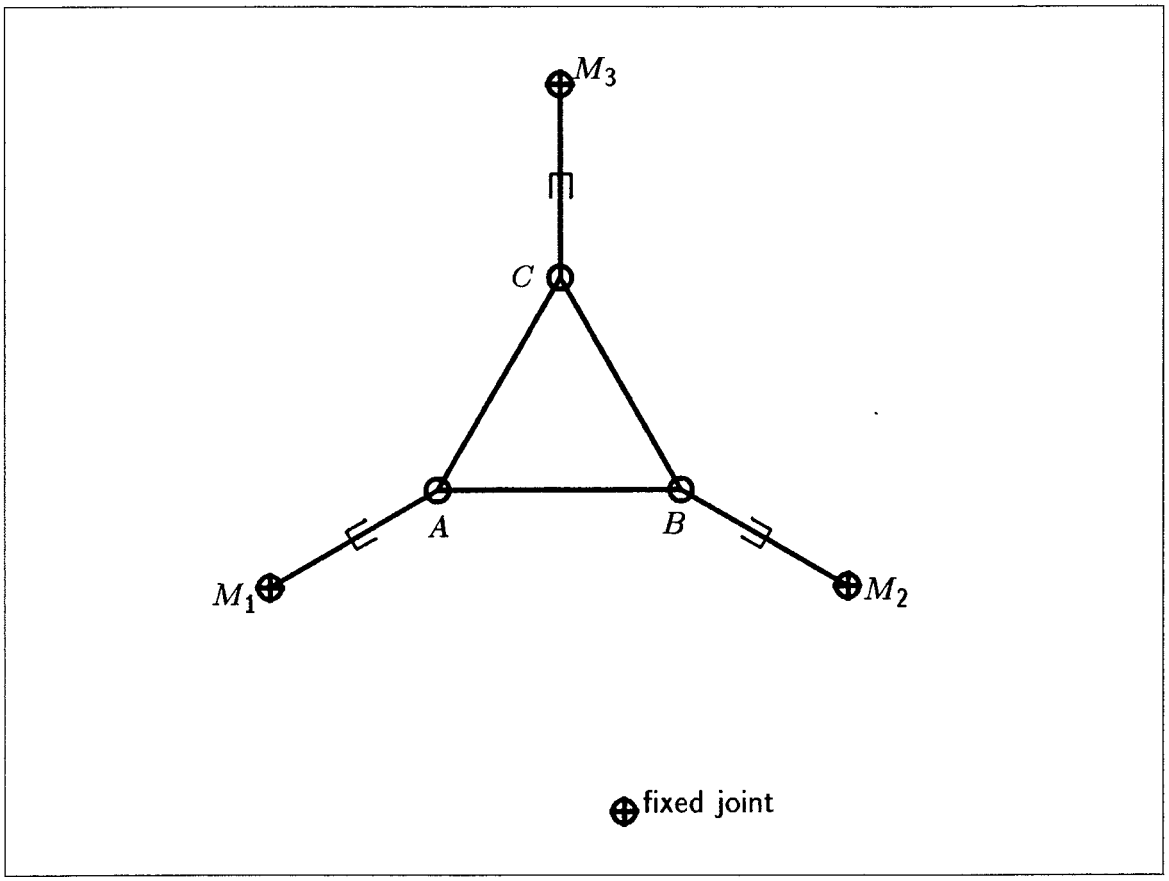

Figure 4.7 An example of the second type of singularity for the planar three-degree-of-freedom parallel manipulator with prismatic actuators.

Similarly, we define a set of three vectors connecting the centroid of the gripper with the fixed pinned joints as

$$\mathbf{v}_i = \begin{bmatrix} x - x_{oi} \\ y - y_{oi} \end{bmatrix}, \qquad i = 1,2,3 \tag{4.51}$$

Using these definitions, we can express the elements of the third column of the Jacobian matrix as

$$J_{i3} = \frac{l_3}{p_i}(\mathbf{u}_i \cdot \mathbf{v}_i), \qquad i = 1,2,3 \tag{4.52}$$

Therefore, when vectors $\mathbf{u}_i$ and $\mathbf{v}_i$ $(i = 1,2,3)$ are orthogonal, i.e., when the three lines along the legs intersect at the centroid of the gripper, the last column of the Jacobian matrix vanishes and the determinant vanishes. The nullspace of the Jacobian matrix is spanned by vector $[0\,0\,1]^T$, which means that Cartesian velocities associated with pure rotations of the gripper about its centroid will produce zero velocities at the actuators. The resulting configuration is shown in Fig. 4.7.

As in the case of the manipulator with revolute actuators, there exists a second type of configuration which will cause the second type of singularities. Indeed, when all the legs are parallel, the second column of the Jacobian matrix is proportional to the first one, which results in a singularity. The proof of this fact was already given in Section 4.1.5. The set of Cartesian velocities that produce vanishing joint rates is given by the set of pure translations along a direction orthogonal to the legs.

Third type of singularities

The condition on the kinematic parameters of the manipulator that are required for the third type of singularities to occur is now given as:

$$l_3 = \frac{1}{\sqrt{3}} \tag{4.53}$$

In other words, the gripper triangle has the same dimension as the base triangle. Therefore, if the three legs are extended to the same length and are all parallel to each other, i.e.:

$$p_1 = p_2 = p_3 \quad \text{and} \quad \phi = 0 \tag{4.54}$$

then the four-bar linkage M_1ABM_2 is a parallelogram and point C of its coupler will trace a circle of radius p_i and centred at point M_3. The resulting linkage, which is shown in Fig. 4.8 can then undergo finite motions while the actuators are locked.

4.3 Spherical Three-Degree-of-Freedom Manipulator

Previous research on parallel manipulators has been confined, almost exclusively, to the consideration of planar and spatial kinematic chains while spherical parallel manipulators have received little attention. As a matter of fact, the only reference that the author could find on a spherical parallel manipulator is (Asada and Cro Granito 1985), where a mechanism similar the the one studied here is briefly introduced. A spherical parallel manipulator could be applied as an orientation wrist in robotics. Applications outside of robotics, that could be mentioned, are mechanisms for the orientation of machine-tool

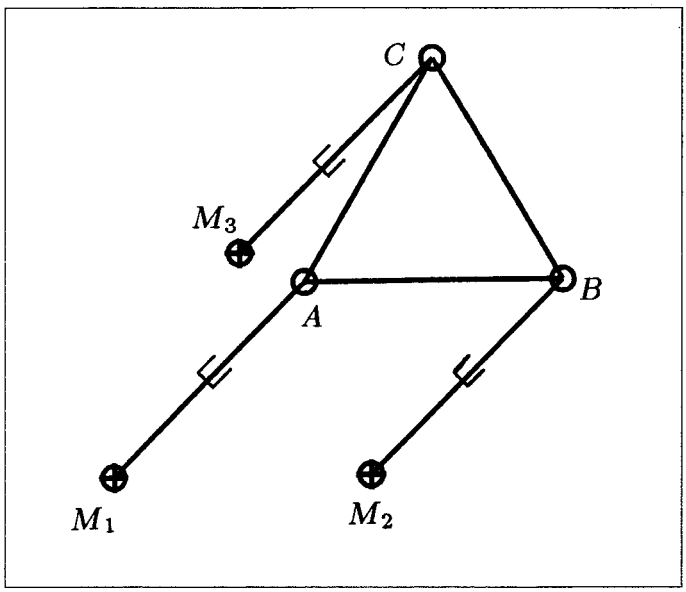

Figure 4.8 Third type of singularity for the planar three-degree-of-freedom parallel manipulator with prismatic actuators.

beds and workpieces, solar panels, antennas, etc. Hence the motivation to study this type of kinematic chains.

A spherical parallel manipulator is represented in Fig. 4.9, all of whose joints are of the revolute type, and the three motors M_1, M_2, M_3 are fixed. The manipulator consists of a kinematic chain with three closed loops, namely M_1DABEM_2, M_2EBCFM_3, and M_3FCADM_1, and the gripper is rigidly attached to triangle ABC. Again, only two of the loops are independent. For reasons that were explained in Section 4.1, a symmetric layout has been chosen here. By symmetry, then, the axes of the motors will be located in a common plane, intersecting a point defining the *centre* of the spherical manipulator. Moreover, the joints attached to the gripper have the same relative orientation, and the link angles will be the same for each leg, i.e.,

$$\alpha_i = \alpha_i' = \alpha_i'', \quad i = 1, 2 \tag{4.55}$$

These assumptions will be used throughout.

4.3.1 Inverse Kinematic Problem

Since the spherical manipulator is aimed at orienting a rigid body in space,

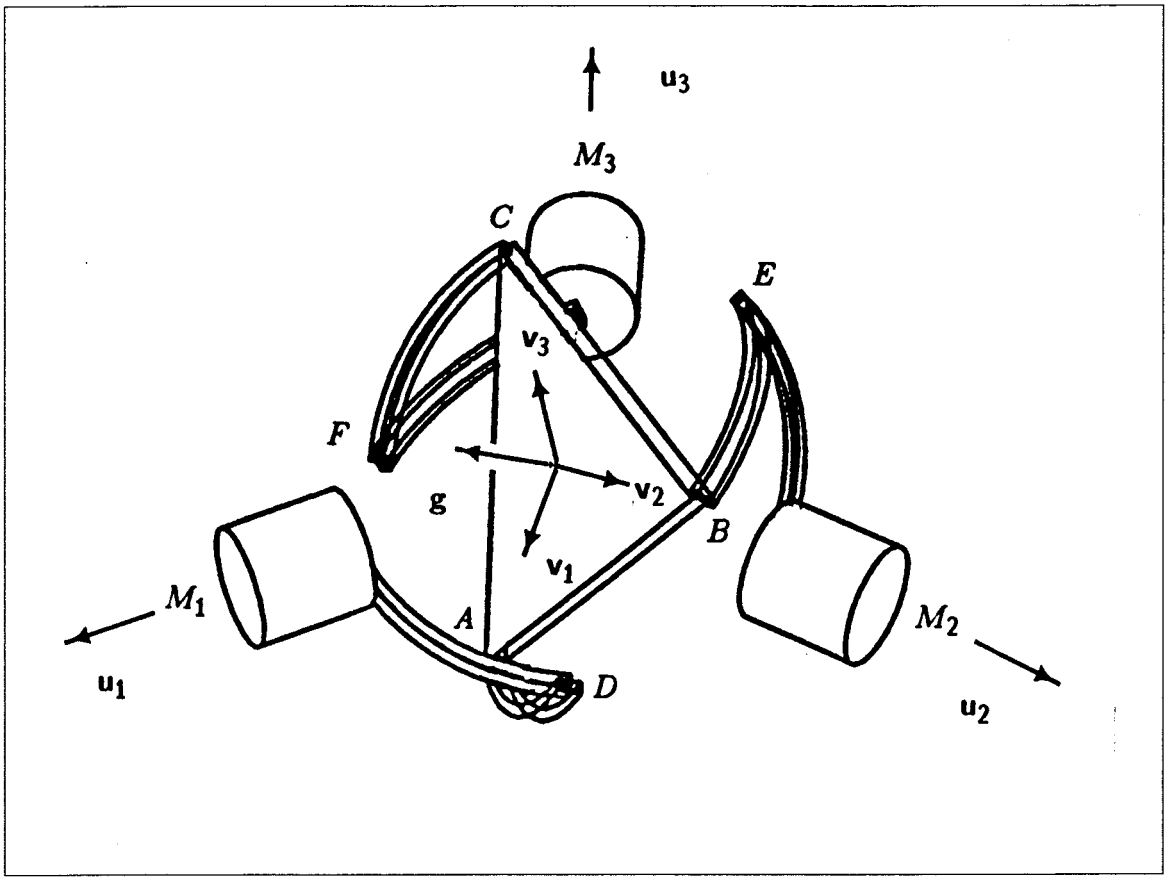

Figure 4.9 Spherical three-degree-of-freedom parallel manipulator.

the Cartesian coordinates of the gripper are given by its orientation only (with respect to a reference configuration C_0), which can be described by a rotation tensor $\mathbf{Q}$ or, alternatively, by the linear vector and scalar invariants of this tensor (Angeles 1985), which are defined as follows:

$$\mathbf{q} = \text{vect}(\mathbf{Q}) = \mathbf{e} \sin \phi \tag{4.56a}$$

$$q_0 = \frac{\text{tr}(\mathbf{Q}) - 1}{2} = \cos \phi \tag{4.56b}$$

where $\mathbf{e}$ is a unit vector along the axis of rotation and ϕ is the angle of rotation. A discussion on the linear invariants is presented in Appendix B. These invariants are related through

$$||\mathbf{q}||^2 + q_0^2 = 1 \tag{4.57}$$

The inverse kinematic problem for this manipulator consists, then, of finding

the motor angles corresponding to a given orientation of the gripper. The solution of this problem contains eight branches, i.e., two branches per leg, since the solutions for the input motor angles, $\theta_1, \theta_2, \theta_3$, are decoupled. The situation is similar to the one encountered in the case of the planar manipulator with revolute actuators except that, in this case, each of the legs can be thought of as a spherical four-bar mechanism.

Let us define $\mathbf{u}_i$ as a unit vector along the axis of the ith input motor, and $\mathbf{v}_i$ as a unit vector along the axis of the revolute joints connecting the gripper and the adjacent link (Fig. 4.10), for $i = 1, 2, 3$.

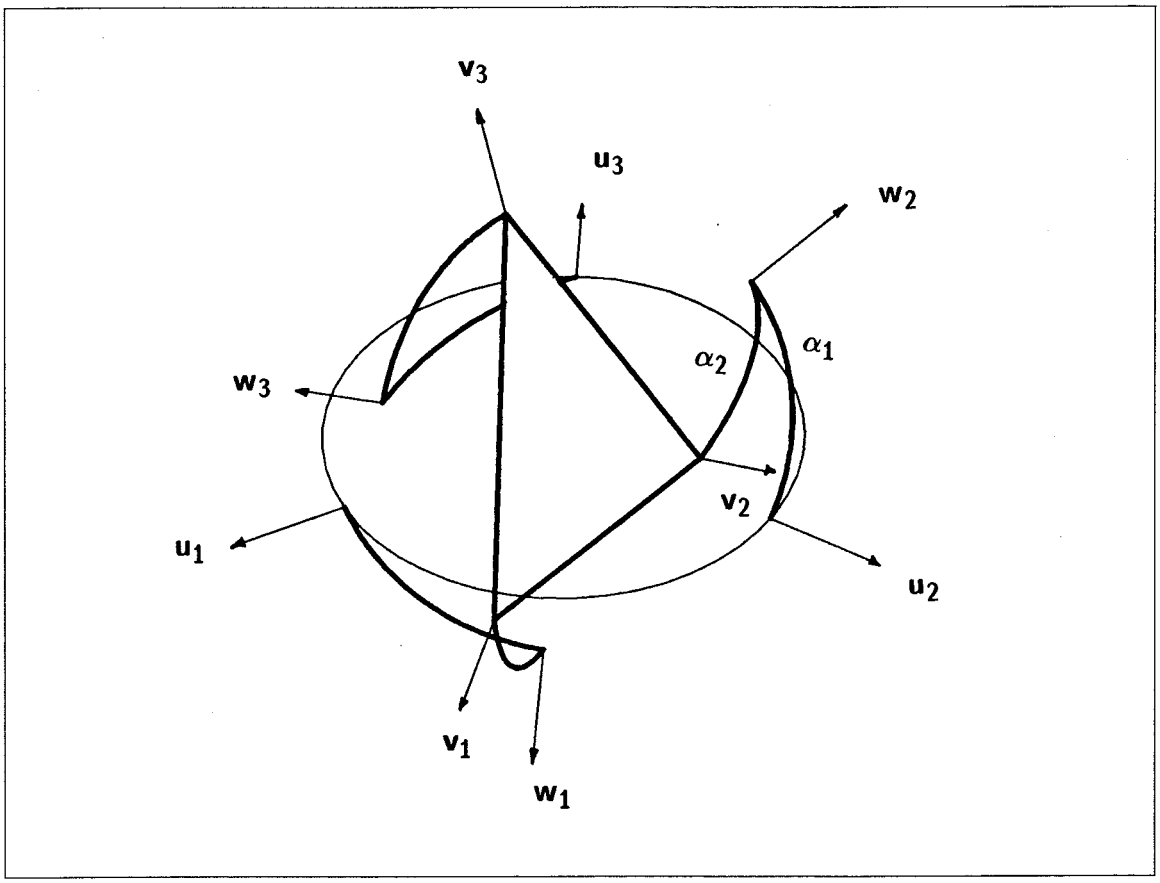

Figure 4.10 Definition of the unit vectors $\mathbf{u}_i$, $\mathbf{v}_i$ and $\mathbf{w}_i$, for $i = 1, 2, 3$.

Moreover, let us denote by α_1 and α_2 the link angles and choose the reference configuration as the one in which $\mathbf{u}_i = \mathbf{v}_i$ for $i = 1, 2, 3$ (Fig. 4.11).

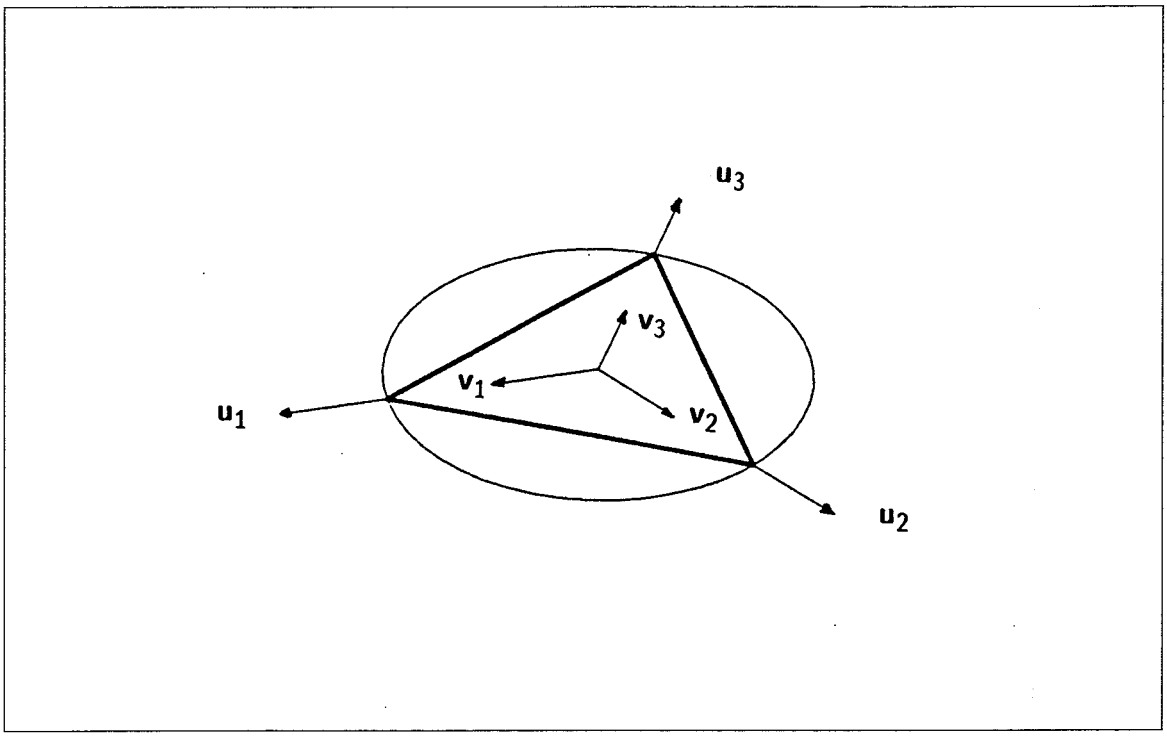

Figure 4.11 Reference configuration for the spherical three-degree-of-freedom parallel manipulator.

We can define another set of unit vectors $\mathbf{w}_i$, for $i = 1,2,3$, along the axes of the intermediate revolute pairs of each leg. These are given by

$$\mathbf{w}_i = \begin{bmatrix} \cos\eta_i \cos\theta_i \sin\alpha_1 + \sin\eta_i \cos\alpha_1 \\ \sin\eta_i \cos\theta_i \sin\alpha_1 - \cos\eta_i \cos\alpha_1 \\ \sin\theta_i \sin\alpha_1 \end{bmatrix}, \quad i = 1,2,3 \tag{4.58}$$

where

$$\eta_1 = \pi/2,\ \eta_2 = -5\pi/6,\ \eta_3 = -\pi/6 \tag{4.59}$$

and θ_i is the angle of rotation of the ith motor where we have chosen

$$\mathbf{u}_i = [\sin\eta_i, -\cos\eta_i, 0]^T, \quad i = 1,2,3 \tag{4.60a}$$

or, explicitly,

$$\mathbf{u}_1 = \begin{bmatrix} 1 \\ 0 \\ 0 \end{bmatrix}, \quad \mathbf{u}_2 = \begin{bmatrix} -1/2 \\ \sqrt{3}/2 \\ 0 \end{bmatrix}, \quad \mathbf{u}_3 = \begin{bmatrix} -1/2 \\ -\sqrt{3}/2 \\ 0 \end{bmatrix} \tag{4.60b}$$

The solution to the inverse kinematic problem is then obtained by writing the closure equations as follows:

$$\mathbf{w}_i \cdot \mathbf{v}_i = \cos\alpha_2, \quad i = 1,2,3 \tag{4.61}$$

which, for each leg, leads to a quadratic equation of the form:

$$A_i T_i^2 + 2B_i T_i + C_i = 0, \quad i = 1,2,3 \tag{4.62}$$

where

$$T_i = \tan(\theta_i/2) \tag{4.63a}$$

and

$$A_i = (\sin\eta_i v_{i1} - \cos\eta_i v_{i2})\cos\alpha_1 - (\cos\eta_i v_{i1} + \sin\eta_i v_{i2})\sin\alpha_1 - \cos\alpha_2 \tag{4.63b}$$

$$B_i = \sin\alpha_1 v_{i3} \tag{4.63c}$$

$$C_i = (\sin\eta_i v_{i1} - \cos\eta_i v_{i2})\cos\alpha_1 + (\cos\eta_i v_{i1} + \sin\eta_i v_{i2})\sin\alpha_1 - \cos\alpha_2 \tag{4.63d}$$

v_{ij} being the jth component of vector $\mathbf{v}_i$. The solution of the inverse kinematic problem is therefore completed by solving the quadratic equation above for each of the legs, which leads to:

$$T_i = \frac{-B_i \pm \sqrt{B_i^2 - A_i C_i}}{A_i}, \quad i = 1,2,3 \tag{4.64}$$

The spherical parallel manipulator mentioned in (Asada and Cro Granito 1985) exhibits a kinematic structure slightly different from the one shown in Fig. 4.9. Indeed, in the former arrangement, the three powered revolute joints are mounted on a common axis, i.e., using concentric shafts, while the rest of the structure remains essentially unchanged. The equations for the solution of the inverse kinematic problem have to be consequently modified. We now have:

$$\mathbf{w}_i = \begin{bmatrix} \cos\theta_i \sin\alpha_1 \\ \sin\theta_i \sin\alpha_1 \\ -\cos\alpha_1 \end{bmatrix}, \qquad i = 1,2,3 \tag{4.65}$$

since the shafts of the three motors are now aligned with the unit vector:

$$\mathbf{s} = [0,\ 0,\ 1]^T \tag{4.66}$$

Using eq.(4.61), a quadratic equation similar to the one given in eq.(4.62), is obtained with coefficients A_i, B_i and C_i defined as follows:

$$A_i = -\sin\alpha_1 v_{i1} - \cos\alpha_1 v_{i3} - \cos\alpha_2 \tag{4.67a}$$

$$B_i = \sin\alpha_1 v_{i2} \tag{4.67b}$$

$$C_i = \sin\alpha_1 v_{i1} - \cos\alpha_1 v_{i3} - \cos\alpha_2 \tag{4.67c}$$

the solution of which is obtained using eq.(4.64).

4.3.2 Direct Kinematic Problem

The solution of the direct kinematic problem for the spherical manipulator can be derived using an approach similar to the one used for the planar manipulator. The reasoning allowing us to establish the number of expected solutions can be repeated here by replacing planar four-bar linkages with spherical four-bar linkages. However, since the equations describing the motion of a point of the coupler of a spherical four-bar mechanism take on rather complicated forms, the formulation derived here for the numerical solution of the direct kinematic problem is slightly different.

First of all, when the input angles are known, the vectors along the intermediate joints of each of the legs $\mathbf{w}_i$, $i = 1,2,3$, are readily computed from eq.(4.58), or alternatively from eq.(4.65), if the manipulator has the kinematic structure presented in (Asada and Cro Granito 1985). Therefore, the equations to be satisfied are

$$\mathbf{w}_i \cdot \mathbf{v}_i = \cos\alpha_2, \qquad i = 1,2,3 \tag{4.68a}$$

$$\mathbf{v}_i \cdot \mathbf{v}_j = -1/2, \quad i \neq j, \quad i,j = 1,2,3 \tag{4.68b}$$

$$||\mathbf{v}_i|| = 1, \qquad i = 1,2,3 \tag{4.68c}$$

which thus lead to nine equations in nine unknowns, i.e., the three components of each of the three vectors $\mathbf{v}_i$, $i = 1,2,3$ where three of the equations are linear. The solution of this problem can be computed using, for instance, the Newton-Raphson method. Once the three vectors $\mathbf{v}_i$, $i = 1,2,3$ are obtained, the rotation matrix $\mathbf{Q}$ describing the orientation of the gripper can be computed using, for instance, the procedure described in (Angeles 1986b). An example is shown in Table 4.1 where the six solutions of the direct kinematic problem for a particular configuration are given.

4.3.3 Velocity Inversion

The definition of the Jacobian matrix of the spherical parallel manipulator is

Solution #	1	2	3	4	5	6
$\mathbf{v}_{1x}$	.407	.149	.963	−.560	−.244	.980
$\mathbf{v}_{1y}$	.588	−.202	−.030	.829	.060	−.197
$\mathbf{v}_{1z}$	−.699	.968	−.269	.000	.968	.000
$\mathbf{v}_{2x}$	.101	−.455	−.713	−.438	−.714	−.319
$\mathbf{v}_{2y}$	.230	.849	.059	−.899	.035	.948
$\mathbf{v}_{2z}$	.968	−.269	−.699	.000	−.699	.000
$\mathbf{v}_{3x}$	−.508	.307	−.250	.998	.959	−.661
$\mathbf{v}_{3y}$	−.818	−.646	−.028	.070	−.094	−.750
$\mathbf{v}_{3z}$	−.269	−.699	.968	.000	−.269	.000

Table 4.1 The six solutions of the inverse kinematic problem for a spherical three-degree-of-freedom parallel manipulator with $\alpha_1 = \pi/3$ and $\alpha_2 = 7\pi/18$ when $\theta_1 = \theta_2 = \theta_3 = 30^\circ$.

similar to the one used for the planar manipulator, i.e., it is defined as the matrix representing the transformation mapping the Cartesian velocities into the joint rates. This is written as

$$\mathbf{J}\omega = \dot{\theta} \tag{4.69}$$

where ω is the angular velocity of the end effector and $\dot{\theta}$ is the vector of actuated joint rates. The Jacobian matrix can be found by differentiation of both sides of eq.(4.61), which leads to:

$$\dot{\mathbf{w}}_i \cdot \mathbf{v}_i + \mathbf{w}_i \cdot \dot{\mathbf{v}}_i = 0 \tag{4.70}$$

Now, the following relations are introduced:

$$\mathbf{v}_i = \mathbf{Q}\mathbf{u}_i \tag{4.71a}$$

and

$$\dot{\mathbf{Q}} = \mathbf{\Omega}\mathbf{Q} \tag{4.71b}$$

with $\mathbf{\Omega}$ defined as the following skew-symmetric matrix

$$\mathbf{\Omega} \equiv \frac{\partial(\omega \times \mathbf{a})}{\partial \mathbf{a}} \tag{4.71c}$$

for any $\mathbf{a}$. Thus,

$$\text{vect}(\mathbf{\Omega}) = \omega \tag{4.71d}$$

We now write the time derivative of vectors $\mathbf{w}_i$ as

$$\frac{1}{\dot{\theta}_i}\dot{\mathbf{w}}_i = \begin{bmatrix} -\cos\eta_i \sin\theta_i \sin\alpha_1 \\ -\sin\eta_i \sin\theta_i \sin\alpha_1 \\ \cos\theta_i \sin\alpha_1 \end{bmatrix} = \mathbf{u}_i \times \mathbf{w}_i \tag{4.72}$$

Moreover, the differentiation of both sides of eq.(4.71a) leads to the following, when eq.(4.71b) is used:

$$\dot{\mathbf{v}}_i = \dot{\mathbf{Q}}\mathbf{u}_i = \mathbf{\Omega}\mathbf{Q}\mathbf{u}_i = \mathbf{\Omega}\mathbf{v}_i \tag{4.73}$$

Therefore, eq.(4.70) can be rewritten as:

$$\dot{\theta}_i(\mathbf{u}_i \times \mathbf{w}_i) \cdot \mathbf{v}_i + \mathbf{w}_i \cdot \mathbf{\Omega}\mathbf{v}_i = 0 \tag{4.74a}$$

or

$$\dot{\theta}_i(\mathbf{u}_i \times \mathbf{w}_i) \cdot \mathbf{v}_i - \omega \cdot (\mathbf{w}_i \times \mathbf{v}_i) = 0 \tag{4.74b}$$

which leads to

$$\dot{\theta}_i = \frac{(\mathbf{w}_i \times \mathbf{v}_i) \cdot \omega}{(\mathbf{u}_i \times \mathbf{w}_i) \cdot \mathbf{v}_i} \tag{4.75}$$

The ith row of the Jacobian, $\mathbf{j}_i^T$, can then be written as

$$\mathbf{j}_i = \frac{(\mathbf{w}_i \times \mathbf{v}_i)}{(\mathbf{u}_i \times \mathbf{w}_i) \cdot \mathbf{v}_i} \tag{4.76}$$

which completes the velocity inversion.

It is pointed out that the essence of the derivation given above is also valid for the kinematic structure of the spherical manipulator studied in (Asada and Cro Granito 1985). However, a few changes in the expressions arise. Indeed, eq.(4.72) has to be rewritten as

$$\frac{1}{\dot{\theta}_i}\dot{\mathbf{w}}_i = \begin{bmatrix} -\sin\theta_i \sin\alpha_1 \\ \cos\theta_i \sin\alpha_1 \\ 0 \end{bmatrix} = \mathbf{s} \times \mathbf{w}_i \tag{4.77}$$

and the ith row of the Jacobian matrix then becomes

$$\mathbf{j}_i = \frac{(\mathbf{w}_i \times \mathbf{v}_i)}{(\mathbf{s} \times \mathbf{w}_i) \cdot \mathbf{v}_i} \tag{4.78}$$

4.3.4 Acceleration Inversion

The acceleration equation is obtained by taking the time derivative of both sides of eq.(4.69), which leads to

$$\ddot{\theta} = \dot{\mathbf{J}}\omega + \mathbf{J}\dot{\omega} \tag{4.79}$$

where all the entities are known except for the time derivative of the Jacobian matrix, which can be obtained by differentiation of both sides of eq.(4.76). The ith row of matrix $\dot{\mathbf{J}}$, denoted by $\mathbf{k}_i^T$, is then written as

$$\mathbf{k}_i = \frac{[(\mathbf{u}_i \times \mathbf{w}_i) \cdot \mathbf{v}_i]\mathbf{b} - a(\mathbf{w}_i \times \mathbf{v}_i)}{[(\mathbf{u}_i \times \mathbf{w}_i) \cdot \mathbf{v}_i]^2} \tag{4.80a}$$

where

$$\mathbf{b} = \mathbf{w}_i \times \dot{\mathbf{v}}_i + \dot{\mathbf{w}}_i \times \mathbf{v}_i \tag{4.80b}$$

and

$$a = (\mathbf{u}_i \times \mathbf{w}_i) \cdot \dot{\mathbf{v}}_i + (\mathbf{u}_i \times \dot{\mathbf{w}}_i) \cdot \mathbf{v}_i \tag{4.80c}$$

The time derivatives of vectors $\mathbf{v}_i$ and $\mathbf{w}_i$ can be obtained from eqs.(4.72), (4.73) and (4.77).

The equivalent expression for the kinematic structure presented in (Asada and Cro Granito 1985) is obtained by replacing vectors $\mathbf{u}_i$ by vector $\mathbf{s}$ in the above equations.

4.3.5 Singularity Analysis

First type of singularities

The first kind of singularities is known to lie on the boundary of the workspace and appears whenever $\det(\mathbf{J}) \rightarrow \infty$. The conditions under which this type of singularities arises can be obtained from the expression of the Jacobian, i.e., eq.(4.76) which produces:

$$(\mathbf{u}_i \times \mathbf{w}_i) \cdot \mathbf{v}_i = 0, \qquad i = 1 \text{ or } 2 \text{ or } 3 \tag{4.81}$$

Equation (4.81) states that vectors $\mathbf{u}_i$, $\mathbf{v}_i$, and $\mathbf{w}_i$ are coplanar, i.e., that the corresponding leg is totally unfolded or folded. In the case of the second kinematic arrangement (Asada and Cro Granito 1985), vector $\mathbf{u}_i$ is replaced by vector $\mathbf{s}$ in the above expression. When such a configuration is attained, a certain set of velocitites of the gripper cannot be produced. This set of velocities corresponds to the motions of the gripper that involve a velocity of the point of attachment of the fully extended or folded leg to the gripper along the direction of the leg.

Second type of singularities

The second type of singularities—which occurs when $\det(\mathbf{J}) = 0$—appears in configurations in which the different motor rates are not independent. This type of configuration should be avoided for the manipulator is not controllable in such a configuration. An additional proof of that is now given.

If we regard the manipulator as a control system where the orientation of the gripper is the state variable vector and $\dot{\theta}$ the input variable vector, then eq.(4.69) can be rewritten as

$$\omega = \mathbf{K}\dot{\theta} \tag{4.82}$$

where $\mathbf{K} = \mathbf{J}^{-1}$. Moreover, using the following relation between ω and $\dot{\lambda}$ (Angeles 1985):

$$\dot{\lambda} = \mathbf{\Lambda}\omega \tag{4.83a}$$

where

$$\mathbf{\Lambda} = \begin{bmatrix} \frac{1}{2}(\mathbf{1}\mathrm{tr}\mathbf{Q} - \mathbf{Q}) \\ -\mathbf{q}^T \end{bmatrix} \tag{4.83b}$$

eq.(4.82) can be rewritten in standard state-variable form as

$$\dot{\lambda} = \mathbf{\Lambda K}\dot{\theta} \tag{4.84}$$

where λ is the four-dimensional state variable and $\dot{\theta}$ is the three-dimensional input variable. Therefore, for this system, the 4×12 controllability matrix (Wonham, 1979) is given by

$$\mathbf{R} = [\mathbf{\Lambda K}, \mathbf{0}, \mathbf{0}, \mathbf{0}] \tag{4.85}$$

where $\mathbf{0}$ is a 4×3 zero matrix. If $\mathbf{\Lambda}$ is of full rank, which is the case if the angle of rotation, ϕ, is different from π, then rank($\mathbf{\Lambda K}$) =rank($\mathbf{K}$). The rank of the controllability matrix $\mathbf{R}$ is then equal to the rank of $\mathbf{K}$ and hence the system becomes uncontrollable when $\mathbf{K}$ becomes singular.

For the spherical manipulator, the condition under which det($\mathbf{J}$)=0 can be derived from expression (4.76) obtained for the Jacobian. Since, by definition, vectors $\mathbf{w}_i$ and $\mathbf{v}_i$ cannot be identical, then this condition is that the three vectors $(\mathbf{w}_i \times \mathbf{v}_i, i = 1,2,3)$ are coplanar. Since $\mathbf{v}_1, \mathbf{v}_2$ and $\mathbf{v}_3$ are coplanar, this condition states that the three planes defined, respectively, by the pairs of vectors $(\mathbf{v}_i, \mathbf{w}_i)$, for $i = 1,2,3$, either have a common intersection along an axis or are identical. This corresponds to configurations in which the links of dimension α_2 either lie on the plane of the gripper or are orthogonal to this plane. It is pointed out that this result is in perfect agreement with the one obtained in Section 3.2.3.3 with an alternate approach.

Third type of singularities:

Two sets of spherical manipulators for which the third type of singularities can occur are identified here, the second one being a subset of the first one.

First, for the set of spherical manipulators having $\alpha_1 = \alpha_2$, the configuration that we defined as the reference configuration is attainable and it constitutes a special case because condition (4.81) is verified for all three legs. Therefore, in this case, any motion of the input links will not affect the gripper since the former are just rotating, together with the intermediate link, around the axis defined by vectors $\mathbf{u}_i = \mathbf{v}_i$, leaving the gripper at rest. The rank of $\mathbf{K}$ is then equal to zero in this configuration, which means that system (4.84) is completely uncontrollable, i.e., none of the three Cartesian components of ω can be produced in the said configuration. Moreover, if $\theta_1 = \theta_2 = \theta_3 = 0$ or if $\theta_1 = \theta_2 = \theta_3 = \pi/2$, from the discussion above, the first and the second type of singularities meet.

Furthermore, if we have, more specifically, $\alpha_1 = \alpha_2 = \pi/2$, all the configurations for which $\mathbf{v}_1, \mathbf{v}_2, \mathbf{v}_3$ are coplanar to $\mathbf{u}_1, \mathbf{u}_2, \mathbf{u}_3$, are singular. This set of configurations is

characterized by the fact that the gripper can be rotated around the axis described by the unit vector $[0,0,1]^T$ without moving the input links.

In order to illustrate the foregoing comments, a plot of the reciprocal of the condition number for a full rotation of the gripper of a spherical manipulator having $\alpha_1 = \alpha_2 = \pi/3$ is given in Fig. 4.12. The reciprocal of the condition number can be thought of as a measure of the 'distance' of the Jacobian to a singularity. This concept will be clarified in Chapter 5.

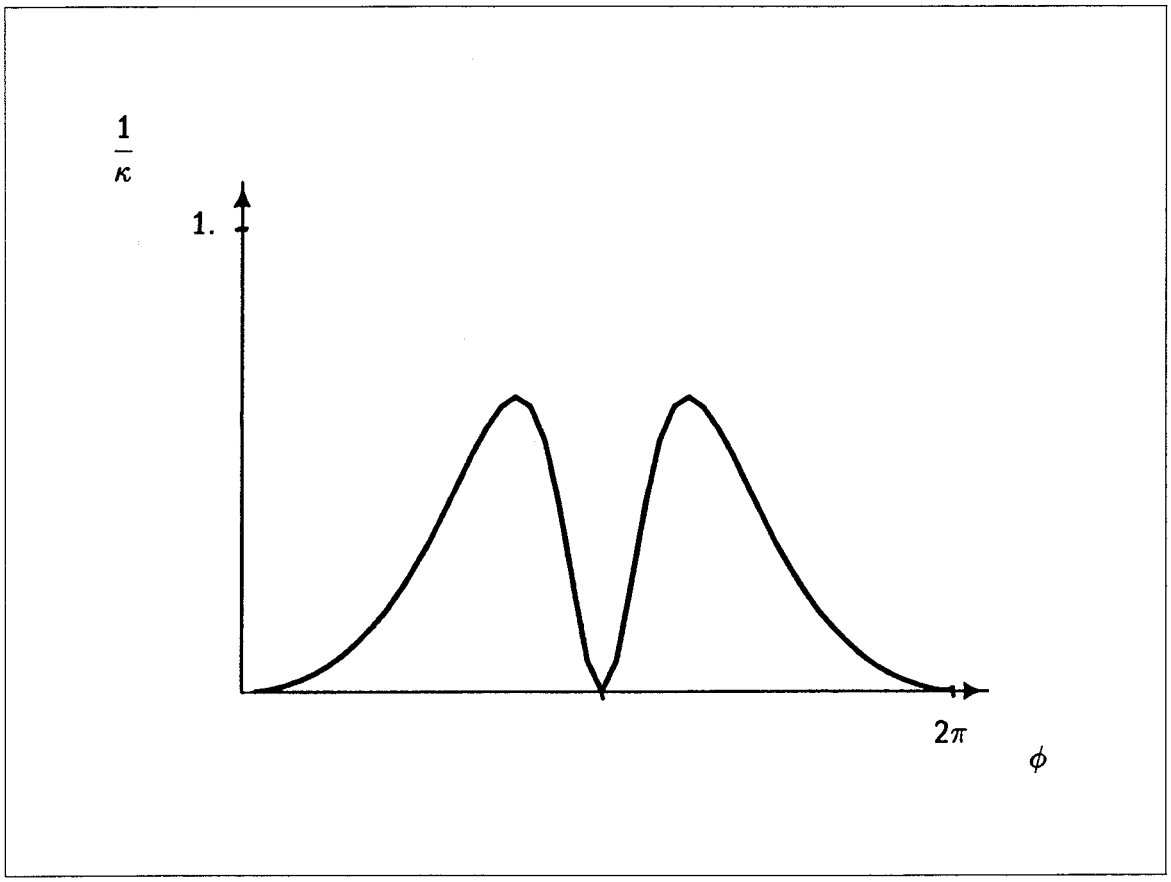

Figure 4.12 Reciprocal of the condition number for a full rotation of the gripper of a spherical manipulator with $\alpha_1 = \alpha_2 = \pi/3$. The axis of rotation is along $\mathbf{e} = [0\,0\,1]^T$.

4.4 Spatial Three-Degree-of-Freedom Manipulator

A spatial three-degree-of-freedom parallel manipulator is shown in Fig. 4.13.

The moving platform is attached to the base link by three legs which constitute kinematic chains of the *RPS* type. Only the prismatic joints are actuated. Therefore, by varying the length of each of the three legs, the position and orientation of the platform is modified. However, since the platform has only three degrees of freedom, the six coordinates defining its position and orientation are coupled and cannot be specified arbitrarily.

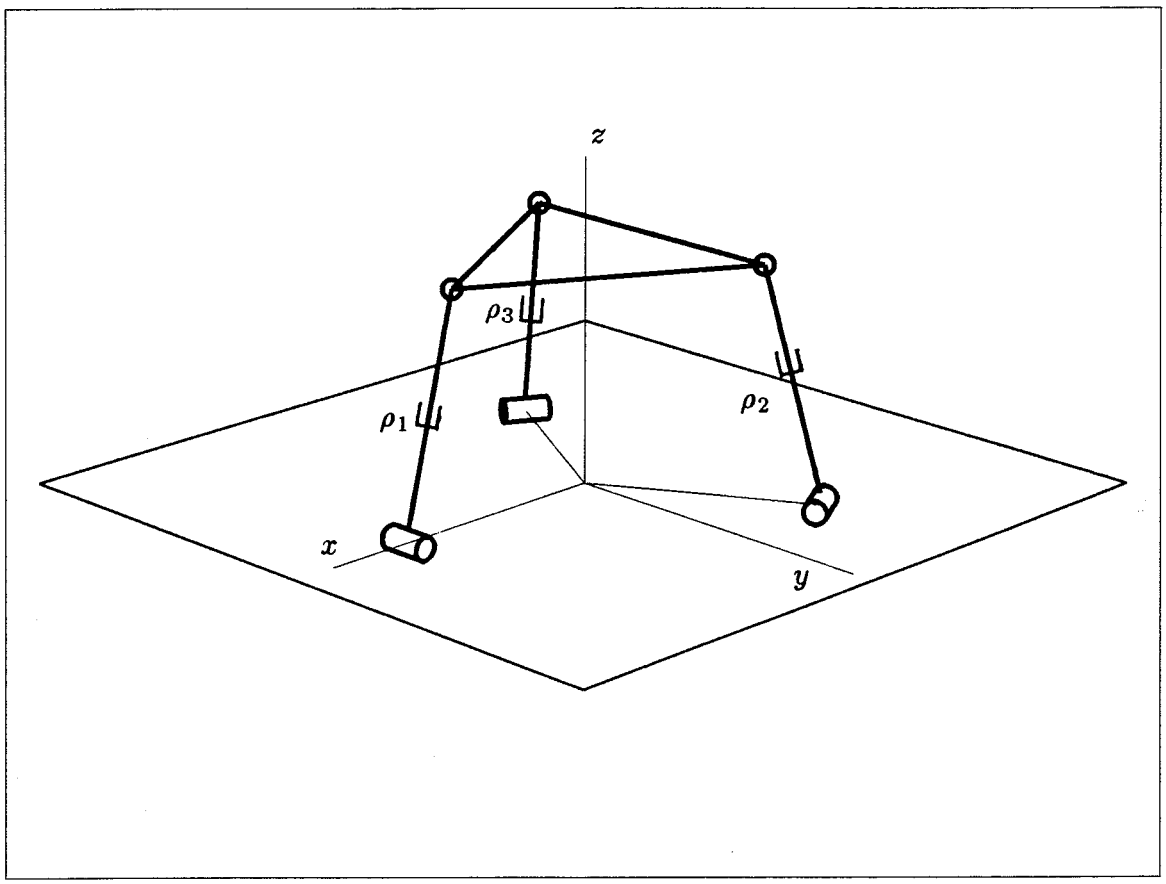

Figure 4.13 Spatial three-degree-of-freedom parallel manipulator.

This type of manipulator has been proposed by Hunt (1983) and revisited by Lee and Shah (1987) and Waldron et al. (1988a & b). In the last two references, a ten-degree-of-freedom manipulation system called *ARTISAN*, which is a hybrid serial-parallel manipulator, is discussed. The parallel part of *ARTISAN* is of the type discussed here. It is termed a micro-manipulator because of its relatively small physical dimensions and it is intended for fine accurate motion.

The potential applications of the spatial manipulator described here arise when the demand on workspace and maneuverability is low but the dynamic loading is severe and high speed and precision motion are of primary concern. For instance, it could be used as a regional structure for a manipulator which would be completed by mounting a spherical parallel manipulator of the type described in Section 4.3 on the platform, thereby leading to a hybrid structure. However, for this type of application, and whenever it is intended to use the spatial three-degree-of-freedom manipulator as a positioning device, it is necessary to solve the inverse kinematic problem where the position of a point of the platform—for instance its centroid—is prescribed and it is desired to compute the corresponding actuator motions. This problem remains unsolved in the references given above since, in all of them, the Cartesian coordinates specified for the platform contain at least one variable describing the orientation. The solution of this problem is given here and it will be shown in Chapter 5 that it leads to a simple description of the workspace of the manipulator.

4.4.1 Inverse Kinematic Problem

The notation used to describe the kinematics of the manipulator is now introduced. Referring to Fig. 4.13, we consider a coordinate system fixed to the base of the manipulator with its x and y axes lying in the plane of the base and its z axis normal to that plane. Moreover, the x axis is placed along the line joining the centroid of the base triangle—which is the origin of the coordinate system—to the revolute joint at the base of the first leg. Therefore, if we denote the position vectors of the points of attachment of each of the three legs to the base by $\mathbf{s}_i = [x_i, y_i, z_i]^T$, we will have:

$$\mathbf{s}_i = L\mathbf{u}_i \tag{4.86}$$

where L is the distance from the centroid of the base to each of the legs and the unit vectors $\mathbf{u}_i$, $i = 1,2,3$ are defined in eqs.(4.59) and (4.60a). Moreover, we define three coplanar unit vectors $\mathbf{v}_i$ as the vectors attached to the moving platform and directed along the three lines connecting the centroid of the platform, $P(x,y,z)$, with the spherical joints. As in the case of the planar and spherical manipulators, symmetry is also assumed here so

the base triangle and the platform are equilateral triangles. The extension of each of the three actuators is given by ρ_i, $i = 1,2,3$, and the position of the three spherical joints is denoted by $\mathbf{s}'_i = [x'_i, y'_i, z'_i]^T$. Similar to the case of the spherical manipulator, the reference orientation for the platform is chosen as the one for which $\mathbf{v}_i = \mathbf{u}_i$, $i = 1,2,3$. Therefore, if $\mathbf{Q}$ denotes the rotation tensor representing the attitude of the platform with respect to the reference frame, we have

$$\mathbf{v}_i = \mathbf{Q}\mathbf{u}_i, \qquad i = 1,2,3 \tag{4.87}$$

In what follows, we will denote the (i,j) component of tensor $\mathbf{Q}$, in the given reference frame, by q_{ij}.

As specified in the introduction of this section, it is now desired to solve the inverse kinematic problem for the positioning of the platform. The input variables are then the coordinates giving the position of the centroid of the platform, i.e., x, y, and z, and the corresponding values of the actuator extensions ρ_1, ρ_2 and ρ_3 are the output variables to be computed. If we assume that the orientation of the platform is known, we can write:

$$\begin{bmatrix} x'_i \\ y'_i \\ z'_i \end{bmatrix} = \begin{bmatrix} x \\ y \\ z \end{bmatrix} + l\mathbf{v}_i, \qquad i = 1,2,3 \tag{4.88}$$

where l is the distance between the centroid of the platform and each of the spherical joints and $\mathbf{v}_i$ is given by eq.(4.87). The extensions of the actuators are then computed as the distances between the points of attachment on the platform and the base, i.e., as

$$\rho_i = \sqrt{(x'_i - x_i)^2 + (y'_i - y_i)^2 + (z'_i - z_i)^2}, \qquad i = 1,2,3 \tag{4.89}$$

which leads to a unique solution for each of the legs.

However, before this solution can be used, we have to compute the rotation tensor $\mathbf{Q}$ corresponding to a given position of the platform. Because of this intermediate step, the inverse kinematic problem, as defined here, might have multiple solutions, as will be shown later.

The structure of the manipulator allows us to write some constraint equations that will lead to the derivation of the rotation tensor. Indeed, due to the revolute joint at the base of each leg, the tip of the leg, i.e., the spherical joint, is constrained to move on a plane orthogonal to the axis of rotation of the revolute. This leads to a constraint for each of the legs, namely,

$$y_1' = 0 \tag{4.90a}$$

$$\sqrt{3}x_2' + y_2' = 0 \tag{4.90b}$$

$$\sqrt{3}x_3' - y_3' = 0 \tag{4.90c}$$

Moreover, using eqs.(4.87) and (4.88), we obtain:

$$y_1' = y + lq_{21} \tag{4.91a}$$

$$x_2' = x + l(-1/2q_{11} + \sqrt{3}/2q_{12}) \tag{4.91b}$$

$$y_2' = y + l(-1/2q_{21} + \sqrt{3}/2q_{22}) \tag{4.91c}$$

$$x_3' = x + l(-1/2q_{11} - \sqrt{3}/2q_{12}) \tag{4.91d}$$

$$y_3' = y + l(-1/2q_{21} - \sqrt{3}/2q_{22}) \tag{4.91e}$$

Substitution of the foregoing expressions, (4.91a–e), into eqs.(4.90a–c), leads to:

$$q_{21} = -y/l \tag{4.92a}$$

$$\sqrt{3}(-q_{11} + \sqrt{3}q_{12} + q_{22}) = -3y - 2\sqrt{3}x \tag{4.92b}$$

$$\sqrt{3}(-q_{11} - \sqrt{3}q_{12} + q_{22}) = 3y - 2\sqrt{3}x \tag{4.92c}$$

which can be rearranged to give:

$$q_{21} = -y/l \tag{4.93a}$$

$$q_{12} = q_{21} = -y/l \tag{4.93b}$$

$$q_{11} - q_{22} = 2x/l \tag{4.93c}$$

Furthermore, since the rotation tensor $\mathbf{Q}$ is orthogonal, its components are constrained by the following:

$$\sum_{j=1}^{3} q_{ij}^2 = 1, \qquad i = 1,2,3 \tag{4.94a}$$

and

$$\sum_{k=1}^{3} q_{ik}q_{jk} = 0, \qquad i \neq j, \qquad i,j = 1,2,3 \tag{4.94b}$$

If we now consider the first two rows of **Q**, substitution of eqs.(4.93a&b) into eqs.(4.94a&b) allows us to write:

$$-q_{11}y/l - q_{22}y/l + q_{13}q_{23} = 0 \tag{4.95a}$$

$$q_{11}^2 + q_{13}^2 + (y/l)^2 = 1 \tag{4.95b}$$

$$q_{22}^2 + q_{23}^2 + (y/l)^2 = 1 \tag{4.95c}$$

which, together with eq.(4.93c), constitutes a system of four nonlinear equations in four unknowns, q_{11}, q_{22}, q_{13}, q_{23}. In order to solve this system, we first substitute eq.(4.93c) into eqs.(4.95a&b) to eliminate q_{11}. Then, expressions for q_{13}^2 and q_{23}^2 as functions of q_{22} only, are derived from eqs.(4.95b&c) and substituted into eq.(4.95a). This results into a quartic equation in q_{22} that can be written as

$$q_{22}^4 + Aq_{22}^3 + Bq_{22}^2 + Cq_{22} + D = 0 \tag{4.96a}$$

where

$$A = 4X \tag{4.96b}$$

$$B = 4X^2 - 2Y^2 - 2 \tag{4.96c}$$

$$C = -4X(1 + Y^2) \tag{4.96d}$$

$$D = Y^4 - 2Y^2 - 4X^2 + 1 \tag{4.96e}$$

with

$$X = x/l \qquad \text{and} \qquad Y = y/l \tag{4.96f}$$

The four roots of this equation, which are all always real, can be found using the procedure described in Appendix A and can be written in closed form as

$$(q_{22})_{1,2} = \sqrt{X^2 + Y^2} - X \pm 1 \tag{4.97a}$$

$$(q_{22})_{3,4} = -\sqrt{X^2 + Y^2} - X \pm 1 \tag{4.97b}$$

However, because of the nature of the unknown q_{22}, we must have

$$-1 \leq q_{22} \leq 1 \tag{4.98}$$

Therefore, only 2 out of the 4 solutions are acceptable—the other 2 solutions do not fall into that range—and they are given by:

$$(q_{22})_{1,2} = -X \pm (\sqrt{X^2 + Y^2} - 1) \tag{4.99}$$

The value of q_{11} corresponding to each of these two solutions is obtained from eq.(4.93c) and hence 4 of the entries of $\mathbf{Q}$ are known, i.e., q_{11}, q_{12}, q_{21} and q_{22}. The absolute value of all the remaining components—i.e., the last row and the last column of $\mathbf{Q}$—can be computed using the fact that the columns and rows of $\mathbf{Q}$ should have a unit Euclidean norm. There will remain a sign ambiguity on each of these quantities but, as shown in Appendix C, only two solutions for matrix $\mathbf{Q}$ can arise due to the constraints on the orthogonality of the rows and columns of $\mathbf{Q}$. As a matter of fact, it is also shown, in the aforementioned appendix that, when a solution for $\mathbf{Q}$ is found, the second one can be obtained by changing the signs of q_{13}, q_{23}, q_{31} and q_{32}.

It is pointed out that the two sets of two solutions each, obtained by choosing the plus or minus sign in eq.(4.99), correspond to two different geometric interpretations. To explain that result, we will define a unit vector $\mathbf{z}'$ attached to the platform as:

$$\mathbf{z}' = \frac{\mathbf{v}_1 \times \mathbf{v}_2}{||\mathbf{v}_1 \times \mathbf{v}_2||} \tag{4.100}$$

This unit vector is orthogonal to the plane of the platform and points along the positive direction of the z axis when the platform is in its reference configuration.

It can be shown that the two solutions of the inverse kinematic problem obtained when the positive sign is chosen in eq.(4.99) correspond to configurations for which the following holds:

$$\mathbf{z}' \cdot \mathbf{e}_3 \leq 0 \tag{4.101}$$

where $\mathbf{e}_3 = [0, 0, 1]^T$, i.e., $\mathbf{e}_3$ is a unit vector along the positive direction of the z axis. Hence, in these configurations, the upper face of the platform is facing down. Moreover,

for these two solutions, we have

$$q_{13} = q_{31} \qquad \text{and} \qquad q_{23} = q_{32} \tag{4.102}$$

which leads to

$$\text{vect}(\mathbf{Q}) = \mathbf{0} \tag{4.103}$$

and the angle of rotation associated with $\mathbf{Q}$ is equal to 0° or 180°.

On the other hand, the two solutions obtained when the negative sign is chosen in eq.(4.99) correspond to configurations for which:

$$\mathbf{z}' \cdot \mathbf{e}_3 \geq 0 \tag{4.104}$$

i.e., configurations for which the upper face of the platform is facing up. In a practical situation, these would be the solutions of interest. For these two solutions, we have:

$$q_{13} = -q_{31} \qquad \text{and} \qquad q_{23} = -q_{32} \tag{4.105}$$

which may lead to any value for the angle of rotation. However, we have:

$$\text{vect}(\mathbf{Q}) = \begin{bmatrix} a \\ b \\ 0 \end{bmatrix} \tag{4.106}$$

where a and b are arbitrary real numbers. Hence, the axis of rotation is always contained in the plane of the base. This is so because q_{12} is always equal to q_{21}, and hence, the third component of $\text{vect}(\mathbf{Q})$, i.e., $\mathbf{e}\sin\phi$, vanishes, which means that $\mathbf{e}$ lies in the x, y plane.

In summary, the inverse kinematic problem, as defined here for point positioning, leads to up to four solutions. Two of these solutions correspond to configurations in which the platform is facing down and the two remaining ones correspond to configurations in which the platform is facing up.

4.4.2 Direct Kinematic Problem

The solution of the direct kinematic problem, as in the case of the other manipulators, necessitates the utilization of a numerical procedure. The formulation developed

here consists of considering the coordinates of the three spherical joints as the unknowns of the problem. This leads to a system of nine equations in nine unknowns, i.e., the coordinates x_i', y_i' and z_i', for $i = 1,2,3$. The first three equations constraining these unknowns are eqs.(4.90a–c), which state that the legs are forced to rotate on a fixed plane. The other equations are obtained by imposing the length of each of the legs, ρ_i, for $i = 1,2,3$, and by forcing the three spherical joints to remain at a constant distance $\sqrt{3}l$ from each other. This leads to:

$$||\mathbf{s}_i - l\mathbf{u}_i|| = \rho_i, \qquad i = 1,2,3 \tag{4.107a}$$

and

$$||\mathbf{s}_i' - \mathbf{s}_j'|| = \sqrt{3}l, \qquad i \neq j, \qquad i,j = 1,2,3 \tag{4.107b}$$

Furthermore, this system can be reduced, since the first three equations, i.e., eqs.(4.90a–c) are simple linear relationships and can be easily substituted into the other equations, which then leads to a system of six equations in six unknowns, x_1', x_2', x_3', z_1', z_2' and z_3'. The resulting system of equations can be written as

$$\mathbf{f}(x_1', x_2', x_3', z_1', z_2', z_3') = \mathbf{0} \tag{4.108a}$$

where

$$f_1 = (x_1' - 1)^2 + {z_1'}^2 - \rho_1^2 \tag{4.108b}$$

$$f_2 = 4(x_2' + 1/2)^2 + {z_2'}^2 - \rho_2^2 \tag{4.108c}$$

$$f_3 = 4(x_3' + 1/2)^2 + {z_3'}^2 - \rho_3^2 \tag{4.108d}$$

$$f_4 = (x_1' - x_2')^2 + 3{x_2'}^2 + (z_1' - z_2')^2 - 3l^2 \tag{4.108e}$$

$$f_5 = (x_1' - x_3')^2 + 3{x_3'}^2 + (z_1' - z_3')^2 - 3l^2 \tag{4.108f}$$

$$f_6 = (x_2' - x_3')^2 + 3(x_2' + x_3')^2 + (z_2' - z_3')^2 - 3l^2 \tag{4.108g}$$

which can be solved using, for instance, the Newton-Raphson method. Due to the nonlinearity of the equations involved, it is hard to predict how many solutions could be obtained. A reasoning similar to the one used for the planar three-degree-of-freedom manipulator could be used by virtually disassembling one of the spherical joints. The resulting linkage would

be an *RSSR* linkage and the solutions of the direct kinematic problem would correspond to the intersection of its coupler surface—obtained by rotating the input link of the *RSSR* linkage through its range of mobility and by rotating its coupler link about the axis connecting its spherical pairs, i.e., exploiting the two real degrees of freedom of the *RSSR* linkage—with a circle, in a three dimensional space. An example of solution is given in Table 4.2, where the Newton-Raphson method has been used and four different solutions were found by varying the initial guess.

Solution #	1	2	3	4
x_1'	0.482	−0.080	0.607	0.560
x_2'	−0.254	−0.275	0.110	−0.218
x_3'	−0.243	−0.223	−0.187	0.171
z_1'	1.082	0.523	0.113	0.112
z_2'	1.203	1.220	0.450	1.171
z_3'	1.302	1.285	1.253	0.401

Table 4.2 Four solutions found to the inverse kinematic problem of a spatial three-degree-of-freedom parallel manipulator with $l = 0.5$ and when $\rho_1 = 1.2$, $\rho_2 = 1.3$, $\rho_3 = 1.4$.

4.4.3 Velocity Inversion

The relationship between the Cartesian and actuator velocities of the manipulator under study is given by the Jacobian matrix, which is defined as:

$$\dot{\rho} = \mathbf{J}\dot{\mathbf{p}} \tag{4.109}$$

where $\dot{\mathbf{p}} = [\dot{x}, \dot{y}, \dot{z}]^T$ and $\dot{\rho} = [\dot{\rho}_1, \dot{\rho}_2, \dot{\rho}_3]^T$. This equation is obtained by differentiation of the solution to the inverse kinematic problem given in Section 4.4.1. We first take the time derivative of both sides of eq.(4.89) to obtain:

$$\dot{\rho}_i = \frac{1}{\rho_i}[(x_i' - x_i)\dot{x}_i' + (y_i' - y_i)\dot{y}_i' + (z_i' - z_i)\dot{z}_i'], \qquad i = 1,2,3 \tag{4.110}$$

The expressions for the time derivatives of the coordinates of the spherical joints are then obtained by differentiation of both sides of eq.(4.88) as:

$$\dot{\mathbf{s}}_i' = \dot{\mathbf{p}} + l\dot{\mathbf{Q}}\mathbf{u}_i, \qquad i = 1,2,3 \tag{4.111a}$$

or, in component form,

$$\begin{bmatrix} \dot{x}_i' \\ \dot{y}_i' \\ \dot{z}_i' \end{bmatrix} = \begin{bmatrix} \dot{x} \\ \dot{y} \\ \dot{z} \end{bmatrix} + l\cos\gamma_i \begin{bmatrix} \dot{q}_{11} \\ \dot{q}_{21} \\ \dot{q}_{31} \end{bmatrix} + l\sin\gamma_i \begin{bmatrix} \dot{q}_{12} \\ \dot{q}_{22} \\ \dot{q}_{32} \end{bmatrix} \tag{4.111b}$$

where

$$\gamma_i = 2(i-1)\pi/3, \quad i = 1,2,3 \tag{4.111c}$$

Moreover, the time derivatives of the components of the rotation tensor $\mathbf{Q}$ involved in the foregoing equation can be obtained by differentiation of eqs.(4.93a–b), (4.99), and (4.95b–c), which leads to

$$\dot{q}_{11} = \frac{\dot{x}}{l} \pm \left(\frac{x\dot{x} + y\dot{y}}{l\sqrt{x^2 + y^2}} \right) \tag{4.112a}$$

$$\dot{q}_{12} = -\dot{y}/l \tag{4.112b}$$

$$\dot{q}_{21} = -\dot{y}/l \tag{4.112c}$$

$$\dot{q}_{22} = \frac{-\dot{x}}{l} \pm \left(\frac{x\dot{x} + y\dot{y}}{l\sqrt{x^2 + y^2}} \right) \tag{4.112d}$$

$$\dot{q}_{13} = \frac{-1}{q_{13}}[q_{11}\dot{q}_{11} + q_{12}\dot{q}_{12}] \tag{4.112e}$$

$$\dot{q}_{23} = \frac{-1}{q_{23}}[q_{21}\dot{q}_{21} + q_{22}\dot{q}_{22}] \tag{4.112f}$$

Then, substitution of eqs.(4.112a–f) into eq.(4.111b) allows us to rewrite eq.(4.111b) as

$$\dot{x}_i' = A_i\dot{x} + D_i\dot{y} \tag{4.113a}$$

$$\dot{y}_i' = B_i\dot{x} + E_i\dot{y} \tag{4.113b}$$

$$\dot{z}_i' = C_i\dot{x} + F_i\dot{y} + \dot{z} \tag{4.113c}$$

where

$$A_i = 1 + \cos\gamma_i(1 \pm r_x) \tag{4.114a}$$

$$B_i = \sin\gamma_i(-1 \pm r_x) \tag{4.114b}$$

$$C_i = \cos\gamma_i(1 \pm r_x)\left(\frac{-q_{11}}{q_{13}}\right) + \sin\gamma_i(-1 \pm r_x)\left(\frac{-q_{22}}{q_{23}}\right) \tag{4.114c}$$

$$D_i = \pm r_y \cos\gamma_i - \sin\gamma_i \tag{4.114d}$$

$$E_i = 1 - \cos\gamma_i \pm r_y \sin\gamma_i \tag{4.114e}$$

$$F_i = -\left(\frac{\cos\gamma_i}{q_{13}}\right)(-q_{12} \pm q_{11}r_y) - \left(\frac{\sin\gamma_i}{q_{23}}\right)(-q_{21} \pm q_{22}r_y) \tag{4.114f}$$

and

$$r_x = \frac{x}{\sqrt{x^2+y^2}} \tag{4.115a}$$

$$r_y = \frac{y}{\sqrt{x^2+y^2}} \tag{4.115b}$$

and hence the ith row of the Jacobian matrix, $\mathbf{j}_i^T$, can be written as

$$\mathbf{j}_i = \frac{1}{\rho_i}[\,\lambda_{i1},\quad \lambda_{i2},\quad (z_i' - z_i)\,]^T \tag{4.116a}$$

with

$$\lambda_{i1} = A_i(x_i' - x_i) + B_i(y_i' - y_i) + C_i(z_i' - z_i) \tag{4.116b}$$

$$\lambda_{i2} = D_i(x_i' - x_i) + E_i(y_i' - y_i) + F_i(z_i' - z_i) \tag{4.116c}$$

and the velocity inversion is completed.

4.4.4 Acceleration Inversion

The time derivative of eq.(4.109) leads to the expression relating the Cartesian and joint accelerations, which is written as

$$\ddot{\rho} = \mathbf{J}\ddot{\mathbf{p}} + \dot{\mathbf{J}}\dot{\mathbf{p}} \tag{4.117}$$

where the acceleration vectors are defined as $\ddot{\rho} = [\ddot{\rho}_1, \ddot{\rho}_2, \ddot{\rho}_3]^T$ and $\ddot{\mathbf{p}} = [\ddot{x}, \ddot{y}, \ddot{z}]^T$. To complete the acceleration inversion, the time derivative of the Jacobian matrix, $\dot{\mathbf{J}}$, has to be derived. This leads to the following expression for $\mathbf{k}_i^T$, the ith row of this matrix

$$\mathbf{k}_i = \frac{1}{\rho_i^2}[\,\rho_i\dot{\lambda}_{i1} - \lambda_{i1}\dot{\rho}_i,\quad \rho_i\dot{\lambda}_{i2} - \lambda_{i2}\dot{\rho}_i,\quad \rho_i\dot{z}_i' - \dot{\rho}_i(z_i' - z_i)\,]^T \tag{4.118}$$

where the time derivative of the λ_i's have not been derived yet. They are obtained from eq.(4.116b&c) and can be written as:

$$\dot{\lambda}_{i1} = (x_i' - x_i)\dot{A}_i + A_i\dot{x}_i' + (y_i' - y_i)\dot{B}_i + B_i\dot{y}_i' + (z_i' - z_i)\dot{C}_i + C_i\dot{z}_i' \quad (4.119a)$$

$$\dot{\lambda}_{i2} = (x_i' - x_i)\dot{D}_i + D_i\dot{x}_i' + (y_i' - y_i)\dot{E}_i + E_i\dot{y}_i' + (z_i' - z_i)\dot{F}_i + F_i\dot{z}_i' \quad (4.119b)$$

where

$$\dot{A}_i = \pm w_1 \cos\gamma_i \quad (4.120a)$$

$$\dot{B}_i = \pm w_1 \sin\gamma_i \quad (4.120b)$$

$$\dot{C}_i = \pm w_1 \cos\gamma_i(-q_{11}/q_{31}) + t_1 \cos\gamma_i(1 \pm r_x) \pm w_1 \sin\gamma_i(-q_{22}/q_{32}) + t_2 \sin\gamma_i(-1 \pm r_x) \quad (4.120c)$$

$$\dot{D}_i = \pm w_2 \cos\gamma_i \quad (4.120d)$$

$$\dot{E}_i = \pm w_2 \sin\gamma_i \quad (4.120e)$$

$$\dot{F}_i = \cos\gamma_i[\pm w_2(-q_{11}/q_{31}) \pm r_y t_1 + t_3] + \sin\gamma_i[\pm w_2(-q_{22}/q_{32}) \pm r_y t_2 + t_4] \quad (4.120f)$$

with

$$w_1 = \left(\frac{y^2\dot{x} - xy\dot{y}}{(x^2+y^2)^{3/2}}\right) \quad (4.121a)$$

$$w_2 = \left(\frac{x^2\dot{y} - xy\dot{x}}{(x^2+y^2)^{3/2}}\right) \quad (4.121b)$$

and

$$t_1 = \left(\frac{q_{11}\dot{q}_{31} - q_{31}\dot{q}_{11}}{q_{31}^2}\right) \quad (4.121c)$$

$$t_2 = \left(\frac{q_{22}\dot{q}_{32} - q_{32}\dot{q}_{22}}{q_{32}^2}\right) \quad (4.121d)$$

$$t_3 = \left(\frac{q_{31}\dot{q}_{21} - q_{21}\dot{q}_{31}}{q_{31}^2}\right) \quad (4.121e)$$

$$t_4 = \left(\frac{q_{32}\dot{q}_{12} - q_{12}\dot{q}_{32}}{q_{32}^2}\right) \quad (4.121f)$$

4.4.5 Singularity Analysis

First type of singularities:

Under the assumption that the linear actuators have an infinite range of motion, the first type of singularities would occur only when one of the legs has a length of zero, i.e.,

$$\rho_i = 0, \qquad i = 1 \text{ or } 2 \text{ or } 3 \tag{4.122}$$

This result is obtained from eq.(4.116a), which clearly shows that such a situation produces a Jacobian matrix whose determinant tends to infinity.

However, in a real manipulator, the actuators have a finite range of motion, i.e.,

$$\rho_{min} < \rho_i < \rho_{max}, \quad i = 1,2,3 \tag{4.123}$$

where ρ_{min} is, in general, positive. In this case, the first type of singularities occurs when one of the actuators reaches one of its limits, i.e.:

$$\rho_i = \rho_{min} \qquad \text{or} \qquad \rho_i = \rho_{max}, \qquad i = 1 \text{ or } 2 \text{ or } 3 \tag{4.124}$$

which, again, corresponds to the limit of the workspace. Since one of the actuators cannot move further in one direction, a certain set of velocities, corresponding to that motion of the actuator, cannot be produced.

Second type of singularities:

The second type of singularities occurs in configurations where we can find a set of velocities of the platform that produce vanishing joint velocity vectors. In other words, this type of singularities happens when there exists a set of velocities of the paltform that will correspond to velocities of the spherical joints which are orthogonal to the leg to which they are attached.

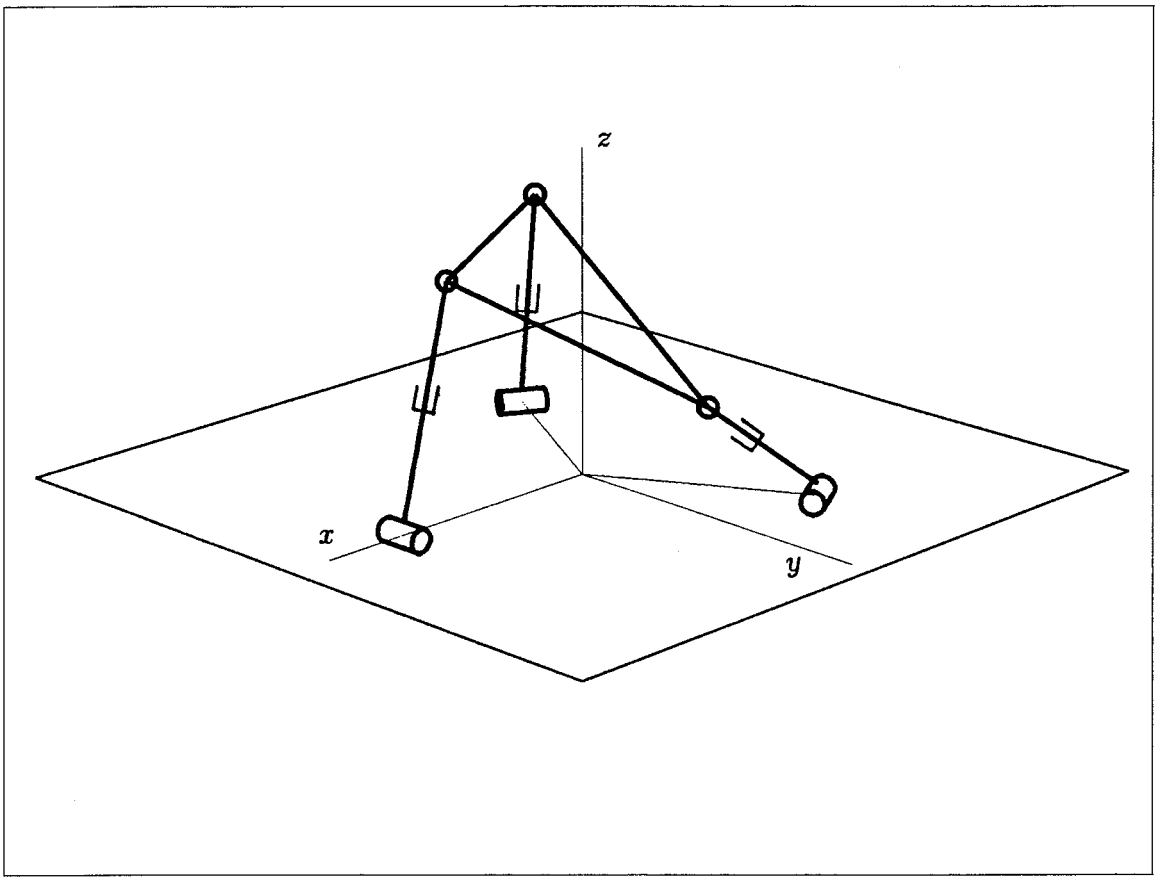

Figure 4.14 Example of the second type of singularity for the spatial three-degree-of-freedom parallel manipulator.

An example of this is shown in Fig. 4.14, where the first leg is contained in the plane of the platform. Therefore, a rotation of the platform around the axis connecting the spherical joints attached to legs 2 and 3 will produce a vanishing joint velocity vector. Another example is represented in Fig. 4.15, where the whole manipulator is contained in the base plane. In that configuration, a translational velocity of the platform along a direction perpendicular to the base plane will produce a zero joint velocity vector.

Third type of singularities:

For this type of manipulator, the third type of singularities occurs when the base triangle and the platform have the same dimensions, i.e., when $l = L$. The first two kinds of singularities can then meet when all the legs have a length of zero but since this would not be possible in a real manipulator, this type of singularities will generally not happen.

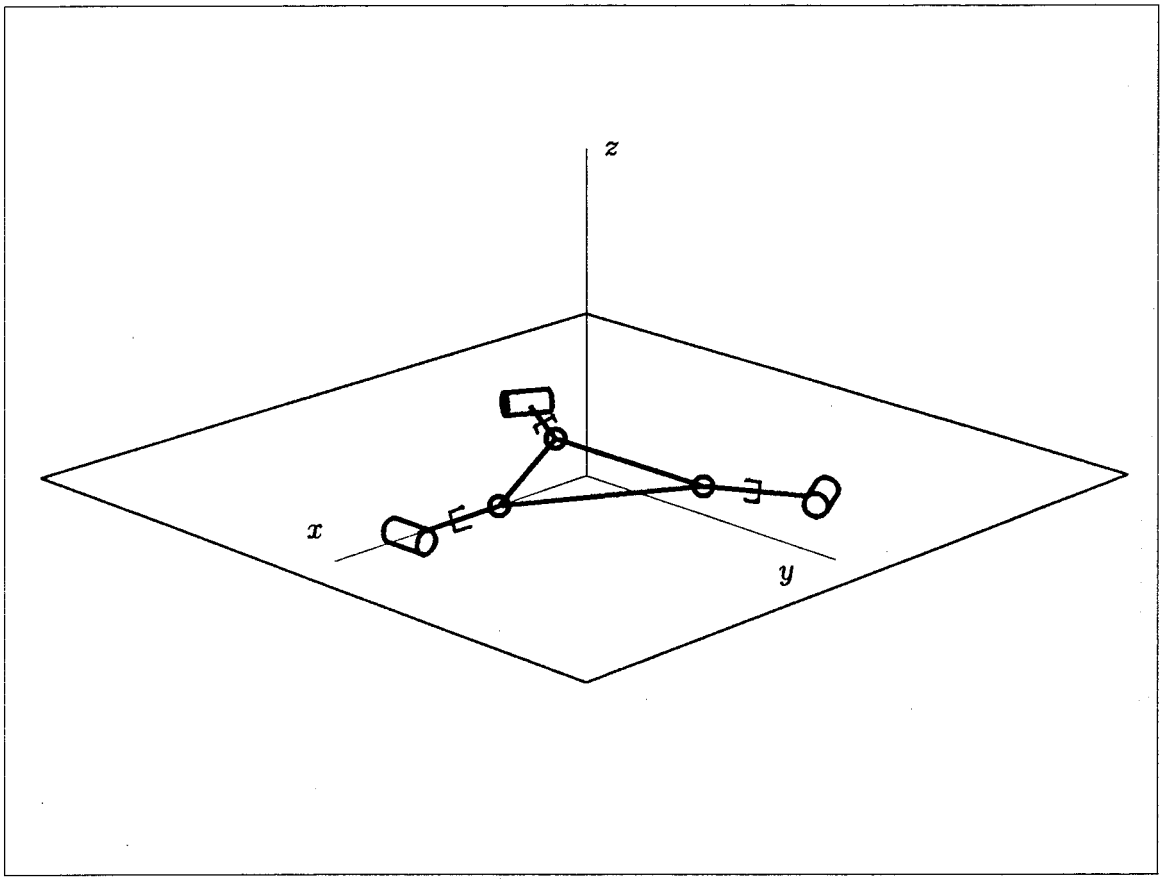

Figure 4.15 Example of the second type of singularity for the spatial three-degree-of-freedom parallel manipulator.

4.5 Spatial Six-Degree-of-Freedom Manipulator

A general six-degree-of-freedom parallel manipulator is shown in Fig. 4.16. Each of the six legs connecting the platform to the base are kinematic chains having six degrees of freedom, i.e., they are equivalent to a six-axis manipulator. This type of device has been the subject of more intensive research than the parallel manipulators studied in the preceeding sections of this chapter because of its use as a flight simulator. This application was suggested by Stewart (1965) although it would seem that the first machine of this type was built by Gough in 1949 (Stewart 1965) and was used to test tires.

However, only rather recently, namely, in the seventies, researchers started considering to use this kinematic structure as a robotic device. The idea seems to have been suggested by Hunt (1978)—although Tindale (Stewart 1965) had already suggested to

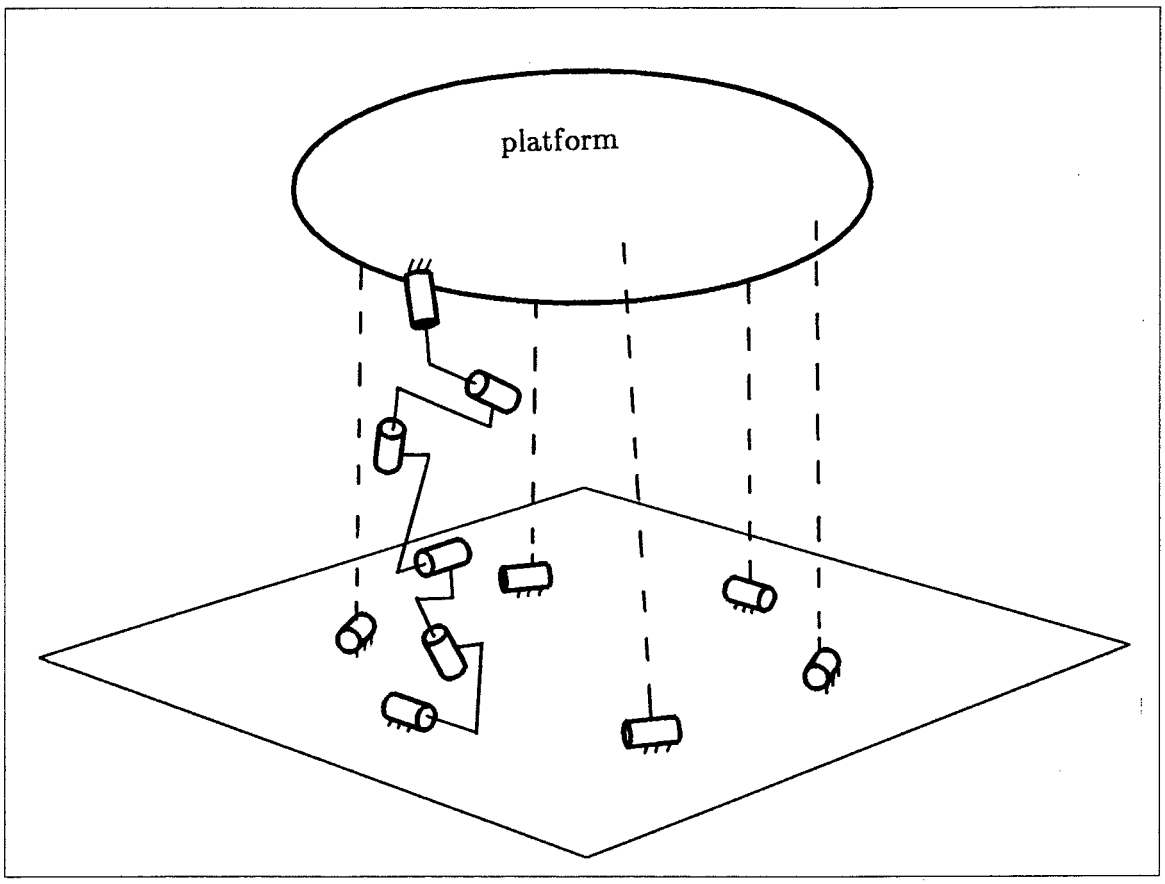

Figure 4.16 General six-degree-of-freedom parallel manipulator.

use the platform as a machine tool—and it was further developed in (Hunt 1978, 1983; MacCallion and Pham 1979; Yang and Lee 1984; Mohamed and Duffy 1985; Inoue et al. 1985; Fichter 1986; Merlet 1987, 1988; Reboulet 1988) and led to robotic systems based on this architecture such as, for instance, the SPACE-1 system (Système Poignet à Contrôle d'Effort) developed in France by CERT (Centre d'Etudes et de Recherches de Toulouse).

However, in all the aforementioned references, only special cases of spatial six-degree-of-freedom parallel manipulators are considered. In fact, the complexity of a spatial parallel manipulator can be described by the number of branches that can possibly be obtained in the solution of the inverse kinematic problem. This number is given by b^6, where b denotes the number of branches for each of the chains constituting the legs, since there are six legs. The total number of branches for different cases of chains is shown in Table 4.3. In the most general case, a six-degree-of-freedom serial manipulator leads to 16 solutions

(Primrose 1986; Lee and Liang 1988) and therefore, the fully-general parallel manipulator may lead to roughly 16.8 million solutions. In all the references mentioned above but one, the simplest case of parallel manipulator, having only one branch, is considered. It is only in (Inoue et al. 1985) that a manipulator of the second type (two solutions per leg) is considered and no reference was found where cases of greater complexity are handled.

b	n
1	1
2	64
4	4096
8	262144
16	16777216

Table 4.3 Number of branches (n) in six-degree-of-freedom, six-leg parallel manipulators as a function of the number of branches of each of the legs (b).

4.5.1 Inverse Kinematic Problem

The solution of the inverse kinematic problem of a spatial six-degree-of-freedom parallel manipulator is very similar to the solution of the same problem for a serial six-axis manipulator. Indeed, when the pose—position and orientation—of the platform is given, the solution of the inverse kinematic problem consists of computing the joint coordinates for each of the legs. Therefore, the solution of the inverse kinematic problem for each of the legs is analogous to the solution of the inverse kinematic problem of a serial six-axis manipulator, except that only one of the joint coordinates, on each leg, is really required for control. In general, however, the computation of one of the joint coordinates entails the computation of all of them. The solution of the inverse kinematic problem for the parallel six-degree-of-freedom manipulator is therefore, in the most general case, a repetition (six times) of the solution of the inverse kinematics of a six-axis serial manipulator. The general numerical methods of solution of the inverse kinematic problem developed for serial manipulators (Tsai and Morgan 1985; Takano 1985; Angeles 1985; Gupta and Kazerounian 1985) are then also applicable to parallel manipulators.

In some particular cases, like the Stewart platform, i.e., case 1 in Table 4.3, the solution of the inverse kinematic problem of a parallel six-degree-of-freedom manipulator becomes very simple. It is emphasized here that this is the case because each of the legs of the manipulator have a very simple kinematic structure, which leads to simple closed-form solutions for the inverse kinematic problem of the corresponding serial manipulator. The kinematic equations of such an arrangement can be found in many references on the subject. They are included here for quick reference.

The term *Stewart platform* is generally used to designate a six-degree-of-freedom parallel manipulator of the first type in Table 4.3, i.e., a manipulator for which each of the legs is equivalent to a kinematic structure of the *SPS* type. It is pointed out that both spherical joints are not necessary and one of them can be replaced by a Hooke joint, i.e., two revolutes with intersecting axes. A manipulator of this type is shown in Fig. 4.17a, where the notation used is now described. Again, symmetry is assumed and the points of attachment of the legs, i.e., the centres of the spherical joints, are located on the base and on the platform as shown in Figs. 4.17b & c, i.e., on the circumference of circles of radii R_B (base) and R_P (platform), respectively. The points of attachment are grouped by pairs which are uniformly spaced along the circle. The angles between the points and the average position of each of the pairs along the circle are given by ϕ_B (base) and ϕ_P (platform). Moreover, the points of attachment of the legs on the base and the platform are denoted by B_i and P_i, for $i = 1,\ldots,6$, respectively. Furthermore, the position vectors of points B_i and P_i are given by vectors $\mathbf{b}_i$ and $\mathbf{p}_i$, for $i = 1,\ldots,6$, respectively, in a coordinate frame fixed to the base of the manipulator, while the position vectors of points P_i in a coordinate frame fixed to the platform are given by vectors $\mathbf{p}'_i$, for $i = 1,\ldots,6$.

We can then write

$$\mathbf{b}_i = \begin{bmatrix} R_B \cos\theta_i \\ R_B \sin\theta_i \\ 0 \end{bmatrix}, \qquad i = 1,\ldots,6 \tag{4.125a}$$

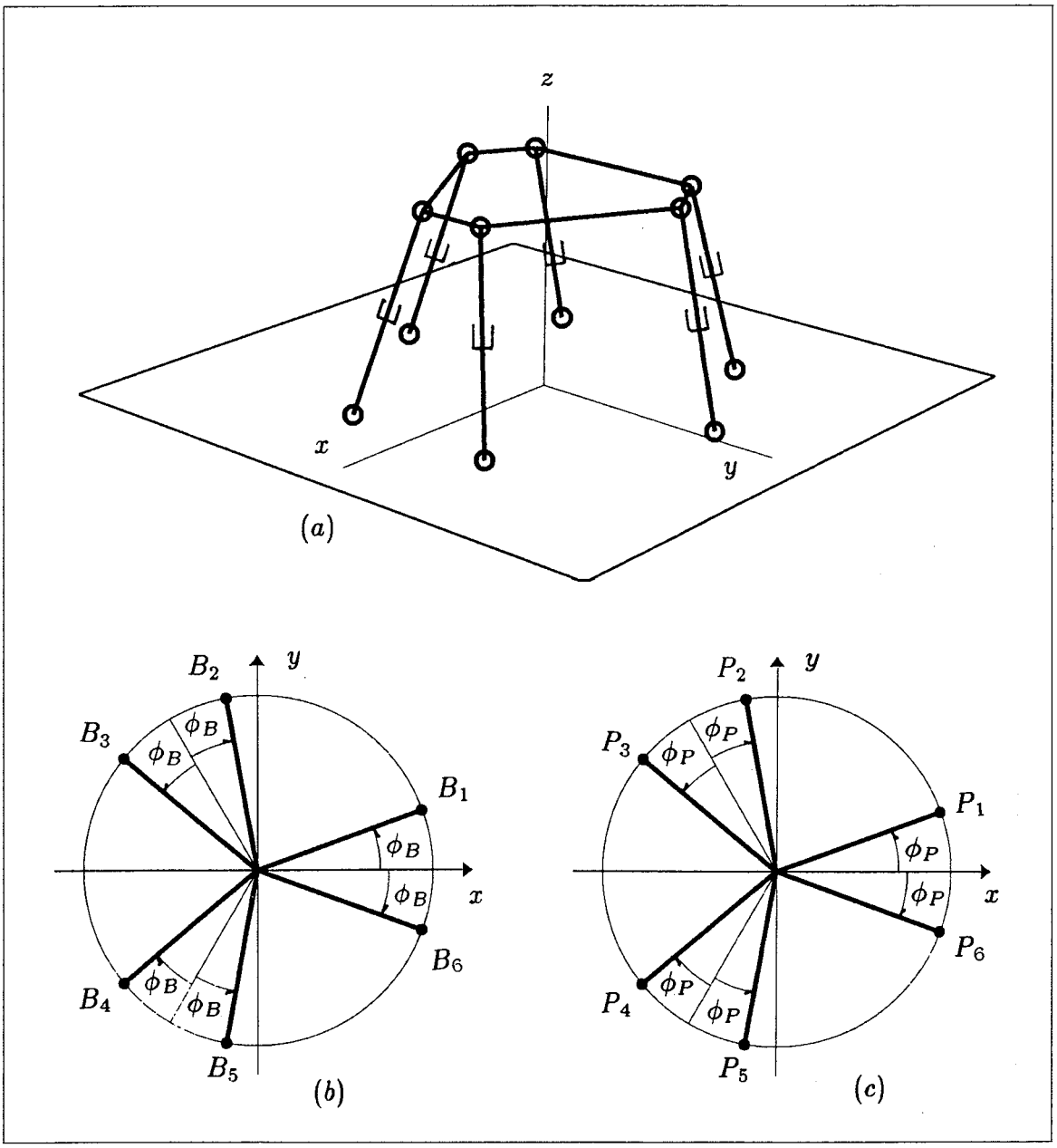

Figure 4.17 (*a*)Stewart platform (*b*)position of the joints on the base (*c*)position of the joints on the platform.

where

$$\theta \equiv \begin{bmatrix} \theta_1 \\ \theta_2 \\ \theta_3 \\ \theta_4 \\ \theta_5 \\ \theta_6 \end{bmatrix} = \begin{bmatrix} \phi_B \\ 2\pi/3 - \phi_B \\ 2\pi/3 + \phi_B \\ 4\pi/3 - \phi_B \\ 4\pi/3 + \phi_B \\ -\phi_B \end{bmatrix} \tag{4.125b}$$

and

$$\mathbf{p}_i' = \begin{bmatrix} R_P \cos\eta_i \\ R_P \sin\eta_i \\ 0 \end{bmatrix}, \qquad i = 1,\ldots,6 \tag{4.126a}$$

Moreover,

$$\eta \equiv \begin{bmatrix} \eta_1 \\ \eta_2 \\ \eta_3 \\ \eta_4 \\ \eta_5 \\ \eta_6 \end{bmatrix} = \begin{bmatrix} \phi_P \\ 2\pi/3 - \phi_P \\ 2\pi/3 + \phi_P \\ 4\pi/3 - \phi_P \\ 4\pi/3 + \phi_P \\ -\phi_P \end{bmatrix} \tag{4.126b}$$

We denote the position vector of the centroid of the platform by $\mathbf{x}$, while the rotation tensor defining the orientation of the platform by $\mathbf{Q}$. The position of each of the spherical joints attached to the platform is therefore written as:

$$\mathbf{p}_i = \mathbf{x} + \mathbf{Q}\mathbf{p}_i', \qquad i = 1,\ldots,6 \tag{4.127}$$

Subtracting vector $\mathbf{b}_i$ from both sides of eq.(4.127) leads to

$$\mathbf{p}_i - \mathbf{b}_i = \mathbf{x} + \mathbf{Q}\mathbf{p}_i' - \mathbf{b}_i, \qquad i = 1,\ldots,6 \tag{4.128}$$

Now, taking the Euclidean norm of both sides of eq.(4.128), we finally derive

$$||\mathbf{p}_i - \mathbf{b}_i|| = ||\mathbf{x} + \mathbf{Q}\mathbf{p}_i' - \mathbf{b}_i|| = c_i, \qquad i = 1,\ldots,6 \tag{4.129}$$

where c_i is the length of the ith leg, i.e., the value of the ith joint coordinate. The solution of the inverse kinematic problem of the Stewart platform is therefore completed and can be rewritten as

$$c_i = \sqrt{U_i^2 + V_i^2 + W_i^2}, \qquad i = 1,\ldots,6 \tag{4.130a}$$

where

$$U_i = x + q_{11}R_P \cos\eta_i + q_{12}R_P \sin\eta_i - R_B \cos\theta_i \tag{4.130b}$$

$$V_i = y + q_{21}R_P \cos\eta_i + q_{22}R_P \sin\eta_i - R_B \sin\theta_i \tag{4.130c}$$

$$W_i = z + q_{31}R_P \cos\eta_i + q_{32}R_P \sin\eta_i \tag{4.130d}$$

in which variables x, y, z and q_{ij}, for $i, j = 1, 2, 3$, are the components of the Cartesian coordinates, i.e., vector $\mathbf{x}$ and matrix $\mathbf{Q}$. Thus, in the coordinate frame fixed to the base,

$$\mathbf{x} = \begin{bmatrix} x \\ y \\ z \end{bmatrix} \quad \text{and} \quad \mathbf{Q} = \begin{bmatrix} q_{11} & q_{12} & q_{13} \\ q_{21} & q_{22} & q_{23} \\ q_{31} & q_{32} & q_{33} \end{bmatrix} \tag{4.131}$$

4.5.2 Direct Kinematic Problem

The problem of finding the Cartesian position and orientation of the platform, associated with given actuator lengths is now discussed. This problem consists, in fact, of the solution of the nonlinear system of equations given in eq.(4.130a) for the Cartesian coordinates. The problem can be formulated using any kind of convention for the representation of the orientation of the platform. For instance, a formulation based on Euler angles is presented in (Dieudonne et al. 1972), where numerical results obtained with the Newton-Raphson method are shown. In the aforementioned formulation, a system of six equations in six unknowns is solved, the unknowns being the position coordinates x, y, z of the centroid of the platform and three Euler angles ψ_1, ψ_2, ψ_3 giving the attitude of the platform. This implies, of course, that we have expressed the rotation tensor as

$$\mathbf{Q} = \mathbf{Q}(\psi_1, \psi_2, \psi_3) \tag{4.132}$$

using a Euler angle convention.

Alternatively, the orientation of the platform could be represented by all the components of the rotation matrix or by some of its invariants. This formulation would lead to a larger system of equations since the constraints on the orthogonal matrix, or on the said invariants, would have to be introduced as additional equations. This formulation would have the merit of eliminating the singularities introduced by the Euler angles, but, depending on the invariants used, other singularities may be introduced (cf. Appendix B). It is to be noted that the use of Euler parameters does not introduce any spurious singularity.

4.5.3 Velocity Inversion

Again, we can write the relationship between the Cartesian and joint velocities as follows:

$$\dot{\mathbf{c}} = \mathbf{J}\dot{\mathbf{x}} \tag{4.133}$$

where $\dot{\mathbf{c}}$ and $\dot{\mathbf{x}}$ are defined as $\dot{\mathbf{c}} = [\dot{c}_1, \ldots, \dot{c}_6]^T$ and $\dot{\mathbf{x}} = [\dot{x}, \dot{y}, \dot{z}, \omega_1, \omega_2, \omega_3]^T$, in which the angular velocity of the platform is defined as $\omega = [\omega_1, \omega_2, \omega_3]^T$. This equation, and hence, an expression for the Jacobian matrix $\mathbf{J}$, is obtained by differentiation of eqs.(4.130a–d). Moreover, we can again make use of the following property of the rotation tensor:

$$\dot{\mathbf{Q}} = \mathbf{\Omega Q} \tag{4.134a}$$

where

$$\mathbf{\Omega} = \mathbf{1} \times \omega \tag{4.134b}$$

to obtain the time derivative of this tensor. Also, we define a set of vectors $\mathbf{w}_i$, for $i = 1, \ldots, 6$ as

$$\mathbf{w}_i = c_i \mathbf{e}_i = \begin{bmatrix} U_i \\ V_i \\ W_i \end{bmatrix} \tag{4.135}$$

where $\mathbf{e}_i$ is a unit vector along the ith leg, pointing from the base to the platform. The ith row of the Jacobian matrix, $\mathbf{j}_i^T$, can then be written as

$$\mathbf{j}_i = \frac{1}{c_i} \left[\mathbf{w}_i^T, (-\mathbf{W}_i \mathbf{Q} \mathbf{p}_i')^T \right]^T, \quad i = 1, \ldots, 6 \tag{4.136a}$$

where

$$\mathbf{W}_i = \mathbf{1} \times \mathbf{w}_i \tag{4.136b}$$

and the velocity inversion is completed.

4.5.4 Acceleration Inversion

Differentiation with respect to time of both sides of the velocity equation, i.e., eq.(4.133), leads to the expression relating Cartesian and joint accelerations for this manipulator, namely,

$$\ddot{\mathbf{c}} = \mathbf{J}\ddot{\mathbf{x}} + \dot{\mathbf{J}}\dot{\mathbf{x}} \tag{4.137}$$

where the time derivative of the Jacobian matrix needs to be defined. The ith row of this matrix, denoted as $\mathbf{k}_i^T$, can be obtained as

$$\mathbf{k}_i = \frac{1}{l_i^2} \left[\mathbf{r}_i^T, \mathbf{s}_i^T \right]^T, \quad i = 1, \ldots, 6 \tag{4.138a}$$

where

$$\mathbf{r}_i = c_i\dot{\mathbf{w}}_i - \dot{c}_i\mathbf{w}_i \tag{4.138b}$$

$$\mathbf{s}_i = -c_i[\dot{\mathbf{W}}_i\mathbf{Q}\mathbf{p}_i' + \mathbf{W}_i\dot{Q}p_i'] + \dot{c}_i\mathbf{W}_i\mathbf{Q}\mathbf{p}_i' \tag{4.138c}$$

and

$$\dot{\mathbf{W}}_i = \mathbf{1} \times \dot{\mathbf{w}}_i \tag{4.138d}$$

with

$$\dot{\mathbf{w}}_i = \begin{bmatrix} \dot{x} + (\omega_2 q_{31} - \omega_3 q_{21})R_P \cos\eta_i + (\omega_2 q_{32} - \omega_3 q_{22})R_P \sin\eta_i \\ \dot{y} + (\omega_3 q_{11} - \omega_1 q_{31})R_P \cos\eta_i + (\omega_3 q_{12} - \omega_1 q_{32})R_P \sin\eta_i \\ \dot{z} + (\omega_1 q_{21} - \omega_2 q_{11})R_P \cos\eta_i + (\omega_1 q_{22} - \omega_2 q_{12})R_P \sin\eta_i \end{bmatrix} \tag{4.138e}$$

which completes the acceleration inversion.

4.5.5 Singularity Analysis

First type of singularities:

Since the actuators of the Stewart platform are prismatic, the first type of singularities occurs when one of these actuators reaches its limit, just as in the case of the three-degree-of-freedom spatial parallel manipulator.

Second type of singularities:

The singularities of the second type for the Stewart platform have been discussed in some references, namely (Fichter 1986; Reboulet 1988; Merlet 1988). In the latter reference, several types of configurations in which the platform's Jacobian is singular are described in detail. For each of these configurations, there exists a set of velocities of the platform that will produce vanishing velocities at all the actuators.

Third type of singularities:

The situation is similar to the one encountered in the case of the three-degree-of-freedom spatial parallel manipulator, i.e., the third type of singularities occurs when the platform and the base have the same dimensions, i.e.,

$$R_P = R_B \quad \text{and} \quad \phi_P = \phi_B \tag{4.139}$$

If this is the case, the manipulator becomes uncontrollable when all the actuator lengths are the same. Indeed, the platform can undergo pure translations when all the actuators are locked and the manipulator is in the said configuration.

Chapter 5 OPTIMIZATION OF PARALLEL MANIPULATORS

The kinematic optimization of parallel manipulators is addressed in this chapter. The detailed analysis of the kinematics of the parallel manipulators conducted in Chapter 4 will now be used to define and optimize their properties.

An important question that arises in the process of designing robotic manipulators is the choice of the optimization criteria. In the context of kinematics, several concepts have been used as design guidelines. In fact, most of the serial robots currently in use have been designed considering invertibility as a constraint, i.e., requiring that the solution to the inverse kinematic problem be available in closed-form. Many authors (Cwiakala and Lee 1985; Kohli and Spanos 1985; Lin and Freudenstein 1986; Gupta 1986a; Kumar and Patel 1986) have also analyzed the workspace of manipulators and have sometimes used it as a design criterion. Other authors (Vijaykumar et al 1986; Yang and Lai 1985, Yoshikawa 1985) have investigated the possibility of defining dexterity or manipulability indices which could be used for optimization. A review of these is given in (Klein and Blaho 1987).

The recent development of numerical algorithms (Tsai and Morgan 1985; Takano 1985; Angeles 1985; Gupta and Kazerounian 1985), capable of inverting serial manipulators of arbitrary architecture, allows designers to relax the constraint of invertibility and thus opens the avenue for new design criteria. Moreover, since this thesis is devoted to parallel manipulators which exhibit, most of the time, a simple closed-form solution to their inverse kinematic problem, the invertibility constraint disappears.

In this chapter, we will be mainly considering two optimization criteria, i.e., the *workspace* or reachable volume and the *dexterity* of robotic manipulators. The dexterity index used here is based on the condition number of the Jacobian matrix of the manipulator, a quantity that has attracted the attention of some researchers (Salisbury and Craig 1982; Angeles and Rojas 1987; Angeles and López-Cajún 1987). A discussion on the condition number can be found in Appendix D. It is pointed out that this concept was already used for the kinematic optimization of a closed-loop manipulator by Stoughton and Kokkinis (1987).

The aforementioned condition number, which can also be termed *local dexterity*, is of great interest for the planning of optimum trajectories of given robots, as will be shown in Chapter 6. However, for the task at hand, i.e., the optimum kinematic design of a manipulator, one may be interested in an index that represents a global property of the manipulator. This motivates the introduction of a new performance index which is defined here and termed the *global conditioning index* (GCI). This index is based on the distribution of the condition number of the Jacobian matrix, i.e., it is a measure of the conditioning of the manipulator over the whole workspace.

The first section of this chapter will be devoted to a discussion on the dexterity of manipulators and to the definition of the GCI. Then, the two design criteria mentioned above, i.e., workspace and dexterity, will be applied to the kinematic optimization of some of the parallel manipulators presented in Chapter 4.

5.1 Dexterity of Robotic Manipulators

As stated in the introduction of this chapter, the dexterity index defined here is based on the condition number of the Jacobian matrix. This quantity, which is a measure of the local dexterity, can be used for both serial and parallel manipulators as will now be shown.

The Jacobian matrix of a serial-type manipulator is defined as the matrix representing the transformation mapping the joint rates into the Cartesian velocities. This transformation is written as:

$$\mathbf{J}\dot{\theta} = \dot{\mathbf{x}} \tag{5.1}$$

where $\dot{\theta}$ is the vector of joint rates and $\dot{\mathbf{x}}$ is the vector of Cartesian velocities. However, as we have seen in Chapter 4, it is more convenient to define the Jacobian matrix of closed-loop manipulators in terms of the inverse transformation, i.e.,

$$\mathbf{K}\dot{\mathbf{x}} = \dot{\theta} \tag{5.2}$$

The accuracy of the control of the manipulator is dependent on the condition number of the Jacobian matrix (Salisbury and Craig 1982; Angeles and Rojas 1987; Angeles and López-Cajún 1987). This is so because the condition number represents the amplification factor by which the error on the input vector of a linear system are multiplied when the solution vector is computed (Strang 1980). In the case of a manipulator, the condition number is therefore an indication of the amplification of the error on the position or the force at the gripper for a given accuracy of the actuators. This number is to be kept as small as possible, the smallest value that can be attained being 1, which is obtained by rendering the matrix isotropic. The condition number of the manipulator is defined as:

$$\kappa = \|\mathbf{J}\|\|\mathbf{J}^{-1}\| \tag{5.3a}$$

where $\|\cdot\|$ denotes *any* norm of its matrix argument. In this thesis, the following frame-invariant Euclidean norm is adopted throughout:

$$\|\mathbf{J}\| = \sqrt{\mathrm{tr}(\mathbf{J}\mathbf{W}\mathbf{J}^T)} \tag{5.3b}$$

$\mathbf{W}$ being defined as $w\mathbf{1}$ where $w = 1/n$, and n is the dimension of the square matrix $\mathbf{J}$. Of course, the same definition applies to $\mathbf{K}$. A more detailed discussion on the condition number can be found in Appendix D. The local dexterity index can now be formally defined as the reciprocal of the condition number of the Jacobian matrix of the manipulator, i.e.,

$$\nu = \left(\frac{1}{\kappa}\right) \tag{5.4}$$

It is important to notice that, since the Jacobian is configuration dependent, its condition number is a local property of the manipulator—which is the reason behind the term *local dexterity index*—and therefore bears information on the accuracy of the control in this particular configuration only. This criterion can be used for design by minimizing the condition number over the space of manipulator parameters together with the space of configurations. Isotropic configurations can then be isolated and the corresponding designs are termed *isotropic*. However, since isotropy is a property of a limited subset of the workspace, either a curve or a surface within the manipulator's workspace (Salisbury and Craig 1982, Angeles and Rojas 1987), it does not guarantee, in general, that the overall conditioning of the manipulator is optimum.

To obtain a measure of the global behaviour of the condition number of the manipulator, the following *global conditioning index* η is now proposed:

$$\eta = \frac{A}{B} \tag{5.5a}$$

where

$$A = \int_W \left(\frac{1}{\kappa}\right) \mathrm{d}W = \int_W \nu \mathrm{d}W \tag{5.5b}$$

and

$$B = \int_W \mathrm{d}W \tag{5.5c}$$

in which κ is the condition number at a particular point of W, the manipulator's workspace, and the denominator B is the volume of the workspace. The reciprocal of the condition number, i.e., the local dexterity index ν has been used for it is better behaved than κ itself over the whole workspace. In fact, it is bounded as follows:

$$0 \leq \nu \leq 1 \tag{5.6}$$

which thus produces a bounded performance index, i.e.,

$$0 < \eta < 1 \tag{5.7}$$

An alternative definition of A can also be given as:

$$A = \int_W \left(\frac{1}{\kappa}\right)^2 \mathrm{d}W = \int_W \nu^2 \mathrm{d}W \tag{5.8}$$

The squaring of the local dexterity index is not necessary here, since the condition number is a positive definite quantity. However, the definition given in eq.(5.8) can sometimes simplify the algebra since the condition number, as defined in eq.(5.3a), is given by the square root of a product. Both definitions are acceptable.

In the context of the optimum design of robotic manipulators, the GCI is to be maximized over the space of manipulator parameters. Thus, the closer to unity the index is, the better the overall behaviour of the condition number and hence, of the manipulator. The normality condition necessary for a stationary value of η is given by:

$$\frac{\partial \eta}{\partial \mathbf{h}} = 0 \tag{5.9a}$$

where $\mathbf{h}$ is the vector containing the parameters defining the architecture of the manipulator. For example, for an n-axis serial manipulator, these parameters can be those of Hartenberg and Denavit (Hartenberg and Denavit 1964), i.e.,

$$\mathbf{h} = [a_1, b_1, \alpha_1, \ldots, a_n, b_n, \alpha_n]^T \tag{5.9b}$$

Since the Hartenberg-Denavit parameters are not appropriate for the description of parallel manipulators (Kleinfinger and Khalil 1986), for this class of manipulators, vector $\mathbf{h}$ may represent an alternative set of kinematic parameters that fully describe the manipulator.

Application of condition (5.9a) to eqs.(5.5a,b&c) leads to the normality condition given below:

$$\int_W \frac{\partial}{\partial \mathbf{h}} \left(\frac{1}{\kappa}\right) \mathrm{d}W - \eta \frac{\partial B}{\partial \mathbf{h}} = 0 \tag{5.10}$$

The integration over the workspace can be performed in the Cartesian space providing that its boundary is known. This will be done in the examples presented here, which involve closed-loop manipulators. However, for current open-loop manipulators, the workspace is not always known in the Cartesian space and it is, in general, much easier to describe it in the joint space. If we want the GCI to still be a measure based on the Cartesian space metric, the transformation from one coordinate system to the other can be

introduced in the integral where we have to include the absolute value of the determinant of the Jacobian matrix, Δ. The normality condition, eq.(5.10), then becomes:

$$\int_R \frac{\partial}{\partial \mathbf{h}} \left(\frac{1}{\kappa}\right) |\Delta| \mathrm{d}\theta_n \ldots \mathrm{d}\theta_2 \mathrm{d}\theta_1 - \eta \frac{\partial B}{\partial \mathbf{h}} = 0 \tag{5.11}$$

where R denotes the workspace (in joint coordinates), and each of A and B are computed accordingly, i.e., as:

$$A = \int_R \left(\frac{1}{\kappa}\right) |\Delta| \mathrm{d}\theta_n \ldots \mathrm{d}\theta_2 \mathrm{d}\theta_1 \tag{5.12a}$$

and

$$B = \int_R |\Delta| \mathrm{d}\theta_n \ldots \mathrm{d}\theta_2 \mathrm{d}\theta_1 \tag{5.12b}$$

It is pointed out that an alternative definition of the GCI based on the joint space metric would take away the determinant of the Jacobian from the above integrals. This GCI would have a slightly different, but also meaningful interpretation and in many instances it may be easier to handle mathematically, when serial manipulators are considered.

As a demonstration of its applicability, the concept of *global conditioning index* will now be used on two different serial manipulators for which optimum designs will be obtained. We will also use the GCI in the forthcoming sections of this chapter, where the kinematic optimization of parallel manipulators is addressed.

5.1.1 Examples

5.1.1.1 Planar, Open-Loop, Two-Link Manipulator

The open-loop, two-link manipulator under study is shown in Fig. 5.1. This manipulator is capable of positioning a point on its plane.

The Jacobian matrix, as defined in eq.(5.1), can be written in a coordinate frame attached to link 1 as:

$$\mathbf{J} = \begin{bmatrix} -a_2 \sin\theta_2 & -a_2 \sin\theta_2 \\ a_1 + a_2 \cos\theta_2 & a_2 \cos\theta_2 \end{bmatrix} \tag{5.13}$$

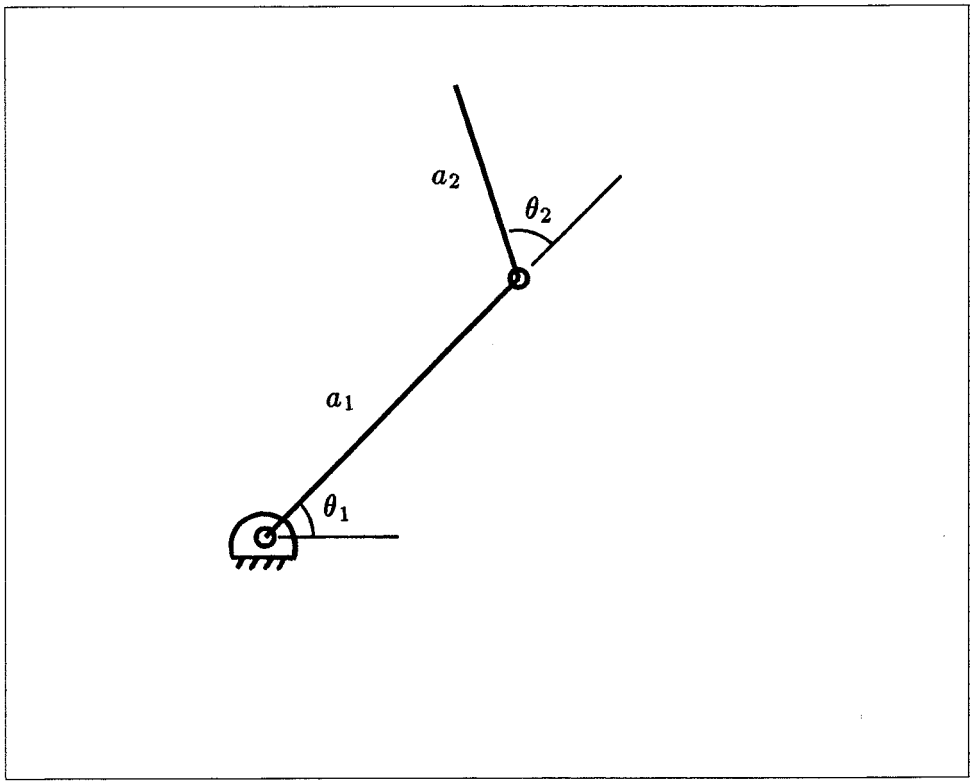

Figure 5.1 Open-loop planar two-link manipulator.

Therefore, we have:

$$\mathbf{J}^{-1} = \frac{1}{\Delta}\begin{bmatrix} a_2\cos\theta_2 & a_2\sin\theta_2 \\ -(a_1 + a_2\cos\theta_2) & -a_2\sin\theta_2 \end{bmatrix} \tag{5.14}$$

where

$$\Delta = a_1 a_2 \sin\theta_2 \tag{5.15}$$

The condition number of **J**, can then be computed from eqs.(5.3a&b) (Angeles and Rojas 1987), and is given by:

$$\kappa = (a_1^2 + 2a_2^2 + 2a_1 a_2\cos\theta_2)/2a_1 a_2\sin\theta_2 \tag{5.16a}$$

or

$$\kappa = (1/\alpha + 2\alpha + 2\cos\theta_2)/2\sin\theta_2 \tag{5.16b}$$

where

$$\alpha = a_2/a_1 > 0, \quad a_1 > 0 \tag{5.16c}$$

Some plots of the condition number against θ_2 are shown in Fig. 5.2 for a few values of α. It can be seen that the only value that leads to an isotropic manipulator is $\alpha = \sqrt{2}/2$, a fact that was pointed out in (Salisbury and Craig 1982). However, it is interesting to notice that, from a figure presented in the latter reference, it is not obvious that this value of α gives the best GCI. The curves shown in Fig. 5.2 are plotted against θ_2 and this way of presenting the curves allows us to see that the isotropic manipulator should lead to an optimum GCI since the value of the condition number for this value of α is always the lowest.

Now, in order to compute the manipulator's GCI, we have to integrate the reciprocal of κ over the workspace. Since we have expressed the condition number as a function of joint angle θ_2 and the linkage parameter α only, it is convenient to evaluate the integrals described in eqs.(5.5a–c) in the joint space, i.e., to use the formulation developed in eqs.(5.12a&b). We cover the workspace of the manipulator by integrating on one of the two branches of the manipulator. For example, letting angle θ_2 vary between 0 and π, we have:

$$B = \int_{\theta_1=0}^{2\pi} \int_{\theta_2=0}^{\pi} a_1 a_2 \sin\theta_2 \mathrm{d}\theta_2 \mathrm{d}\theta_1 = 4\pi a_1 a_2 \tag{5.17}$$

which leads to:

$$\eta = \frac{1}{4\pi a_1 a_2} \int_0^{2\pi} \int_0^{\pi} \left(\frac{2\sin\theta_2}{1/\alpha + 2\alpha + 2\cos\theta_2} \right) a_1 a_2 \sin\theta_2 \mathrm{d}\theta_2 \mathrm{d}\theta_1 \tag{5.18}$$

and can be further simplified to:

$$\eta = \int_0^{\pi} \left(\frac{\sin^2\theta_2}{1/\alpha + 2\alpha + 2\cos\theta_2} \right) \mathrm{d}\theta_2 \tag{5.19}$$

Then, taking the derivative with respect to the only parameter involved, i.e., α, and setting it equal to zero, one obtains:

$$(2 - 1/\alpha^2) \int_0^{\pi} \frac{\sin^2\theta_2 \mathrm{d}\theta_2}{(1/\alpha + 2\alpha + 2\cos\theta_2)^2} = 0 \tag{5.20}$$

The integral in eq.(5.20) is a positive definite quantity. Therefore, this equation is satisfied if, and only if,

$$\alpha = \frac{\sqrt{2}}{2} \tag{5.21a}$$

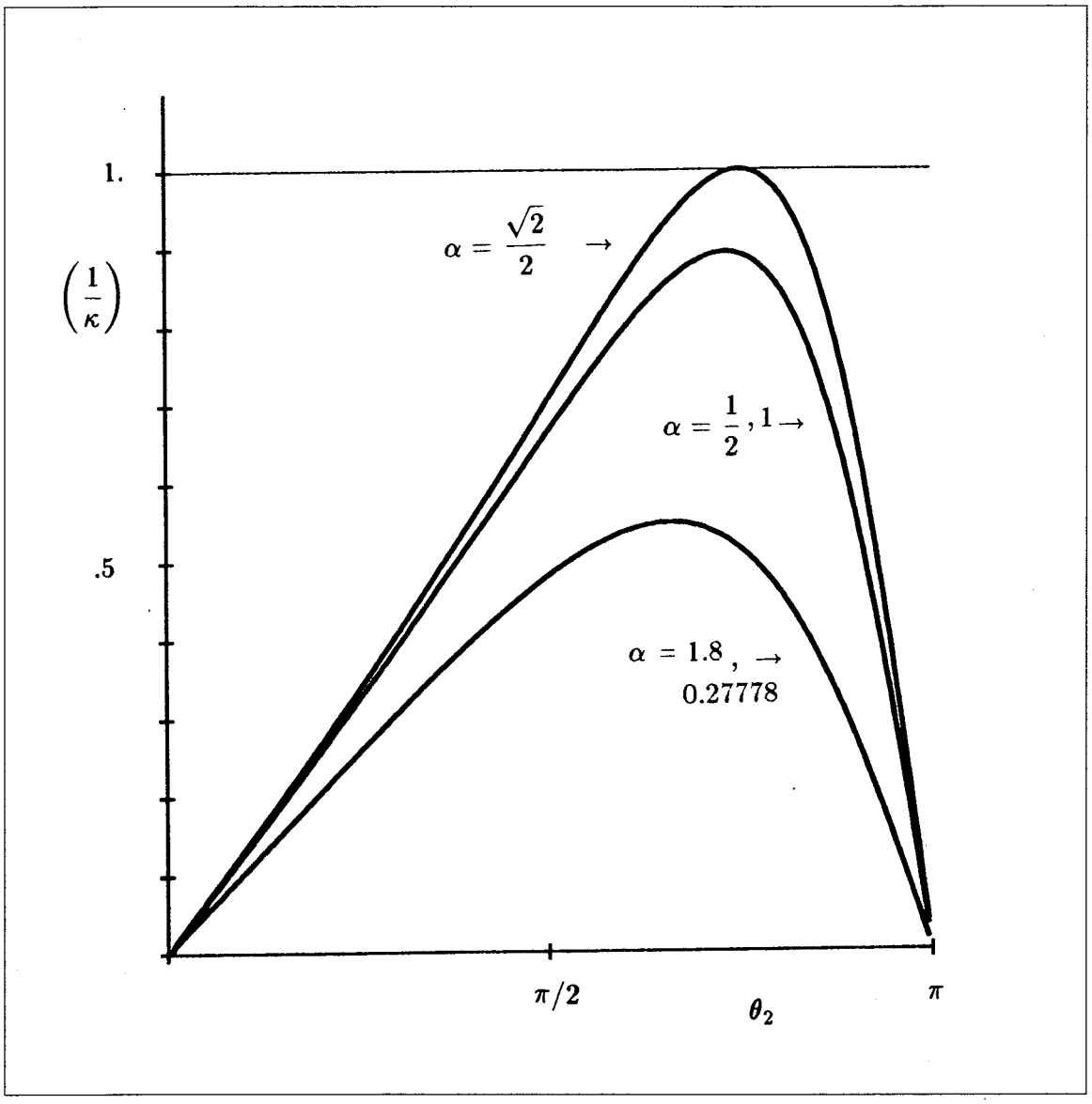

Figure 5.2 Reciprocal of the condition number of the planar two-link manipulator as a function of θ_2 for three different values of α.

The investigation of the denominator of the integrand in eq.(5.20) shows that the integrand does not suffer from any singularity. In fact, the condition under which the denominator vanishes can be written as:

$$\cos\theta_2 = -(\alpha + \frac{1}{2\alpha}) \tag{5.21b}$$

which leads to:

$$1 + 4\alpha^4 < 0 \tag{5.21c}$$

and cannot be satisfied for real α.

In this case, the optimum design in the sense of the *global conditioning index* is found to lead to the isotropic manipulator already discussed in (Salisbury and Craig 1982; Angeles and Rojas 1987). The *global conditioning index* of the two-link manipulator as a function of α is shown in Fig. 5.3. Its maximum value is $\eta_{\max} = 0.6506$, for $\alpha = \sqrt{2}/2$.

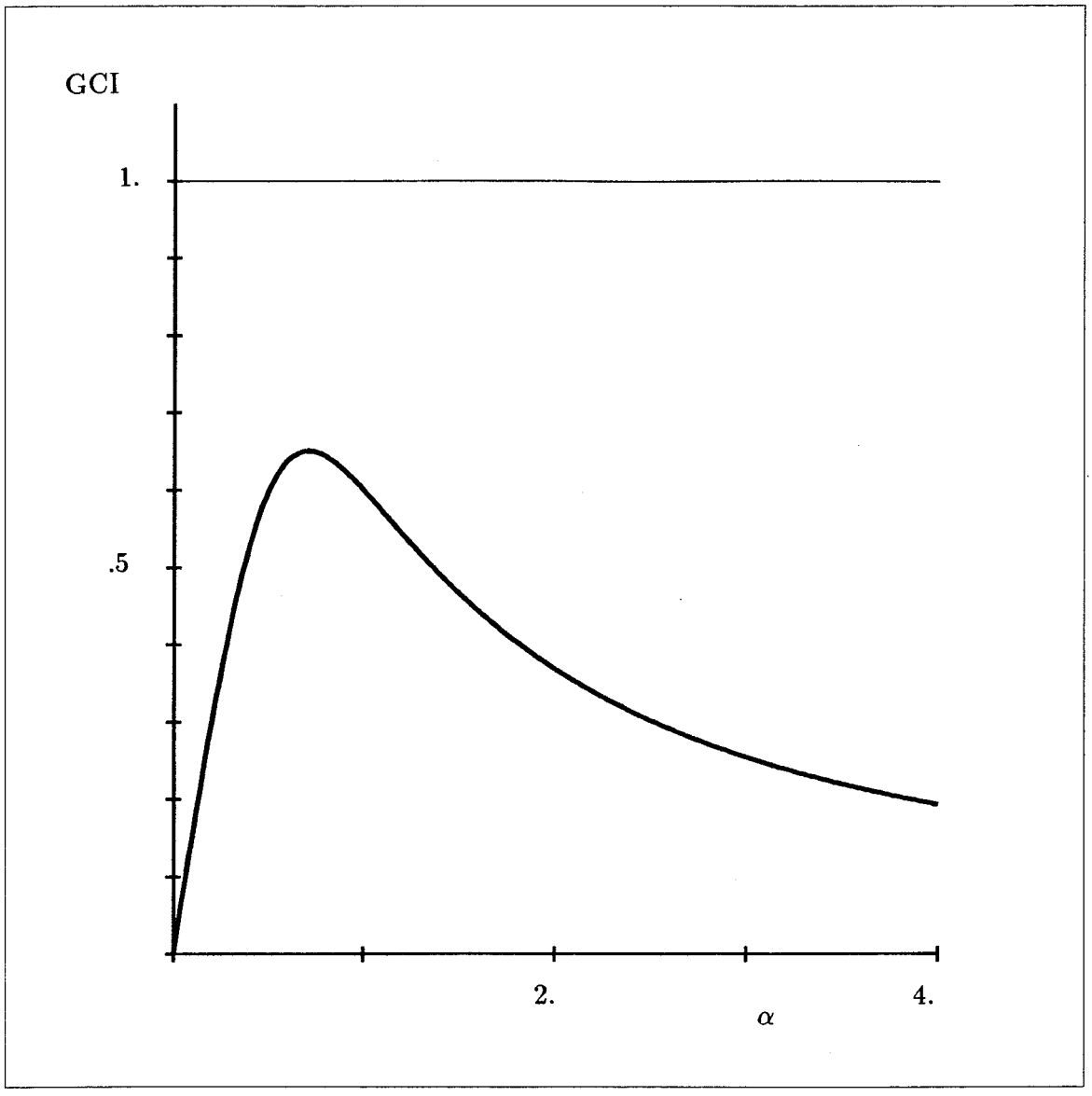

Figure 5.3 Global conditioning index of the planar two-link manipulator for different values of α.

5.1.1.2 Spherical, Open-Loop, Three-Degree-of-Freedom Wrist

A spherical wrist is shown in Fig. 5.4. Since the axes of the three joints intersect at a common point, the parameters defining the architecture of the wrist are reduced to the angles α_1 and α_2. We then have:

$$\mathbf{h} = [\, \alpha_1, \, \alpha_2 \,]^T \tag{5.22}$$

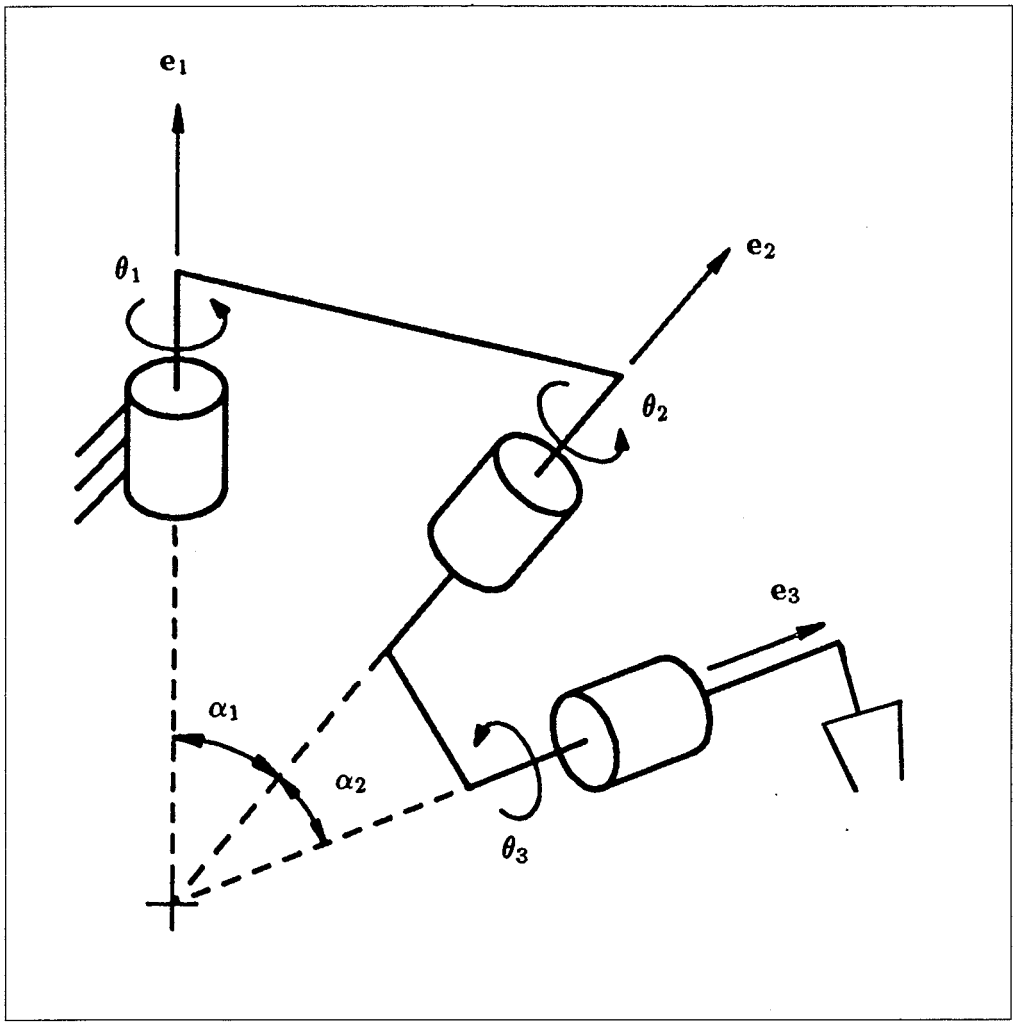

Figure 5.4 Open-loop three-degree-of-freedom wrist.

If we denote by $\mathbf{e}_1$, $\mathbf{e}_2$ and $\mathbf{e}_3$ the three unit vectors along the kinematic pairs of the wrist, we can write the Jacobian matrix as:

$$\mathbf{J} = [\, \mathbf{e}_1 \quad \mathbf{e}_2 \quad \mathbf{e}_3 \,] \tag{5.23}$$

This matrix is now represented in a coordinate frame attached to the second link, i.e.,

$$\mathbf{J} = \begin{bmatrix} 0 & 0 & \sin\theta_2 \sin\alpha_2 \\ \sin\alpha_1 & 0 & -\cos\theta_2 \sin\alpha_2 \\ \cos\alpha_1 & 1 & \cos\alpha_2 \end{bmatrix} \tag{5.24}$$

from which we can write:

$$\Delta = \sin\alpha_1 \sin\alpha_2 \sin\theta_2 \tag{5.25}$$

Using eqs.(5.3a&b) one can then derive an expression for the condition number (Angeles and Rojas 1987), which gives:

$$\left(\frac{1}{\kappa}\right)^2 = \frac{3N}{D} \tag{5.26a}$$

where

$$N = \sin^2\alpha_1 \sin^2\alpha_2 \sin^2\theta_2 \tag{5.26b}$$

and

$$\begin{aligned} D = {} & \sin^2\alpha_1(1+\cos^2\alpha_2) + \sin^2\alpha_2(1+\sin^2\theta_2) + \cos^2\alpha_1 \sin^2\alpha_2 \cos^2\theta_2 \\ & + 2\cos\alpha_1 \sin\alpha_1 \cos\alpha_2 \sin\alpha_2 \cos\theta_2 \end{aligned} \tag{5.26c}$$

As in the case of the first example, the spherical wrist has two branches and the integration can be performed on one of them. For instance, we can choose the branch for which the determinant of the Jacobian matrix is positive, i.e., integrate over θ_2 from 0 to π. Now, eq.(5.10) will lead to two equations since $\mathbf{h}$ is of dimension 2. The integrand of the first term of each of these equations can be written as:

$$\frac{\partial}{\partial\alpha_1}\left[\left(\frac{1}{\kappa}\right)^2 \Delta\right] = \frac{3}{D^2}\left[3\sin^2\alpha_1 \cos\alpha_1 \sin^3\alpha_2 \sin^3\theta_2 D - 2\sin^3\alpha_1 \sin^3\alpha_2 \sin^3\theta_2 D'\right] \tag{5.27a}$$

where

$$D' = \sin\alpha_2 \cos\alpha_2 \cos\theta_2 \cos 2\alpha_1 + \sin\alpha_1 \cos\alpha_1(1+\cos^2\alpha_2 - \sin^2\alpha_2 \cos^2\theta_2) \tag{5.27b}$$

and

$$\frac{\partial}{\partial\alpha_2}\left[\left(\frac{1}{\kappa}\right)^2 \Delta\right] = \frac{3}{D^2}\left[3\sin^3\alpha_1 \sin^2\alpha_2 \cos\alpha_2 \sin^3\theta_2 D - 2\sin^3\alpha_1 \sin^3\alpha_2 \sin^3\theta_2 D''\right] \tag{5.28a}$$

where

$$D'' = \sin\alpha_1 \cos\alpha_1 \cos\theta_2 \cos 2\alpha_2 + \sin\alpha_2 \cos\alpha_2 \cos^2\alpha_1 + \sin\alpha_2 \cos\alpha_2 (\sin^2\theta_2 + \cos^2\alpha_1 \cos^2\theta_2) \tag{5.28b}$$

Moreover, the second term of each of the normal equations, eq.(5.10), contains a factor $\partial B/\partial \mathbf{h}$ whose integrand, for the first equation, is given by,

$$\frac{\partial \Delta}{\partial \alpha_1} = \cos\alpha_1 \sin\alpha_2 \sin\theta_2 \tag{5.29a}$$

and, for the second equation, by,

$$\frac{\partial \Delta}{\partial \alpha_2} = \sin\alpha_1 \cos\alpha_2 \sin\theta_2 \tag{5.29b}$$

By inspection of eqs.(5.27a–5.29b), it becomes obvious that the normality condition is verified if $\alpha_1 = \alpha_2 = \pi/2$. Therefore, these angles constitute an optimum design in the sense of the *global conditioning index*. Again, this design is found to be an isotropic manipulator which has been discussed in (Angeles and Rojas 1987).

The results obtained for these first two examples can be reproduced using a GCI based on the joint space metric, which actually leads to simpler integrals. The procedure is identical to the one described above.

5.2 Planar Three-Degree-of-Freedom Manipulator with Revolute Actuators

The workspace and dexterity of the planar three-degree-of-freedom parallel manipulator studied in Section 4.1 will now be optimized. The symmetry assumptions used in Chapter 4 are maintained here.

5.2.1 Workspace Optimization

The mobility region can be found for each leg of this manipulator, this region being bounded by the *singularity curve* which is the closed curve separating the region

where the leg has mobility from that in which it does not. For the points of the workspace located on this curve, the solution of the inverse kinematic problem is unique since the two branches meet. Indeed, for a given leg to have mobility for prescribed Cartesian coordinates, the expression in brackets in eq.(4.4) has to have a magnitude smaller than or equal to one. Thus, the *singularity curve*, i.e., the limit of the workspace, for the ith leg is obtained by writing:

$$\frac{l_1^2 - l_2^2 + x_{2i}^2 + y_{2i}^2}{2l_1\sqrt{x_{2i}^2 + y_{2i}^2}} = \pm 1 \tag{5.30}$$

The workspace of the manipulator, dashed in Fig. 5.5, is then obtained by the intersection of the three foregoing mobility regions. Those regions are, in fact, annular regions in the x-y plane described by the following equations:

$$(x - x_i)^2 + (y - y_i)^2 = (l_1 \pm l_2)^2, \; i = 1,2,3 \tag{5.31a}$$

where

$$x_1 = l_3 \cos(\phi + \pi/6) \tag{5.31b}$$

$$y_1 = l_3 \sin(\phi + \pi/6) \tag{5.31c}$$

$$x_2 = 1 - l_3 \cos(\phi - \pi/6) \tag{5.31d}$$

$$y_2 = -l_3 \sin(\phi - \pi/6) \tag{5.31e}$$

$$x_3 = 1/2 + l_3 \sin\phi \tag{5.31f}$$

$$y_3 = \sqrt{3}/2 - l_3 \cos\phi \tag{5.31g}$$

a result that is derived directly from eq.(5.30).

Each of the three annular regions is bounded by two concentric circles whose centres, C_i, have coordinates (x_i, y_i) for $i = 1,2,3$. This is shown in Fig. 5.5.

The concentric circles are obtained by choosing alternatively the plus and minus sign in eq.(5.30), which gives rise to circles of radii $(l_1 + l_2)$ and $|l_1 - l_2|$. From the particular form of the expressions of the coordinates of the centres, C_i, given in eqs.(5.31b–g), it can be realized that these are located on the circumference of three other circles of radii l_3,

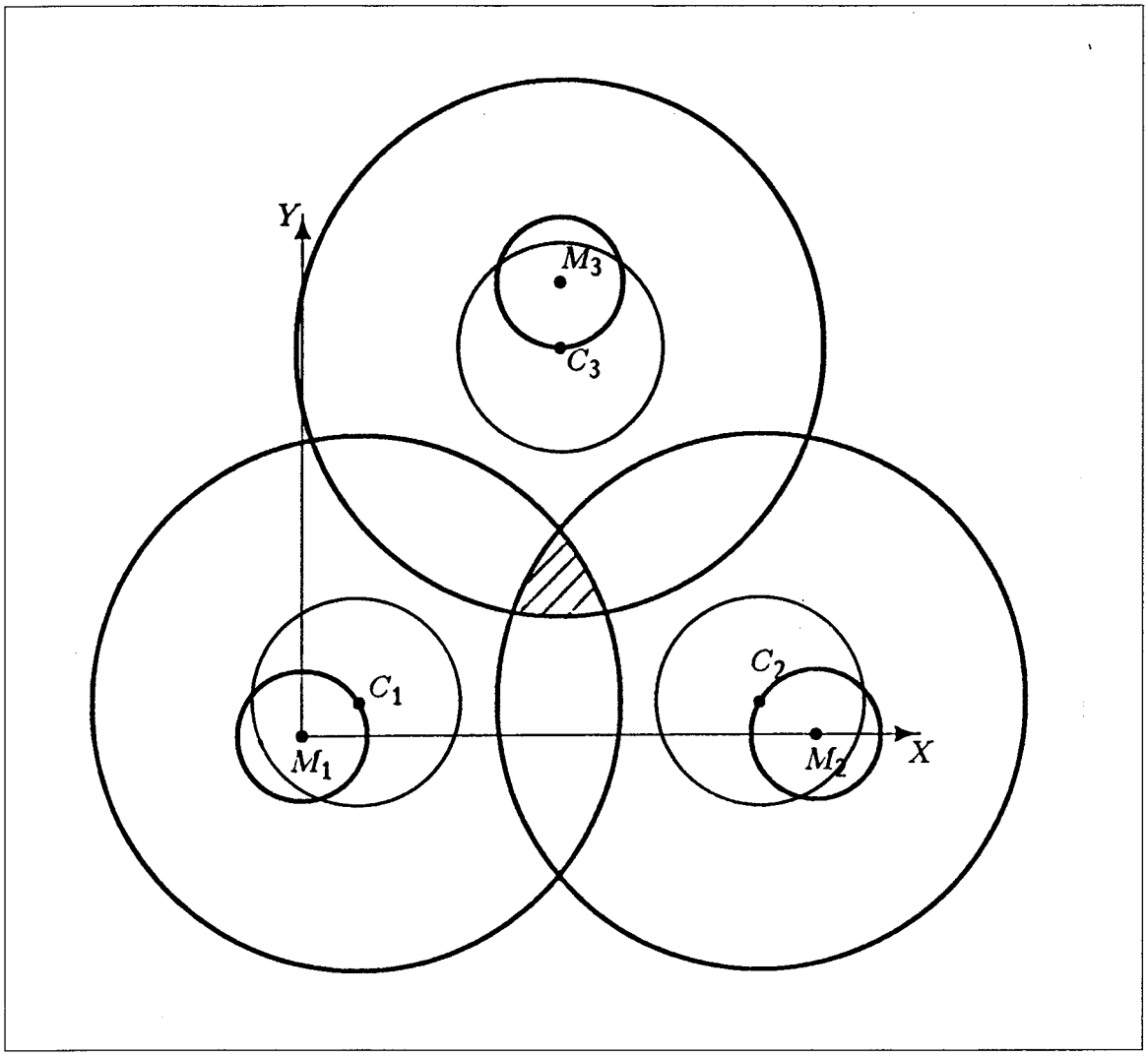

Figure 5.5 Workspace of the planar manipulator for $l_1 = 0.355$, $l_2 = 0.15$ and $l_3 = 0.125$ when $\phi = 0°$. For this value of ϕ, the annular regions whose intersection form the workspace are centred at points C_1, C_2 and C_3, respectively.

centred at the driven joints. Their location on this circumference depends on the gripper orientation, which is given by angle ϕ. For example, if ϕ is equal to zero, the centres C_i are located as shown in Fig. 5.5, i.e., bringing the annular regions as close as possible to each other. As ϕ is incremented, centres C_i will move around the circles of radii l_3 and, for $\phi = \pi$, they reach the configuration shown in Fig. 5.6, i.e., the one for which the annular regions are as far as possible from each other. The geometric construction of Fig. 5.5 can then be redrawn for any angle ϕ. It can be realized, from the foregoing discussion, that the area of the workspace will be a minimum when angle ϕ is equal to π, since in this case the

distance between the regions, whose intersection defines the workspace of the manipulator, is a maximum.

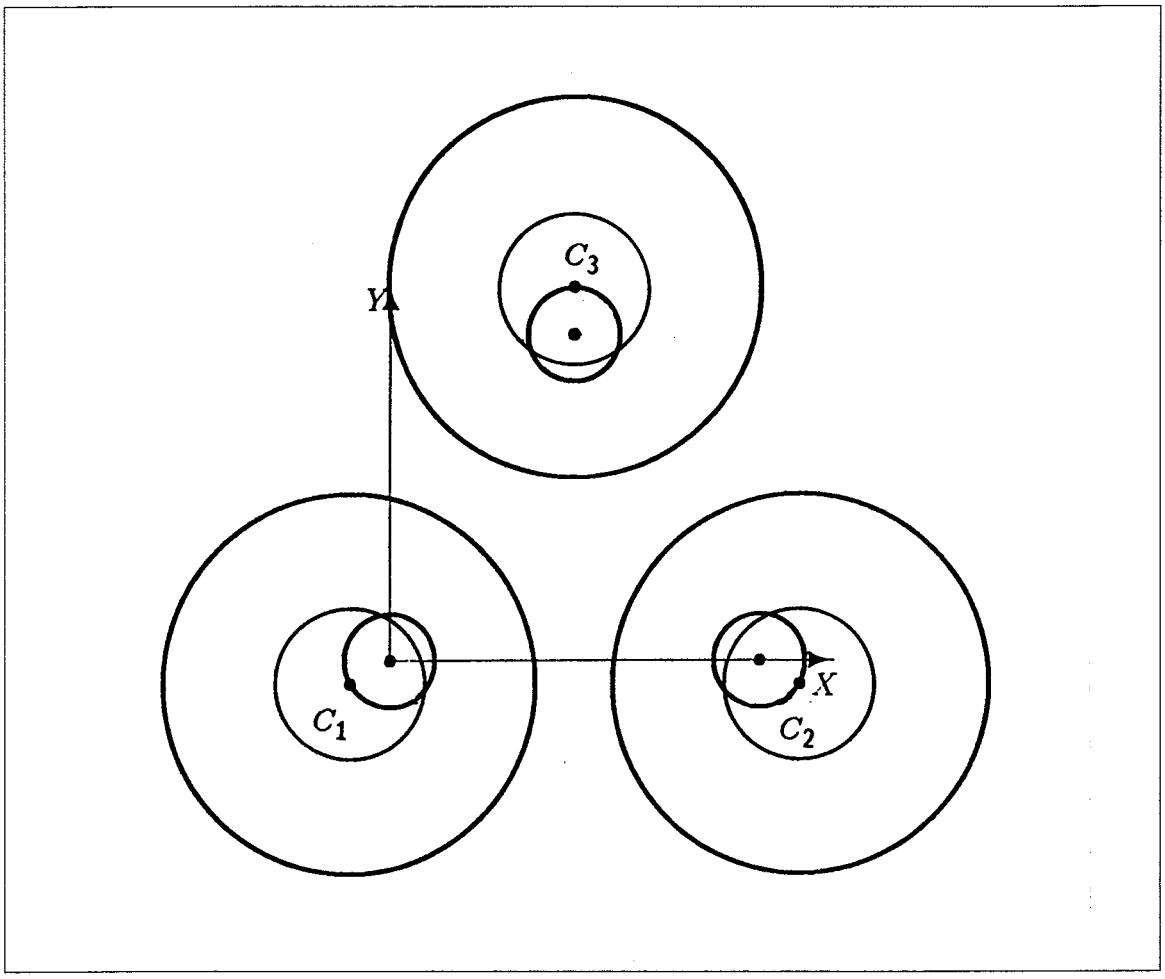

Figure 5.6 Same construction as in Fig. 5.5 but with $\phi = \pi$. The workspace vanishes.

One important criterion for the usefulness of the manipulator is that we have a non-vanishing workspace for every angle ϕ. This can be achieved by imposing a non-vanishing workspace for $\phi = \pi$, i.e., by setting $\phi = \pi$ in equations (5.31a) and the condition that the intersection of two of the circles defining the outer boundary of the annular regions be inside the third one and that the three circles defining the inner boundary of the annular regions do not have a common intersection. This leads to:

$$3(l_1 + l_2)^2 \geq (\sqrt{3}l_3 + 1)^2 \qquad (5.32a)$$

and

$$3(l_1 - l_2)^2 \leq (\sqrt{3}l_3 - 1)^2 \tag{5.32b}$$

The manipulators verifying these conditions will have a non-vanishing workspace for every angle ϕ.

The global workspace of the manipulator can now be represented as a volume in the (x, y, ϕ) space, as shown in Fig. 5.7, where the origin of the coordinates has been placed on the centroid of the base triangle formed by the motors M_1, M_2, M_3. This figure has been obtained by incrementing ϕ and calculating the coresponding workspace in the (x, y) plane, for every angle ϕ. The volume of the workspace, W, can then be approximated numerically using discrete integration over ϕ from 0 to 2π. The introduction of Simpson's rule, for example, leads to:

$$W = \int_0^{2\pi} A(\phi)d\phi \simeq \frac{\Delta\phi}{3}[A_0 + 4A_1 + 2A_2 + \ldots + 4A_{2n-1} + A_{2n}] \tag{5.33a}$$

where

$$A_i = A(i\Delta\phi), \qquad \Delta\phi = \pi/n, \qquad i = 0, 1, \ldots, 2n \tag{5.33b}$$

and A_i = area of the workspace for $\phi = \phi_i = i\Delta\phi$, i.e., A_i is the area of the region $\alpha(\phi_i)$, and n can be chosen large enough to provide an acceptable accuracy.

Equation (5.33a) requires the evaluation of A_i for many different values of ϕ. This can be done more efficiently by resorting to integration on the boundary using the Gauss Divergence Theorem (Brand 1955). The application of this theorem to the planar region $\alpha(\phi)$ gives:

$$A(\phi) = \frac{1}{2}\int_{\partial\Omega} \mathbf{s} \cdot \mathbf{n} d\partial\Omega \tag{5.34a}$$

where

$\partial\Omega$: the boundary of the region $\alpha(\phi)$

$\mathbf{s}$: the position vector of an arbitrary point of $\partial\Omega$

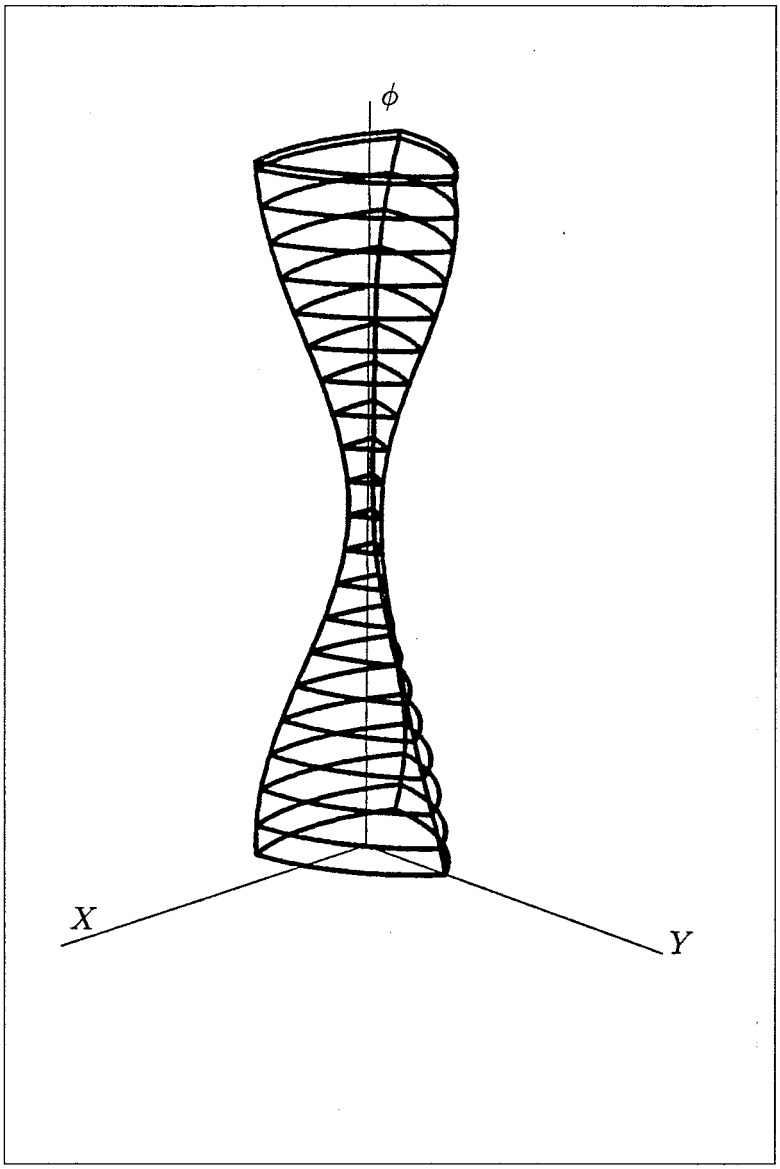

Figure 5.7 Workspace of the planar manipulator as a volume in the (x, y, ϕ) space obtained for $l_1 = l_2 = \sqrt{2}/4$ and $l_3 = 0.1$.

n : the outward unit normal vector to the curve $\partial\Omega$

This integral is more easily evaluated by first computing the area of region MNP and then subtracting three times the area of region PQR, where M, N, P, Q, and R are as indicated in Fig. 5.8. This gives:

$$A(\phi) = A_1(\phi) - 3A_2(\phi) \tag{5.34b}$$

The first line integral $A_1(\phi)$ can be broken down into three parts, one for each

of the three arcs forming the border of this region. This leads to:

$$\begin{aligned} A_1(\phi) =& \frac{R}{2}\{a[\sin\theta]_{\theta_{P1}}^{\theta_{N1}} - b[\cos\theta]_{\theta_{P1}}^{\theta_{N1}} + R(\theta_{N1} - \theta_{P1})\} \\ &+ \frac{R}{2}\{e[\sin\theta]_{\theta_{M3}}^{\theta_{P3}} - f[\cos\theta]_{\theta_{M3}}^{\theta_{P3}} + R(\theta_{P3} - \theta_{M3})\} \\ &+ \frac{R}{2}\{c[\sin\theta]_{\theta_{N2}}^{\theta_{M2}} - d[\cos\theta]_{\theta_{N2}}^{\theta_{M2}} + R(\theta_{M2} - \theta_{N2})\} \end{aligned} \tag{5.35a}$$

where (a,b), (c,d), and (e,f) are the coordinates of the centres of circles corresponding to the first, second and third circle, respectively and θ_{Ni} is the angle associated with point N when considering the ith circle; θ_{Pi} and θ_{Mi} are defined similarly to θ_{Ni}, all angles being measured from the positive direction of the X axis, and $R = l_1 + l_2$. The area of region PQR is computed in a similar fashion, as

$$\begin{aligned} A_2(\phi) =& \frac{R}{2}\{a[\sin\theta]_{\theta_{P1}}^{\theta_{R1}} - b[\cos\theta]_{\theta_{P1}}^{\theta_{R1}} + R(\theta_{R1} - \theta_{P1})\} \\ &+ \frac{R}{2}\{e[\sin\theta]_{\theta_{Q3}}^{\theta_{P3}} - f[\cos\theta]_{\theta_{Q3}}^{\theta_{P3}} + R(\theta_{P3} - \theta_{Q3})\} \\ &+ \frac{r}{2}\{c[\sin\theta]_{\theta_{R2}}^{\theta_{Q2}} - d[\cos\theta]_{\theta_{R2}}^{\theta_{Q2}} + r(\theta_{Q2} - \theta_{R2})\} \end{aligned} \tag{5.35b}$$

where θ_{Ri} and θ_{Qi} are defined similarly to θ_{Mi}, θ_{Ni} and θ_{Pi}, while $r = |l_1 - l_2|$.

The sine and cosine functions involved in eqs.(5.35a&b) can be readily calculated using simple differences between abscissae and ordinates, and the difference between the angles can be evaluated using the inverse sine function. These considerations allow us to write these equations in a form that is more efficient for computational purposes. Equations (5.35a&b) can then be rewritten as:

$$\begin{aligned} A_1(\phi) =& \frac{1}{2}[a(y_N - y_P) - b(x_N - x_P) + e(y_P - y_M) \\ &- f(x_P - x_M) + c(y_M - y_N) - d(x_M - x_N)] \\ &+ 3R^2 \sin^{-1}(\frac{D}{2R}) \end{aligned} \tag{5.36a}$$

and

$$\begin{aligned} A_2(\phi) =& \frac{1}{2}[a(y_R - y_P) - b(x_R - x_P) + e(y_P - y_Q) \\ &- f(x_P - x_Q) + c(y_Q - y_R) - d(x_Q - x_R)] \\ &+ 2R^2 \sin^{-1}(\frac{D}{2R}) + r^2 \sin^{-1}(\frac{d}{2r}) \end{aligned} \tag{5.36b}$$

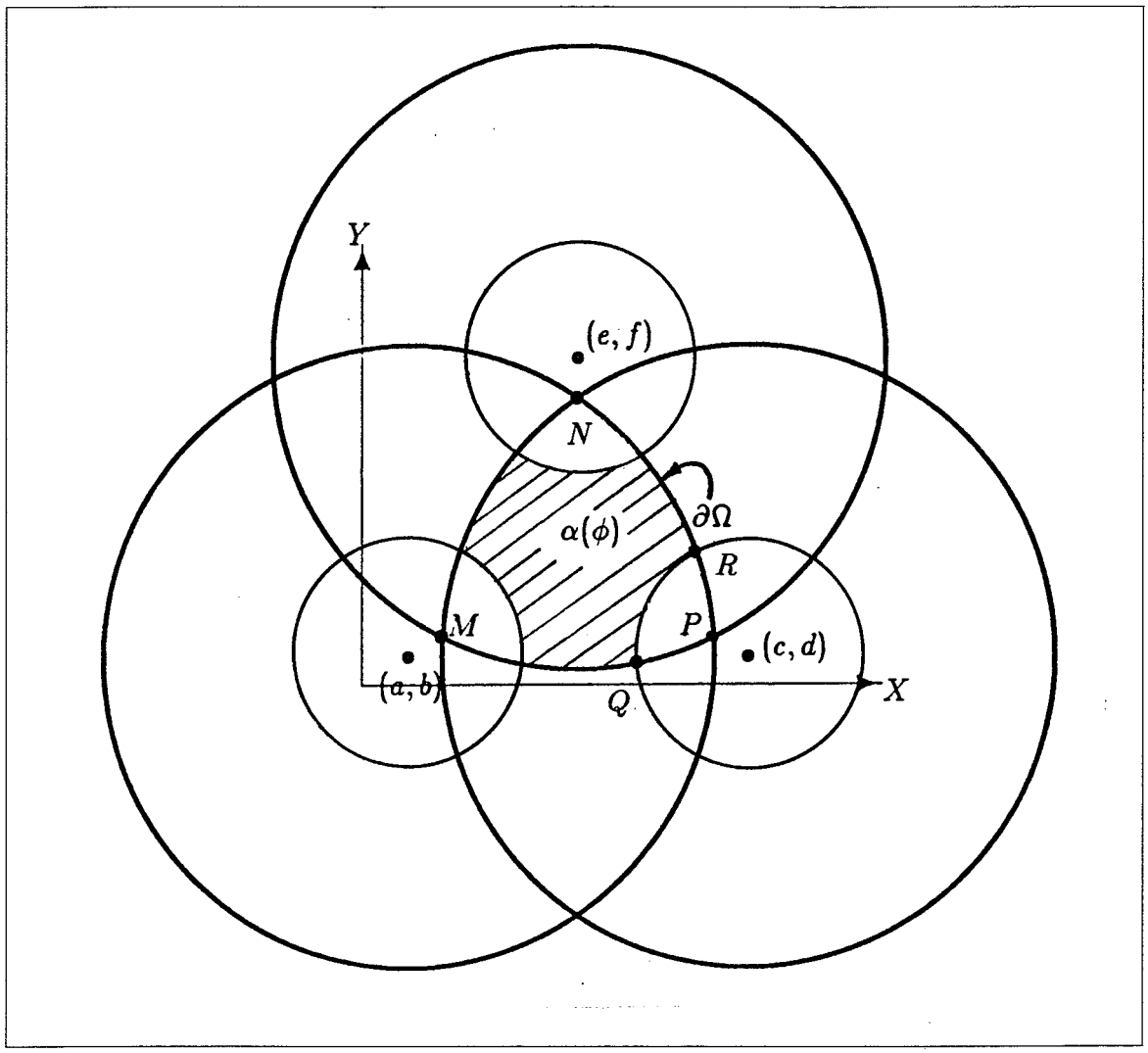

Figure 5.8 Workspace $\alpha(\phi)$ obtained for $l_1 = 11\sqrt{2}/32$, $l_2 = 5\sqrt{2}/32$, $l_3 = 0.125$ and $\phi = 0°$. The centres of the intersecting annular regions are denoted by (a, b), (c, d), and (e, f). The curve $\partial\Omega$ is the boundary of the workspace.

where $(x_M, y_M), (x_N, y_N), (x_P, y_P), (x_Q, y_Q), (x_R, y_R)$ are the coordinates of points M, N, P, Q, and R. The quantities D and d are the distances between any two of the points M, N, P and any two of the points P, Q, R, respectively.

We can thus evaluate the volume W of the workspace of the manipulator in the (x, y, ϕ) space. It can be seen from Fig. 5.8 that, for a given value of R, there is a maximum value of r for which the workspace is given simply by the intersection of the three larger circles defining the outer boundary of the annular regions. If r is larger than this value,

the workspace is reduced due to regions similar to region PQR in Fig. 5.8. Moreover, it becomes obvious, from eq.(5.31a) that the volume of the workspace will be monotonically increasing with R since this is the radius of the larger intersecting circles. The optimization problem will then be to find, for a given value of R, the value of l_3 that maximizes the workspace, and then compute the maximum value of r that is acceptable. The optimum value of l_3 is found using a numerical one-dimensional direct search where the step size is halved whenever the centrepoint of the current interval gives a larger workspace volume than the extreme points of the said interval. This method converges to a local maximum. The maximum acceptable value of r is then computed from this optimum design. The results of this optimization procedure are shown in Fig. 5.9. Points on the curve represent manipulators having maximum global workspace. It is interesting to note that when R is larger than 1, the optimum design is obtained with $l_3 = 0$. On the other hand, when $R \to 0$, then $l_3 \to \sqrt{3}/3$, which corresponds to the case of a fixed gripper having the same dimensions as the base triangle. It also turns out that the maximum acceptable value of r associated with these optimum designs is always zero, which means that we have $l_1 = l_2 = R/2$ for the optimum designs.

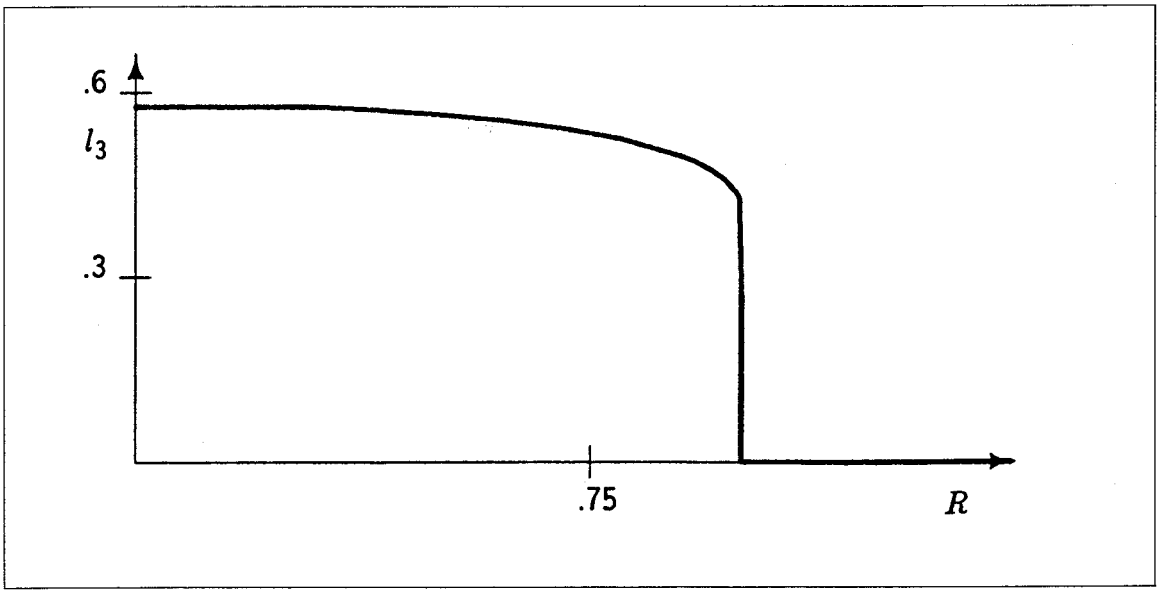

Figure 5.9 Optimum values of l_3 which maximize the workspace for a given value of R.

5.2.2 Isotropy of the Jacobian Matrix

It is recalled from Chapter 4 that the Jacobian matrix of this manipulator is defined as

$$\mathbf{J}\dot{\mathbf{c}} = \dot{\theta} \tag{5.37}$$

where $\dot{\mathbf{c}} = [\dot{x}, \dot{y}, \dot{\phi}]^T$ is the vector of Cartesian velocities and $\dot{\theta} = [\dot{\theta}_1, \dot{\theta}_2, \dot{\theta}_3]^T$ is the vector of joint rates. Moreover, an expression for this matrix was given as

$$\mathbf{J} = \begin{bmatrix} a_1/d_1 & b_1/d_1 & c_1/d_1 \\ a_2/d_2 & b_2/d_2 & c_2/d_2 \\ a_3/d_3 & b_3/d_3 & c_3/d_3 \end{bmatrix} \tag{5.38}$$

where

$$a_i = -g_1 g_2 (x - x_{oi}) + g_2 \cos\theta_i + g_1 \cos\phi_i \tag{5.39a}$$

$$b_i = -g_1 g_2 (y - y_{oi}) + g_2 \sin\theta_i + g_1 \sin\phi_i \tag{5.39b}$$

$$c_i = g_1[(y - y_{oi})\cos\phi_i - (x - x_{oi})\sin\phi_i] - \sin(\theta_i - \phi_i) \tag{5.39c}$$

$$d_i = -g_2[(y - y_{oi})\cos\theta_i - (x - x_{oi})\sin\theta_i] - \sin(\theta_i - \phi_i) \tag{5.39d}$$

with g_1 and g_2 defined, in turn, as

$$g_1 = 1/l_1, \qquad g_2 = 1/l_3 \tag{5.39e}$$

(x_{oi}, y_{oi}) being the coordinates of the centre of the ith motor and angles ϕ_i being defined as

$$\phi_1 = \phi + \pi/6 \tag{5.40a}$$

$$\phi_2 = \phi + 5\pi/6 \tag{5.40b}$$

$$\phi_3 = \phi - \pi/2 \tag{5.40c}$$

It is now desired to find isotropic designs for this manipulator, i.e., kinematic parameters that will lead to manipulators for which at least one point of the workspace corresponds to a configuration for which the condition number is equal to unity. One

simple way of obtaining this minimum value of the condition number is to render the matrix proportional to an orthogonal matrix. Indeed, it is known (Strang 1980) that orthogonal matrices and their multiples are the only isotropic matrices, i.e., the only ones having a condition number of 1. This, however, can be done only in specific configurations since the Jacobian matrix is configuration dependent. The mobility region shown in Fig. 5.7 being symmetric about the centroid of the triangle defined by the motors, this point of the x-y plane is the one where the manipulator attains the maximum mobility in terms of the different values of the angle ϕ that it can reach. Therefore, this position is one in which we would like the Jacobian to be isotropic. We call this position the *home configuration*. This is then defined as that in which the centroid of the gripper is located at the centroid of the base triangle and, for example, $\phi = 0°$. If we write the Jacobian matrix in this configuration, we will derive expressions in $g_1, g_2, \theta_1, \theta_2, \theta_3$. However, due to the symmetry of the manipulator, θ_2 and θ_3 will be related to θ_1 by:

$$\theta_2 = \theta_1 + 2\pi/3 \qquad \theta_3 = \theta_1 + 4\pi/3 \tag{5.41}$$

which leaves us with only 3 variables namely g_1, g_2, and θ_1. If we now want the Jacobian to be proportional to an orthogonal matrix, then we have to specify that its rows be of equal norm and orthogonal with respect to each other, the same holding for its columns. This brings 12 potential equations, some of which are redundant. In fact, in this case, due to simplifications that arise, we end up with only one independent equation, i.e.,

$$g_1^2\left(\frac{\sqrt{3}}{3}g_2 - \frac{1}{2} - \frac{1}{6}g_2^2\right) + g_1 g_2\left(\frac{1}{2}g_2 - \frac{\sqrt{3}}{2}\right)\cos\theta_1 + g_1 g_2\left(\frac{\sqrt{3}}{6} - \frac{1}{2}\right)\sin\theta_1 - \frac{\sqrt{3}}{2}\sin\theta_1\cos\theta_1 + \left(\frac{1}{4} - \frac{1}{2}g_2^2\right)\cos^2\theta_1 + \left(\frac{3}{4} - \frac{1}{2}g_2^2\right)\sin^2\theta_1 = 0 \tag{5.42}$$

We can think of the left-hand side of this nonlinear equation as being a function of l_1, l_2, l_3, since θ_1 will bear the information on l_2. We can therefore simultaneously specify isotropy in other configurations. To satisfy our need for symmetry, we will choose two other configurations which have the same position of the gripper but in which the angle ϕ is $2\pi/3$ and $4\pi/3$. Moreover, since each of these also leads to only one independent equation, we will end up with as many equations as unknowns and *exact* solutions, within roundoff errors,

of course, should be possible. The condition for isotropy in the two last configurations can be expressed as

$$-\frac{g_1^2}{2}(\frac{g_2^2}{3}+\frac{\sqrt{3}}{3}g_2+\frac{1}{2})+\frac{g_1}{2}(g_2^2+\sqrt{3}g_2-1)\cos\theta_1'+\frac{g_1}{2}(\frac{\sqrt{3}}{3}g_2^2-g_2-\sqrt{3})\sin\theta_1' + \frac{\sqrt{3}}{2}\sin\theta_1'\cos\theta_1'+(\frac{1}{4}-\frac{1}{2}g_2^2)\cos^2\theta_1'+(\frac{3}{4}-\frac{1}{2}g_2^2)\sin^2\theta_1'=0 \tag{5.43}$$

and

$$-\frac{g_1^2}{2}(\frac{g_2^2}{3}-\frac{\sqrt{3}}{3}g_2-\frac{1}{2})+g_1(\frac{1}{2}g_2^2-1)\cos\theta_1''+g_1g_2(\frac{\sqrt{3}}{6}g_2+1)\sin\theta_1'' + (1-\frac{1}{2}g_2^2)\cos^2\theta_1''-(\frac{g_2^2}{2})\sin^2\theta_1''=0 \tag{5.44}$$

Equations (5.43) and (5.44) seem to intoduce two new unknowns, namely, θ_1' and θ_1'', which represent the value of the first motor angle in configurations 2 and 3 respectively. However, they are not independent variables since the value of l_2 has to be the same in the 3 configurations. For computational purposes, we will keep these variables as if they were independent, and write the equations constraining them, i.e.,

$$l_2^{(1)}=l_2^{(2)}=l_2^{(3)} \tag{5.45}$$

where $l_2^{(i)}$ denotes the value of l_2 in the ith configuration. Equation (5.45) leads to the following:

$$g_2(\cos\theta_1'-\cos\theta_1)+\sqrt{3}(\cos\theta_1+\cos\theta_1')-\sqrt{3}g_1+(\sin\theta_1'-\sin\theta_1)(\frac{\sqrt{3}}{3}g_2-1)=0 \tag{5.46}$$

and

$$g_2(\cos\theta_1''-\cos\theta_1)+\sqrt{3}\cos\theta_1-\sqrt{3}g_1+\frac{\sqrt{3}}{3}g_2(\sin\theta_1''-\sin\theta_1)+(\sin\theta_1+2\sin\theta_1'')=0 \tag{5.47}$$

Now the sines and the cosines of the angles appearing in eqs.(5.42–5.44) and (5.46–5.47) are considered as independent variables as well. Thus, the following constraints are adjoined:

$$\sin^2\theta_1+\cos^2\theta_1-1=0 \tag{5.48}$$

$$\sin^2\theta_1' + \cos^2\theta_1' - 1 = 0 \tag{5.49}$$

$$\sin^2\theta_1'' + \cos^2\theta_1'' - 1 = 0 \tag{5.50}$$

Equations (5.42–5.44) and (5.46–5.50), therefore, constitute a system of 8 nonlinear equations in 8 unknowns. The solution, if there is any, may then not be unique. This problem has been solved using the Newton-Raphson method and convergence has been obtained to 8 different solutions. The corresponding link lengths are given in Table 5.1 and the manipulators are shown in Fig. 5.10(a)–(h).

Solution #	l_1	l_2	l_3
1	0.783261	5.896342	−5.399776
2	1.166456	5.054792	−5.393759
3	1.154665	3.722528	−4.041159
4	2.010278	2.518945	1.240155
5	1.265630	7.244370	6.767731
6	1.344719	3.828894	3.257859
7	−7.942812	7.854237	0.780640
8	1.575610	2.587595	−1.185050

Table 5.1 Link lengths for the isotropic manipulators (8 solutions).

The solutions converging to a positive value of l_3 correspond to manipulators which are isotropic in the home configuration with $\phi = 0, 2\pi/3, 4\pi/3$, while the ones having a negative value of l_3 represent manipulators for which the third link length is $|l_3|$ but which are isotropic in the home configuration when $\phi = \pi/3, \pi, 5\pi/3$. Both results are acceptable. It should be noticed also that the sign obtained for l_1 has a well-defined geometric interpretation, but this link length should always be taken as positive, of course.

5.2.3 Global Conditioning Index

Unlike the serial manipulators studied in Section 5.1, it is not possible to obtain a closed-form expression for the condition number of the Jacobian matrix of the planar

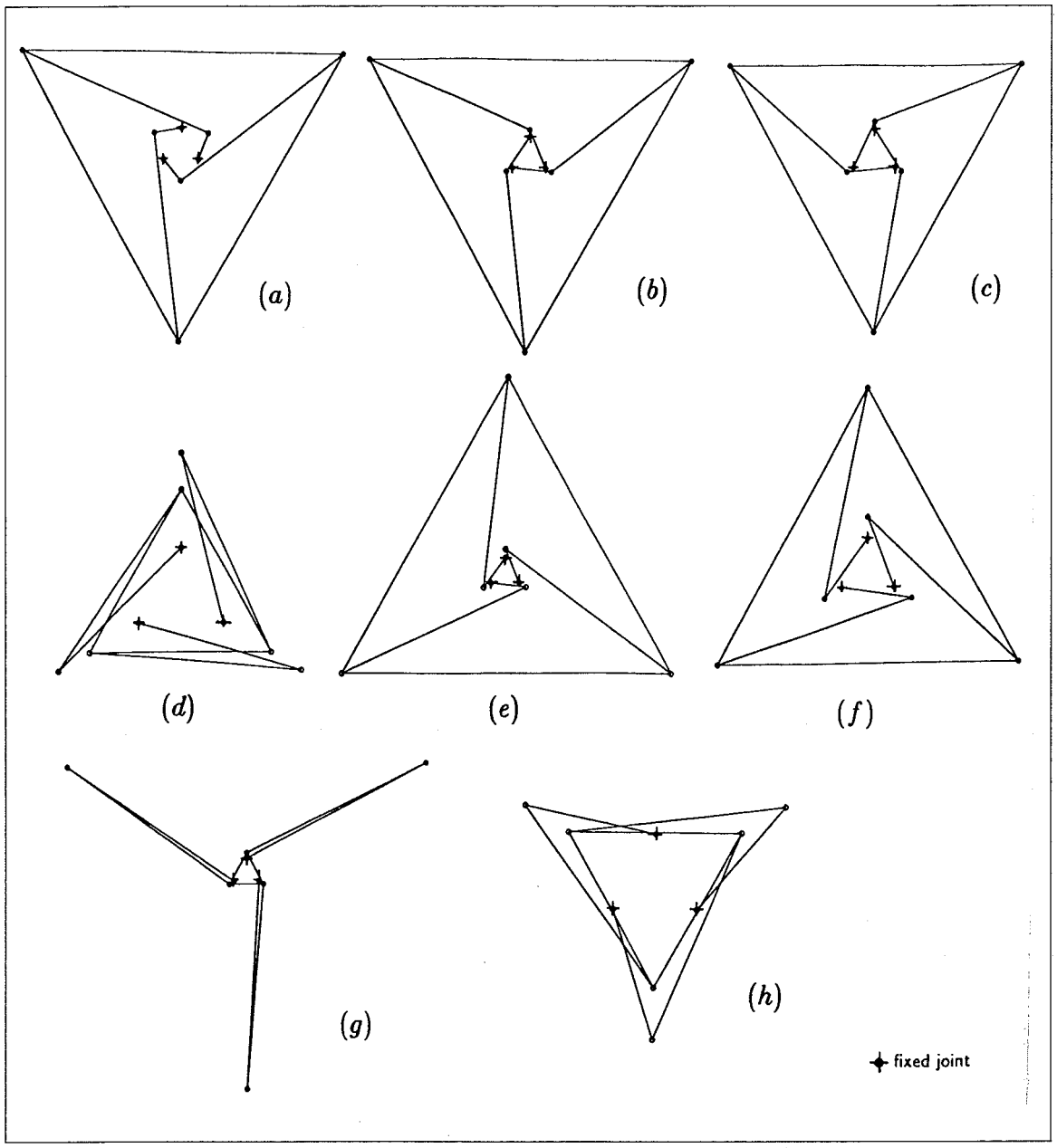

Figure 5.10 Representation of the eight different manipulators that were found to be isotropic in the home position and for three different orientations. They are shown here in one of their isotropic configurations.

parallel manipulator. This forces us to resort to a numerical integration in order to evaluate the GCI. The integration has been carried out over the workspace in the Cartesian space. The algorithm to compute the volume of this workspace, B, developed in Section 5.2.1 was used and a triple numerical integration was introduced to compute the numerator of

η, i.e.,

$$A = \int_{\phi}\int_{y}\int_{x}\left(\frac{1}{\kappa}\right)\mathrm{d}x\mathrm{d}y\mathrm{d}\phi \tag{5.51}$$

The optimization was then performed using the complex method (Box 1965). Optimum results are shown in Table 5.2, where three cases are reported. The first one represents the solution obtained when no constraints are imposed on the maximization of the GCI. However, the manipulator then obtained has a rather limited workspace. Therefore, a second optimization was conducted with a constraint on the workspace. This presents no particular problem since the optimization method used is well suited for handling inequality const15aev ery angle ϕ of the gripper, a criterion that was introduced in Section 5.2.1 where the associated inequality constraints were derived. The solution obtained for this problem is identified as case 2 in Table 5.2. The corresponding optimum manipulator now has a much larger workspace. However, the link lengths are quite long, which may induce major mechanical interference problems. A new optimization problem can be set up by imposing additional inequality constraints in order to remedy this situation. For instance, case 3 of Table 5.2 shows the solution obtained when the link lengths are forced to be less than the distance between the motors, i.e., $(0 < l_i < 1, i = 1,2,3)$ and the constraint on the workspace used in case 2 is imposed. Notice that the introduction of the constraints has led to a reduction of the GCI. The three cases reported here are obviously not the only possible designs and they are shown to illustrate how one can use the GCI to optimize a manipulator while meeting other design constraints associated with a particular problem.

Parameters	Case1	Case2	Case3
l_1	0.9940	1.1855	0.9968
l_2	1.3274	4.5987	0.7838
l_3	2.6293	5.1739	0.9719
η	0.79156	0.69691	0.42961

Table 5.2 Planar three-degree-of-freedom parallel manipulators having an optimum GCI.

5.3 Planar Three-Degree-of-Freedom Manipulator with Prismatic Actuators

5.3.1 Workspace Optimization

The properties of the workspace of this manipulator are very similar to the ones of the manipulator with revolute actuators. Indeed, the limits of the mobility region of each of the legs is obtained by setting the actuator length equal to p_{min} and p_{max} respectively, i.e., the minimum and maximum value that the actuator length can take. This leads to an equation similar to eq.(5.31a) with the difference that the radii of the two concentric circles are replaced by p_{min} and p_{max}, i.e.,

$$(x - x_i)^2 + (y - y_i)^2 = p_{min}^2, \qquad i = 1,2,3 \tag{5.52a}$$

and

$$(x - x_i)^2 + (y - y_i)^2 = p_{max}^2, \qquad i = 1,2,3 \tag{5.52b}$$

where the x_i's, y_i's, for $i = 1,2,3$ are defined in eqs.(5.31b–g). The graphical representation of the workspace is therefore identical to the one shown in Figs. (5.5–5.8) in which $(l_1 + l_2)$ and $|l_1 - l_2|$ should be replaced by p_{max} and p_{min}.

The condition under which the manipulator has a non-vanishing workspace for every angle ϕ can also be derived by imposing a non-vanishing workspace for $\phi = \pi$. This leads to two conditions analog to inequalities (5.32a&b) and that can be written as:

$$3p_{max}^2 \geq (\sqrt{3}l_3 + 1)^2 \tag{5.53a}$$

and

$$3p_{min}^2 \leq (\sqrt{3}l_3 - 1)^2 \tag{5.53b}$$

The manipulators verifying these conditions will have a non-vanishing workspace for every angle ϕ.

As stated above, the workspace of this manipulator is very similar to the one of the planar manipulator with revolute actuators which is shown in Fig. 5.7. Therefore, the evaluation of the volume of the workspace presented in eqs.(5.33a–5.36b) is also applicable to the manipulator with prismatic actuators provided that the variables r and R are redefined as follows:

$$r = p_{min} \quad \text{and} \quad R = p_{max} \tag{5.54}$$

The optimization performed on the global workspace of the manipulator in Section 5.2.1 can be repeated here, leading to the same optimum curve, i.e., the one plotted in Fig. 5.9, where the values of l_3 that correspond to a maximum global workspace of the manipulator, for a given value of $R = p_{max}$, are shown. The fact that the maximum acceptable value of r associated with these optimum designs is equal to zero is now interpreted as that p_{min} should be as small as possible for the volume of the workspace to be a maximum.

5.3.2 Isotropy of the Jacobian Matrix

It is recalled from Section 4.2.3 that the Jacobian matrix of this manipulator is defined as:

$$\mathbf{J}\dot{\mathbf{c}} = \dot{\mathbf{p}} \tag{5.55}$$

where $\dot{\mathbf{c}} = [\dot{x}, \dot{y}, \dot{\phi}]^T$ and $\dot{\mathbf{p}} = [\dot{p}_1, \dot{p}_2, \dot{p}_3]^T$ are the vectors of Cartesian and joint rates, respectively, and the expression for $\mathbf{J}$ is given in eqs.(4.42–4.43c).

Contrary to the case of the manipulator with revolute actuators, the configuration in which the centroid of the gripper is located at the centroid of the motors, i.e., $x = 1/2$ and $y = \sqrt{3}/6$, and for which $\phi = 0°$—which we termed the home configuration in Section 5.2.2—is a singular configuration for the manipulator with prismatic actuators for any value of l_3 and p_{max}. This is so because, in this configuration, the lines along the three legs intersect at the centroid of the gripper, which leads to the second type of singularity, as mentioned in Section 4.2.5. It is therefore impossible to render the Jacobian

matrix isotropic in the home configuration. This is clearly seen in Fig. 5.11, where plots of the local dexterity with respect to the orientation angle ϕ are given for $x = 1/2$, $y = \sqrt{3}/6$ and for different values of l_3. It is clear that, for any value of l_3, the Jacobian matrix is singular when $\phi = 0$ or $\phi = \pi$ in the home configuration. Moreover, the configuration for which the condition number is a minimum is attained when $x = 1/2$, $y = \sqrt{3}/6$, $\phi = 0.75$ rad and $l_3 = 0.79$, which leads to a dexterity index of 0.98, i.e., a Jacobian matrix very close to isotropy is obtained.

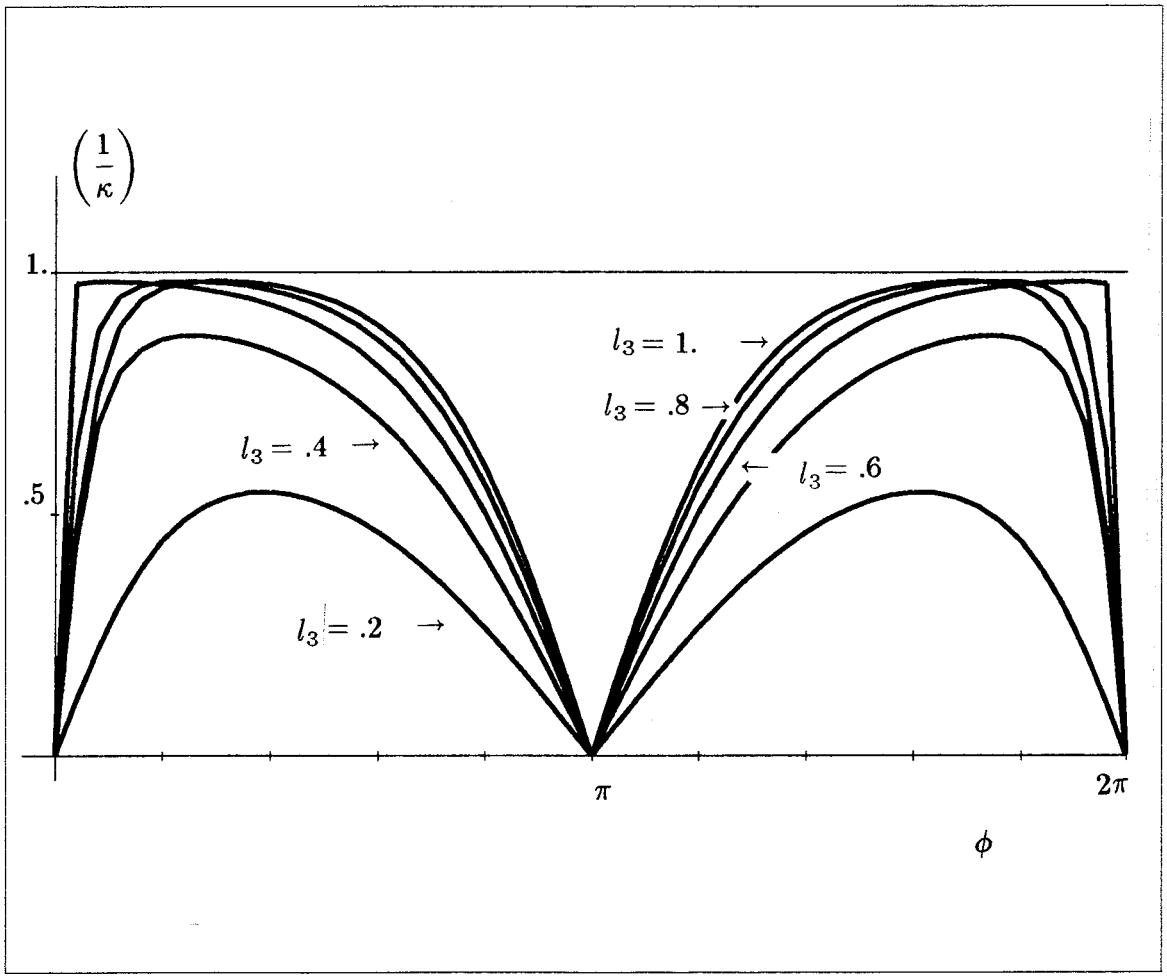

Figure 5.11 Reciprocal of the condition number of the planar manipulator with prismatic actuators as a function of the angle of orientation ϕ when $x = 1/2$ and $y = \sqrt{3}/6$, i.e., when the centroid of the gripper is located at the centroid of the motors, for different values of l_3.

5.3.3 Global Conditioning Index

Again, the GCI has been used and the integration carried out numerically over the workspace in the Cartesian space, using eq.(5.51). A graphical representation of the GCI of the manipulator as a function of l_3 and p_{max} is shown in Fig. 5.12. The maximum value of the GCI is attained when $l_3 = 4.2$ and $p_{max} = 4.6$, which leads to a GCI of 0.498 when a value of $p_{min} = 0.1$ is assumed. It is pointed out that this value of the global dexterity is lower than the ones that were found for the manipulator with revolute actuators, which suggests that the manipulator with revolute actuators is better conditioned.

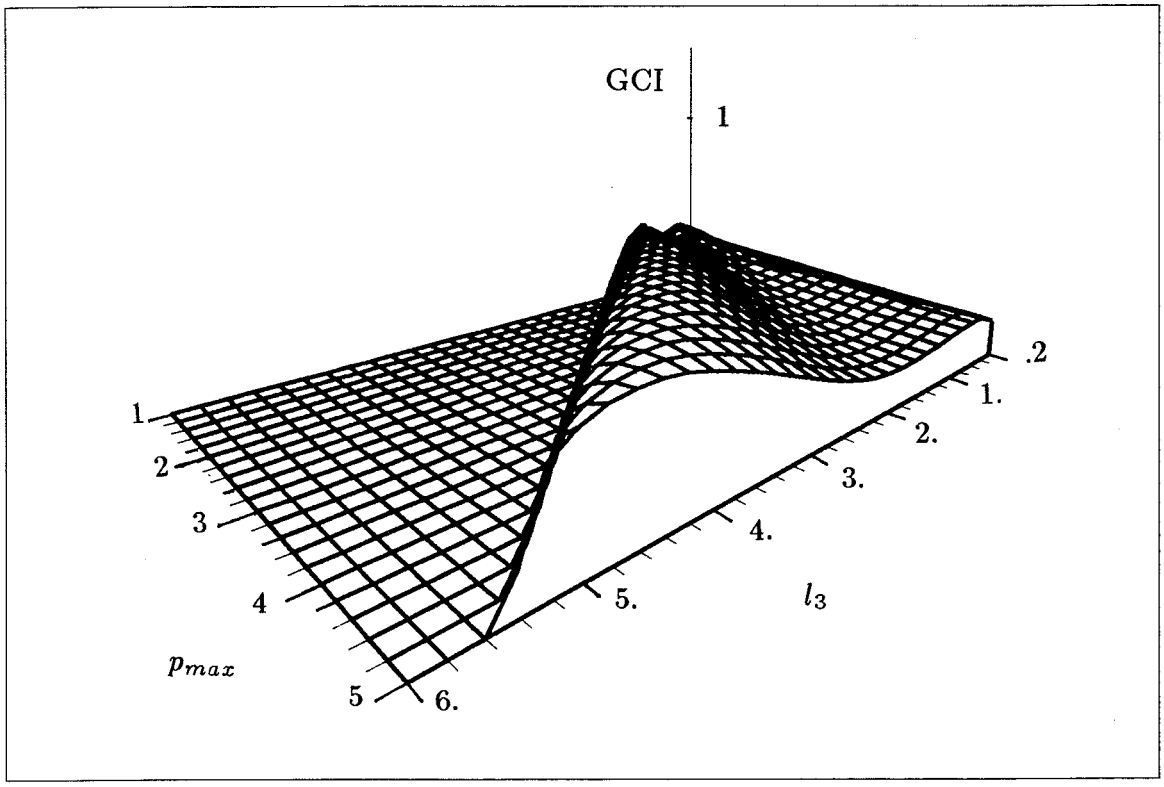

Figure 5.12 GCI of the planar manipulator with prismatic actuators as a function of l_3 and p_{max}.

5.4 Spherical Three-Degree-of-Freedom Manipulator

The spherical manipulator studied in Section 4.3 will now be optimized for

its workspace and dexterity. The symmetry assumptions used in Chapter 4 are again maintained here.

5.4.1 Workspace Optimization

Since the purpose of this manipulator is to orient a rigid body in space, i.e., we are concerned with the orientation of the gripper only, the workspace of the manipulator will be embedded in the space of rigid body rotations which can be represented, for instance, using the linear invariants of the rotation matrix $\mathbf{Q}$, introduced in Chapter 4 and described in Appendix B. Again, the workspace is found by computing the intersection of the mobility region of all the legs. The mobility region for each individual leg is given by the set of possible orientations that the gripper can attain, given the link dimensions of this leg. This region is bounded by the *singularity surface*, which can be found for each leg as the closed surface separating the region where the leg has mobility from that in which it does not. The *global* mobility region will then be the intersection of all these three regions. As previously stated, we can represent the set of all possible rotations using the linear invariants, which can be grouped in a 4-dimensional vector $\lambda = [\mathbf{q}^T \quad q_0]^T$ with $\mathbf{q} = [q_1, q_2, q_3]^T$. One possibility for this representation consists of using the three-dimensional subspace (q_0, q_1, q_2) in which the set of points located inside or on the surface of the unit sphere centred at the origin, represent all possible rotations, the distance from a given point to the origin being equal to $\sqrt{1 - q_3^2}$.

The singularity surface can be obtained using eq.(4.64), where we set the discriminant equal to zero:

$$z_i = B_i^2 - A_i C_i = 0 \tag{5.56}$$

This equation, written for the first leg, leads to:

$$q_1^2 = (1 + q_0)(\cos\alpha_1 \cos\alpha_2 - q_0) \pm (1 + q_0) \sin\alpha_1 \sin\alpha_2 \tag{5.57}$$

which represents two circles in the (q_0, q_1) plane (Fig. 5.13), or two cylinders in the (q_0, q_1, q_2) space (the inner cylinder is shown in Fig. 5.14).

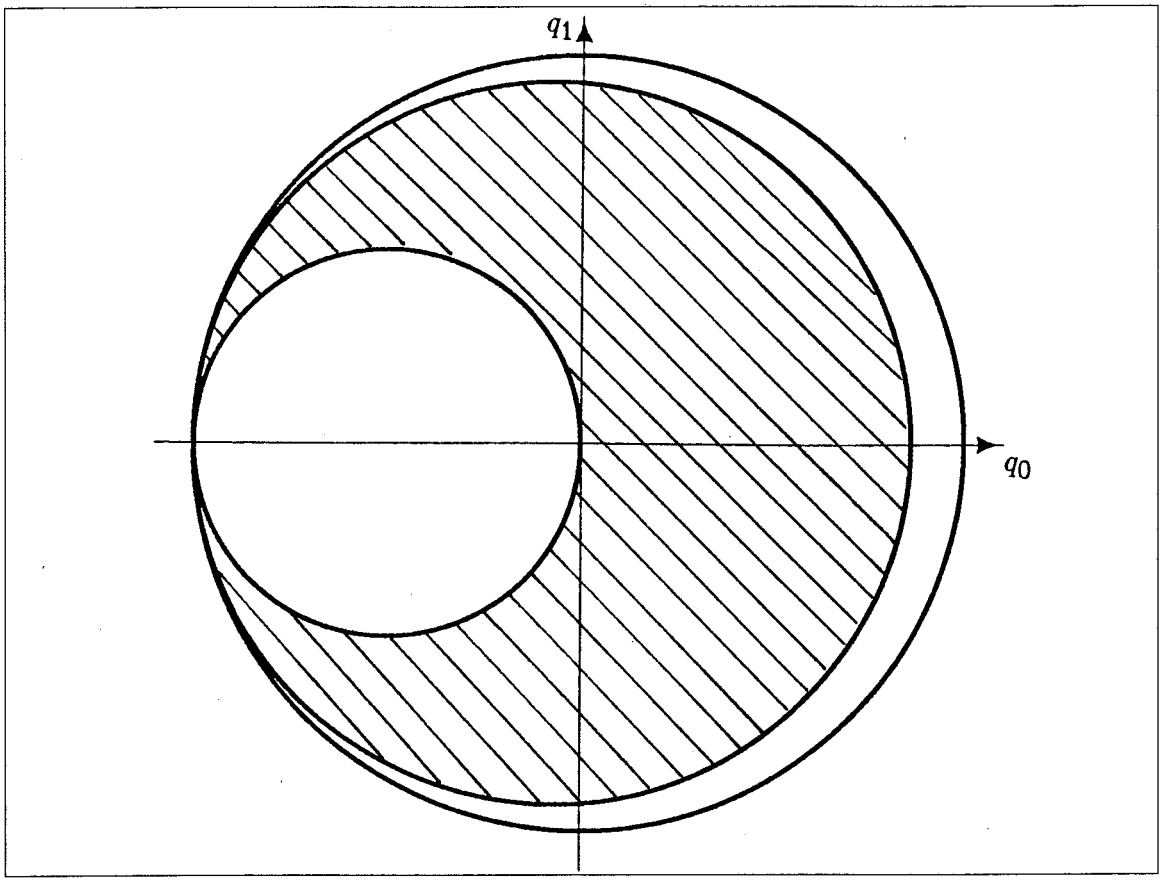

Figure 5.13 Mobility region for the first leg of the spherical manipulator.

The equations describing these circles are obtained by choosing alternatively the plus and minus signs in equation (5.57), which gives:

$$q_1^2 + \{q_0 + \frac{1}{2}[1 - \cos(\alpha_1 - \alpha_2)]\}^2 = \frac{1}{4}[1 + \cos(\alpha_1 - \alpha_2)]^2 \qquad (5.58a)$$

Thus, eq.(5.58a) represents a circle of radius $\frac{1}{2}[1 + \cos(\alpha_1 - \alpha_2)]$ centred at a point of coordinates $(C, 0)$, where

$$C = \frac{1}{2}[\cos(\alpha_1 - \alpha_2) - 1] \qquad (5.58b)$$

and

$$q_1^2 + \{q_0 + \frac{1}{2}[1 - \cos(\alpha_1 + \alpha_2)]\}^2 = \frac{1}{4}[1 + \cos(\alpha_1 + \alpha_2)]^2 \qquad (5.59a)$$

Similarly, eq.(5.59a) represents a circle of radius $\frac{1}{2}[1 + \cos(\alpha_1 + \alpha_2)]$ centred at a point of coordinates $(C', 0)$, where:

$$C' = \frac{1}{2}[\cos(\alpha_1 + \alpha_2) - 1] \qquad (5.59b)$$

Moreover, it can be shown that the region located between these circles is the one where the leg has mobility, i.e., where the discriminant is positive—this region is hatched on Fig. 5.13.

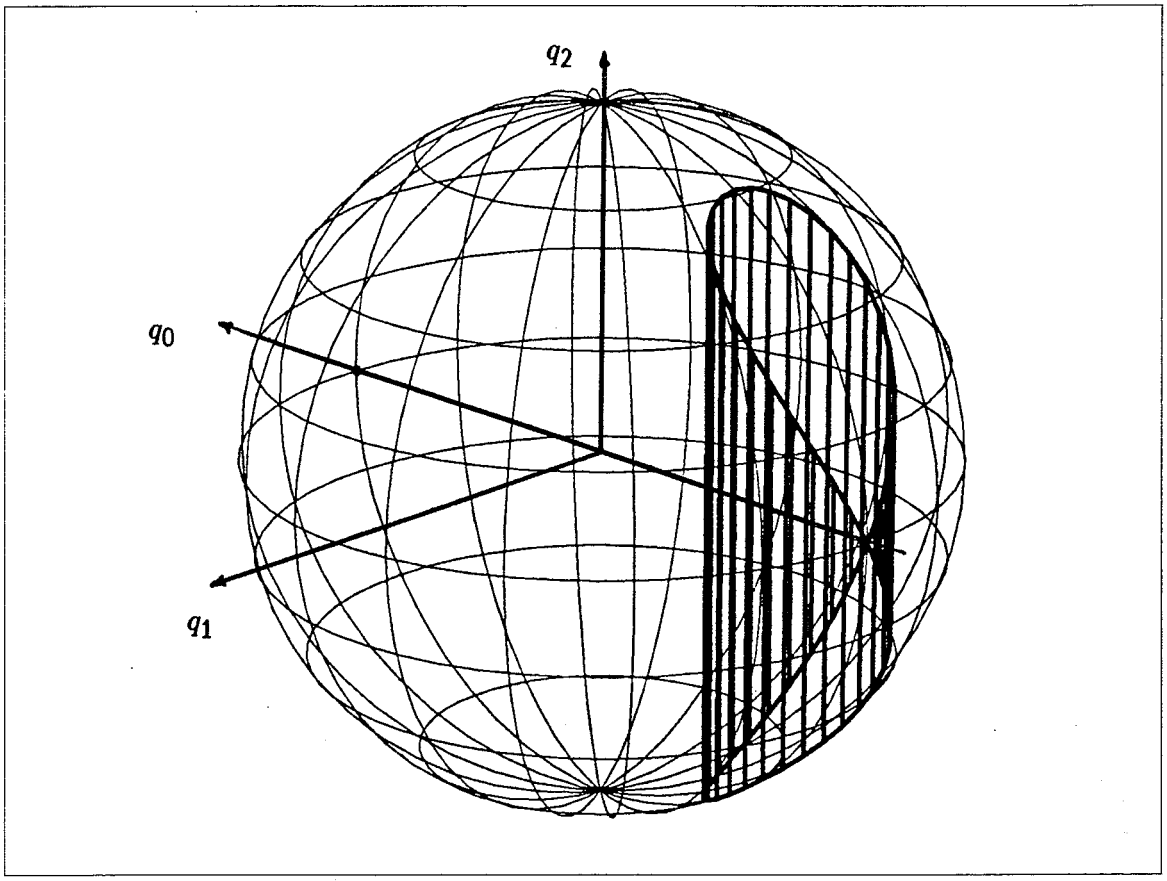

Figure 5.14 Inner cylinder defining the mobility region of the first leg of the spherical manipulator in the (q_0, q_1, q_2) space.

A similar analysis is repeated for each of the legs. This defines two other pairs of cylinders, which also have their axes in a plane parallel to the (q_1, q_2) plane. These axes intersect the first ones on the q_0 axis with and angle of $\pm 60°$ and the global mobility region is therefore completely defined. It can be seen from equations (5.58a) and (5.59a) that the conditions under which the manipulator is capable of producing all possible rotations are:

$$\alpha_1 - \alpha_2 = 0 \tag{5.60a}$$

and

$$\alpha_1 + \alpha_2 = \pi \tag{5.60b}$$

which means

$$\alpha_1 = \alpha_2 = \pi/2 \tag{5.60c}$$

If this condition is met, the *singularity surface* degenerates into three *singularity curves* which are major circles on the surface of the unit sphere in the (q_0, q_1, q_2) space at 60° from each other as shown in Fig. 5.15. A projection of this figure onto the $q_1 - q_2$ plane is given in Fig. 5.16 for clarity. This result is similar to the one obtained for an open-loop three-axis spherical wrist (Gupta and Roth 1982), for which condition (5.60c) has to be met if we want the wrist to be able to reach all possible orientations. Notice, however, that in the case of the open-loop wrist having $\alpha_1 = \alpha_2 = \pi/2$, there would be only one singularity curve on the sphere of Fig. 5.15.

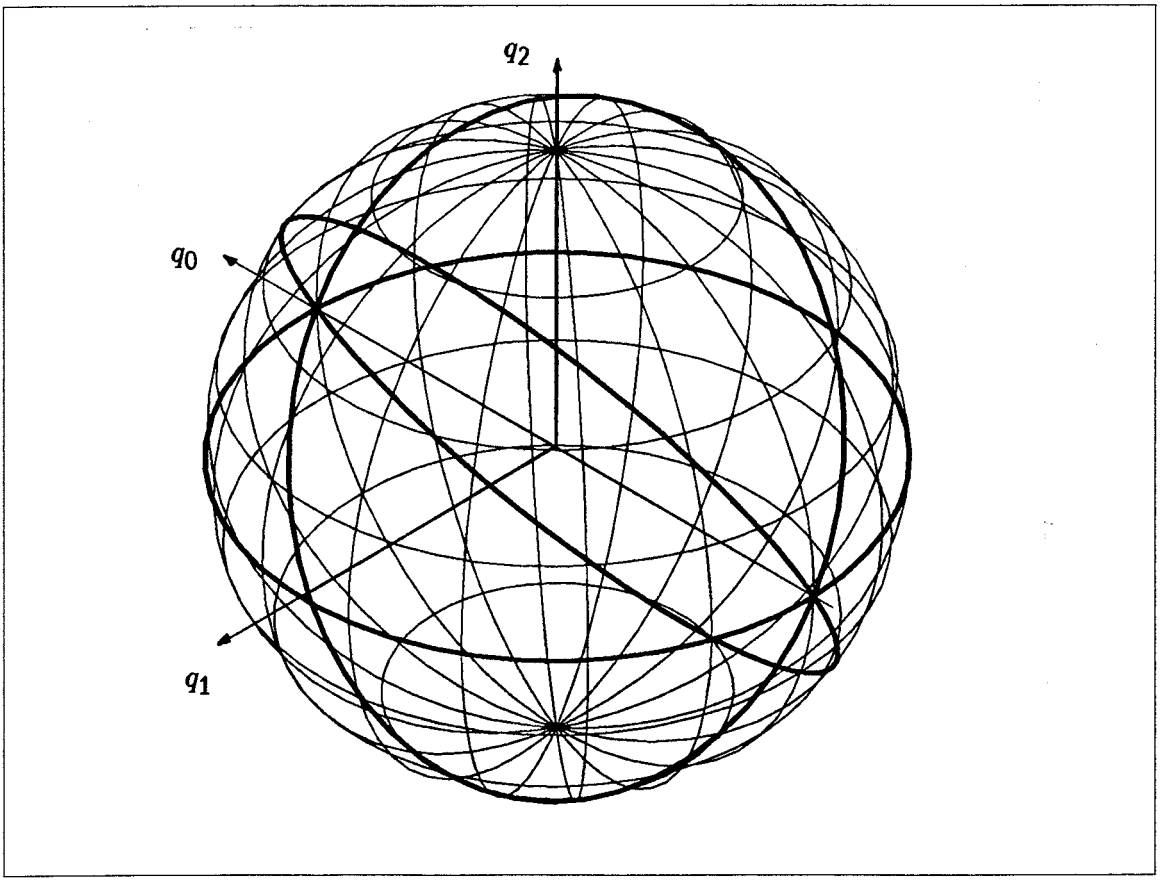

Figure 5.15 Singularity curves for a manipulator with $\alpha_1 = \alpha_2 = 90°$.

Furthermore, notice that, in the case of a manipulator having $\alpha_1 = \alpha_2 = \pi/2$,

the solution to the inverse kinematic problem simplifies to:

$$\theta_i = \tan^{-1}\left(\frac{\cos\eta_i v_{i1} + \sin\eta_i v_{i2}}{-v_{i3}}\right) \tag{5.61}$$

where the η_i's and the v_{ij}'s are defined in Section 4.3.

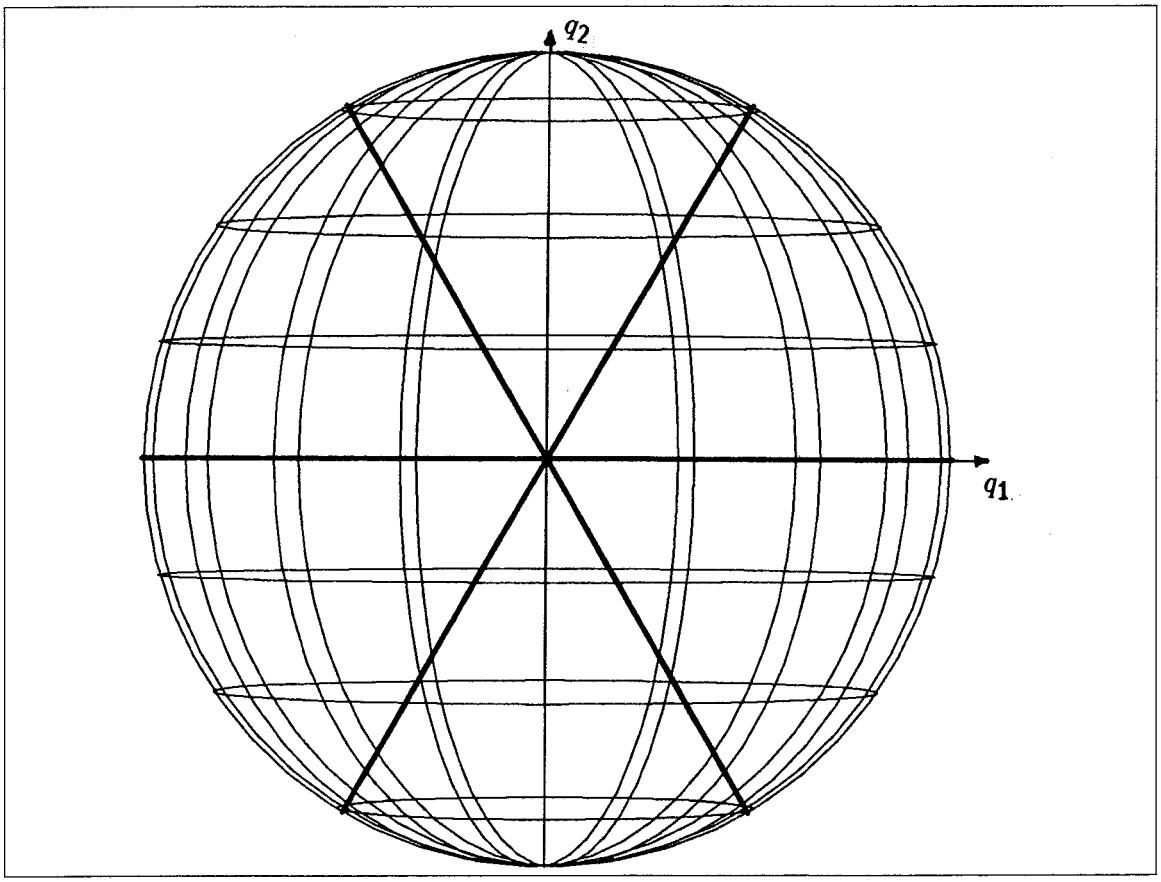

Figure 5.16 Projection of the singularity curves of Fig. 5.15 in the (q_1, q_2) plane.

5.4.2 Isotropy of the Jacobian Matrix

The definition of the Jacobian matrix of the spherical parallel manipulator was given in Chapter 4. It is repeated here for quick reference. We have defined:

$$\mathbf{J}\omega = \dot{\theta} \tag{5.62}$$

where ω is the angular velocity of the end-effector and $\dot{\theta}$ is the vector of powered joint rates and $\mathbf{J}$ is given as

$$\mathbf{J} = \begin{bmatrix} \mathbf{j}_1 \\ \mathbf{j}_2 \\ \mathbf{j}_3 \end{bmatrix} \tag{5.63a}$$

with

$$\mathbf{j}_i = \frac{(\mathbf{w}_i \times \mathbf{v}_i)^T}{(\mathbf{u}_i \times \mathbf{w}_i) \cdot \mathbf{v}_i} \tag{5.63b}$$

A direct-search method has been used to minimize the condition number of this Jacobian matrix. The minimization method referred to is that of bisection (Brent 1973) on one of the variables, while the other ones are kept fixed. The procedure is repeated alternatively for each of the variables until convergence is reached. This has been done for the general case of a manipulator with arbitrary link angles and also in the case where the link angles are assumed to be both of 90° due to the particularly interesting properties of this design that were discussed in Section 5.4.1. The results are given in Table 5.3. It is pointed out that the manipulator cannot be rendered isotropic with any link angles.

Solution #	α_1	α_2	$\mathbf{e}_1$	$\mathbf{e}_2$	$\mathbf{e}_3$	ϕ	κ
1	99.10	90.00	−.2363	.8818	.4081	135.60	1.1103
2	91.17	128.56	.8827	.4700	.0000	130.22	1.2073
3	123.36	60.00	.6411	−.3176	.6986	63.43	1.5502
4	140.02	100.00	.5443	.3594	.7580	40.05	1.9431
5	90.00	90.00	.0000	±1.0000	.0000	137.36	1.5728
6	90.00	90.00	±.8660	±.5000	.0000	137.36	1.5728
7	90.00	90.00	.9217	−.2470	.2992	146.69	1.1559
8	90.00	90.00	.2470	−.9217	.2992	146.69	1.1559

Table 5.3 Solutions corresponding to local minima of the condition number of the spherical manipulator. Solutions 1–4 are unconstrained while solutions 5–8 have been obtained when link angles of $\alpha_1 = \alpha_2 = 90°$ are assumed.

5.4.3 Global Conditioning Index

The workspace of the spherical manipulator was described in Section 5.4.1 as

a region in the (q_0, q_1, q_2) space. A numerical integration can then be carried out on this workspace in order to evaluate the GCI. This is done as:

$$\eta = \frac{\mathrm{A}}{\mathrm{B}} \tag{5.64a}$$

with

$$\mathrm{A} = \int_{q_2}\int_{q_1}\int_{q_0}\left(\frac{1}{\kappa}\right)\mathrm{d}q_0\mathrm{d}q_1\mathrm{d}q_2 = \int_{q_2}\int_{q_1}\int_{q_0}\nu\mathrm{d}q_0\mathrm{d}q_1\mathrm{d}q_2 \tag{5.64b}$$

and

$$\mathrm{B} = \int_{q_2}\int_{q_1}\int_{q_0}\mathrm{d}q_0\mathrm{d}q_1\mathrm{d}q_2 \tag{5.64c}$$

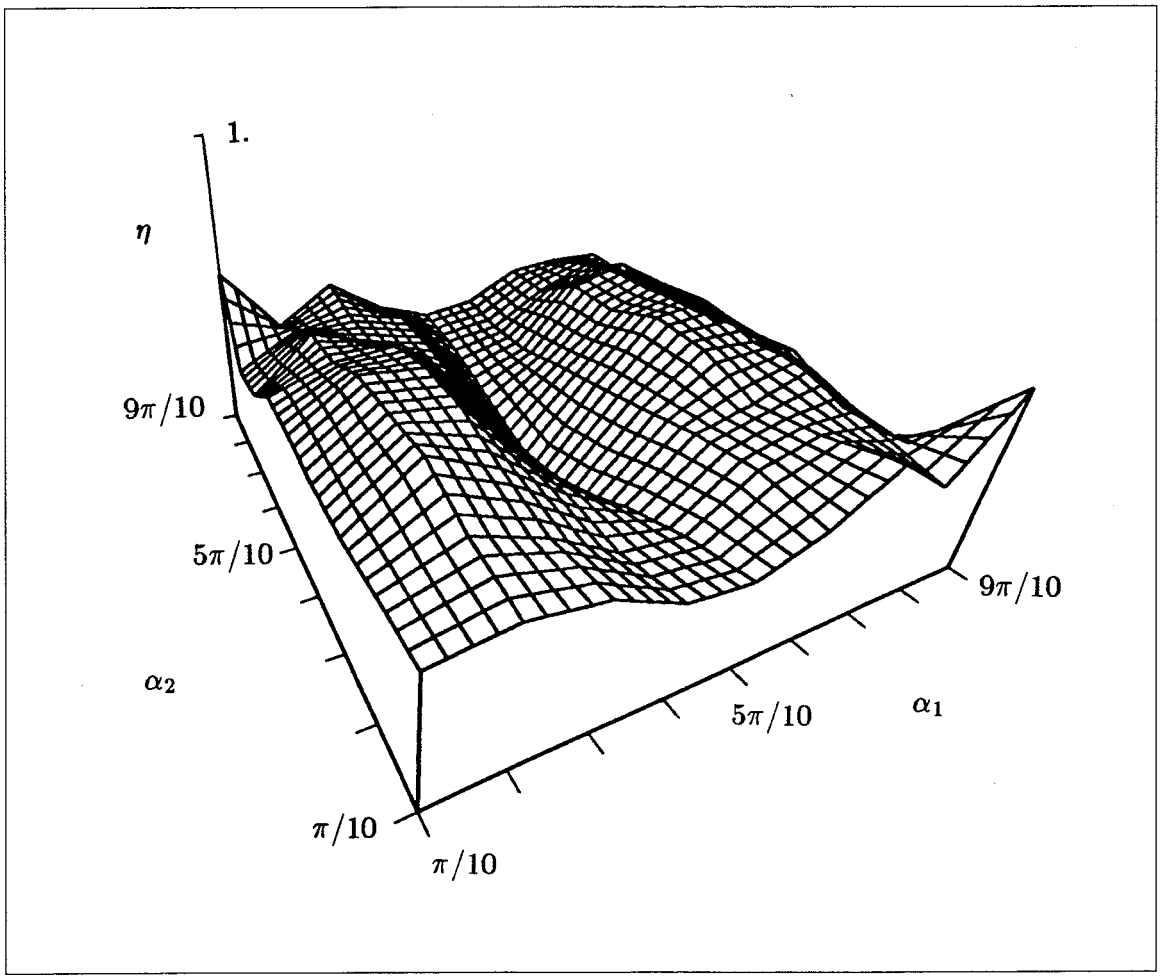

Figure 5.17 GCI of the spherical parallel manipulator as a function of α_1 and α_2.

These integrations were performed for different values of α_1 and α_2 and the results are given in Fig. 5.17 where the GCI is plotted as a function of α_1 and α_2. It is

interesting to note that the maximum GCI ($\eta = 0.52$), is obtained for $\alpha_1 = 7\pi/30$ and $\alpha_2 = 13\pi/30$, approximately. A symmetry about the central point $\alpha_1 = \alpha_2 = \pi/2$ is also observed. This point is found to be the one having the minimum GCI ($\eta = 0.056$), which indicates that, for this manipulator, the optimization of the GCI conflicts seriously with the maximization of the workspace. Indeed, it was shown in the workspace optimization performed in this chapter, that the central point of the $\alpha_1 - \alpha_2$ region of interest, shown in Figs. 5.17 and 5.18, is the one having the maximum workspace. This can be clearly seen in Fig. 5.18, where the volume of the workspace of the manipulator is plotted as a function of α_1 and α_2, according to the results of Section 5.4.1.

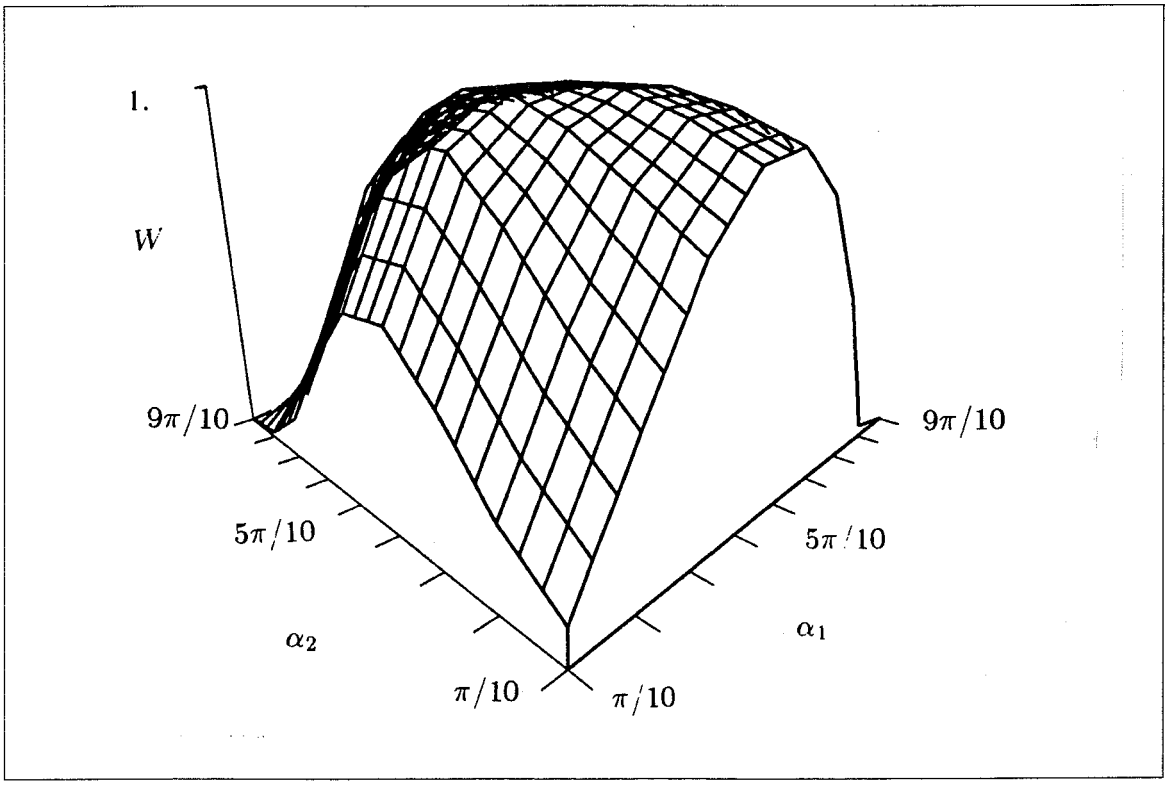

Figure 5.18 Normalized workspace of the spherical parallel manipulator as a function of α_1 and α_2.

5.5 Spatial Three-Degree-of-Freedom Manipulator

The workspace and dexterity of the spatial three-degree-of-freedom manipulator

will now be optimized. The approach used here is similar to the one used for planar and spherical manipulators, i.e., it is based on the analysis performed in Chapter 4.

5.5.1 Workspace Optimization

In the first stage of the analysis, we will assume that the actuators have an infinite range of motion and derive the corresponding workspace of the manipulator, i.e., the region that it can attain when only the constraints due to the architecture of the manipulator are considered. It is recalled from Chapter 4 that the solution of the inverse kinematic problem is obtained through two of the solutions of a quartic equation in q_{22}—a component of the rotation matrix $\mathbf{Q}$ defining the orientation of the platform—, each of which leads to two solution for the global problem. The roots of the quartic equation are given in eq.(4.99) and repeated here for quick reference

$$(q_{22})_{1,2} = -X \pm (\sqrt{X^2 + Y^2} - 1) \tag{5.65a}$$

where

$$X = x/l \quad \text{and} \quad Y = y/l \tag{5.65b}$$

The other components of the upper left corner of matrix $\mathbf{Q}$ are computed as follows:

$$q_{12} = q_{21} = -Y \tag{5.66a}$$

and

$$q_{11} = q_{22} + 2X \tag{5.66b}$$

while the last row and the last column of $\mathbf{Q}$ are computed using the properties of the orthogonal matrix (Appendix C).

The workspace of the manipulator can be determined by noting that the solutions given above are components of an orthogonal matrix and hence have to be comprised within the following range:

$$-1 \leq q_{ij} \leq 1, \qquad i,j = 1,2,3 \tag{5.67}$$

The foregoing constraint is now applied to each of the roots given in eq.(5.65a).

Root 1

We obtain

$$q_{22} = \sqrt{X^2 + Y^2} - X - 1 \tag{5.68a}$$

$$q_{11} = \sqrt{X^2 + Y^2} + X - 1 \tag{5.68b}$$

$$q_{12} = q_{21} = -Y \tag{5.68c}$$

and the first constraint to be applied is

$$q_{13}^2 = q_{31}^2 = 1 - q_{11}^2 - q_{12}^2 \geq 0 \tag{5.69}$$

Upon substitution of eqs.(5.68b&c) into eq.(5.69), this equation becomes

$$-2Y^2 - 2X^2 + 2X - 2(X-1)\sqrt{X^2 + Y^2} \geq 0 \tag{5.70}$$

which can be further simplified to lead to

$$(1 - \sqrt{X^2 + Y^2})(X + \sqrt{X^2 + Y^2}) \geq 0 \tag{5.71}$$

Since the second factor on the left-hand side of eq.(5.71) is a positive semidefinite quantity, we are left with only

$$1 - \sqrt{X^2 + Y^2} \geq 0 \tag{5.72a}$$

i.e.

$$x^2 + y^2 \leq l^2 \tag{5.72b}$$

The second constraint to be applied can be written as

$$q_{23}^2 = q_{32}^2 = 1 - q_{21}^2 - q_{22}^2 \geq 0 \tag{5.73}$$

Upon substitution of eqs.(5.68a&c) into eq.(5.73), this equation becomes

$$-2Y^2 - 2X^2 - 2X + 2(X+1)\sqrt{X^2 + Y^2} \geq 0 \tag{5.74}$$

which can be rewritten as

$$(\sqrt{X^2+Y^2}-1)(X-\sqrt{X^2+Y^2}) \geq 0 \tag{5.75}$$

Since the second factor on the left-hand side of eq.(5.75) is a negative semidefinite quantity, eq.(5.75) leads to

$$\sqrt{X^2+Y^2}-1 \leq 0 \tag{5.76a}$$

i.e.

$$x^2+y^2 \leq l^2 \tag{5.76b}$$

Root 2

We obtain

$$q_{22} = -\sqrt{X^2+Y^2}-X+1 \tag{5.77a}$$

$$q_{11} = -\sqrt{X^2+Y^2}+X+1 \tag{5.77b}$$

$$q_{12} = q_{21} = -Y \tag{5.77c}$$

Again, the first constraint is written as

$$q_{13}^2 = q_{31}^2 = 1-q_{11}^2-q_{12}^2 \geq 0 \tag{5.78}$$

Upon substitution of eqs.(5.77b&c) into eq.(5.78), this equation becomes

$$-2Y^2-2X^2-2X+2(X+1)\sqrt{X^2+Y^2} \geq 0 \tag{5.79}$$

which is identical to eq.(5.74) and hence, the first constraint leads to:

$$x^2+y^2 \leq l^2 \tag{5.80}$$

The second constraint applied on the second root is

$$q_{23}^2 = q_{32}^2 = 1-q_{21}^2-q_{22}^2 \geq 0 \tag{5.81}$$

Upon substitution of eqs.(5.77a&c) into eq.(5.81), this equation becomes

$$-2Y^2 - 2X^2 + 2X - 2(X-1)\sqrt{X^2+Y^2} \geq 0 \tag{5.82}$$

which is identical to eq.(5.70) and hence, the second constraint leads to

$$x^2 + y^2 \leq l^2 \tag{5.83}$$

Since all the constraints lead to one and the same inequality, i.e., eqs.(5.72b), (5.76b), (5.80) and (5.83), which are all identical, this inequality defines the boundary of the workspace which is, in this case, a circular cylinder of radius l whose axis of symmetry is the z axis, i.e., an axis orthogonal to the base plane and located at the centroid of the base triangle. Hence, if the actuators have an infinite range of motion, the foregoing cylinder represents the set of points that the centroid of the platform can attain when all mechanical interferences are neglected.

In a real manipulator, however, the actuators have a finite range of motion and the workspace is consequently reduced. To find the workspace of a manipulator whose actuators have limited motion, the cylinder described above will be discretized and a description of the accessible region will be obtained in terms of a sum of elements of volume.

First of all, we have to compute the minimum and maximum height, from the base plane, that the platform can reach in z. This is given by

$$\begin{aligned} h_{min} &= \sqrt{p_{min}^2 - (1-l)^2} \quad \text{if} \quad p_{min} < |1-l| \\ h_{min} &= 0 \qquad \text{otherwise} \end{aligned} \tag{5.84}$$

and

$$h_{max} = \sqrt{p_{max}^2 - (1-l)^2} \tag{5.85}$$

This potential region can then be divided in a certain number of sections, or 'slices', parallel to the base plane and located between $z = h_{min}$ and $z = h_{max}$. In each of these sections, the trace of the workspace on a plane parallel to the base is found using

the following algorithm: A certain number of rays originating from the point $x = y = 0$ are equally spaced around a circle centred at that point. For each of the rays, a direct-search method is used to locate its intersection with the boundary of the workspace. The surface of the element is then approximated by a sector of a circle, i.e.,

$$S_{el} = \frac{r_{el}^2 \theta}{2} \tag{5.86}$$

where θ is the angle between two consecutive rays and r_{el} is the radius associated with a given element. This is illustrated in Fig. 5.19. It is pointed out that, due to the symmetry of the workspace, only one third of the rays need be actually computed. The surface of all the elements of a planar region—or 'slice'—are then summed and multiplied by the increment in z to give the volume of that 'slice' of the workspace, which is, in turn, added to the volume of the other elements.

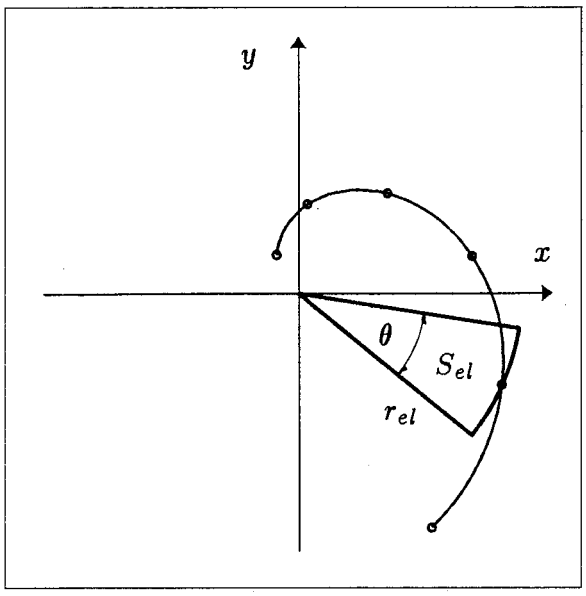

Figure 5.19 Discretization and approximation of the workspace of the spatial three-degree-of-freedom manipulator.

An example of the workspace of a manipulator, with actuators having limited motion, is plotted in Fig. 5.20. The workspace is represented by the projection of its boundary, onto the base plane, for different values of z, or 'slices', used in the numerical evaluation of the volume.

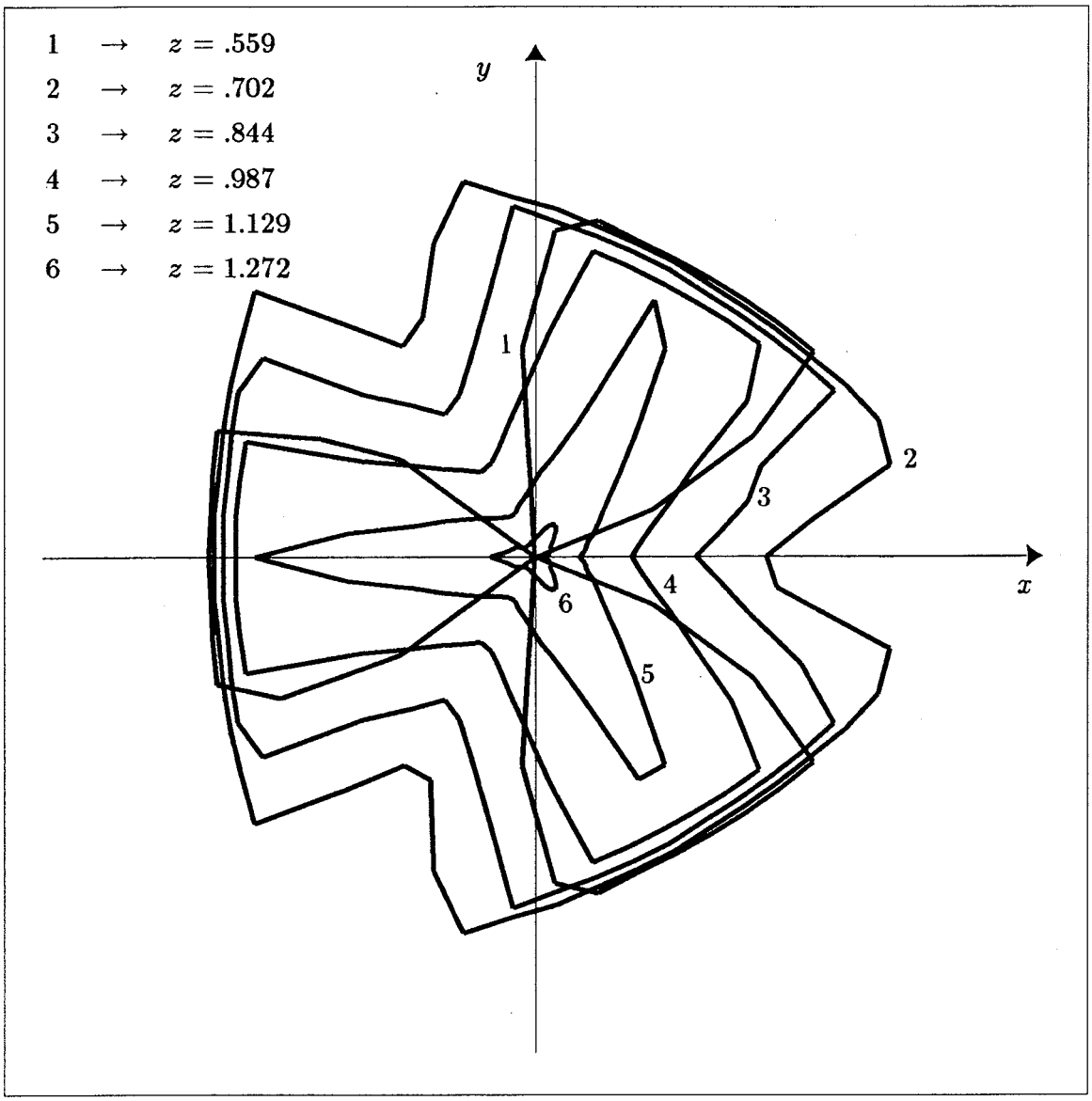

Figure 5.20 Example of the workspace of a spatial three-degree-of-freedom parallel manipulator with $l = 0.5$ and $p_{max} = 1.5$. The workspace is represented by the projection of its boundary, in the base plane, for different values of z.

The problem of the optimization of the workspace is now formulated as follows: For a given value of the range of motion of the actuators, find the value of l, the characteristic dimension of the platform, that will produce the workspace with a maximum volume. This problem will be solved as a series of workspace maximization problems obtained by incrementing the value of the maximum extension of the actuators p_{max}. The minimum

extension of the actuators is assumed to be given by

$$p_{min} = \frac{1}{2} p_{max} \tag{5.87}$$

For a given value of p_{max}, we can compute the volume of the workspace corresponding to a certain value of l and, therefore, use a search technique to find the value of l that leads to the maximum workspace. The results for different values of p_{max} are shown in Fig. 5.21, where the values of l corresponding to a maximum workspace are plotted vs. p_{max}.

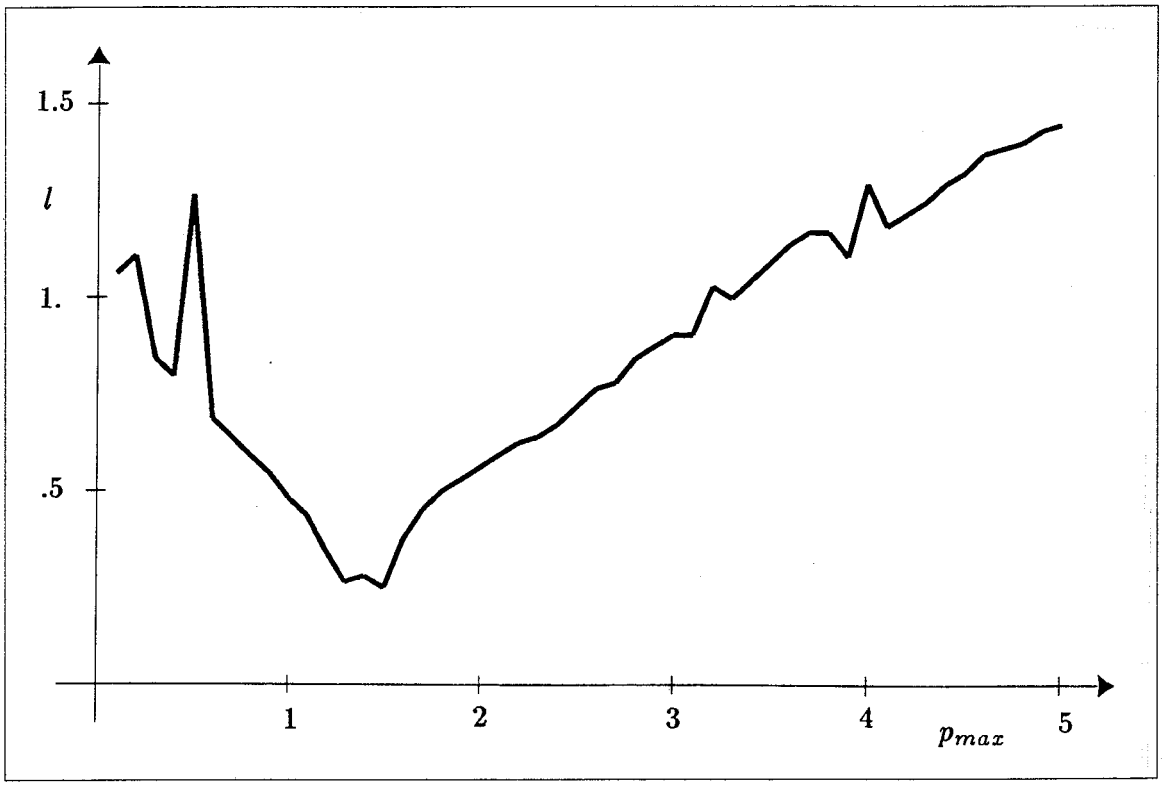

Figure 5.21 Optimum values of l that maximize the volume of the workspace as a function of p_{max}.

5.5.2 Isotropy of the Jacobian Matrix

The Jacobian matrix of the spatial three-degree-of-freedom parallel manipulator is defined in eq.(4.109) and an explicit expression for this matrix is given in eq.(4.116a).

It is now desired to find isotropic designs, i.e., to find kinematic parameters for which at least one point of the workspace corresponds to a configuration for which the condition number of the Jacobian matrix is equal to unity.

As a first analysis, the complex method (Box 1965) was used to minimize the condition number over the variables x, y, z and l, i.e., over the whole set of kinematic parameters and position variables. It was then observed that the minimization procedure tends to converge to points for which $x = y = 0$. Therefore, a more detailed investigation of these points was undertaken. This is shown in Fig. 5.22 where curves of the reciprocal of the condition number as a function of z are shown for a few values of l and for $x = y = 0$.

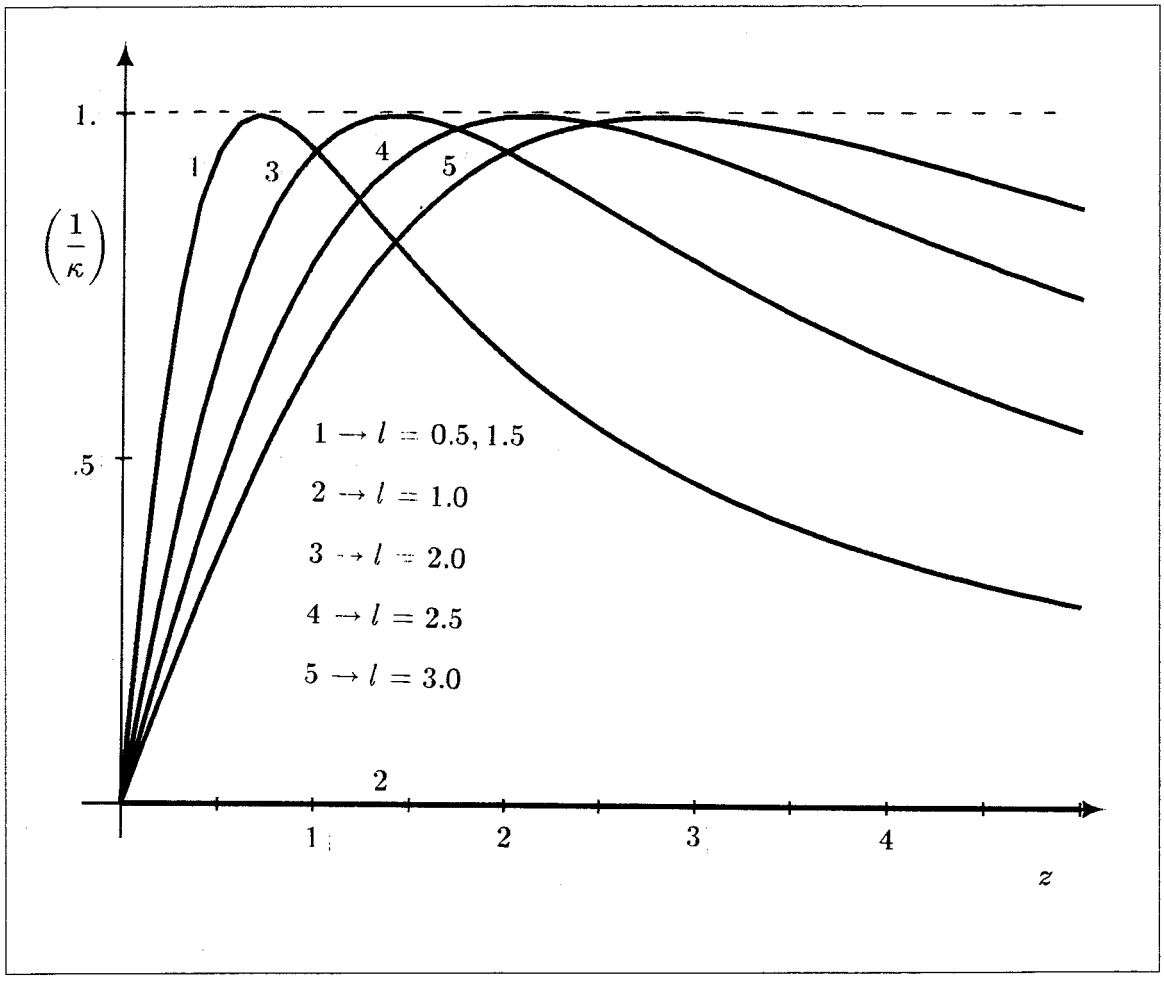

Figure 5.22 Reciprocal of the condition number of the spatial three-degree-of-freedom parallel manipulator as a function of z, for $x = y = 0$ and for a few values of l.

The following is readily observed: for every value of the characteristic dimension l, there exists an isotropic point located on the z axis, i.e., the axis defined by $x = y = 0$, at a certain height z^*. Moreover, the value of z^* is a linear function of l, as it can clearly be seen in Fig 5.23, where the value of z^* is plotted as a function of l. This plot was obtained by minimizing the condition number over z for every value of l. The linear relationship can be expressed as

$$z^* = |al - b| \tag{5.88a}$$

where

$$a = b = \sqrt{2} \tag{5.88b}$$

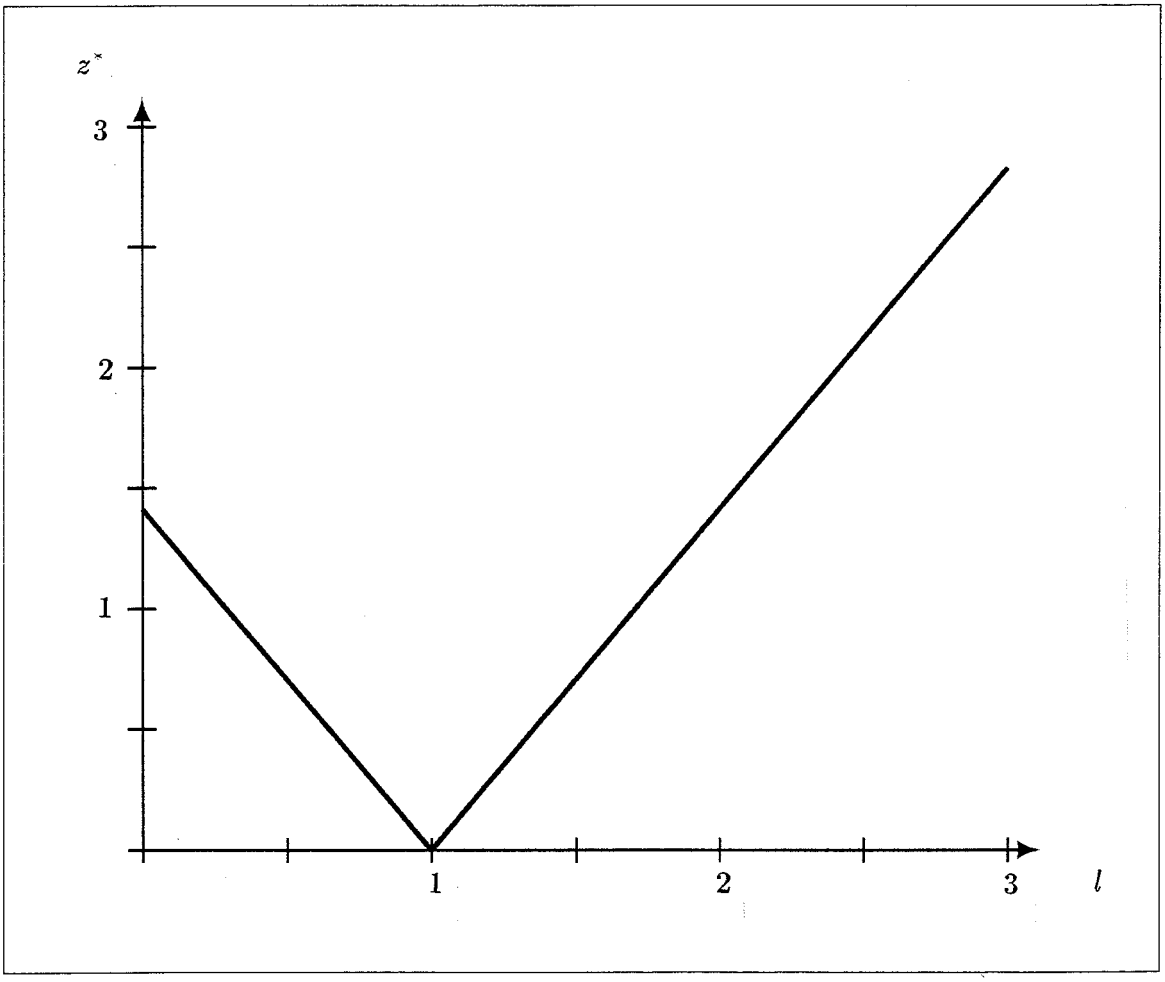

Figure 5.23 Values of z^*, i.e., values of z for which the spatial three-degree-of-freedom parallel manipulator is isotropic when $x = y = 0$ as a function of l.

No other point of the workspace was found to be isotropic. As an example of the behaviour of the condition number over the workspace, this quantity is plotted as a function of z in Fig. 5.24 for $x = y = 0.2$, and for a few values of the characteristic dimension l.

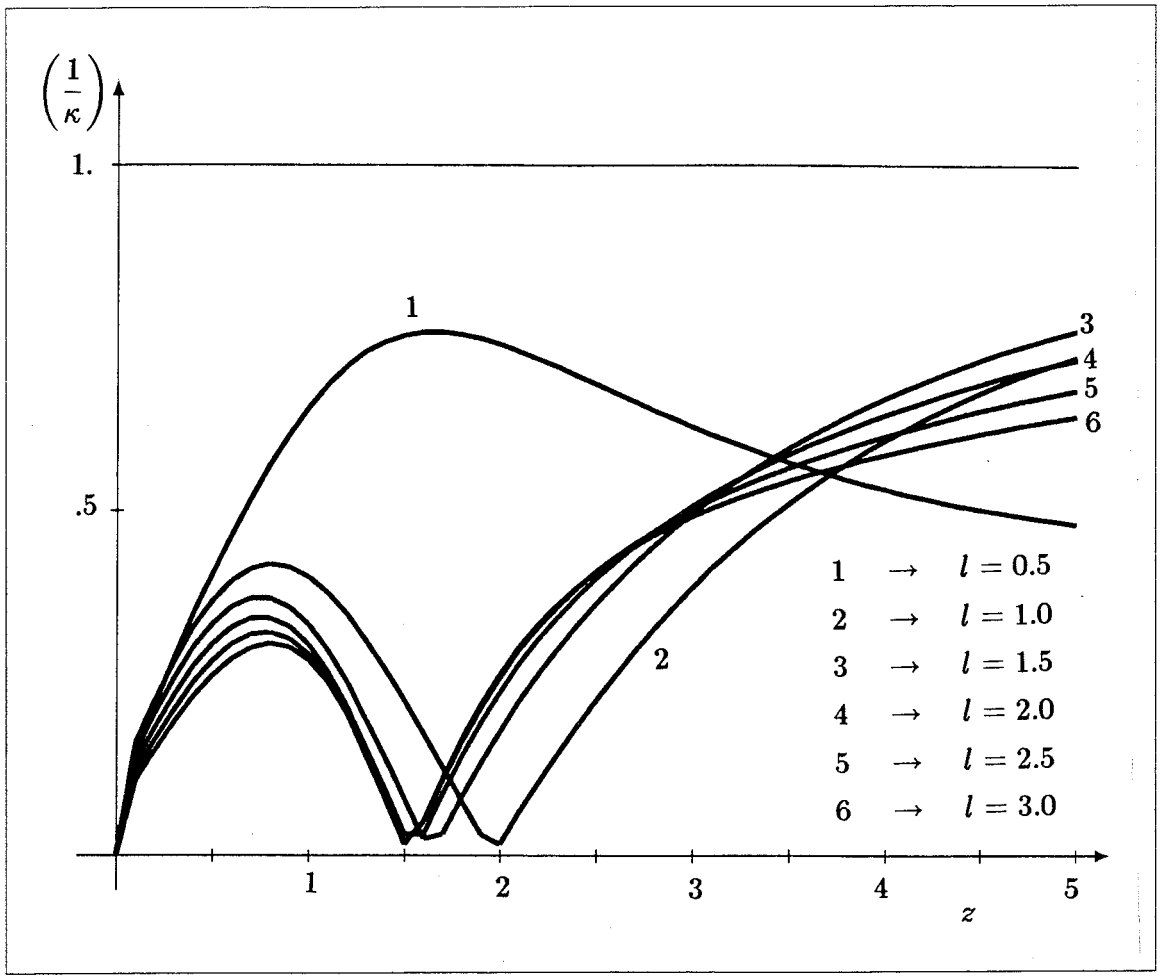

Figure 5.24 Reciprocal of the condition number of the spatial three-degree-of-freedom parallel manipulator as a function of z for $x = y = 0.2$ and for different values of l.

5.5.3 Global Conditioning Index

The global conditioning index of the spatial three-degree-of-freedom manipulator can be evaluated by resorting to a numerical integration over the workspace. It is known, from Section 5.5.1, that the workspace is included in a circular cylinder of radius l and

length $h_{max} - h_{min}$ whose axis of symmetry is along the z axis. Therefore, this volume can be discretized and a test can be performed on each of the elements then obtained to check whether or not it is part of the workspace. When the element is part of the workspace, the condition number of the Jacobian matrix is computed, for one point of the element, as well as the volume of the element. These quantities are then summed over all the elements to lead to the values of A and B as defined in eqs.(5.5b&c). Since the integration is performed over a cylinder, it is natural to choose a cylindrical coordinate system. After discretizing the potential workspace as shown in Fig. 5.25, the integrals to be performed can be written as the following sums where, it is recalled, each element has to be tested before it is included:

$$A = \sum_{i=1}^{n_z} \sum_{j=1}^{n_\theta} S_{ij}^A \Delta h \tag{5.89a}$$

and

$$B = \sum_{i=1}^{n_z} \sum_{j=1}^{n_\theta} S_{ij}^B \Delta h \tag{5.89b}$$

where

$$S_{ij}^A = \sum_{k=1}^{n_r} a_{ijk} \tag{5.90a}$$

and

$$S_{ij}^B = \sum_{k=1}^{n_r} b_{ijk} \tag{5.90b}$$

with

$$a_{ijk} = \left(\frac{1}{\kappa_{ijk}} \right) (r_{k+1}^2 - r_k^2) \frac{\Delta\theta}{2} \tag{5.91a}$$

if element ijk is in the workspace. Otherwise,

$$a_{ijk} = 0 \tag{5.91b}$$

Similarly,

$$b_{ijk} = (r_{k+1}^2 - r_k^2) \frac{\Delta\theta}{2} \tag{5.92a}$$

if element ijk is in the workspace. Otherwise,

$$b_{ijk} = 0 \tag{5.92b}$$

In the above expressions, we have

$$\Delta h = (h_{max} - h_{min})/n_z \tag{5.93}$$

$$r_i = l(i-1)/n_r \tag{5.94}$$

and

$$\Delta\theta = 2\pi/3n_\theta \tag{5.95}$$

the variables n_r, n_θ and n_z representing the number of elements chosen when discretizing in r, θ and z, respectively. It is pointed out that the symmetry of the workspace allows us to integrate on only one third of the actual workspace, a fact that is taken into account by eq.(5.95).

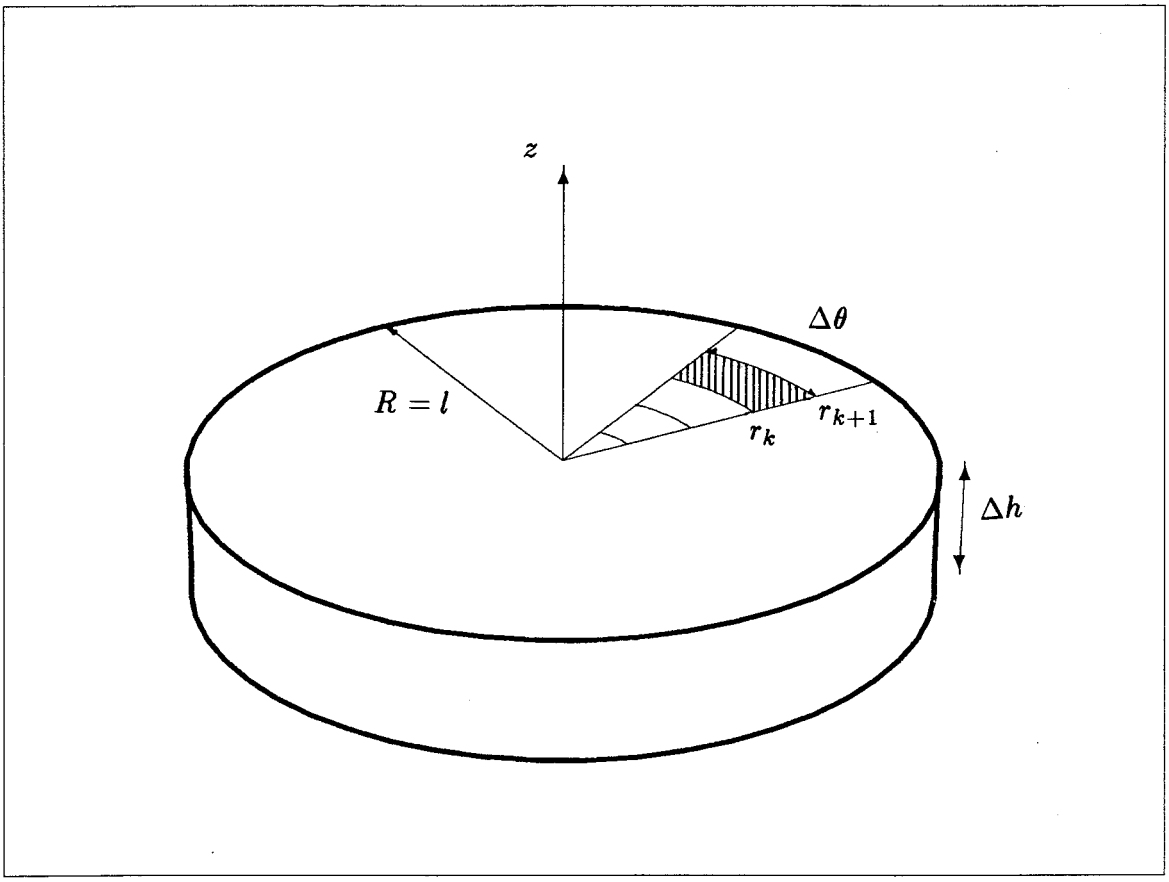

Figure 5.25 Discretization of the workspace of the spatial three-degree-of-freedom parallel manipulator.

The algorithm described above was used to compute the global conditioning index of the manipulator under study for different values of p_{max} and l. Again, the relation

given in eq.(5.87) was assumed. The results are shown graphically in Fig. 5.26, where the GCI is plotted as a function of the two variables. The best design is obtained when we have $p_{max} = 1.2$ and $l = 1.4$, which leads to a GCI of 0.5783.

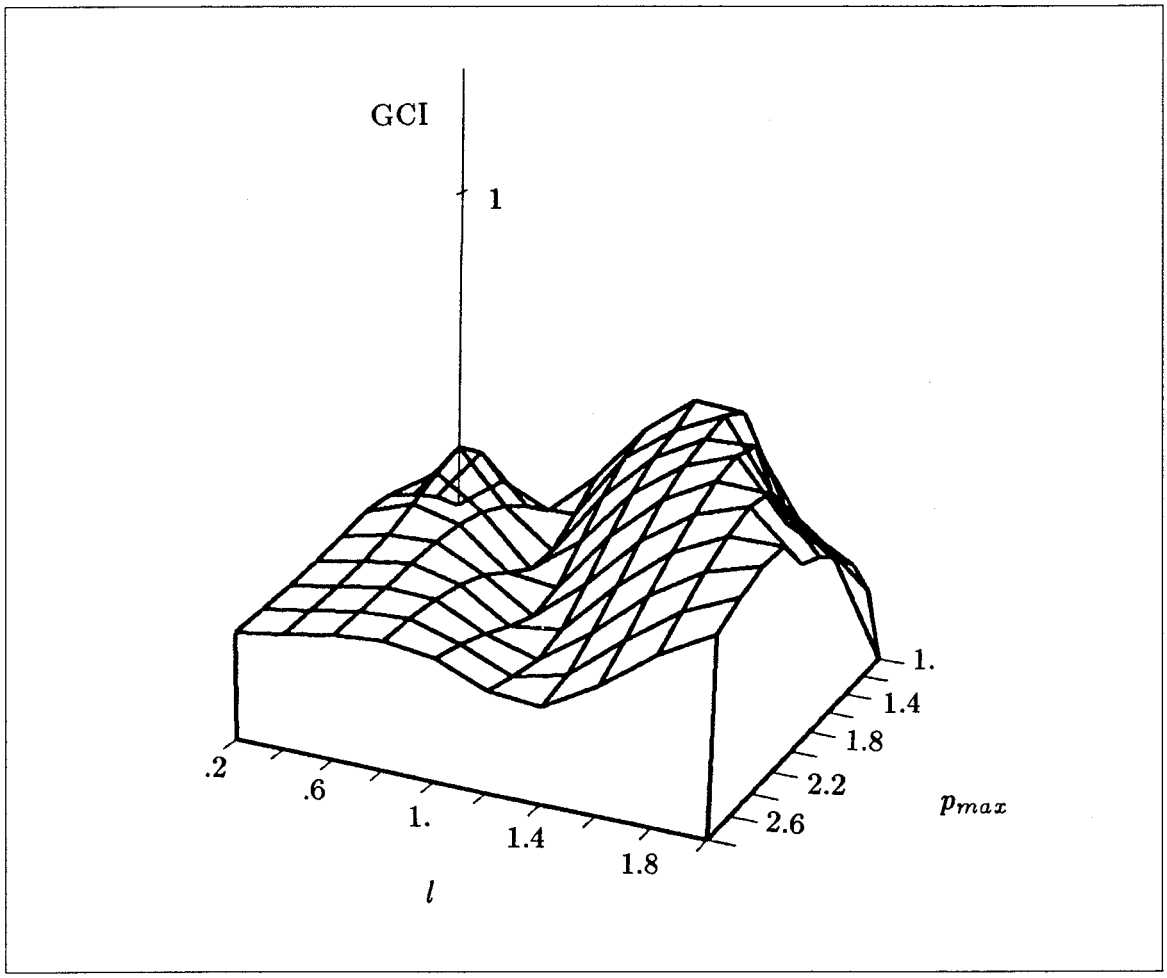

Figure 5.26 GCI of the spatial three-degree-of-freedom parallel manipulator as a function of l and p_{max}.

Chapter 6 KINEMATIC INVERSION AND TRAJECTORY PLANNING OF REDUNDANT PARALLEL MANIPULATORS

The kinematics of manipulators in the presence of redundancies has attracted the attention of many researchers over the past decade. Liégeois (1977), Klein and Huang (1983), Baillieul (1985, 1986) and Stanišić and Pennock (1985), among others, have tackled the associated inverse kinematic problem considering various types of approaches and optimization criteria. This problem is still a subject of current research (Anderson and Angeles 1987; Suh and Hollerbach 1987; Wampler 1987; Mayorga and Wong 1987; Chevallereau and Khalil 1987; Nakamura et al. 1987). Klein and Blaho (1987) presented a review of different optimization criteria that have been used for the design and control of redundant manipulators. However, to the knowledge of the author, the study of redundancies has so far been limited to serial manipulators only.

The kinematic problem addressed in this chapter is associated with parallel manipulators. In many instances, it may be desirable to use a parallel manipulator with a degree of freedom greater than the number of Cartesian coordinates to be controlled. This allows one to optimize a performance index in the process of solving the inverse kinematic problem. After having formulated this problem as one of condition-number minimization, it will be shown that the optimum value of the free parameter that minimizes the condition number is not a continuous function of the prescribed Cartesian coordinates. In fact, the

performance index used, i.e., the condition number of the Jacobian matrix of the manipulator, is a measure of the local dexterity, as stated in Chapter 5. In order to optimize this index along a partially prescribed Cartesian trajectory, the concept of *trajectory map* is introduced. The Cartesian trajectory to be followed is said to be partially prescribed because, as stated above, the task to be performed—and hence the Cartesian trajectory to be followed—requires less degrees of freedom than the manipulator can provide. Therefore, the description of the task itself does not completely define the associated motions of the manipulator. The trajectory map is, in fact, a representation of the field of possible solutions over which the optimum trajectory will be chosen in order to fully specify the motion of the manipulator.

An on-line trajectory planning solution is then derived and the results obtained with this method for a planar three-degree-of-freedom parallel manipulator and a spherical three-degree-of-freedom parallel manipulator, which were studied in Chapters 4 and 5, are given.

6.1 Problem Formulation

The problem to be solved here can be described as follows: Given an incompletely specified trajectory in the Cartesian space of the manipulator, find the joint histories that will produce this trajectory while optimizing a certain performance index. Of course, the choice of this performance index will strongly affect the resulting joint histories. It is therefore crucial that the index chosen be a relevant meaningful quantity. The condition number of the Jacobian matrix of the manipulator will be used here as a performance index to be minimized. It is recalled, from Chapter 5, that the condition number of the Jacobian matrix of a manipulator is a measure of the accuracy of the kinematic control of this manipulator (Salisbury and Craig 1982), which makes it a very significant index. Moreover, since the condition number becomes infinity at singularities, the minimization of this quantity will tend to keep the manipulator away from these undesirable configurations. It is pointed out here that the approach used in (Anderson and Angeles 1987), consisting of minimiz-

ing the deviation of the joint angles from a certain value—this measure is termed JRAE in (Klein and Blaho 1987)—, produced unsatisfactory results when tested on the planar parallel manipulator. Hence, known results for serial manipulators cannot be extrapolated to parallel manipulators.

6.1.1 Planar Three-Degree-of-Freedom Manipulator

The planar three-degree-of-freedom parallel manipulator considered here (Fig. 4.1) was studied in detail in Chapters 4 and 5. This manipulator can be thought of as a redundant manipulator if one is interested in positioning a point of the gripper on the plane disregarding its orientation. That case would arise, for instance, when the manipulator is used to guide a mill, a drill, or any other axially symmetric object. The partially prescribed Cartesian trajectory is therefore given by the position $C(x, y)$ of the centroid of the gripper. The inverse kinematic problem for this manipulator can be solved in closed form as shown in Chapter 4, its solution θ being represented here as

$$\theta = \theta(x, y, \phi) \tag{6.1}$$

where θ is the 3-dimensional vector of actuated joint coordinates. The problem consists, then, of generating the joint histories that will guide point C of the gripper through the prescibed positions (x, y) and will minimize the condition number of the manipulator over the free variable, i.e., angle ϕ. Once this angle is specified, we can explicitly compute the joint variables θ using the kinematic inversion mentioned above. Since this inversion leads to two solutions per leg, we will choose these solutions so that the manipulator remains on the same branch, the procedure being then capable of avoiding undesirable branching effects. In the discussion that follows, a coordinate frame is defined fixed to the manipulator's base, with its origin O located at the centroid of triangle $M_1M_2M_3$ of Fig. 4.1. Moreover, the X and Y axes of this frame lie in the plane of motion and Y is directed from O to M_3. The branching of the planar manipulator can be readily verified as follows: We first define $M_i(x_{oi}, y_{oi})$, $I_i(x_{1i}, y_{1i})$ and $G_i(x_{2i}, y_{2i})$, for $i = 1, 2, 3$, as the centres of the driven joints, the intermediate joints and the joints attached to the gripper, respectively.

Then we define $\mathbf{s}_i = [x_{2i} - x_{1i}, y_{2i} - y_{1i}, 0]^T$ and $\mathbf{t}_i = [x_{oi} - x_{1i}, y_{oi} - y_{1i}, 0]^T$, which are the vectors connecting I_i to G_i and I_i to M_i, respectively. We can then write:

$$\mathbf{s}_i \times \mathbf{t}_i = \alpha_i \mathbf{e}_3 \tag{6.2}$$

where $\mathbf{e}_3 = [0,0,1]^T$ and

$$\alpha_i = x_{oi}(y_{1i} - y_{2i}) + y_{oi}(x_{2i} - x_{1i}) + x_{1i}y_{2i} - x_{2i}y_{1i} \tag{6.3}$$

The sign of α_i will tell the branch for the ith leg and therefore, by recording this quantity for each of the legs, at every configuration, we can ensure that the manipulator remains on the same branch. A change in sign of this quantity would mean that we have chosen the wrong root of the quadratic equation arising in the solution of the inverse kinematic problem.

6.1.2 Spherical Three-Degree-of-Freedom Manipulator

The spherical three-degree-of-freedom parallel manipulator considered here is represented in Fig. 4.9. This manipulator was studied in detail in Chapters 4 and 5, where it was shown that it can be used to orient a gripper in the three-dimensional space. However, we would like to use it here to orient a line of the gripper, regardless of the orientation of the gripper itself about the said line. This task requires only two degrees of freedom, which allows us to optimize a performance index. Applications requiring such a task definition comprise, e.g., the orientation of solar panels, radar antennas and telescopes.

In what follows, a coordinate frame is defined, fixed to the manipulator's base, with its origin O located at the point of the gripper that remains fixed, with its X and Y axes in the plane of the motors. Moreover, the X axis is defined along the axis of one of the motors. We can, therefore, define the unit vectors $\mathbf{u}_i$, $i = 1,2,3$ along the motors' axes (Fig. 4.10), i.e.,

$$\mathbf{u}_i = [\cos\gamma_i, \sin\gamma_i, 0]^T, \qquad i = 1,2,3 \tag{6.4a}$$

with

$$\{\gamma_i\}_1^3 = \left\{0, \frac{2\pi}{3}, \frac{4\pi}{3}\right\} \tag{6.4b}$$

The orientation of the gripper is described by three unit vectors $\mathbf{v}_i$, for $i = 1,2,3$, fixed to the gripper and directed from O to the joints attached to the gripper, which are represented by points A, B, C in Fig. 4.9.

Let us assume that the line to be oriented is parallel to the unit vector $\mathbf{g}$, which is orthogonal to the plane defined by vectors $\mathbf{v}_1, \mathbf{v}_2, \mathbf{v}_3$ (Fig. 4.9). In Chapter 4, the reference configuration of the manipulator was defined as the one in which $\mathbf{u}_i = \mathbf{v}_i$, for $i = 1,2,3$, and therefore, in this configuration, the unit vector $\mathbf{g}$ would be coincident with the z axis, since vectors $\mathbf{u}_i$, for $i = 1,2,3$, are located in the xy plane.

We can then write tensor $\mathbf{Q}$, describing the rotation of the gripper from the reference configuration to the current configuration, as a combination of two rotations. The first one, represented by the rotation tensor $\mathbf{Q_1}$, is specified as a rotation mapping vector $\mathbf{e}_3$ into $\mathbf{g}$ and vector $\mathbf{u_1}$ into a unit vector $\mathbf{r}$ which is orthogonal to $\mathbf{g}$ and is located in the xy plane. This first rotation is fully specified, for the task to be accomplished here, and is equivalent to a rotation carrying vector $\mathbf{g}$ into its desired orientation with an arbitrary rotation about an axis parallel to $\mathbf{g}$. The second rotation, represented by tensor $\mathbf{Q}_2$, is a rotation of a certain angle ψ about vector $\mathbf{g}$. We can then write:

$$\mathbf{Q} = \mathbf{Q}_2\mathbf{Q}_1 \tag{6.5a}$$

The rotation tensor $\mathbf{Q_1}$ is, in turn, written as:

$$\mathbf{Q}_1 = [\mathbf{r} \quad \mathbf{h} \quad \mathbf{g}] \tag{6.5b}$$

where

$$\mathbf{h} = \mathbf{g} \times \mathbf{r} \tag{6.5c}$$

which follows from the definitions of vectors $\mathbf{r}$ and $\mathbf{g}$. Indeed, we want the unit vector $\mathbf{r} = [r_1, r_2, r_3]^T$ to be orthogonal to $\mathbf{g}$ and located in the xy plane, which leads to:

$$r_3 = 0 \tag{6.6a}$$

$$r_1^2 + r_2^2 + r_3^2 = 1 \tag{6.6b}$$

$$r_1 g_1 + r_2 g_2 + r_3 g_3 = 0 \tag{6.6c}$$

The solution of these equations can be written as:

$$r_1 = \pm\sqrt{\frac{g_2^2}{g_1^2 + g_2^2}}, \quad r_2 = -\frac{r_1 g_1}{g_2} \tag{6.7}$$

To ensure continuity of the angle of rotation ψ about the axis parallel to $\mathbf{g}$ in matrix $\mathbf{Q}_2$, we will choose the positive sign in eq.(6.7) when $g_2 > 0$ and the negative sign when $g_2 < 0$. Two special cases may also arise:

i) If $g_2 = 0$, then we will have, from eqs.(6.6), $r_1 = 0$ and $r_2 = \pm 1$. We will choose the positive sign when $g_1 < 0$ and the negative sign when $g_1 > 0$.

ii) If $g_1^2 + g_2^2 = 0$, then we necessarily have $g_3 = \pm 1$, in which case we will specify that $\mathbf{r} = \pm\mathbf{u}_1$.

We can now write the second rotation, i.e., the rotation through an angle ψ about an axis parallel to vector $\mathbf{g}$, as (Angeles 1982)

$$\mathbf{Q}_2 = \mathbf{g}\mathbf{g}^T + \cos\psi(\mathbf{1} - \mathbf{g}\mathbf{g}^T) - \sin\psi(\mathbf{1} \times \mathbf{g}) \tag{6.8a}$$

where $\mathbf{1}$ denotes the 3×3 identity tensor. Therefore, eq.(6.5a) can be written as:

$$\mathbf{Q} = \mathbf{Q}_2(\psi)\mathbf{Q}_1 \tag{6.8b}$$

from which it becomes obvious that once vector $\mathbf{g}$ is specified, matrix $\mathbf{Q}$ becomes a function of angle ψ, over which the optimization will be performed, since its value does not affect the orientation of vector $\mathbf{g}$.

Once the optimum angle ψ has been determined, matrix $\mathbf{Q}$ can be computed and the joint variables can be obtained from the kinematic inversion. Again, this inversion leads to two solutions per leg and we will choose the solutions so that the manipulator always remains on the same branch. The branching of the spherical manipulator can be

verified as follows: we define two vectors that are tangent to the unit sphere associated with the manipulator at the tip of $\mathbf{w}_i$. Therefore, these vectors are orthogonal to $\mathbf{w}_i$ and can be written as:

$$\mathbf{s}_i = \mathbf{v}_i - (\mathbf{v}_i \cdot \mathbf{w}_i)\mathbf{w}_i \tag{6.9a}$$

$$\mathbf{t}_i = \mathbf{u}_i - (\mathbf{u}_i \cdot \mathbf{w}_i)\mathbf{w}_i \tag{6.9b}$$

These vectors play the same role as the corresponding ones for the planar manipulator. We then have,

$$\mathbf{s}_i \times \mathbf{t}_i = \alpha_i \mathbf{w}_i \tag{6.9c}$$

Again, the sign of α_i will tell the branch for the ith leg.

6.2 Local-Dexterity Maximization

As pointed out in the introduction, the optimization performed along the trajectory will consist of a minimization of the condition number of the Jacobian matrix of the manipulator. Since we are dealing with parallel manipulators, the Jacobian matrix is defined as the matrix mapping the Cartesian velocities into the joint rates. For the planar manipulator, we can write:

$$\mathbf{J}_p \dot{\mathbf{c}} = \dot{\theta} \tag{6.10}$$

where $\dot{\mathbf{c}} = [\dot{x}, \dot{y}, \dot{\phi}]$ is the vector of Cartesian velocities and $\dot{\theta}$ is the vector of joint rates. For the spherical manipulator, we have:

$$\mathbf{J}_s \omega = \dot{\theta} \tag{6.11}$$

where ω is the angular-velocity vector of the gripper and $\dot{\theta}$ is the vector of joint rates. The expressions of these matrices are given in Chapter 4 as functions of the Cartesian coordinates and the joint angles. They are repeated next for quick reference:

$$\mathbf{J}_p = \begin{bmatrix} -a_1/c_1 & -b_1/c_1 & -d_1/c_1 \\ -a_2/c_2 & -b_2/c_2 & -d_2/c_2 \\ -a_3/c_3 & -b_3/c_3 & -d_3/c_3 \end{bmatrix} \tag{6.12}$$

where

$$\begin{aligned} a_i &= -g_1 g_2 (x - x_{oi}) + g_2 \cos\theta_i + g_1 \cos\phi_i \\ b_i &= -g_1 g_2 (y - y_{oi}) + g_2 \sin\theta_i + g_1 \sin\phi_i \\ c_i &= g_2[(y - y_{oi})\cos\theta_i - (x - x_{oi})\sin\theta_i] + \sin(\theta_i - \phi_i) \\ d_i &= g_1[(y - y_{oi})\cos\phi_i - (x - x_{oi})\sin\phi_i] - \sin(\theta_i - \phi_i) \end{aligned} \tag{6.13}$$

with g_1 and g_2 defined, in turn, as

$$g_1 = 1/l_1, \qquad g_2 = 1/l_3 \tag{6.14}$$

(x_{oi}, y_{oi}) being the coordinates of the centre of the ith motor, angles ϕ_i being defined as:

$$\begin{aligned} \phi_1 &= \phi + \pi/6 \\ \phi_2 &= \phi + 5\pi/6 \\ \phi_3 &= \phi - \pi/2 \end{aligned} \tag{6.15}$$

For the spherical manipulator, the ith row of the Jacobian matrix, $(\mathbf{j}_s^i)^T$, can be written as:

$$\mathbf{j}_s^i = \frac{(\mathbf{w}_i \times \mathbf{v}_i)}{(\mathbf{u}_i \times \mathbf{w}_i) \cdot \mathbf{v}_i} \tag{6.16}$$

where $\mathbf{u}_i, \mathbf{v}_i, \mathbf{w}_i$ are the unit vectors along the axes of the driven joint, the gripper joint and the intermediate joint, respectively, for the ith leg.

We have chosen, as an optimization criterion, to minimize the value of the condition number of the Jacobian matrix. This quantity was introduced in Section 5.1 where it was called the local dexterity of the manipulator. The definition of the condition number is recalled to be:

$$\kappa = ||\mathbf{J}||\,||\mathbf{J}^{-1}|| \tag{6.17}$$

where the norm is the same as the one used in Chapter 5, i.e.,

$$||\mathbf{J}|| = \sqrt{\mathrm{tr}(\mathbf{J}^T \mathbf{W} \mathbf{J})} \tag{6.18}$$

with $\mathbf{W} = \frac{1}{n}\mathbf{1}$, n being the dimension of the square matrix $\mathbf{J}$. From eqs.(6.12–6.18), we can see that, given a set of fully specified Cartesian coordinates (from which we derive the joint coordinates using the kinematic inversion), it is straightforward to compute the

condition number of the Jacobian matrix. However, to compute derivatives of the condition number with respect to the free variable of a redundant manipulator would be a tremendous task. Therefore, it was decided to use a direct-search technique to minimize the condition number over the free parameter. The method used was taken from (Brent 1973), where it is referred to as the *localmin* procedure. This method combines the golden-search technique and successive parabolic interpolation. It leads to an algorithm retaining the advantages of both of these methods, i.e., superlinear convergence is garanteed.

Since the condition number of a matrix becomes infinity when this matrix is singular, it is preferable to use the reciprocal of the condition number as an optimization parameter. Indeed, as stated in Chapter 5, this quantity has a very convenient behaviour, for it is bounded as follows:

$$0 \leq \left(\frac{1}{\kappa}\right) \leq 1 \tag{6.19}$$

However, this quantity, which can be thought of as a measure of the *distance* to singularity, should be maximized and, since the direct search technique we are using is devised to minimize an objective function, we will rather use the complement of this quantity, which can be thought of as a measure of the *distance* to isotropy for a certain matrix and which, therefore, is to be minimized. It is recalled that isotropic matrices are the ones which have a condition number of 1, i.e., the lowest value that this quantity can attain. As stated in Chapter 5, only orthogonal matrices and their multiples have this property (Strang 1980). The objective function to minimize is then written as:

$$\varsigma = 1 - \left(\frac{1}{\kappa}\right) \tag{6.20}$$

The procedure consists of minimizing this quantity over the free variable for each point of the partially prescribed Cartesian trajectory. For the planar manipulator, this amounts to a minimization over the angle of orientation ϕ when x and y are specified for each of the m points of the trajectory, i.e.,

$$\min_{\phi} \left[1 - \frac{1}{\kappa_i}\right] \tag{6.21a}$$

$$\text{s.t.} \quad x = x_i,\ y = y_i, \quad i = 1, \ldots, m \tag{6.21b}$$

where

$$\kappa_i = \kappa(\phi_i), \quad 0 \leq \phi_i' < 2\pi \tag{6.21c}$$

Once the m values of ϕ, $\{\phi_i\}_1^m$, along the trajectory are obtained, we can compute the joint histories $\theta_j(t)$, for $j = 1, 2, 3$.

The procedure used for the spherical manipulator is very similar. Again, we do:

$$\min_{\psi} \left[1 - \frac{1}{\kappa_i}\right] \tag{6.22a}$$

$$\text{s.t.} \quad \mathbf{g} = \mathbf{g}_i, \quad i = 1, \ldots, m \tag{6.22b}$$

where

$$\kappa_i = \kappa(\psi_i), \quad 0 \leq \psi_i < 2\pi \tag{6.22c}$$

Once the m values of ψ, $\{\psi_i\}_1^m$, are obtained, the joint histories $\theta_j(t)$ can be computed, for $j = 1, 2, 3$.

6.2.1 Undesirable Side Effects

The general idea presented above has to be studied in more detail before we can implement a stable algorithm that would minimize the condition number along a partially prescribed Cartesian trajectory.

The reciprocal of the condition number of the planar manipulator is plotted in Fig. 6.1 as a function of angle ϕ for three consecutive points of a circular trajectory. Two important problems can arise, as shown by this graph.

First of all, one can realize that, in the case shown here, there are two feasible regions, i.e., two ranges of values of ϕ that are attainable for a given point of the trajectory, and that these regions are separated by unfeasible regions which have been assigned a value of $(1/\kappa) = 0$ on the plot. Therefore, when computing optimum values of ϕ for consecutive

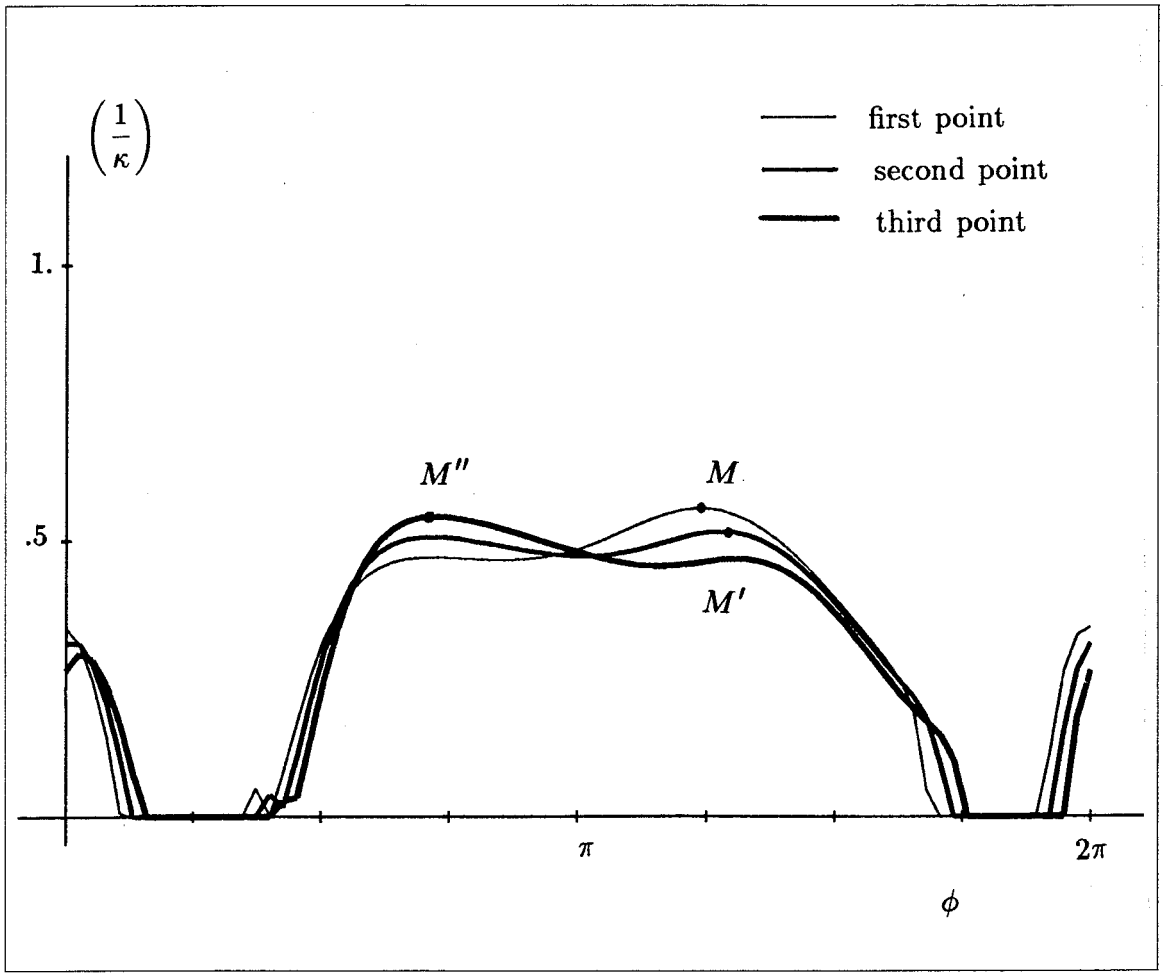

Figure 6.1 Reciprocal of the condition number of the planar manipulator as a function of the angle of orientation ϕ for three consecutive points of a given trajectory.

points of a trajectory, one must avoid unfeasible regions and jumping from one feasible region to another, disconnected, one.

Moreover, even though in the case presented here the solutions for the optimum values of ϕ remain within the same feasible region, discontinuities can arise in these solutions. This is clearly shown in Fig. 6.1, where points M, M' and M'' denote the optimum values of ϕ for each of the three trajectory points. It can be realized from this plot that, although the curve undergoes slight variations from point to point, there is a large 'jump' of the optimum value of ϕ (from point M' to M'') between the second and third points. Hence, as a result, the optimum value of ϕ that maximizes the reciprocal of the condition number *is not a continuous function* of the prescribed Cartesian coordinates.

The foregoing considerations will have to be taken into account in the trajectory-planning procedure.

6.2.2 Trajectory Maps

As pointed out above, there may be values of angle ϕ that are not attainable for a given point of the partially prescribed Cartesian trajectory. We can identify these regions for each of the points and draw the resulting diagram which is here termed *trajectory map*. Examples of these maps are shown in Fig. 6.2 and Fig. 6.3. The regions identified with a minus sign are the unfeasible ones. The trajectories corresponding to these maps will be described later.

The map shown in Fig. 6.2 was obtained for the planar manipulator. In this case, it is possible to obtain a closed-form expression for the limits of the workspace for a given point of the trajectory. It was shown in Chapter 5 that the boundary of the workspace can be obtained by setting the discriminant equal to zero in the quadratic equation that arises in the solution of the inverse kinematic problem for each of the legs of the manipulator. In the aforementioned chapter, the equations obtained when equating the discriminant to zero are:

$$(X_i - x_i)^2 + (Y_i - y_i)^2 = (l_1 + l_2)^2, \qquad i = 1,2,3 \tag{6.23a}$$

$$(X_i - x_i)^2 + (Y_i - y_i)^2 = (l_1 - l_2)^2, \qquad i = 1,2,3 \tag{6.23b}$$

where

$$x_i = l_3 \cos(\phi + \phi_i), \qquad i = 1,2,3 \tag{6.24a}$$

$$y_i = l_3 \sin(\phi + \phi_i), \qquad i = 1,2,3 \tag{6.24b}$$

$$X_i = x - x_{oi}, \qquad i = 1,2,3 \tag{6.24c}$$

$$Y_i = y - y_{oi}, \qquad i = 1,2,3 \tag{6.24d}$$

and

$$\{\phi_i\}_1^3 = \left\{\frac{\pi}{6}, \frac{5\pi}{6}, \frac{3\pi}{2}\right\} \tag{6.25}$$

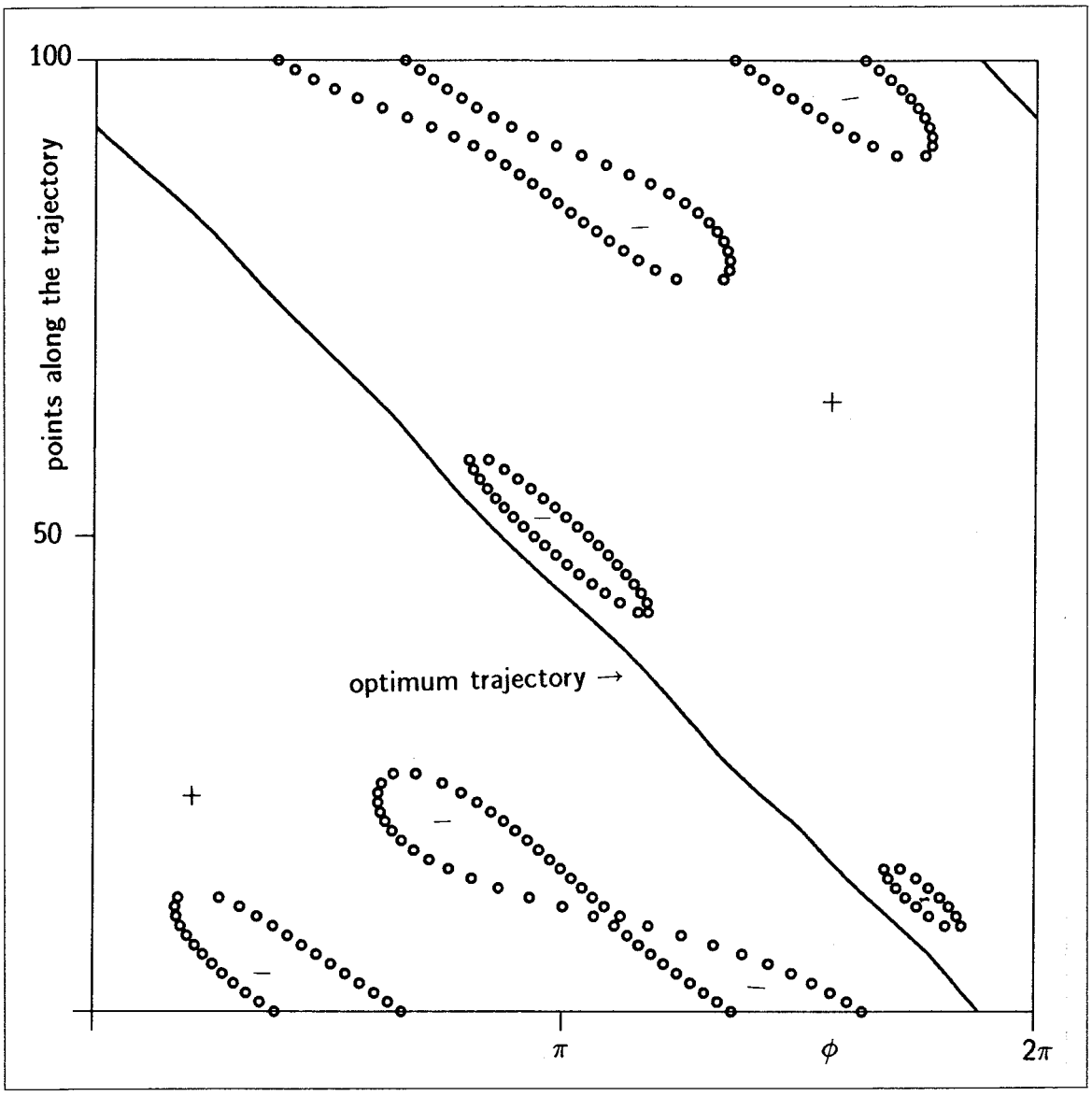

Figure 6.2 A trajectory map for the planar manipulator of example 1.

It is recalled that (x, y, ϕ) are the Cartesian coordinates of the gripper. Expansion of eqs.(6.23a&b) leads to:

$$2X_i l_3 \cos(\phi + \phi_i) + 2Y_i l_3 \sin(\phi + \phi_i) - \epsilon_i = 0, \qquad i = 1,2,3 \tag{6.26a}$$

$$2X_i l_3 \cos(\phi + \phi_i) + 2Y_i l_3 \sin(\phi + \phi_i) - \eta_i = 0, \qquad i = 1,2,3 \tag{6.26b}$$

with

$$\epsilon_i = X_i^2 + Y_i^2 + l_3^2 - (l_1 + l_2)^2, \qquad i = 1,2,3 \tag{6.27a}$$

$$\eta_i = X_i^2 + Y_i^2 + l_3^2 - (l_1 - l_2)^2, \qquad i = 1,2,3 \tag{6.27b}$$

It is then desired to find, for given values of x and y, the values of ϕ for which any one of these six equations (6.26a&b) can be satisfied. Therefore, we introduce the following substitutions:

$$\cos(\phi + \phi_i) = \frac{1 - T_i^2}{1 + T_i^2}, \qquad i = 1,2,3 \tag{6.28a}$$

and

$$\sin(\phi + \phi_i) = \frac{2T_i}{1 + T_i^2}, \qquad i = 1,2,3 \tag{6.28b}$$

where

$$T_i = \tan[\frac{1}{2}(\phi + \phi_i)], \qquad i = 1,2,3 \tag{6.29}$$

which leads to six quadratic equations, namely,

$$T_i^2(2X_i l_3 + \epsilon_i) - 2T_i(2Y_i l_3) + (\epsilon_i - 2X_i l_3) = 0, \qquad i = 1,2,3 \tag{6.30a}$$

$$T_i^2(2X_i l_3 + \eta_i) - 2T_i(2Y_i l_3) + (\eta_i - 2X_i l_3) = 0, \qquad i = 1,2,3 \tag{6.30b}$$

The solutions of these equations can be written as:

$$T_i = \frac{2Y_i l_3 \pm \sqrt{4Y_i^2 l_3^2 - (\epsilon_i^2 - 4X_i^2 l_3^2)}}{(\epsilon_i + 2X_i l_3)}, \qquad i = 1,2,3 \tag{6.31a}$$

and

$$T_i = \frac{2Y_i l_3 \pm \sqrt{4Y_i^2 l_3^2 - (\eta_i^2 - 4X_i^2 l_3^2)}}{(\eta_i + 2X_i l_3)}, \qquad i = 1,2,3 \tag{6.31b}$$

We therefore have a maximum of twelve solutions, i.e., a maximum of four solutions per leg. Equations (6.31a) and (6.31b) have been used to generate the trajectory map shown in Fig. 6.2.

The equations describing the motion of the spherical manipulator being more complicated, it is not possible to obtain closed-form expressions for the limits of the workspace and hence, the trajectory map shown in Fig. 6.3 has been generated by mere scanning of the values of angle ψ for each of the points of the trajectory.

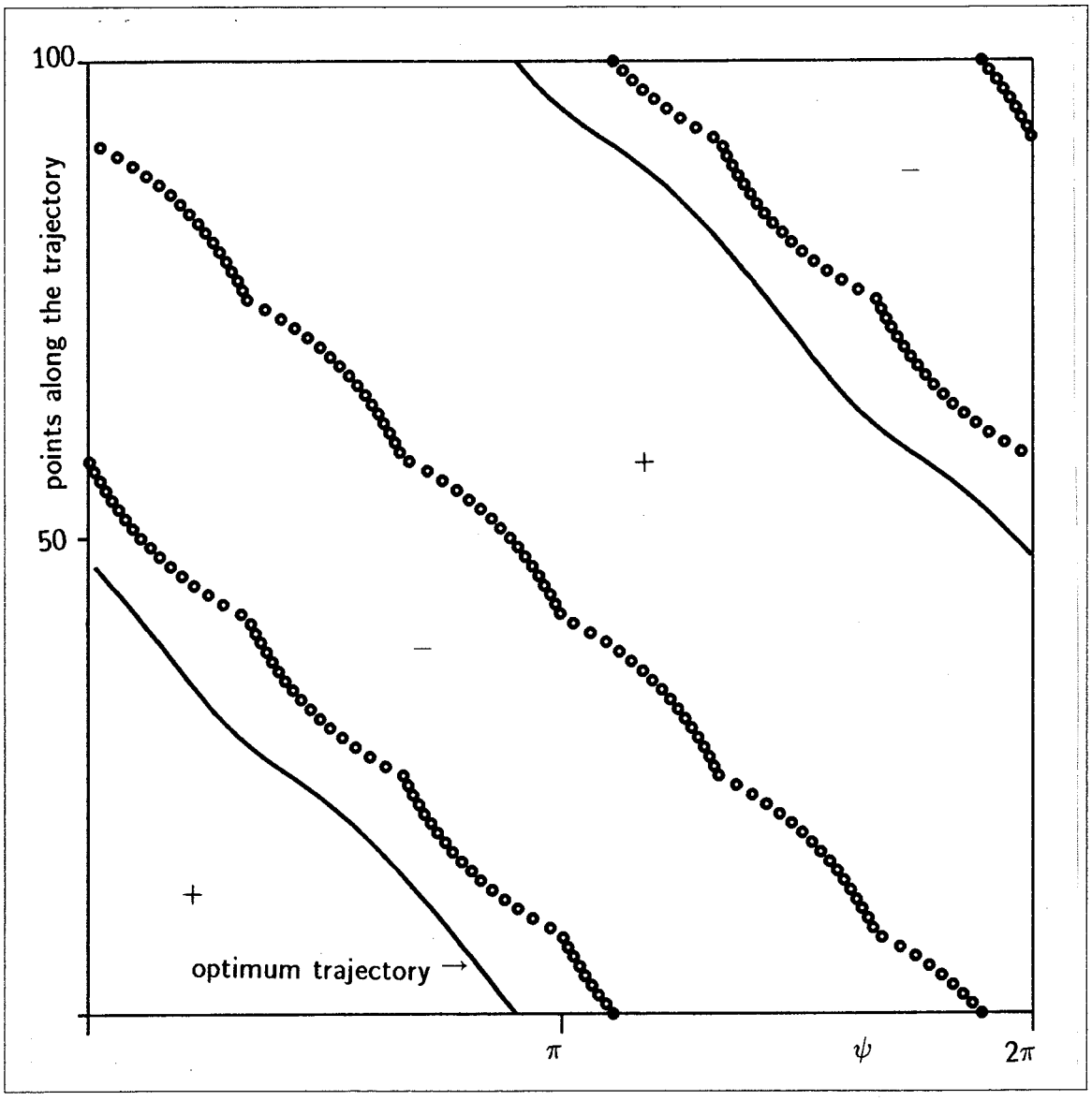

Figure 6.3 A trajectory map for the spherical manipulator of example 2.

6.2.3 On-Line Programming of Smooth Trajectories

Once a trajectory is decided upon and the corresponding trajectory map is obtained, it is desired to compute a smooth path that would go from the bottom to the top of the map while minimizing the condition number of the manipulator. This is accomplished using the algorithm shown in Fig. 6.4, where superscripts denote the step numbers.

This algorithm seeks optimum values of the condition number which are within

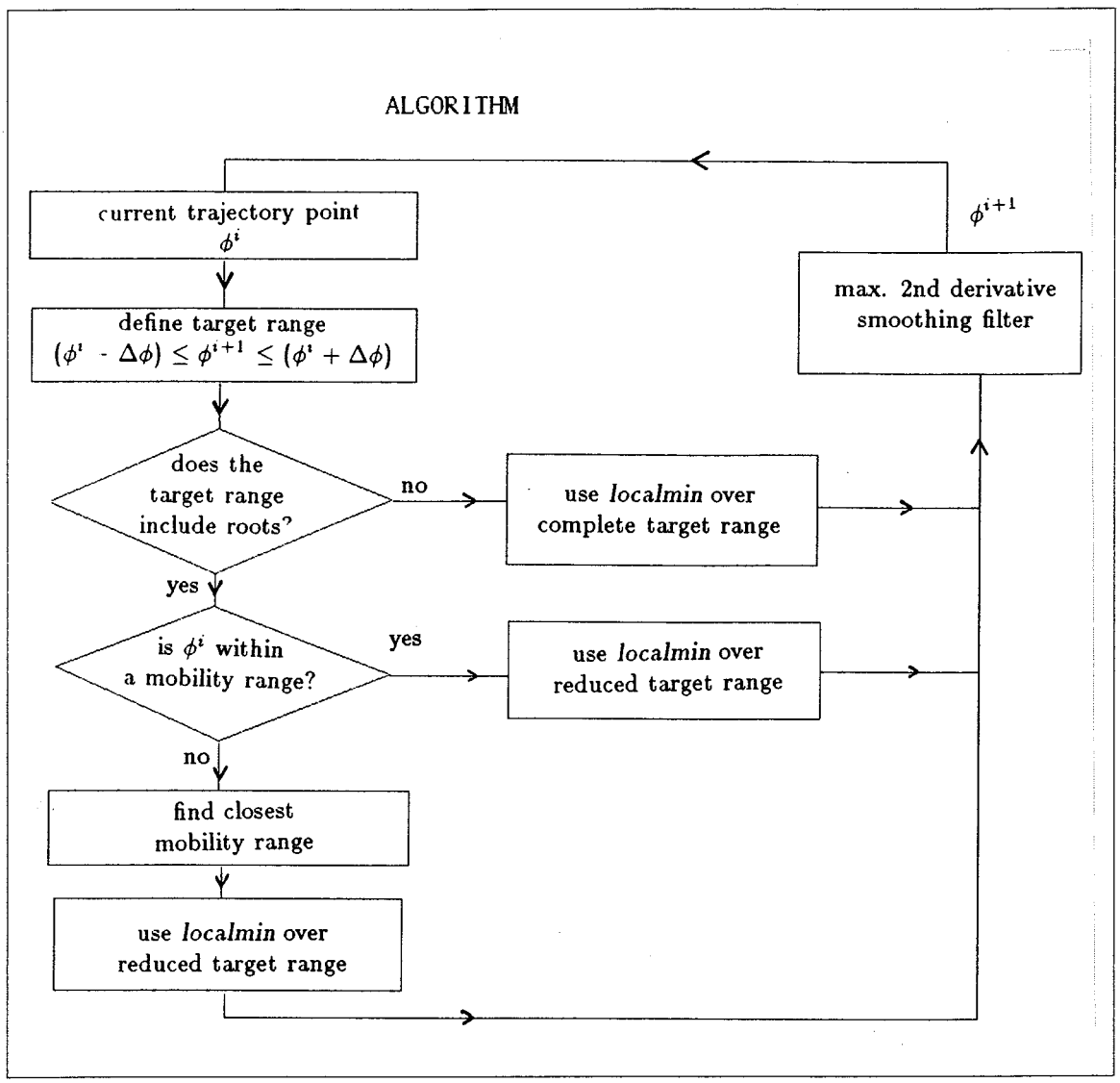

Figure 6.4 Algorithm for the on-line planning of smooth trajectories for redundant parallel manipulators.

a certain neighbourhood of the current value of the free variable. This neighbourhood, or target range, is defined as:

$$(\phi^i - \Delta\phi) \leq \phi^{i+1} \leq (\phi^i + \Delta\phi) \tag{6.32}$$

where $\Delta\phi$ is specified for a given trajectory or manipulator. The occurrence of roots, i.e., of boundaries of the accessible region, within the target range is also verified. Should roots be present, the procedure would still garantee that the solution remains in a continuous feasibility region. This is accomplished by reducing the target range, i.e., by keeping only

the portion of this range lying in the feasible region which is contiguous to the current trajectory point. The direct-search procedure (localmin) described in the first part of this section is then used. Finally, one last stage is added to the procedure in order to smooth the jumps that could occur within the feasible region, as described in Section 6.2.1. This procedure consists of imposing a maximum value of the second derivative of the free variable with respect to a normalized time, i.e., with respect to the progression along the trajectory. The second derivative is approximated using central finite differences. We have

$$\frac{\mathrm{d}^2 X^i}{\mathrm{d}t^2} \simeq X^{i+1} - 2X^i + X^{i-1} \tag{6.33}$$

At step $i+1$ of the trajectory, this quantity is computed. If its magnitude is greater than the prescribed tolerance, we then use:

$$X^{i+1} = \mathrm{sgn}\left(\frac{\mathrm{d}^2 X^i}{\mathrm{d}t^2}\right) X''_{\mathrm{max}} + 2X^i - X^{i-1} \tag{6.34}$$

where X''_{max} denotes the prescribed maximum value of the second derivative. This completes this algorithm.

6.3 Examples

Two examples of the application of the method proposed above are discussed here.

planar manipulator	$l_1 = 2.01$	$l_2 = 2.52$	$l_3 = 1.24$
spherical manipulator	$\alpha_1 = 60°$	$\alpha_2 = 60°$	

Table 6.1 Link lengths and angles used in the examples.

The first example deals with the planar parallel manipulator. The problem here consists of guiding the gripper along the contour of a cam that is to be cut with a mill. The orientation of the gripper is therefore irrelevant to the task since the tool is axiallly

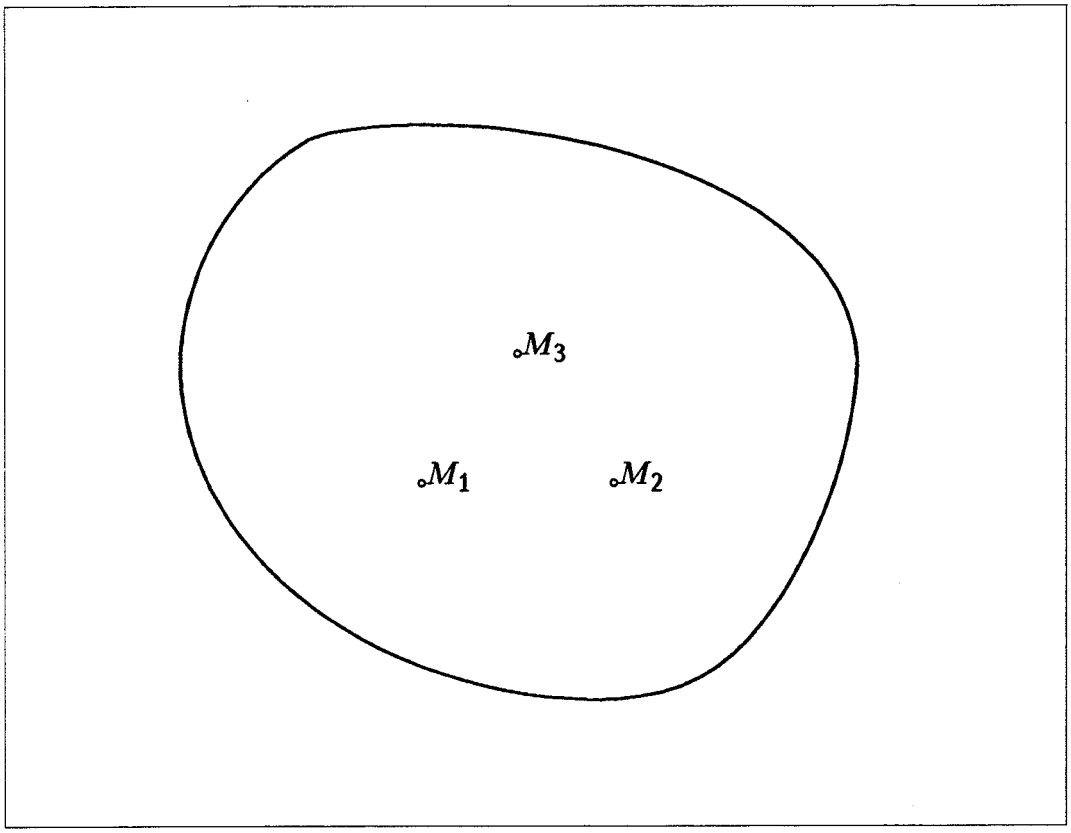

Figure 6.5 Cam contour used as a trajectory for the planar parallel manipulator (example 1).

symmetric. The cam contour is shown in Fig. 6.5, where the location of the fixed joints of the manipulator is also represented.

The link lengths of the manipulator are given in Table 6.1. The trajectory map and the optimum path were computed and are represented in Fig. 6.2. The neighbourhood of a current point was taken as $\Delta\phi = 0.5$ rad and, for the trajectory shown here, no jump discontinuity was observed, i.e., the filtering based on a maximum value of the second derivative was not used. The reciprocal of the condition number obtained along the optimum trajectory is shown in Fig. 6.6.

The second example presents an application of the method to the spherical manipulator. The trajectory along which the manipulator is to be guided is prescribed as:

$$\mathbf{g} = \begin{bmatrix} \cos\beta\cos\lambda_i \\ \cos\beta\sin\lambda_i \\ \sin\beta \end{bmatrix} \tag{6.35a}$$

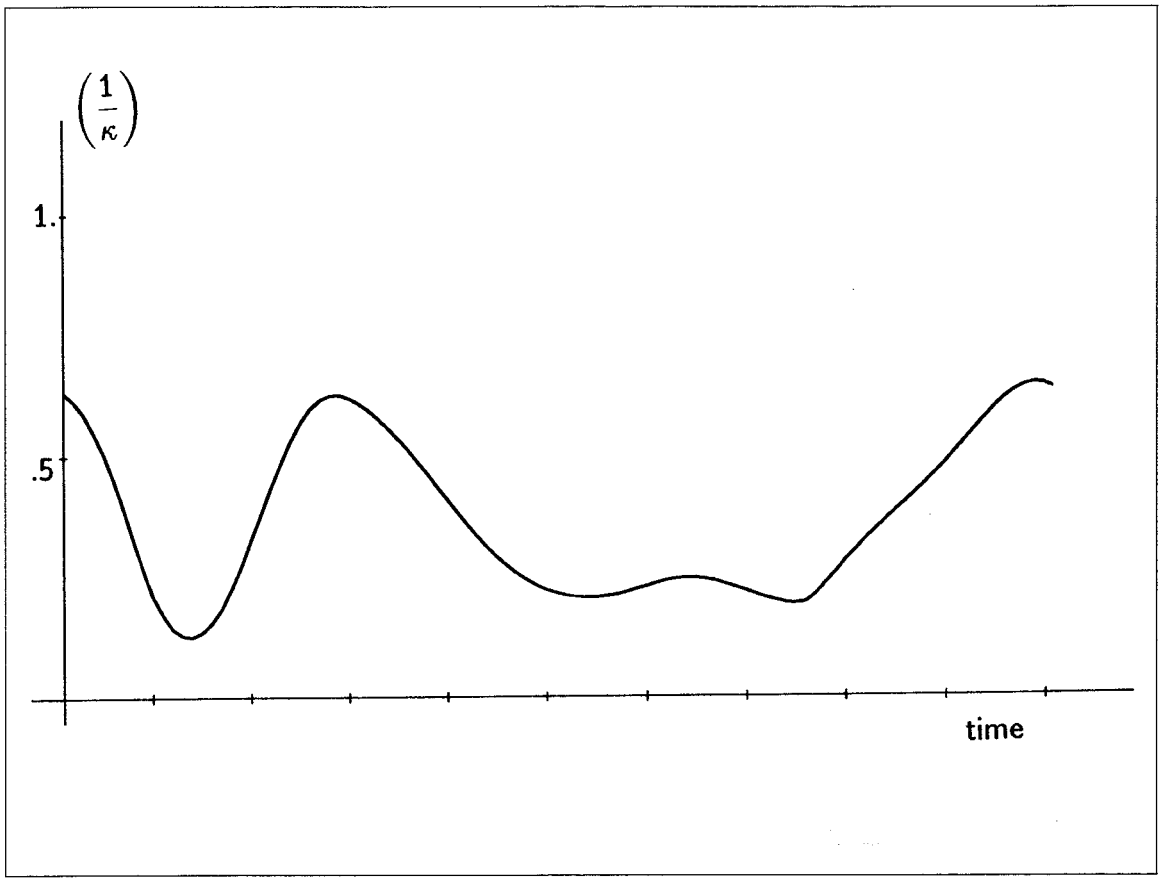

Figure 6.6 Reciprocal of the condition number along the optimum trajectory for the planar manipulator (example 1).

where

$$\beta = \pi/6, \quad \lambda_i = (i-1)\pi/50, \qquad i = 1,101 \tag{6.35b}$$

The link angles of the manipulator are given in Table 6.1. The trajectory map and the optimum path were computed and are represented in Fig. 6.3. The value of $\Delta\psi$ used to define the target range was taken as 0.5 rad. The reciprocal of the condition number along this trajectory is plotted in Fig. 6.7.

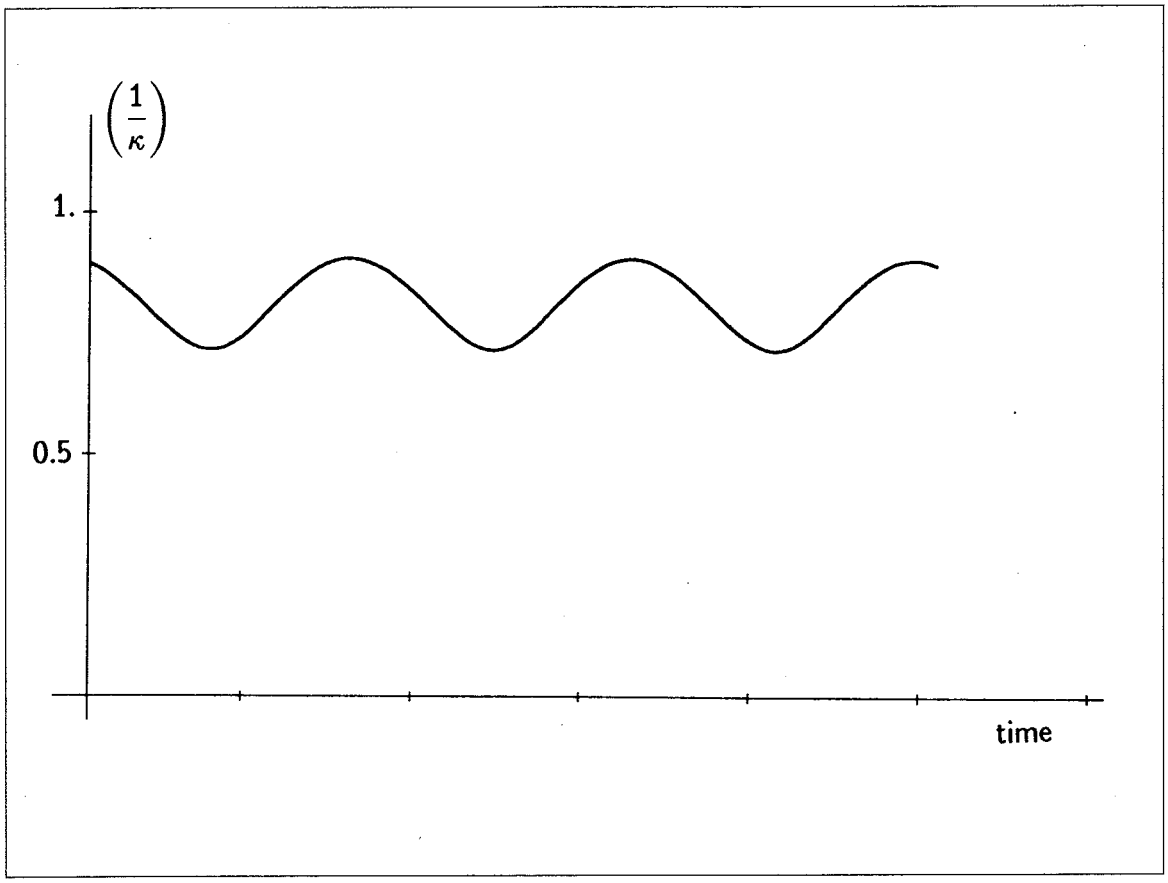

Figure 6.7 Reciprocal of the condition number along the optimum trajectory for the spherical parallel manipulator (example 2).

Chapter 7

CONCLUSIONS AND RECOMMENDATIONS FOR FUTURE RESEARCH

This thesis has presented several results concerning the kinematic analysis, optimization and programming of parallel manipulators.

As a prelude to the study of these manipulators, some properties of simple kinematic chains were revisited, which led to a graphical representation of the mobility regions of planar and spherical four-bar linkages and which allowed the formulation of the transmission quality problem for these linkages as a minimization of the transmission defect. Further investigations could be carried on to apply these concepts to spatial linkages. However, the simple graphical representation obtained here for the mobility regions of planar and spherical linkages would not be possible due to the larger number of kinematic parameters involved. Moreover, the concept of linkage discriminant used here takes on more complicated forms when the input-output equation of a mechanism is of a degree higher than two.

A solution of the branch identification problem for wrist-partitioned manipulators which makes use of the eigenvalues of the Jacobian matrix was given. The Jacobian matrix being the representation of the transformation mapping the joint rates of a serial manipulator into the Cartesian velocities of its end-effector, it is conjectured that the eigenvalues and the determinant of this matrix contains the information necessary to identify the branches, a fact that was verified for a 3×3 positioning Jacobian, leading to the solution

mentioned above. However, in the case of a general six-axis manipulator for which the Jacobian matrix has to be written as a matrix of order six which contains information on the position and orientation, the eigenvalues and the determinant were found to be insufficient for branch identification since different branches led to eigenvalues and determinants of the same nature. A more detailed study could be pursued to find a function of the eigenvalues or of other invariants of the Jacobian matrix that would distinguish between the branches.

Complex kinematic chains were then analyzed and a method to determine their degree of freedom was derived. The fact that this method is based on both the topology and the geometry of the chain makes it very general and applicable to any kinematic chain. A detailed analysis of the singularities encountered in a complex kinematic chain was then performed and led to the classification of all possible singularities into three types. The physical interpretation of each of these singularities was also given. The classification of singularities developed here provides a systematic way of describing the singularities of complex kinematic chains and, hence, of parallel manipulators, which is of primary importance in both analysis and design of robots.

The kinematic analysis of five types of parallel manipulators was conducted. The direct and inverse kinematic problems were discussed together with the velocity and acceleration inversions and a singularity analysis based on the classification mentioned above. For most of the manipulators discussed, a simple closed-form solution of the inverse kinematic problem can be found. However, it was pointed out that a six-degree-of-freedom parallel manipulator with fully general architecture would not exhibit such a solution. It was also shown that the direct kinematic problem does not lead to closed-form solutions even for the simplest cases of parallel manipulators. Numerical methods have to be used and methods of reducing the order of the systems of equations to be solved were discussed.

The optimization of the design of parallel manipulators presented was based on two main performance criteria, i.e., the workspace and the dexterity. Workspace representations were obtained for four types of parallel manipulators and optimum designs were derived. The dexterity criterion led to the definition of a new performance index for the

optimization of manipulators which was shown to be applicable to both serial and parallel manipulators. This index is based on the condition number of the matrix representing the mapping between the Cartesian velocities and the joint rates—which is also an indication of the force transmission quality—over the whole workspace of the manipulator, as opposed to existing indices which are based on the properties of the manipulator at some particular points of the workspace. The new index seems to be more appropriate to the design of manipulators since the tasks to be performed by a robot are unknown *a priori*. The optimization of the workspace of a fully general six-degree-of-freedom parallel manipulator—which has to be described in a six-dimensional space—and the study of its singularities and dexterity presents a formidable challenge. This is a subject for future research. However, it was pointed out in Chapter 4 that this problem can be approached as a set of serial manipulator analyses.

The programming of redundant parallel manipulators was discussed and an algorithm for the trajectory planning of these robots was given. The cases on which the algorithm was tested involved manipulators with a degree of redundancy of unity. The scheme developed here could be extended to manipulators for which the degree of redundancy with respect to a certain task is greater than one, in which case the local dexterity maximization would have to be performed over a set of variables. This is an avenue to be explored in the future.

Finally, it is pointed out that the analyses and optimizations presented in this thesis involved only the kinematics of parallel manipulators and that the dynamics of these manipulators still remains a subject which brings about several unsolved problems.

References

Anderson, K., and Angeles, J., 1987, 'Kinematic inversion of manipulators in the presence of redundancies', *Technical Report*, Dept. of Mech. Engng. and McGill Research Centre for Intelligent Machines, McGill University, Montréal.

Angeles, J., 1982, *Spatial kinematic chains*, Springer–Verlag, Berlin.

Angeles, J., 1985, 'On the numerical solution to the inverse kinematic problem', *The International Journal of Robotics Research*, Vol. 4, No. 2, pp. 21–37.

Angeles, J., 1986a, 'Optimierung ebener, sphärischer und räumlicher Getriebe zur approximierten Lagenzuordnung', *Mechanism and Machine Theory*, Vol. 21, pp. 187–197.

Angeles, J., 1986b, 'Automatic computation of the screw parameters of rigid-body motions. Part-I: Finitely-Separated positions', *ASME Journal of Dynamic Systems, Measurement, and Control*, Vol. 108, No. 1, pp. 32–38.

Angeles, J., 1987, 'Détermination du degré de liberté des chaînes cinématiques', *Proceedings of the 7th World Congress on Theory of Machines and Mechanisms*, Seville, September, pp. 199–202.

Angeles, J., Anderson, K., and Gosselin, C., 1987, 'An orthogonal-decomposition algorithm for constrained least-square optimization', proceedings of the 13th *ASME Design Automation Conference*, Boston Ma., Sept., pp. 215–220.

Angeles, J., and Bernier, A., 1987a, 'A general method of four-bar linkage mobility analysis', *ASME Journal of Mechanisms, Transmissions, and Automation in Design*, Vol. 109, No. 2, pp. 197–203.

Angeles, J., and Bernier, A., 1987b, 'The global least-square optimization of function-generating linkages', *ASME Journal of Mechanisms, Transmissions, and Automation in Design*, Vol. 109, No. 2, pp. 204–209.

Angeles, J., and Callejas, M., 1984, 'An algebraic formulation of Grashof's mobility criteria with application to linkage optimization using gradient-dependent methods', *ASME Journal of Mechanisms, Transmissions, and Automation in Design*, Vol. 106, No. 3, pp. 327–332.

Angeles, J., and López-Cajún, C.S., 1987, 'The dexterity index of serial-type robotic manipulators', Technical Report, Dept. of Mech. Eng., RMSL, McGill Research Centre for Intelligent Machines, McGill University, Montréal.

Angeles, J. and Rojas, A.A., 1987 'Manipulator inverse kinematics via condition number minimization and continuation', *The International Journal of Robotics and Automation*, Vol. 2, No. 2, pp. 61–69.

Asada, H., and Cro Granito, J.A., 1985, 'Kinematic and static charecterization of wrist joints and their optimal design', *Proc. IEEE Conf. on Robotics and Automation*, St-Louis, pp. 244–250.

Asada, H., and Kanade, T., 1982, 'Design of direct-drive mechanical arms', *ASME Journal of Mechanical Design*, Vol. 104, No. 3.

Asada, H., Kanade, T., and Takeyama, I., 1982, 'Control of a direct-drive arm', Proceedings of the *Winter Annual Meeting of the ASME*, Phoenix, Arizona, pp. 63–72.

Asada, H., and Youcef-Toumi, K., 1984, 'Analysis and design of a direct-drive arm with a five-bar-link parallel drive mechanism', *ASME Journal of Dynamic Systems, Measurements, and control*, Vol. 106, No. 3, pp. 225–230.

Asada, H., and Youcef-Toumi, K., 1987, *Direct-drive robots: theory and practice*, MIT Press, Cambridge, Mass.

Baillieul, J., 1985, 'Kinematic programming alternatives for redundant manipulators', *Proc. IEEE Conf. on Robotics and Automation*, St-Louis, March, pp. 722–728.

Baillieul, J., 1986, 'Avoiding obstacles and resolving kinematic redundancy', *Proc. IEEE Conf. on Robotics and Automation*, San Francisco, April, pp. 1698–1704.

Bajpai, A., and Roth, B., 1986, 'Workspace and mobility of a closed-loop manipulator', *The International Journal of Robotics Research*, Vol. 5, No. 2, pp. 131–142.

Barker, C.R., and Lo, J., 1986, 'Classification of spherical four-bar mechanisms', *ASME* paper 86-DET-144.

Bennett, G. T., 1903, 'A new mechanism', *Engineering*, Vol. 76, pp. 777–778.

Box, M.J., 1965, 'A new method of constrained optimization and a comparision with other methods', *Computer Journal*, Vol. 8, pp. 42–52.

Brand, L., 1955, *'Advanced Calculus'*, John Wiley & sons Inc., New-York, pp. 355–361.

Brent, R.P., 1973, *Algorithms for minimization without derivatives*, Englewood Cliffs, N.J., Prentice-Hall.

Chevallereau, C., and Khalil, W., 1987, 'Efficient method for the calculation of the pseudo inverse kinematic problem', *Proc. IEEE Conf. on Robotics and Automation*, Raleigh, March, pp. 1842–1848.

Cleghorn, W.L., and Fenton, R.G., 1984, 'Optimum synthesis of an angular function generating mechanism with prescribed time ratio and rocker angular swing amplitude', *Mechanism and Machine Theory*, Vol. 19, pp. 319–324.

Cwiakala, M., and Lee, T.W., 1985, 'Generation and evaluation of a manipulator workspace based on optimum path search', *ASME Journal of Mechanisms, Transmissions, and Automation in Design*, Vol. 107, No. 2, pp. 245–255.

Davies, T.H., 1981, 'Kirchoff's circulation law applied to multi-loop kinematic chains' , *Mechanism and Machine Theory*, Vol. 16, No. 3, pp. 171–183.

Dieudonne, J.E., Parrish, R.V., and Bardusch, R.E., 1972, 'An actuator extension transformation for a motion simulator and an inverse transformation applying Newton-Raphson's method', NASA Technical Report TN D-7067.

Duditza, F., and Dittrich, G., 1969, 'Die Bedingungen für die Umlauffähigkeit sphärischer viergliedriger Kurbelgetriebe', *Industrie–Anzeiger*, Vol. 91, pp. 1687–1690.

Earl, C.F. and Rooney, J., 1983, 'Some kinematic structures for robot manipulator designs', *ASME Journal of Mechanisms, Transmissions and Automation in Design*, Vol. 105, No. 1, pp. 15–22.

Eddie Baker, J., 1980a, 'Screw system algebra applied to special linkage configurations', *Mechanism and Machine Theory*, Vol. 15, No. 4, pp. 255–265.

Eddie Baker, J., 1980b, 'On the relative freedom between links in kinematic chains with cross-jointing', *Mechanism and Machine Theory*, Vol. 15, No. 5, pp. 397–413.

Eddie Baker, J., 1981, 'On mobility and relative freedoms in multiloop linkages and structures', *Mechanism and Machine Theory*, Vol. 16, No. 6, pp. 583–597.

Fichter, E.F., 1986, 'A Stewart platform-based manipulator: general theory and practical construction', *The International Journal of Robotics Research*, Vol. 5, No. 2, pp. 157–182.

Forsythe, G.E., Malcom, M.A., and Moler, C.B., 1977, *Computer Methods for Mathematical Computations*, Prentice-Hall, Englewood Cliffs, N.J..

Freudenstein, F., 1954, 'Design of four-link mechanisms', Ph.D. dissertation at Columbia University, publication No. 8252 of Univerity Microfilms Inc., Ann Arbor, Michigan.

Freudenstein, F., 1955, 'Approximate synthesis of four-bar linkages', *Trans. ASME*, Vol. 77, pp. 853–861.

Freudenstein, F., 1962, 'On the variety of motions generated by mechanisms', *Trans. ASME Journal of Engineering for Industry*, Vol. 84, pp. 156–160.

Freudenstein, F., 1965, 'On the determination of the type of spherical four link mechanisms', *Contemporary Problems in the Theory of Machines and Mechanisms*, pp.193–196, USSR Academy of Sciences.

Freudenstein, F., and Primrose, E.J.F., 1973, 'The classical transmission angle problem', Proceedings of the Conference on Mechanisms, *Institution of Mechanical Engineers*, London, pp. 105–110.

Goldberg, M., 1943, 'New five-bar and six-bar linkages in three dimensions', *Trans. ASME*, Vol. 65, pp. 649–661.

Golub, G. H., and Van Loan, C., 1983, *Matrix Computations*, The Johns Hopkins University Press, Baltimore.

Gosselin, C., and Angeles, J., 1987a, 'Représentation graphique de la région de mobilité des mécanismes plans et sphériques à barres articulées', *Mechanism and Machine Theory*, Vol. 22, No. 6, pp. 557–562.

Gosselin, C., and Angeles, J., 1987b, 'The optimum kinematic design of a spherical three-degree-of-freedom parallel manipulator', proceedings of the 13th *ASME Design Automation Conference*, Boston Ma., Sept., pp. 111–115.

Gosselin, C., and Angeles, J., 1987c, 'Application des techniques de moindres carrés contraints à des problèmes de robotique', *Journées de l'optimisation*, Montréal 13–15 mai 1987.

Gosselin, C., and Angeles, J., 1987d, 'Optimization of planar and spherical function generators as minimum-defect linkages', submitted for publication to *Mechanism and Machine Theory*.

Gosselin, C., and Angeles, J., 1988a, 'The optimum kinematic design of a planar three-degree-of-freedom parallel manipulator', *ASME Journal of Mechanisms, Transmissions, and Automation in Design*, Vol. 110, No. 1, pp. 35–41.

Gosselin, C., and Angeles, J., 1988b, 'Mobility analysis of planar and spherical linkages at a glance', to appear in *ASME Computers in Mechanical Engineering*.

Gosselin, C., and Angeles, J., 1988c, 'A new performance index for the kinematic optimization of robotic manipulators', accepted for presentation at the *ASME 20th biennial mechanisms conference*, sept. 25–28 1988, Kissimmee Florida.

Gosselin, C., and Angeles, J., 1988d, 'Kinematic inversion of parallel redundant manipulators', accepted for presentation at the *ASME 20th biennial mechanisms conference*, sept. 25–28 1988, Kissimmee Florida.

Grashof, F., 1883, *Theorethische Maschinenlehre*, Berlin.

Gupta, K.C., 1977, 'A note on the optimum design of four bar crank-rocker mechanisms', *Mechanism and Machine Theory*, Vol. 12, pp. 247–254.

Gupta, K.C., 1980, 'Synthesis of position, path and function generating 4-bar mechanisms with completely rotatable driving links', *Mechanism and Machine Theory*, Vol. 15, pp. 93–101.

Gupta, K.C., 1986a, 'On the nature of robot workspace', *The International Journal of Robotics Research*, Vol. 5, No. 2, pp. 112–121.

Gupta, K.C., 1986b, 'Rotatability considerations for spherical four bar linkages with applications to robot wrist design', *ASME Journal of Mechanisms, Transmissions, and Automation in Design*, Vol. 108, No. 3, pp. 387–391.

Gupta, K.C., and Kazerounian, S.M.K., 1983, 'Synthesis of fully rotatable R-S-S-R linkages', *Mechanism and Machine Theory*, Vol. 18, pp. 199–205.

Gupta, K.C., and Kazerounian, K., 1985, 'Improved numerical solutions of inverse kinematics of robots', *Proc. IEEE Conf. on Robotics and Automation*, St-Louis.

Gupta, V.K., and Radcliffe, C.W., 1971, 'Mobility analysis of plane and spatial mechanisms', *Trans. ASME Journal of Engineering for Industry*, Vol. 93, pp. 125–130.

Gupta, K.C., and Roth, B., 1982, 'Design considerations for manipulator workspace', *ASME Journal of Mechanical Design*, Vol. 104, No. 3, pp. 704–711.

Hain, K., 1967, *Applied Kinematics*, McGraw-Hill.

Hall, A.S., 1966, *Kinematics and Linkage Design*, Balt Publishers, West Lafayette, Indiana.

Harary, F., 1969, *Graph Theory*, Addison-Wesley Publishing Company Inc.

Hartenberg, R.S., and Denavit, J., 1964, *Kinematic Synthesis of Linkages*, McGraw-Hill Book Co., New-york.

Hervé, J.M., 1978, 'Analyse structurelle des mécanismes par groupe des déplacements', *Mechanism and Machine Theory*, Vol. 13, No. 4, pp. 437–450.

Hunt, K.H., 1978, *Kinematic Geometry of Mechanisms*, Clarendon Press, Oxford.

Hunt, K.H., 1983, 'Structural kinematics of in-parallel-actuated robot arms', *ASME Journal of Mechanisms, Transmissions, and Automation in Design*, Vol. 105, No. 4, pp. 705–712.

Hunt, K.H., 1986, 'Special configurations of robot-arms via screw theory- Part I: The Jacobian and its matrix cofactors', *Robotica*, Vol. 4, pp. 171–179.

Hunt, K.H., 1987, 'Special configurations of robot-arms via screw theory- Part II: Available end-effector displacements', *Robotica*, Vol. 5, pp. 17–22.

Inoue, H., Tsusaka, Y., and Fukuizumi, T., 1985, 'Parallel manipulator', 3rd Int. Symposium on Robotics Research, Gouvieux, France.

Klein, C.A., and Blaho, B.E., 1987, 'Dexterity measures for the design and control of kinematically redundant manipulators', *The International Journal of Robotics Research*, Vol. 6, No. 2, pp. 72–83.

Klein, C.A., and Huang, C.H., 1983, 'Review of pseudoinverse control for use with kinematically redundant manipulators', *IEEE Trans. Sys., Man, Cyber.* SMC-13, pp. 245–250.

Kleinfinger, J.F., and Khalil, W., 1986, 'Dynamic modeling of robots with closed kinematic chains', Technical Report, Laboratoire d'Automatique (LAN), Ecole Nationale Supérieure de Mécanique, Nantes, France.

Kohli, D., and Spanos, J., 1985, 'Workspace analysis of mechanical manipulators using polynomial discriminants', *ASME Journal of Mechanisms, Transmissions, and Automation in Design*, Vol. 107, No. 2, pp. 209–215.

Kumar, A., and Patel, M.S., 1986, 'Mapping the manipulator workspace using interactive computer graphics', *The International Journal of Robotics Research*, Vol. 5, No. 2, pp. 122–130.

Lai, Z.C., and Yang, D.C.H., 1986, 'A new method for the singularity analysis of simple six link manipulators', *The International Journal of Robotics Research*, Vol. 5, No. 2, pp. 66–74.

Lee, H.-Y., and Liang, C.-G., 1988, 'Displacement analysis of the general spatial 7-link 7R mechanism', *Mechanism and Machine Theory*, Vol. 23, No. 3, pp. 219–226.

Lee, K.-M., and Shah, D.K., 1987, 'Kinematic analysis of a three degree of freedom in-parallel actuated manipulator', *Proc. IEEE Conf. on Robotics and Automation*, Raleigh, pp. 345–350.

Liégeois, J., 1977, 'Automatic supervisory control of the configuration and behavior of multi-body mechanisms', *IEEE Trans. Sys., Man., Cyber.* SMC-7, pp. 868–871.

Lin, C.C.-D., and Freudenstein, F., 1986, 'Optimization of the workspace of a three-link turning-pair connected robot arm', *The International Journal of Robotics Research*, Vol. 5, No. 2, pp. 104–111.

Litvin, F.L., and Parenti Castelli, V., 1985, 'Configurations of robot manipulators and their identification, and the execution of prescribed trajectories Part-I: Basic concepts', *ASME*

Journal of Mechanisms, Transmissions, and Automation in Design, Vol. 107, No. 2, pp. 170–178.

Litvin, F.L., Costopoulos, T., Parenti Castelli, V., Shaheen, M., and Yukishige, Y., 1985, 'Configurations of robot manipulators and their identification, and the execution of prescribed trajectories Part-II: Investigation of manipulators having five, seven and eight degrees of freedom', *ASME Journal of Mechanisms, Transmissions, and Automation in Design*, Vol. 107, No. 2, pp. 179–188.

Litvin, F.L., Yi, Z., Parenti Castelli, V., and Innocenti, C., 1986, 'Singularities, configurations, and displacement functions for manipulators', *The International Journal of Robotics Research*, Vol. 5, No. 2, pp. 52–65.

Litvin, F.L., Tan, J., Fanghella, P., and Wu, S., 1987, 'Singularities in motion and displacement functions for the RCRCR, RCRRC and RSRC linkages part-I: Basic concepts', Proceedings of the *13th ASME Design Automation Conference*, Boston, pp. 267–278.

Litvin, F.L., and Tan, J., 1987, 'Singularities in motion and displacement functions for the RCRCR, RCRRC and RSRC linkages part-II: The RCRCR linkage', Proceedings of the *13th ASME Design Automation Conference*, Boston, pp. 279–284.

Litvin, F.L., and Fanghella, P., 1987, 'Singularities in motion and displacement functions for the RCRCR, RCRRC and RSRC linkages part-III: The RCRRC linkage', Proceedings of the *13th ASME Design Automation Conference*, Boston, pp. 285–290.

Litvin, F.L., and Wu, S., 1987, 'Singularities in motion and displacement functions for the RCRCR, RCRRC and RSRC linkages part-IV: The RSRC linkage', Proceedings of the *13th ASME Design Automation Conference*, Boston, pp. 291–298.

Ma, O., and Angeles, J., 1987, 'Positioning-error analysis of planar, spherical, and spatial four-bar linkages', Technical Report, McRCIM, McGill University, Montréal, Qué., Canada.

MacCallion, H., and Pham, D.T., 1979, 'The analysis of a six degree of freedom work station for mechanised assembly', Proceedings of the *5th World Congress on Theory of Machines and Mechanisms*, Montréal.

Mayorga, R.V., and Wong, A.K.C., 1987, 'A singularities avoidance method for the trajectory planning of redundant and nonredundant robot manipulators', *Proc. IEEE Conf. on Robotics and Automation*, Raleigh, March, pp. 1707–1712.

Merlet, J.P., 1987, 'Parallel manipulators, Part I: Theory, design, kinematics, dynamics and control', Technical Report # 646 INRIA, France.

Merlet, J.P., 1988, 'Parallel manipulators, Part II: Theory, singular configurations and Grassman geometry', Technical Report # 791 INRIA, France.

Midha, A., Zhao, Z.-L., and Her, I., 1985, 'Mobility conditions for planar linkages using triangle inequality and graphical interpretation', *ASME Journal of Mechanisms, Transmissions, and Automation in Design*, Vol. 107, No. 3, pp. 394–400.

Mohamed, M.G., 1987, 'Structural kinematics of partially-parallel robotic mechanisms', proceedings of the 13th *ASME Design Automation Conference*, Boston Ma., Sept., pp. 31–35.

Mohamed, M.G., and Duffy, J., 1985, 'A direct determination of the instantaneous kinematics of fully parallel robot manipulators', *ASME Journal of Mechanisms, Transmissions, and Automation in Design*, Vol. 107, No. 2, pp. 226–229.

Nakamura, Y., Hanafusa, H., and Yoshikawa, T., 1987, 'Task-Priority based redundancy control of robot manipulators', *The International Journal of Robotics Research*, Vol. 6, No. 2, pp. 3–15.

Primrose, E.J.F., 1986, 'On the input-output equation of the general 7R mechanism', *Mechanism and Machine Theory*, Vol. 21, No. 6, pp. 509–510.

Rastegar, J., and Deravi, P., 1987, 'Methods to determine the workspace, its subspaces with different numbers of configurations and all the possible configurations of a manipulator', *Mechanism and Machine Theory*, Vol. 22, No. 4, pp. 343–350.

Reboulet, C., 1988, 'Modélisation des robots parallèles', Chapter 8 of the book: 'Techniques de la robotique', Hermès, Paris.

Renaud, M., 1980, 'Calcul de la matrice jacobienne nécessaire à la commande coordonnée d'un manipulateur', *Mechanism and Machine Theory*, Vol. 15, pp. 81–91.

Risbourg, A., 1983, 'Représentation spatiale tétraédrique de l'ensemble des mécanismes à quatre barres', *Mechanism and Machine Theory*, Vol. 18, pp. 501–511.

Russell, R., 1988, 'Kinematic optimization of lower-pair clutch mechanisms', M. Eng. thesis, Dept. of Mech. Eng., McGill University, Montréal, Qué., Canada.

Salisbury, J.K., and Craig, J.J., 1982, 'Articulated hands: force control and kinematic issues', *The International Journal of Robotics Research*, Vol. 1, No. 1, pp. 4–17.

Sandor, G.S., Kohli, D., Reinholtz, C.F., and Ghosal, A., 1984, 'Closed-form analytic synthesis of a five-link spatial motion generator', *Mechanism and Machine Theory*, Vol. 19, No. 1, pp. 97–105.

Sandor, G.S., Kohli, D., and Zhuang, X., 1985, 'Synthesis of RSSR-SRR spatial motion generator mechanism with prescribed crank rotations for three and four finite positions', *Mechanism and Machine Theory*, Vol. 20, No. 6, pp. 503–519.

Sandor, G.N., Xu, Y., and Weng, T.C., 1986a, 'Synthesis of 7-R spatial motion generators with prescribed crank rotations and elimination of branching', *The International Journal of Robotics Research*, Vol. 5, No. 2, pp. 143–156.

Sandor, G.N., Xu, L.J., and Yang, S.P., 1986b, 'Computer-aided synthesis of two-closed-loop RSSR-SS spatial motion generator with branching and sequence constraints', *Mechanism and Machine Theory*, Vol. 21, No. 4, pp. 345–350.

Savage, M. and Hall, A.S., 1970, 'Unique descriptions of all spherical four bar linkages', *Trans. ASME Journal of Engineering for Industry*, Vol. 92, pp. 559–563.

Selby, S.M., 1971, *CRC Standard Mathematical Tables*, 19th edition, The Chemical Rubber Co., Ohio.

Sheth, P.N., and Uicker, J.J.Jr., 1972, 'IMP (Integrated Mechanisms Program), A computer-aided design analysis system for mechanisms and linkages', *ASME Journal of Engineering for Industry*, pp. 454–464.

Shirkhodaie, A.H., and Soni, A.H., 1987, 'Forward and inverse synthesis for a robot with three degrees of freedom', Proceedings of the *1987 Summer Computer Simulation Conference*, Montréal, pp. 851–856.

Soni, A.H., 1974, *Mechanism Synthesis and Analysis*, McGraw-Hill, New-York.

Soni, A.H., and Harrisberger, L., 1967, 'The design of the spherical drag link mechanism', *Trans. ASME Journal of Engineering for Industry*, Vol. 89, pp. 177–181.

Söylemez, E., and Freudenstein, F., 1982, 'Transmission optimization of spatial 4-link mechanisms', *Mechanism and Machine Theory*, Vol. 17, pp. 263–283.

Stanišić, M., and Pennock, G., 1985, 'A nondegenerate kinematic solution of a seven jointed robot manipulator', *The International Journal of Robotics Research*, Vol. 4, No. 2, pp. 10–20.

Stewart, D., 1965, 'A platform with six degrees of freedom', *Proceedings of the Institution of Mechanical Engineers*, Vol. 180, No. 5, pp. 371–378.

Stoughton, R., and Kokkinis, T., 1987, 'Some properties of a new kinematic structure for robot manipulators', Proceedings of the 13th *ASME Design Automation Conference*, Boston Ma., Sept., pp. 73–79.

Strang, G., 1980, *Linear Algebra and its Applications*, 2nd Editon, Academic press, New-York.

Sugimoto, K., 1987, 'Kinematic and dynamic analysis of parallel manipulators by means of motor algebra', *ASME Journal of Mechanisms, Transmissions, and Automation in Design*, Vol. 109, No. 1, pp. 3–7.

Sugimoto, K., and Duffy, J., 1982, 'Application of linear algebra to screw systems', *Mechanism and Machine Theory*, Vol. 17, No. 1, pp. 73–83.

Sugimoto, K., Duffy, J., and Hunt, K.H., 1982, 'Special configurations of spatial mechanisms and robot arms', *Mechanism and Machine Theory*, Vol. 17, No. 2, pp. 119–132.

Suh, K.C., and Hollerbach, J.M., 1987, 'Local versus global torque optimization of redundant manipulators', *Proc. IEEE Conf. on Robotics and Automation*, Raleigh, March, pp. 619–624.

Sutherland, G., and Roth, B., 1973, 'A transmission index for spatial mechanisms', *ASME Journal of Engineering for Industry*, Vol. 95, No. 2, pp. 589–597.

Takano, M., 1985, 'A new effective solution for inverse kinematics problem (synthesis) of a robot with any type of configuration', *Journal of the Faculty of Engineering*, University of Tokyo (B), Vol. 38, No. 2, pp. 107–135.

Tinubu, S.O., and Gupta, K.C., 1984, 'Optimal synthesis of function generators without the branch defect', *ASME Journal of Mechanisms, Transmissions, and Automation in Design*, Vol. 106, pp. 348–354.

Tsai, L.W., and Morgan, A.P., 1985, 'Solving the kinematics of the most general six- and five-degree-of-freedom manipulators by continuation methods', *ASME Journal of Mechanisms, Transmissions, and Automation in Design*, Vol. 107, pp. 189–200.

Vijaykumar, R., Waldron, K.J., and Tsai, M.J., 1986, 'Geometric optimization of serial chain manipulator structures for working volume and dexterity', *The International Journal of Robotics Research*, Vol. 5, No. 2, pp. 91–103.

Waldron, K.J., Raghavan, M., and Roth, B., 1988a, 'Kinematics of a hybrid series-parallel manipulation system part I- Position Kinematics', Ohio-State University Technical Report.

Waldron, K.J., Raghavan, M., and Roth, B., 1988b, 'Kinematics of a hybrid series-parallel manipulation system part II- Rate and force decomposition', Ohio-State University Technical Report.

Waldron, K.J., Wang, S.L., and Bolin, S.J., 1985, 'A study of the Jacobian matrix of serial manipulators', *ASME Journal of Mechanisms, Transmissions, and Automation in Design*,

Vol. 107, No. 2, pp. 230–237.

Wampler, C.W. II, 1987, 'Inverse kinematic functions for redundant manipulators', *Proc. IEEE Conf. on Robotics and Automation*, Raleigh, March, pp. 610–617.

Wang, T.B., Dahan, M., and Gong, Z.Y., 1987, 'Nouvelle architecture pour manipulateur spatial', Proceedings of the 11th *Canadian Congress of Applied Mechanics*, Univ. of Alberta, Edmonton.

Wang, S.-L., and Waldron, K.J., 1987, 'A study of the singular configurations of serial manipulators', *ASME Journal of Mechanisms, Transmissions, and Automation in Design*, Vol. 109, No. 1, pp. 14–20.

Wilde, D.J., 1982, 'Error linearization in the least-squares design of function generating mechanisms', *Trans. ASME Journal of Mechanical Design*, Vol. 104, pp. 881–884.

Wilde, D.J., 1983, 'Degeneracy, singularity, and multiplicity in least-squares design of a function-generating mechanism', *ASME Journal of Mechanisms, Transmissions, and Automation in Design*, Vol. 105, pp. 104–107.

Williams, R.L.II, and Reinholtz, C.F., 1986, 'Proof of Grashof's law using polynomial discriminants', *ASME Journal of Mechanisms, Transmissions, and Automation in Design*, Vol. 108, No. 4, pp. 562–564.

Williams, R.L.II, and Reinholtz, C.F., 1987, 'Mechanism link rotatability and limit position analysis using polynomial discriminants', *ASME Journal of Mechanisms, Transmissions, and Automation in Design*, Vol. 109, No. 2, pp. 178–182.

Wonham, V.M., 1979, *Linear multivariable control: a geometric approach*, Springer–Verlag, New-York–Heidelberg–Berlin.

Yang, D.C.H., and Lai, Z.C., 1985, 'On the dexterity of robotic manipulators–service angle', *ASME Journal of Mechanisms, Transmissions, and Automation in Design*, Vol. 107, No. 2, pp. 262–270.

Yang, D.C.H., and Lee, T.W., 1984, 'Feasibility study of a platform type of robotic manipulators from a kinematic viewpoint', *ASME Journal of Mechanisms, Transmissions, and Automation in Design*, Vol. 106, No. 2, pp. 191–198.

Yoshikawa, T., 1985, 'Manipulability of robotic mechanisms', *The International Journal of Robotics Research*, Vol. 4, No. 2, pp. 3–9.

Appendix A. Solution of a Quartic Equation

The solution of the inverse kinematic problem of the spatial three-degree-of-freedom parallel manipulator given in Chapter 4 is derived through the solution of a quartic equation. A method of solution of such an equation in closed-form is given here which was taken from (Selby 1971).

Let a general quartic equation be given by

$$x^4 + ax^3 + bx^2 + cx + d = 0 \tag{A.1}$$

This equation has a *resolvent cubic equation*, which can be written as

$$y^3 - by^2 + (ac - 4d)y - a^2d + 4bd - c^2 = 0 \tag{A.2}$$

Now, let y be any root of this equation, and let

$$R = \sqrt{\frac{a^2}{4} - b + y} \tag{A.3}$$

Then, if $R \neq 0$, let

$$D = \sqrt{\frac{3a^2}{4} - R^2 - 2b + \frac{4ab - 8c - a^3}{4R}} \tag{A.4a}$$

$$E = \sqrt{\frac{3a^2}{4} - R^2 - 2b - \frac{4ab - 8c - a^3}{4R}} \tag{A.4b}$$

If $R = 0$, however, we will define

$$D = \sqrt{\frac{3a^2}{4} - 2b + 2\sqrt{y^2 - 4d}} \tag{A.5a}$$

$$E = \sqrt{\frac{3a^2}{4} - 2b - 2\sqrt{y^2 - 4d}} \tag{A.5b}$$

Then, the four roots of the original equation are given by

$$x = -\frac{a}{4} + \frac{R}{2} \pm \frac{D}{2} \tag{A.6a}$$

and

$$x = -\frac{a}{4} - \frac{R}{2} \pm \frac{E}{2} \tag{A.6b}$$

This solution entails the computation of the roots of the resolvent cubic equation. This can be done as follows: Let a general cubic equation be written as

$$y^3 + py^2 + qy + r = 0 \tag{A.7}$$

This equation can be reduced to the form

$$z^3 + uz + v = 0 \tag{A.8}$$

where

$$u = \frac{1}{3}(3q - p^2) \tag{A.9a}$$

$$v = \frac{1}{27}(2p^3 - 9pq + 27r) \tag{A.9b}$$

by using the following substitution:

$$y = z - \frac{p}{3} \tag{A.10}$$

Now, let

$$A = \sqrt[3]{-\frac{v}{2} + \sqrt{\frac{v^2}{4} + \frac{u^3}{27}}} \tag{A.11a}$$

and

$$B = \sqrt[3]{-\frac{v}{2} - \sqrt{\frac{v^2}{4} + \frac{u^3}{27}}} \tag{A.11b}$$

then the values of the roots of eq.(A.8) will be given by

$$z_1 = A + B \tag{A.12a}$$

$$z_2 = -\frac{A+B}{2} + \frac{A-B}{2}\sqrt{-3} \tag{A.12b}$$

$$z_3 = -\frac{A+B}{2} - \frac{A-B}{2}\sqrt{-3} \tag{A.12c}$$

and the values of the roots of the original cubic equation are readily computed using eq.(A.10).

Appendix B. The Linear Invariants of a Rotation Tensor

Given any 3×3 tensor $\mathbf{A}$, whose representation in a given coordinate frame comprises the array of real numbers a_{ij} for $i, j = 1, 2, 3$, its *linear invariants* are defined as its *vector*, represented as vect($\mathbf{A}$) and its *trace*, represented as tr($\mathbf{A}$). Let $\mathbf{a}$ denote vect($\mathbf{A}$), its representation in the given coordinate frame comprising the array of real numbers a_i, for $i = 1, 2, 3$. Resorting to index notation, the aforementioned invariants are defined as

$$a_i \equiv \frac{1}{2}\epsilon_{ijk}a_{kj}, \quad \text{tr}(\mathbf{A}) \equiv a_{ii} \tag{B.1}$$

In displayed form, we have

$$\text{vect}(\mathbf{A}) \equiv \mathbf{a} \equiv \frac{1}{2}\begin{bmatrix} a_{32} - a_{23} \\ a_{13} - a_{31} \\ a_{21} - a_{12} \end{bmatrix}, \quad \text{tr}(\mathbf{A}) \equiv a_{11} + a_{22} + a_{33} \tag{B.2}$$

Moreover, from the foregoing definitions, it is apparent that the vector of a symmetric tensor vanishes, whereas the trace of a skew symmetric tensor vanishes.

Now, if the 3×3 tensor is a *rotation tensor*, denoted by $\mathbf{Q}$, i.e., a *proper orthogonal tensor*, it can be expressed as

$$\mathbf{Q} = \mathbf{e}\mathbf{e}^T + \cos\phi(\mathbf{1} - \mathbf{e}\mathbf{e}^T) + \sin\phi(\mathbf{1} \times \mathbf{e}) \tag{B.3}$$

where $\mathbf{e}$ is the unit vector parallel to the axis of the rotation associated with $\mathbf{Q}$ and ϕ is the angle of that rotation. Since the first two terms of the representation of $\mathbf{Q}$ given in eq.(B.3) are symmetric, we can write the vector of $\mathbf{Q}$ as:

$$\text{vect}(\mathbf{Q}) = \text{vect}(\sin\phi\mathbf{1} \times \mathbf{e}) = \sin\phi\mathbf{e} \tag{B.4}$$

Furthermore, the last term of the representation of $\mathbf{Q}$ given in eq.(B.3) being skew symmetric, we can write the trace as

$$\text{tr}(\mathbf{Q}) = \text{tr}[\mathbf{e}\mathbf{e}^T + \cos\phi(\mathbf{1} - \mathbf{e}\mathbf{e}^T)] \equiv \mathbf{e}\cdot\mathbf{e} + \cos\phi(3 - \mathbf{e}\cdot\mathbf{e}) = 1 + 2\cos\phi \tag{B.5}$$

The vector of $\mathbf{Q}$ can be denoted by $\mathbf{q} = [q_1, q_2, q_3]^T$, and rather than using tr($\mathbf{Q}$) as the other linear invariant, $q_0 \equiv \cos\phi$ is introduced to refer to the *linear invariants of the rotation*

tensor. Hence, the rotation tensor is fully defined by *four scalar parameters*, namely $\{q_i\}_0^3$, which can be conveniently stored in the four-dimensional array λ, defined as

$$\lambda \equiv [q_0, q_1, q_2, q_3]^T \tag{B.6}$$

where

$$q_0 = \frac{\mathrm{tr}(\mathbf{Q}) - 1}{2} \tag{B.7}$$

It is pointed out, however, that the four components of λ are not independent, for they must obey the following:

$$||\lambda||^2 = q_0^2 + q_1^2 + q_2^2 + q_3^2 \equiv ||\mathbf{q}||^2 + q_0^2 = \sin^2\phi + \cos^2\phi = 1 \tag{B.8}$$

The rotation of a rigid body about a fixed point can therefore be described in a four-dimensional space by the motion of a point of position vector λ that moves on the surface of the unit sphere centred at the origin of the said space.

Appendix C. Computation of a Rotation Matrix Given its Four Upper-Left Entries

This problem arose from the solution of the inverse kinematic problem for the positioning of the spatial three-degree-of-freedom manipulator presented in Section 4.4.1. In the aforementioned solution, the four upper-left entries, i.e., q_{11}, q_{12}, q_{21} and q_{22} of the rotation matrix $\mathbf{Q}$ representing the orientation of the platform are found from the solution of a quartic equation. It is then desired to find the rotation matrix or the set of rotation matrices that are compatible with these four entries. The absolute value of each of the entries of the last row and the last column of $\mathbf{Q}$ can be computed using the fact that each of the rows and columns of $\mathbf{Q}$ should have a unit Euclidean norm. We can write, then,

$$q_{i3} = \pm\sqrt{1 - q_{i1}^2 - q_{i2}^2}, \qquad i = 1,2 \tag{C.1a}$$

and

$$q_{3i} = \pm\sqrt{1 - q_{1i}^2 - q_{2i}^2}, \qquad i = 1,2,3 \tag{C.1b}$$

Therefore, because of the sign ambiguities on five of the components of $\mathbf{Q}$, a set of up to 32 matrices can be found that will satisfy the column and row unit norm constraints. However, since $\mathbf{Q}$ must be an orthogonal matrix, its rows and columns must be orthogonal to each other. This additional constraint can be used to find which of the 32 matrices are orthogonal and, moreover, the determinant can be used to find which of these are proper orthogonal matrices. The following is next shown:

Theorem C.1 Only up to two of the 32 matrices mentioned above are proper orthogonal matrices.

Proof:

Let $\mathbf{Q}$ be a proper orthogonal matrix which satisfies all the constraints described above and let

$$\mathbf{Q} = \begin{bmatrix} q_{11} & q_{12} & q_{13} \\ q_{21} & q_{22} & q_{23} \\ q_{31} & q_{32} & q_{33} \end{bmatrix} \tag{C.2}$$

It is now desired to find other matrices obtained from **Q** by changing the signs of some or all of the entries of the last row and the last column and that would still be proper orthogonal matrices. It is clear that, if the sign of only one or two of the entries of **Q** is changed, the orthogonality between the rows and the columns cannot be preserved. Furthermore, if the sign of three of the entries of **Q** is changed, the orthogonality of the rows and columns is again lost unless the three entries are chosen on a same row or column, i.e., if we change the sign of the entries of the third row or the third column. However, if these signs are changed, the sign of the determinant will be changed and the resulting matrix will be improper orthogonal, i.e., it will represent a reflexion rather than a rotation and it is therefore not an acceptable solution. It is also readily seen that the orthogonality of the rows and columns cannot be preserved when the sign of all the entries of the last row and the last column of **Q** are changed. Finally, there is only one possibility that will preserve both the orthogonality and the determinant and that is, when the signs of q_{13}, q_{23}, q_{31} and q_{32} are changed, i.e.,

$$\mathbf{Q}' = \begin{bmatrix} q_{11} & q_{12} & -q_{13} \\ q_{21} & q_{22} & -q_{23} \\ -q_{31} & -q_{32} & q_{33} \end{bmatrix} \tag{C.3}$$

Indeed, the orthogonality conditions, on the columns of this new matrix $\mathbf{Q}'$ can then be written as

$$q_{11}q_{12} + q_{21}q_{22} + q_{31}q_{32} = 0 \tag{C.4a}$$

$$-q_{11}q_{13} - q_{21}q_{23} - q_{31}q_{33} = 0 \tag{C.4b}$$

$$-q_{12}q_{13} - q_{22}q_{23} - q_{32}q_{33} = 0 \tag{C.4c}$$

which are equivalent to the orthogonality conditions of **Q** and the determinant can be written as

$$\begin{aligned} \Delta(\mathbf{Q}') =& q_{11}(q_{22}q_{33} - q_{23}q_{32}) - q_{21}(q_{12}q_{33} - q_{13}q_{32}) \\ & - q_{31}(-q_{12}q_{23} + q_{13}q_{22}) \\ =& \Delta(\mathbf{Q}) \end{aligned} \tag{C.5}$$

and hence, only up to two solutions to the original problem, **Q** and $\mathbf{Q}'$, can arise.

Appendix D. Condition Number of a Matrix

Let us consider the following linear system:

$$\mathbf{A}\mathbf{x} = \mathbf{b} \tag{D.1}$$

where $\mathbf{A}$ is an $n \times n$ matrix and $\mathbf{x}$ and $\mathbf{b}$ are n–dimensional vectors. The condition number of the matrix $\mathbf{A}$ is a measure of its natural resistance to roundoff error when the solution of the linear system is computed. This resistance is expressed by the amplification factor by which a *relative error* $||\delta\mathbf{b}||/||\mathbf{b}||$ in the data is multiplied to lead to a *relative error* $||\delta\mathbf{x}||/||\mathbf{x}||$ in the solution and it is called the *condition number* of the matrix. We can write the following:

$$\mathbf{A}(\mathbf{x} + \delta\mathbf{x}) = \mathbf{b} + \delta\mathbf{b} \tag{D.2}$$

or, by subtraction of eq.(D.1),

$$\mathbf{A}(\delta\mathbf{x}) = \delta\mathbf{b} \tag{D.3}$$

or

$$\delta\mathbf{x} = \mathbf{A}^{-1}\delta\mathbf{b} \tag{D.4}$$

We now define the norm of a matrix as its *amplifying power*, i.e.,

$$||\mathbf{A}\mathbf{x}|| \leq ||\mathbf{A}||||\mathbf{x}||, \quad \text{for all vectors } \mathbf{x} \tag{D.5}$$

and equality holds for at least one nonzero vector. We can then write, from eqs.(D.1 & D.4),

$$||\mathbf{b}|| \leq ||\mathbf{A}||||\mathbf{x}|| \tag{D.6}$$

and

$$||\delta\mathbf{x}|| \leq ||\mathbf{A}^{-1}||||\delta\mathbf{b}|| \tag{D.7}$$

which leads to

$$\frac{||\delta\mathbf{x}||}{||\mathbf{x}||} \leq \kappa(\mathbf{A})\frac{||\delta\mathbf{b}||}{||\mathbf{b}||} \tag{D.8}$$

where

$$\kappa(\mathbf{A}) = ||\mathbf{A}||||\mathbf{A}^{-1}|| \tag{D.9}$$

is the condition number of $\mathbf{A}$, which defines an upper bound for the amplification of the relative error. This definition of the condition number can be used with different matrix norms. In this thesis, the Euclidean —or Frobenius— norm was used, which is defined as:

$$||\mathbf{A}|| = \sqrt{\mathrm{tr}(\mathbf{A}\mathsf{W}\mathbf{A}^T)} \qquad (D.10a)$$

where

$$\mathsf{W} = \frac{1}{n}\mathbf{1} \qquad (D.10b)$$

and $\mathbf{A}$ is assumed to be $n \times n$. Other definitions for the norm could be adopted. For instance, the square root of the largest eigenvalue of $\mathbf{A}^T\mathbf{A}$ is often used. This definition has the advantage of being applicable to non-square matrices. When this definition is adopted, the condition number of a matrix $\mathbf{A}$ becomes the square root of the ratio of the largest to the smallest eigenvalue of the matrix $\mathbf{A}^T\mathbf{A}$. The Euclidean norm was used here because it is frame-invariant and it is also very easy to compute.